University of Southampton

HARD/SOFT INTERACTIONS: GROUP IV METAL HALIDE COMPLEXES WITH SOFT DONOR LIGANDS OF GROUPS 15 AND 16

Bhavesh Patel

A Thesis Submitted for the Degree of Doctor of Philosophy
Department of Chemistry

May 2002

UNIVERSITY OF SOUTHAMPTON

ABSTRACT

FACULTY OF SCIENCE
CHEMISTRY
Doctor of Philosophy

Hard/Soft Interactions: Group IV Metal Halide Complexes With Soft Donor Ligands Of Groups 15 And 16

by Bhavesh Patel

The complexes *fac*-$[Mn(CO)_3(\eta^3\text{-}L)]CF_3SO_3$ (L = [12]-, [14], [16]-aneS$_4$ and [15]aneS$_5$) have been prepared and characterised by mass spectrometry, IR and multinuclear (^1H, $^{13}C\{^1H\}$, ^{55}Mn) NMR spectroscopy and elemental analysis. Single crystal X-ray diffraction of adducts with L = [12]aneS$_4$ and [15]aneS$_5$ confirmed *fac* coordination of the ligand. Decarbonylation with Me_3NO afforded *cis*-$[Mn(CO)_2(\eta^4\text{-}L)]CF_3SO_3$ as the first examples of thioether stabilised $[Mn(CO)_2]^+$. These were characterised as above and X-ray crystallography of adducts with L = [12]-, [16]-aneS$_4$ and [15]aneS$_5$ revealed the consequences of increasing macrocyclic coordination.

The coordination chemistry of soft donor ligands with Group IV metal halides has been investigated. The complexes $[TiX_4(L_2)]$ (L_2 = $MeE(CH_2)_nEMe$, *o*-$C_6H_4(EMe)_2$, X = Cl, Br; L_2 = $PhE(CH_2)_nEPh$, X = Cl; E = S, Se, n = 2, 3) and $[TiI_4(L_2)]$ (L_2 = $MeSe(CH_2)_nSeMe$, n = 2, 3; *o*-$C_6H_4(SeMe)_2$) have been prepared and characterised by electronic, IR and multinuclear (^1H, $^{13}C\{^1H\}$, $^{77}Se\{^1H\}$) NMR spectroscopy and elemental analysis. NMR spectroscopy revealed dynamic inversion and dissociation processes in solution. X-ray crystallography of $[TiCl_4(L_2)]$ (L_2 = *o*-$C_6H_4(SeMe)_2$ and $MeE(CH_2)_nEMe$, E = S, n = 2, 3; E = Se, n = 3) confirmed *cis* coordination of the ligands and revealed trends in the coordination geometry at Ti(IV).

Analogous reactions with Group 15 ligands afforded $[TiX_4(L_2)]$ (L_2 = $Ph_2As(CH_2)_2AsPh_2$, $Ph_2P(CH_2)_nPPh_2$ (n = 1, 2, 3), *o*-$C_6H_4(PPh_2)_2$, *o*-$C_6H_4(EMe_2)_2$, E = As, P) and $[TiI_4\{o\text{-}C_6H_4(EMe_2)_2\}]$ (E = As, P). Reactions with 2 equivalents of ligand afforded rare 8-coordinate $[TiX_4(L_2)_2]$ for L_2 = *o*-$C_6H_4(EMe_2)_2$, E = As, P, X = Cl, Br, I. The complexes were characterised by electronic, IR and multinuclear (^1H, $^{13}C\{^1H\}$, $^{31}P\{^1H\}$) NMR spectroscopy and elemental analysis. X-ray crystallography of $[TiCl_4(o\text{-}C_6H_4(PMe_2)_2)]$ and $[TiX_4(o\text{-}C_6H_4(EMe_2)_2)_2]$ (E = P, X = Cl, Br; E = As, X = Br) revealed changes in the geometry at Ti(IV) on increasing coordination number.

While Zr(IV) and Hf(IV) showed a strong preference for hard donor ligands, the complexes $[MCl_4(L_2)]$ (L_2 = *o*-$C_6H_4(AsMe_2)_2$, $MeE(CH_2)_nEMe$, E = S, Se, n = 2, 3, M = Zr, Hf) were prepared from $[MCl_4(Me_2S)_2]$. Reactions with 2 equivalents of ligand afforded 8-coordinate $[MCl_4(L_2)_2]$ for L_2 = $MeE(CH_2)_2EMe$, E = S, Se, M = Zr, Hf. The complexes were characterised by IR spectroscopy and elemental analysis. X-ray crystallography of $[ZrCl_4(Me_2S)_2]$, $[ZrCl_4(MeS(CH_2)_3SMe)]$, $[HfCl_4(MeSe(CH_2)_2SeMe)]$, $[MCl_4(MeS(CH_2)_2SMe)_2]$ (M = Zr, Hf), $[ZrCl_4(o\text{-}C_6H_4(AsMe_2)_2)_2]$ revealed the consequences of changing coordination number, ligand architecture and metal centre.

Rare 7-coordinate complexes $[MX_4(L_3)]$ were prepared using L_3 = [Z]aneS$_4$ (Z = 9, 10) for M = Ti, X = Cl, Br, I; M = Zr, X = Cl. However, tripodal L_3 = $MeC(CH_2EMe)_3$ (E = S, Se) afford only 6-coordinate $[MX_4(\eta^2\text{-}L_3)]$ for M = Ti, X = Cl, Br; M = Zr, X = Cl. While L_3 = $MeC(CH_2AsMe_2)_3$ afforded 6-coordinate $[TiX_4(\eta^2\text{-}L_3)]$ (X = Cl, Br, I) and 8-coordinate $[ZrCl_4(\eta^2\text{-}L_3)_2]$. The complexes were characterised by ^1H, $^{13}C\{^1H\}$ NMR (M = Ti) and IR spectroscopy and elemental analysis. X-ray crystallography of $[TiBr_4\{MeC(CH_2AsMe_2)_3\}]$, $[ZrCl_4([9]aneS_4)]$, $[ZrCl_4\{MeC(CH_2AsMe_2)_3\}_2]$ confirmed 6-, 7- and 8-coordination respectively and allowed comparison with the above structures.

Acknowledgements

On completion of this written work, it has become clearly evident why the thesis is regarded by so many as a labour of love. Through the three or so years it has taken, I have experienced the usual highs and lows and I am extremely grateful for the support and assistance provided by both Dr Gillian Reid and Professor William Levason that has seen me through the many challenges. While the chemistry was obviously of great importance, the door has never been closed for the occasional chat and problem sharing.

On the technical side, there have been a number of mentors throughout my PhD. Thanks go again to Dr Reid and Prof. Levason for the collection of the considerable multinuclear NMR spectra and for facing the 'wrath' when the stench of the complexes inconveniently seeped through the NMR caps. Similarly, many thanks to Prof. Levason for putting up with the awful smell when collecting microanalytical data for the numerous moisture sensitive complexes reported within.

During these postgraduate studies, I have had the opportunity to develop an understanding of single crystal X-ray diffraction on many levels. The art of crystal growing will never be understood, but as a few of my colleagues will no doubt recall, the selection criteria were perhaps too high when I was collecting other peoples diffraction data. Through data collection and structure solution, I must thank Dr Mike Webster, Dr Reid and Dr Anthony Genge for their tutelage. Thanks also to Prof. Mike Hursthouse for the use of the EPSRC service diffractometer over many weekends and the opportunity to assume the position of crystallography referee for Polyhedron.

In the lab, there have been a number of influences over the years. In particular, thanks to Dr Andrew Barton, Dr Simon Pope, Dr Anthony Genge and to soon to be 'Drs' Nick Hill and Mike Popham for sharing their experiences and always being around to lend a hand. Unfortunately it was often the famous hands that landed me in trouble outside university, so thanks also to those who have rescued me from many a dodgy situation, especially when under the influence. Thanks to all other past and present members of the research group that I have had the pleasure to meet.

Over the years I have made many other friends within the Chemistry department so thanks all for your company. Obviously the roll-call would be far too long to mention here, but you know who you are. Finally thanks to the University of Southampton for the opportunity to undertake these postgraduate studies, it has been a pleasure.

CONTENTS

Chapter 3 Titanium (IV) Halide Complexes with Bidentate Thio- and Seleno-ether Ligands *69*

Chapter 4 Titanium (IV) Halide Complexes with Bidentate Phosphine and Arsine Ligands *108*

Chapter 5 Zr(IV) and Hf(IV) Chloride Complexes with Bidentate Thio- and Seleno-ether Ligands 144

Chapter 6 Ti(IV) and Zr(IV) Halide Complexes with Tridentate Soft Donor Ligands 175

LIST OF FIGURES

Chapter 1

Chapter 2

Chapter 3

Chapter 4

Chapter 5

Chapter 6

LIST OF TABLES

Chapter 1

Chapter 2

Chapter 3

Chapter 4

Chapter 5

Chapter 6

ABBREVIATIONS

Techniques

NMR	Nuclear Magnetic Resonance	FT	Fourier Transform
IR	Infrared	UV-vis	Ultra violet-visible
EDX	Energy Dispersive X-ray	CVD	Chemical Vapour Deposition
ES^+	Electrospray	MALDI	Matrix Assisted Laser Desorption / Ionisation

Spectroscopy

Q	Quadrupolar moment	D_p	Relative receptivity to ^1H
δ	Chemical shift	$\{^1H\}$	Proton decoupled NMR
ppm	Parts per million	Hz	Hertz
s	Singlet	*d*	Doublet
t	Triplet	*m*	Multiplet
s	Strong	m	Medium
w	Weak	br	Broad
sh	Shoulder	*m/z*	Mass to charge ratio

Ligands

[9]aneS_3	1,4,7-trithiacyclononane	[10]aneS_3	1,4,7-trithiacyclodecane
[12]aneS_4	1,4,7,10-tetrathiacyclododecane	[14]aneS_4	1,4,8,11-tetrathiacyclotetradecane
[16]aneS_4	1,5,9,13-tetrathiacyclohexadecane	[15]aneS_5	1,4,7,10,13-pentathiacyclopentadecane
dppm	bis(diphenylphosphino)methane	dppe	1,2-bis(diphenylphosphino)ethane
dppp	1,3-bis(diphenylphosphino)propane	dmpe	1,2-bis(dimethylphosphino)ethane
dpae	1,2-bis(diphenylarsino)ethane	acac	Acetylacetonate

Groups

M	Metal centre	L	Donor ligand
E	Donor atom	R	Alkyl or aryl substituent
X	Halide	Me	Methyl
Et	Ethyl	Pr	Propyl
Ph	Phenyl	Cy	Cyclohexyl

Solvents

CH_2Cl_2	Dichloromethane	$CHCl_3$	Chloroform
MeCN	Acetonitrile	Me_2CO	Acetone
THF	Tetrahydofuran	THT	Tetrahydrothiaphene
DMF	N,N-Dimethylformamide	$MeNO_2$	Nitromethane
Et_2O	Diethyl ether	EtOH	Ethanol

Miscellaneous

ΔG	Change in Gibbs free energy	ΔH	Change in enthalpy
ΔS	Change in entropy	K	Equilibrium constant
χ	Electronegativity	*o*	Ortho substituents
Rongalite	Sodium formaldehyde sulfoxylate	mmol	Millimoles
VT	Variable Temperature	LT	Low Temperature

Chapter 1

Introduction

1.1 Introduction to Coordination Chemistry

The chemistry of the transition metals is dominated by the formation of coordination and organometallic compounds. This is not entirely surprising considering the considerable number of possible metal / ligand combinations. However, examination of known transition metal coordination chemistry reveals the majority of these complexes comply with simple trends concerning the properties of the metals and ligands. One such trend relates to the acidity or basicity of the metals and ligands. It was G. N. Lewis[1] who first classified substances that act as ligands as bases and the substances with which they react as acids. Thus was born the formal definition of Lewis acids and bases:

Lewis acid:	electron pair acceptor
Lewis base:	electron pair donor

It is the direct combination of these Lewis acids and bases that leads to the formation of coordinate bonds, and hence the term coordination compounds.

While these Lewis definitions are useful, they provide little information on whether a particular combination of acid and base will react to give a stable compound. In 1958, Ahrland, Chatt and Davies devised a sub-classification of Lewis acids based on their reactivity.[2] Hence, metals were identified as either *class a* or *class b* based on the definitions:

Class a:	metals that form stable complexes with first-row donor elements (N, O, F)
Class b:	metals that form stable complexes with second-row donor elements (P, S, Cl)

However, this definition results in many borderline cases where the degree of *a*- or *b*-character is dependent on the oxidation state of the metal. In 1968, R. G. Pearson developed this concept further to account for the dissimilar chemistries of different metal oxidation states.[3] Hence, Lewis acids and bases were sub-classified either hard or soft according to the definitions:

Hard base:	donor with high electronegativity, low polarisability, resistance to oxidation
Soft base:	donor with low electronegativity, high polarisability and readily oxidised
Hard acid:	acceptor with high positive charge density and low polarisability
Soft acid:	acceptor with low positive charge density and high polarisability

Table 1 shows a selection of Lewis acids and bases classified as hard, soft or borderline. Based on these definitions, it is clear to see that the strongest interactions would result from reactions of acids and bases of equivalent hardness. Thus, a hard acid/hard base interaction combines constituents with high charge density and low polarisability, resulting in bonding ionic in character (eg. $NaClO_4$). Whereas a soft acid/soft base interaction combines highly polarisable constituents and hence the resulting bonding is covalent in character (eg. $[Ag\{o\text{-}C_6H_4(AsMe_2)_2\}_2]^+$).

However, for a hard/soft combination, there is clearly a mismatch in the electronic properties of the acid and base, and therefore these interactions tend to be less stable than hard/hard or soft/soft interactions. Nevertheless, by careful choice of reaction conditions, it is possible to form stable compounds exhibiting hard/soft interactions. For example, the adducts $[CrCl_3([9]aneS_3)]$[4] and $[VOCl_2([9]aneS_3)]$[5] ($[9]aneS_3$ = 1,4,7-trithiacyclononane) can be formed under anhydrous conditions by utilising the superior coordinating ability of the macrocyclic ligand. The chemistry described in this work will mainly concentrate on hard acid/soft base interactions to gain an insight into what properties of the soft bases affect the stability of the acid/base interaction.

Table 1.1 Classification of hard and soft Lewis acids and bases

	Hard	Borderline	Soft
Acids	H^+, Li^+, Na^+, Ca^{2+}, Ti^{4+}, Fe^{3+}, Cr^{3+}, Mn^{2+}, BF_3	Fe^{2+}, Cu^{2+}, Ru^{3+}, NO^+, SO_2	Cu^+, Au^+, Ag^+, Pd^{2+}, Pt^{2+}, Pt^{4+}, Cd^{2+}, Hg^{2+}
Bases	F^-, Cl^-, HO^-, NO_3^-, H_2O, OR_2, NR_3, ClO_4^-, SO_4^{2-}	Br^-, NO_2^-, N_2, N_3^-, SO_3^{2-}	ER_2 (E = S, Se, Te), $E'R_3$ (E′ = P, As, Sb), CO, C_6H_6

1.2 Hard Metals of Group 4

1.2.1 Titanium

Titanium is a common element, with only iron, the fundamental component of the earth's core, more abundant in the earth's crust among the d-block elements. It exists in the form of two principal ores, ilmenite ($FeTiO_3$) and rutile (TiO_2), the latter representing the main use of titanium as a white pigment in the paint industry. Both ores involve titanium in its most common oxidation state, +4, where all four valence electrons are lost to present the d^0 Ti(IV) ion. The coordination chemistry of titanium is not exclusive to Ti(IV) though, with a wide range of complexes reported involving Ti(III). However, the lower oxidation states of titanium are much less common and are often unstable to oxidation.[6,7]

The most common coordination number of titanium is six, evident in all oxidation states of the metal. Again, this is not exclusive and there are examples of both higher and lower coordination numbers.[8,9] Ti(IV) complexes exhibit a large variation in coordination number, ranging from 4-coordinate in the tetrahedral $TiCl_4$ monomer, to 8-coordinate dodecahedral $[Ti(NO_3)_4]$.[10] The latter is however, one of only a small number of 8-coordinate Ti(IV) complexes, with 7-coordination yet less common, for example $[TiCl(tropolone)_3]$ ($tropolone^- = C_7H_5O_2^-$).[11]

The above examples include the halide $TiCl_4$, and indeed this is the major synthetic precursor to Ti(IV) complexes. $TiBr_4$ is also a useful precursor, however very few characterised complexes involving TiI_4 have been reported, partly due to its low solubility in non-coordinating solvents. Moreover, the relative acceptor strengths of these titanium halides has been established as $TiCl_4 \sim TiBr_4 > TiI_4$,[12] with the latter leading to weakly coordinated complexes with donor ligands, if any at all. The few reported TiI_4 coordination complexes are not well characterised, for example $[TiI_2\{o\text{-}C_6H_4(AsMe_2)_2\}_2][I^-]_2$ is speculated on the basis of analytical and infra-red data alone.[13]

1.2.2 Zirconium and Hafnium

Despite a difference in atomic number of 32, these heavier group IV elements exhibit near identical atomic radii due to the lanthanide contraction. Thus, the chemistries of Zr(IV) and Hf(IV) are very similar, more so than for any other pair of elements in the periodic table. Indeed, the two elements invariably occur together in nature, with the principal zirconium ores zircon ($ZrSiO_4$) and baddelyite (ZrO_2) containing *ca.* 2 – 5 % hafnium. However, driven by their attractive, but contrasting nuclear properties, the separation of these elements has received renewed interest. Thus very weakly neutron absorbing zirconium is utilised in nuclear reactor construction, while highly neutron absorbing hafnium may be used within control rods in the reactors.

As with titanium, both zirconium and hafnium show a strong preference for the +4 oxidation state, with only a small number of reported Zr(III) and Hf(III) complexes, and sporadic reports of poorly characterised coordination complexes of the lower oxidation states.[14,15] The larger size of zirconium and hafnium when compared with titanium generally leads to complexes of high coordination number, with eight-coordination most common. For example, bidentate *N,N*-dialkyldithiocarbamate ligands, $S_2CNR_2^-$ are known to stabilise eight-coordination in the range of complexes $[Zr(S_2CNR_2)_4]$ (R = Me, Et, Pr).[16] Although Zr(IV) and Hf(IV) are both strong Lewis acids, their larger ionic radii present less concentrated charge density and hence slightly softer character for the heavier group IV acids. While this lower Lewis acidity of Zr(IV) and Hf(IV) may reduce reactivity with donor ligands, the more diffuse charge may present greater orbital overlap with the polarised orbitals of soft donor ligands. Indeed, a small number of Zr(IV) and Hf(IV) complexes involving phosphine, arsine and thioether ligands are known, (as discussed in Chapters 5 and 6), including six-coordinate $[MCl_4(THT)_2]$ (M = Zr, Hf).[17] Thus, it is possible that Zr(IV) and Hf(IV) halides may form a range of six and eight-coordinate complexes with other soft donor ligands of groups 15 and 16.

1.3 Soft Donor Ligands of Group 15 and 16

1.3.1 Group 15 Ligands

The coordination chemistry of Group 15 ligands has an extensive history. In 1857, Hofmann[18] reported the first phosphine complex, while Cahours and Gal[19] reported the first arsine coordination complex in 1870. The discovery that arsine containing compounds were of therapeutic or, in some cases, poisonous value led to a huge development of arsine chemistry early in the 20th century. However, from the 1930's, the expansion of phosphine chemistry has outstripped that of arsines following the realisation that phosphines were in fact superior ligands. This trend has continued to the present date with the development of FT-NMR techniques greatly enhancing the study of the 100% abundant spin ½ ^{31}P nucleus. As a result, a number of industrially important phosphine compounds have been synthesised, including Wilkinson's catalyst, $[RhCl(PPh_3)_3]$ for the hydrogenation of alkenes.[20]

1.3.1.1 Group 15 Ligand Synthesis

The synthesis of phosphine and arsine ligands follow very similar methods, and outlined below are the some of the possible synthetic routes for a selection of the ligands used throughout this study. Phosphine synthesis is slightly more difficult than for arsines due to the ease of oxidation of P(III) to P(V). However, stibine ligands are even more challenging to synthesise due to the weakness of the Sb-C interaction leading to the facile elimination of the alkyl groups.

- **$Ph_2E(CH_2)_nEPh_2$ (E = P, As)**[21,22,23,24]

$$2EPh_3 \quad + \quad 2Li \xrightarrow{THF} 2LiEPh_2 \xrightarrow{X(CH_2)_nX} Ph_2E(CH_2)_nEPh_2 \quad + \quad 2LiX$$

- **$o\text{-}C_6H_4(PPh_2)_2$**[25,26]

$$2LiEPh_2 \xrightarrow[THF]{o\text{-}C_6H_4F_2} o\text{-}C_6H_4(EPh_2)_2 \quad + \quad 2LiF$$

- **o-$C_6H_4(EMe_2)_2$**[27,28,29,30]

$$2EMe_3 \quad + \quad 2Na \xrightarrow{THF} 2NaEMe_2 \xrightarrow{o\text{-}C_6H_4Cl_2} o\text{-}C_6H_4(EMe_2)_2 + 2NaCl$$

- **$MeC(CH_2AsMe_2)_3$**[31]

$$3NaAsMe_2 \quad \xrightarrow[THF]{MeC(CH_2Br)_3} \quad MeC(CH_2AsMe_2)_3 \quad + \quad 3NaBr$$

1.3.1.2 M-E (E = P, As, Sb) Bonding

The valence electronic configuration for the donor atoms in Group 15 ligands ER_3 (E = P, As, Sb) is $ns^2\ np^3\ nd^0$. Three of these electrons are used in the three E-R bonds, leaving one lone pair of non-bonding electrons. It is this electron pair that is donated into an empty d orbital of a transition metal centre to form a σ-bond. The Group 15 donor elements also possess empty d orbitals that can, according to the Chatt bonding model,[32] accept electrons from filled d orbitals of suitable (π) symmetry on the metal centre. While this π-backbonding is widely accepted to occur in M-E bonding for mid- and late transition metals, it has been argued that the d orbitals on the donor atoms are too diffuse and of too high energy to contribute significantly to the bonding. Recent quantum mechanical calculations, supported by single crystal X-ray diffraction studies, have suggested that π-acceptance may in fact involve the E-C σ^* orbitals which are of more suitable energy.[33] While the latter is the generally accepted model, the X-ray diffraction evidence for this is of marginal significance according to the margins of error associated with the X-ray crystallographic data.

The strength of the transition metal to Group 15 donor interaction has been investigated through the study of ligand exchange properties of the cations $[(\eta^5\text{-}C_5H_5)Fe(CO)_2(ER_3)]^+$ (E = P, As, Sb).[34] The results indicate the strength of the Fe-E interaction decreases down Group 15 to give a donor ability order $PR_3 > AsR_3 > SbR_3$. While the work within this present study will concentrate on d^0 metal centres incapable of π-bonding, the order of σ-donating ability is expected to remain unchanged.

Other than the electronic considerations mentioned above, steric effects also influence the M-E interaction. With three substituents (R) on the Group 15 donor atoms, the ER_3 ligand is potentially a bulky ligand. The extent of this 'bulkiness' has been modelled to some extent by Tolman,[35] who devised a scale based upon the space occupied by the ligand upon coordination to a metal centre. The 'Cone Angle' model has two major assumptions; there is a fixed bond distance between metal and donor (2.28 Å) and that the ligand occupies a complete cone of space emanating from the metal centre, with no intermeshing between neighbouring ligands. The cone angle is then defined as the apex angle of the cone subtended at the metal centre (Figure 1.1). While the assumptions tend to overestimate spatial considerations, this simplistic model does allow semi-quantitative comparison of the steric effects of different ligands. However, it has been shown through X-ray diffraction studies[36] of complexes involving the bulky ligand PCy_3 that the molecules can adapt in order to accommodate steric over-crowding, principally *via* intermeshing ligands or lengthening of the M-P bond and hence reducing the cone angle.

Figure 1.1 Schematic representation of the Tolman Cone Angle in M-PR$_3$

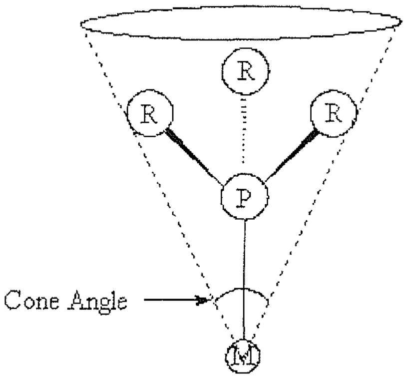

1.3.2 Group 16 Ligands

Although the roots to the coordination chemistry of Group 16 donor ligands can be traced back to the same era as Group 15 ligands, it is only relatively recently that the first major reviews in this area have been reported. This apparent neglect for Group 16 coordination chemistry can be attributed to the generally accepted view that donor ligands of Group 16 are weaker donors than those of Group 15. However, other factors influencing the comparative lack of interest in these ligands must include their toxicity, commercial unavailability and the fact that they are generally extremely malodorous. Recently however, thioether chemistry has benefited from the development of macrocyclic derivatives offering significantly improved donor abilities. Seleno- and telluro-ether chemistry has also received renewed interest through the development of FT-NMR techniques for studying the spin ½ ^{77}Se and ^{125}Te nuclei (7.58 and 6.99% abundance, respectively). As a consequence of this recent interest, Group 16 donor ligands are now an integral part of the development of thin film electronic materials formed *via* Chemical Vapour Deposition (CVD) processes (see Chapter 3).[37]

1.3.2.1 Group 16 Ligand Synthesis

Similar to the ligands of Group 15, the synthesis of thio- and seleno-ether ligands follow very similar methods, and the synthetic routes for the ligands used in this study are outlined below. Again, the lower member of the group of ligands, telluroethers have the most challenging syntheses due to the weakness of the Te-C interaction leading to facile elimination rather than substitution reactions.

- **$PhS(CH_2)_nSPh$**[38]

$$2PhSH \xrightarrow[Na]{EtOH} 2NaSPh \xrightarrow{Cl(CH_2)_nCl} PhS(CH_2)_nSPh + 2NaCl$$

- **$MeS(CH_2)_nSMe$**[38]

$$HS(CH_2)_nSH \xrightarrow[Na]{EtOH} NaS(CH_2)_nSNa \xrightarrow{2MeI} MeS(CH_2)_nSMe + 2NaI$$

- **o-$C_6H_4(SMe)_2$**[39]

$$NaSMe \xrightarrow[THF,\ -NaCl]{o\text{-}C_6H_4Cl_2} o\text{-}C_6H_4(SMe)Cl \xrightarrow[\frac{1}{2}\ MeSSMe]{BuLi} o\text{-}C_6H_4(SMe)_2 + LiCl$$

- **$\mathrm{PhSe(CH_2)_nSePh}$**[40]

$$\mathrm{PhSeSePh} \xrightarrow[\mathrm{LiAlH_4}]{\mathrm{THF}} \mathrm{2LiSePh} \xrightarrow{\mathrm{Br(CH_2)_nBr}} \mathrm{PhSe(CH_2)_nSePh} + \mathrm{2LiBr}$$

- **$\mathrm{MeSe(CH_2)_nSeMe}$**[40]

$$\text{Se powder} \xrightarrow[\mathrm{MeLi}]{\mathrm{Et_2O}} \mathrm{2LiSeMe} \xrightarrow{\mathrm{Cl(CH_2)_nCl}} \mathrm{MeSe(CH_2)_nSeMe} + \mathrm{2LiCl}$$

- **$o\text{-}\mathrm{C_6H_4(SeMe)_2}$**[41]

$$o\text{-}\mathrm{C_6H_4Br_2} \xrightarrow[\mathrm{DMF,\ -2NaBr}]{\mathrm{NaSeSeNa}} [-o\text{-}\mathrm{SeC_6H_4Se}-]_n \xrightarrow[\mathrm{2MeI}]{\text{Rongalite}} o\text{-}\mathrm{C_6H_4(SeMe)_2} + \mathrm{2NaI}$$

- **$\mathrm{MeC(CH_2EMe)_3}$ (E = S, Se)**[42,43]

$$\mathrm{3NaEMe} \xrightarrow[\mathrm{THF}]{\mathrm{MeC(CH_2Br)_3}} \mathrm{MeC(CH_2EMe)_3} + \mathrm{3NaBr}$$

- **Thioether Macrocycles**[44,45,46]

High Dilution: Large volumes of solvent used in final stage to promote cyclisation over polymerisation. Typical route for thioether macrocycles:

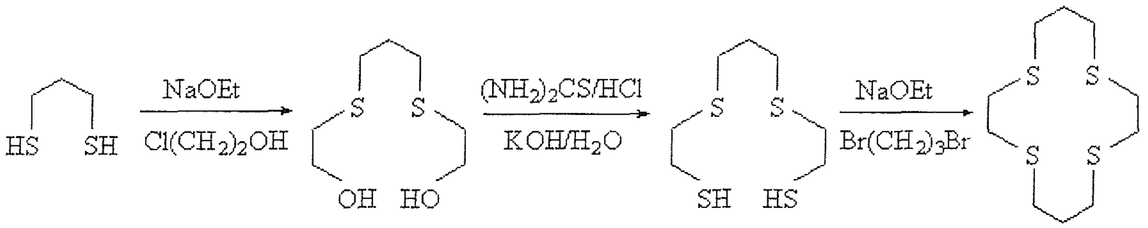

Template: Donor atoms bound to metal ion and preorganised for cyclisation, or binding only possible for cyclised product. Less common for thioether macrocycles due to weak S-donor to metal interaction:

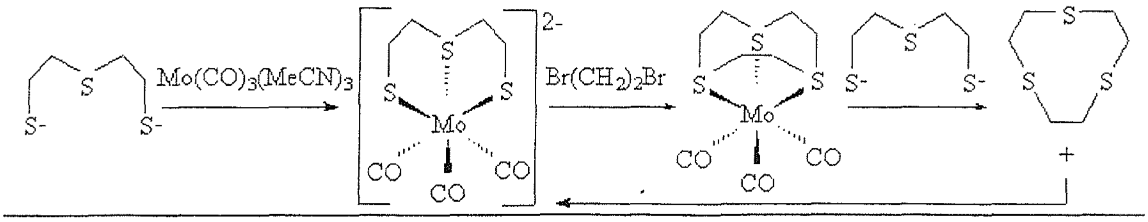

1.3.2.2 M-E (E = S, Se, Te) Bonding

The valence electronic configuration for the donor atoms in Group 16 ligands ER_2 (E = S, Se, Te) is $ns^2\ np^4\ nd^0$. Two of these electrons are used in the two E-R bonds, leaving two lone pairs of non-bonding electrons. As with the Group 15 ligands, one of these electron pairs is donated into an empty d orbital of a transition metal centre to form a σ-bond. However, it is the presence of the second lone pair that increases the complexity of the bonding model for these ligands. If the lone pair remains non-bonding, it is could be a source of π-repulsion when interacting with electron rich metal centres. Alternatively, the lone pair may σ-donate to a second metal centre to give a bridging ER_2 unit, as observed in the adduct $[Br_2Pt(SEt_2)_2PtBr_2]$.[47] Otherwise, the lone pair could π-donate into empty d orbitals of the correct symmetry on a σ-bonded metal centre. While this may be possible during interactions with electron poor metal centres, there is no good evidence to suggest that π-donation is significant for these ligands.

In addition to the uncertainty concerning the contribution of the second lone pair to M-E bonding, empty d orbitals on the Group 16 donor also present the opportunity for π-acceptance from filled d orbitals of the metal centre. However, by similar arguments concerning π-acceptance in Group 15 ligands, it is more likely that any such bonding in Group 16 ligands will involve E-C σ* orbitals, and not the diffuse and high energy d orbitals.[33] While it is difficult to establish unequivocally the presence of π-backbonding, comparison of observed M-E bond lengths with the sum of the covalent radii of the two components has suggested this type of bonding occurs in some cases.[48] Indeed a recent report on macrocyclic thioether complexes suggested that π-acceptance may be a significant part of M-S bonding in certain cases.[49] However, it is the general consensus that for the majority of Group 16 donor ligands, π-bonding is either weak or totally absent, as supported by theoretical studies on thio- and seleno-ether complexes $[Cr(CO)_5(ER_2)]$ (E = S, Se).[50]

As with the donor ligands of Group 15, experimental and theoretical studies have been reported for the Group 16 ligand cations $[(\eta^5\text{-}C_5H_5)Fe(CO)_2(ER_2)]^+$ (E = S, Se, Te).[34] However, in contrast to Group 15, the results indicate the strength of the Fe-E interaction increases down Group 16 to give a donor ability order of $TeR_2 \gg SeR_2 > SR_2$. Recently, work undertaken within this research group at the University of

Southampton has shown the same trend down Group 16 in the complexes [$Mn(CO)_3X$-(L-L)] (X = Cl, Br; L-L = dithio-, diseleno- or ditelluro-ether)[51] and $[Mn(CO)_3(L_3)]^+$ (L_3 = $MeC(CH_2EMe)_3$).[52] These results have been attributed to decreasing electronegativity down Group 16 leading to increasing donation to the metal centre. However, this also leads to increasingly diffuse σ-orbitals on the donor, with the effect most pronounced for telluroether ligands. For low valent metal centres, as in the above examples, the spatial expansion of the d orbitals is also large and so there is good orbital overlap with the diffuse telluroether orbitals. The observed donor ability of ER_2 therefore increases down Group 16, S < Se << Te. However, on increasing the metal oxidation state, the d orbitals contract and interaction with telluroether ligands decreases, giving a donor order S < Se > Te. This is exemplified by the inability of telluroethers to bond to high oxidation state platinum metals, while thio- and seleno-ethers form stable adducts. This contrasts with Group 15 donor ligand behaviour, where donor ability is always P > As > Sb. For the high oxidation state d^0 metals to be used in this study, the latter trend is expected and hence telluroether coordination is expected to be weak. Also, the absence of d electrons will nullify any π-backbonding contributions.

1.3.2.3 Pyramidal Inversion

While the presence of only two R groups removes steric considerations for chalcogenoether ligands (ER_2), two lone pairs of electrons on the donor atoms leads to a pyramidal environment at the chalcogen, E *via sp*^{3} hybridisation. Consequently, if the two R groups are different (RER′), the chalcogen becomes chiral upon coordination σ-donation to a metal centre, assuming the second lone pair remains non-bonding. This chirality leads to the presence of two enantiomeric forms upon inversion at E, and this process is known simply as pyramidal inversion. The most common mechanism (Figure 1.2) for this inversion process involves the interchange of two energetically equivalent configurations *via* a planar transition state.[53] By this definition, pyramidal inversion is simply a subtle molecular rearrangement and involves no bond cleavage. Other mechanisms that do involve dissociation and recombination of one or more of the substituents on E have been shown to exist,[54] however the strength of metal-chalcogen bonds suggest bond cleavage is not a favoured mechanism for Group 16 ligands.

Figure 1.2 Proposed mechanism of pyramidal inversion for chalcogenoethers.

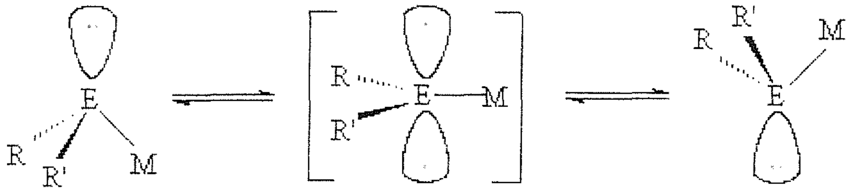

Pyramidal inversion can give rise to subtle variations in the geometry of the molecule; hence it may be possible to elucidate the presence of the diastereoisomers through NMR spectroscopy. For monodentate ligands, rotation about the M-E bond is a low energy process and so the diastereoisomers are NMR indistinguishable. However, for chelating ligands, this rotation is generally not energetically feasible and so the different invertomers can be observed providing they are not interconverting rapidly *via* pyramidal inversion. Thus, pyramidal inversion in chalcogenoether complexes was first observed in the chelate complex $[PtCl_2\{MeS(CH_2)_2SMe\}]$ by Abel and co-workers in 1966.[55] Thereafter, there have been various investigations into pyramidal inversion in other chalcogen-transition metal complexes.[54] A review on the NMR studies of pyramidal inversion has revealed a number of factors which influence the activation energies associated with inversion,[56] including:

- Nature of the inverting centre[57,58,59,60]

  Activation energies to pyramidal inversion generally accepted to increase down Group 16, S < Se < Te, although there is little qualitative data reported for Te.

- Nature of the metal centre[61]

  Coordination of the chalcogen to a metal centre dramatically reduces the energy barrier to inversion at E in two ways. Firstly, the electropositive nature of the metal decreases the *s* character of the non-bonding lone pair, thus allowing easier access to the planar transition state. Secondly, this transition state may be stabilised *via* $(p\text{-}d)\pi$ conjugation between the chalcogen and the metal centre.

- π-Conjugation in the donor ligand[61]

  As with interactions with the metal, π-conjugation in the organic substructure of the ligand may stabilise the transition state and reduce the inversion barrier.

- Chelate ring strain effects[58,59,60]

  Small chelate rings generate strained bite angles that increase the energy barrier to the trigonal transition state. Hence, there is a noticeable decrease in inversion barrier on increasing the chelate ring size from 5- to 6-membered.

- Influence of *trans* ligands[62]

  Highly electronegative ligands *trans* to the chalcogen may weaken the M-E bond and hence increase the energy barrier to inversion by reducing the stabilising influence of the metal centre.

1.3.3 Ligand Architecture

It is expected that the combination of hard Group 4 metal centres with soft donor ligands of Groups 15 and 16 will result in weak interactions, as indicated by the hard/soft acid/base principle discussed earlier. Consequently, the architecture of the ligands used will be carefully chosen to maximise the metal-donor interaction. Multidentate ligands can provide enhanced stability compared with monodentate ligands due to the kinetic advantage of one metal-ligand encounter offering numerous donor atoms. However, the coordination of multidentate ligands has a number of thermodynamic consequences, and the magnitude of stabilisation may also depend on the coordination environment at the metal centre.

1.3.3.1 The Chelate Effect

The thermodynamic advantage of multidentate ligand (L_x, x = denticity) coordination over that of the equivalent number (x) of monodentate ligands (L) can be recognised by observing the equilibrium between the two moieties:

$$M(L)_x \quad + \quad L_x \quad \leftrightarrows \quad M(L_x) \quad + \quad x(L)$$

The equilibrium constant (K) associated with this scheme is related to the standard free energy, and therefore the enthalpy and entropy of the reaction by the equations:

$$\Delta G^\circ = -RT(\ln K)$$

$$\Delta G^\circ = \Delta H^\circ - T\Delta S^\circ$$

Therefore, the direction of the equilibrium is dependent on the enthalpic and entropic contributions of the two systems. For ligands involving the same donor atoms, the strength of individual metal-donor interactions remain relatively independent of ligand denticity and hence the enthalpy terms of each system are comparable. However, when considering the entropic contributions, it is evident that multidentate ligand coordination leads to more free species and hence greater entropy. The net result is a more negative free energy and therefore greater stabilisation for the multidentate complex. This is defined as the Chelate Effect, and the size of chelate stabilisation increases with the number of chelate rings formed during ligand coordination. The effect is also dependent on the size of the chelate rings, with 5- (most stable) and 6-membered chelate rings offering greatest stabilisation.

1.3.3.2 The Macrocyclic Effect

Macrocycles can be defined as cyclic molecules with nine or more atoms, at least three of which are donor heteroatoms. On coordination to a metal centre, a macrocycle of denticity *n* results in the formation of *n* chelate rings. However, the stabilisation observed surpasses that expected for the cumulative chelate stabilisation.[63] This is known as the Macrocyclic Effect[64] and the basis to the thermodynamic stabilisation can be recognised by observing the equilibrium between macrocyclic coordination and that for an analogous open chain ligand of equal denticity:

$$M(L_{chain}) + L_{mac} \leftrightarrows M(L_{mac}) + L_{chain}$$

Here, the entropic contribution relates to the configurational freedom of the respective ligands. The ring structure of the macrocycle results in fewer configurational degrees of freedom, hence little entropic loss on coordination to the metal centre. However, open chain ligands potentially possess a large number of rotational and vibrational degrees of freedom, most of which are lost on coordination. Thus, the entropic term for open chain ligand coordination is unfavourable and therefore favours macrocyclic coordination, as observed for aza-macrocyclic ligands on coordination with Ni(II).[65]

The conformation of ligands can also influence the enthalpic contribution. Macrocyclic coordination is only effective when there is a good match between the macrocycle ring size and the size of the metal centre. Similarly, certain ring sizes lead to conformations where the donor atoms are *exo* to the ring (eg. [14]aneS_4 = 1,4,8,11-tetrathiacyclotetradecane) and therefore require reorganisation prior to coordination. This increases the activation energy to coordination and hence reduces the net enthalpic stabilisation. Other factors also influence the effectiveness of macrocyclic coordination, including solvation effects. However, these are only significant for hard O- and N-donor macrocycles, and less important for the soft S-donor ligands to be used in this study.[63]

1.3.3.3 <u>*Ligand Types*</u>

In order to maximise the chelate and macrocyclic effects discussed above, a range of ligand denticities will be used which generate 5- or 6-membered chelate rings on coordination to a metal centre. These are outlined below:

- Bidentate ligands

Group 15 : E = P, As; n = 1, 2, 3

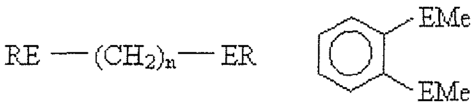

Group 16 : E = S, Se; R = Me, Ph; n = 2, 3

- Tripodal ligands

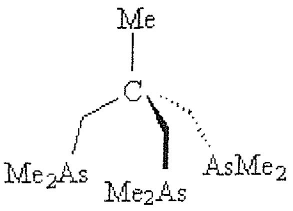

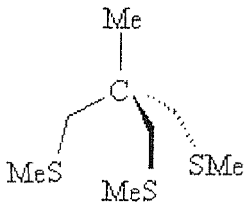

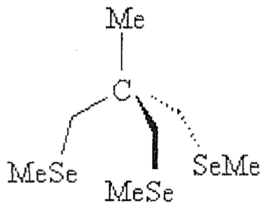

- Macrocyclic ligands

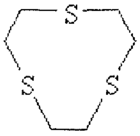

[9]aneS$_3$

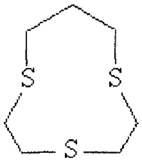

[10]aneS$_3$

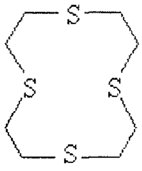

[12]aneS$_4$

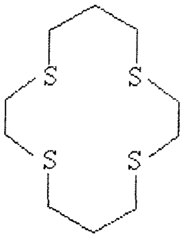

[14]aneS$_4$

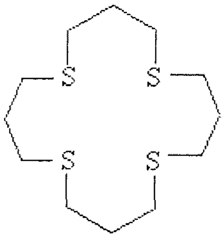

[16]aneS$_4$

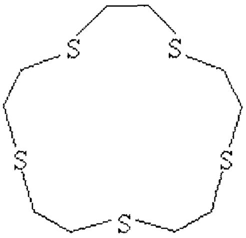

[15]aneS$_5$

1.3.3.4 Coordination Number and Stereochemistry

As mentioned earlier, the common coordination numbers of Group 4 metal complexes range from six for titanium to eight for zirconium and hafnium. Therefore, for the MX_4 (M = Ti, Zr, Hf; X = Cl, Br, I) precursors to be used in this study, coordination of the above multidentate ligands can lead to a number of coordination geometries at the metal centre. Moreover, for the Group 16 donor adducts, the possibility of pyramidal inversion can also lead to a number of diastereoisomeric forms, as shown below. Inversion is not expected to be significant for the macrocyclic adducts due to the energy required for reorganisation of the ring structure.

- 6-coordinate

Formed by coordination of bidentate or η^2-tripodal ligands. The resulting 5- or 6-membered chelate rings cannot span the metal centre for *trans* coordination, hence only the *cis* isomer is observed. Inversion for Group 16 ligands leads to two *meso* invertomers and a *DL* pair of enantiomers.

Bidentates:

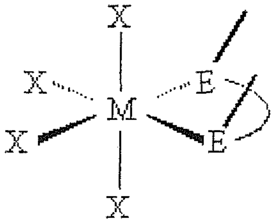

meso

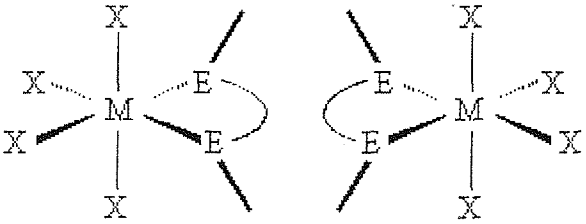

enantiomeric *DL* pair

η^2-Tripods:

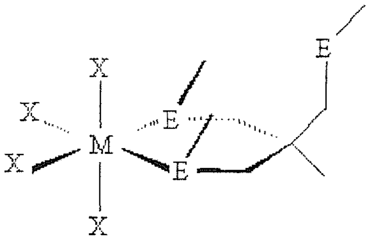

meso-1

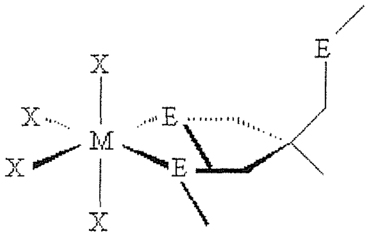

meso-2

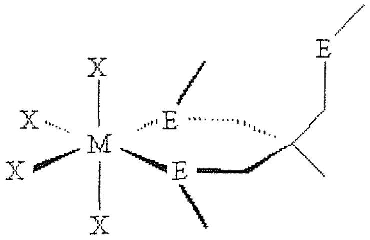

enantiomeric *DL* pair

- 7-coordinate

Numerous geometries are known for 7-coordination. Four of these are capped octahedral (C_{3v}), capped trigonal prismatic (C_{2v}), pentagonal bipyramidal (D_{5h}) and irregular (C_2):[9]

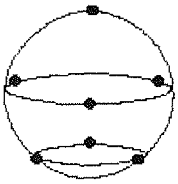

C_{3v}

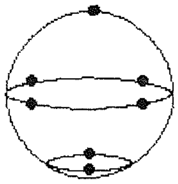

C_{2v}

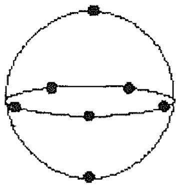

D_{5h}

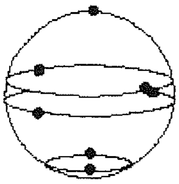

C_2

For the MX_4(tridentate) adducts studied here, the '4 + 3' donor set appears to be best accommodated by the capped octahedral structure. The expected weak interactions between hard metal and soft donor may lead to a distorted structure, with the trigonal base elongated away from the centre. While coordination of tridentate macrocycles in this way leads to only one isomer, tripodal coordination can result in *anti* or *syn* isomers:

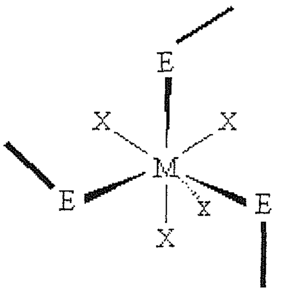

syn

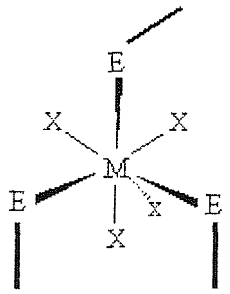

anti

- 8-coordinate

Again, numerous geometries have been observed for 8-coordination:[9]

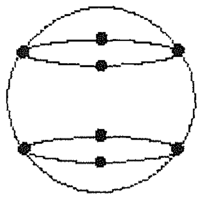

Cubic

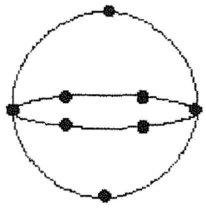

Hexagonal bipyramidal (HBP)

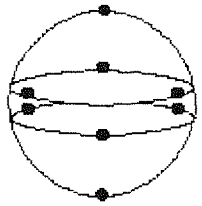

Puckered HBP

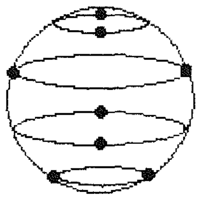

Dodecahedral

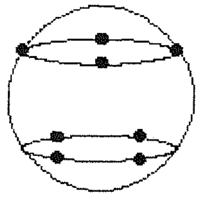

Square anti-prismatic

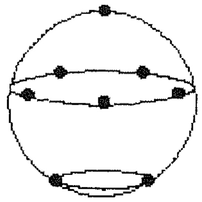

1 : 5 : 2

However, only two of these are commonly observed in coordination complexes, dodecahedral and square anti-prismatic. The two structures are very similar, with the dodecahedral structure formed by simply distorting the square faces within the square anti-prismatic structure. Indeed, studies concerning the potential energy surface for ligand-ligand repulsion in 8-coordinate structures have shown a continuous interconversion between the two geometries. The structures differ only in that the eight ligand sites of the anti-prismatic structure are equivalent, while the dodecahedral geometry contains two different sites. Thus, the two pairs of ligand sites at the apex and base of the above representation are elongated to give four 'A'-type vertices and four 'B'-type vertices along the equator. Each type of ligand site form tetrahedra, hence the dodecahedral structure can be thought of as two interpenetrating tetrahedra.

For the $MX_4(bidentate)_2$ adducts studied here, the '4 + 4' donor set appears to be best accommodated by the dodecahedral structure. Again, the interactions between hard metal and soft donor are likely to be weak, and therefore the donor ligands are expected to occupy the elongated 'A'-type vertices.

1.4 Characterisation Techniques

The weakness of the hard/soft interactions studied in this work presents difficulties during complex characterisation. Due to the preference of the hard metal centres for hard donor ligands, the adducts formed are likely to be extremely moisture sensitive, with the soft ligands readily displaced by hard O-donor ligands. Therefore, it is imperative that the air and moisture free conditions to be used during complex synthesis are maintained during characterisation. In general, this has prompted the use of rigorously anhydrous solvents, sample preparation within a continuously N_2-purged dry glove box and where possible, sealing the samples from external conditions.

A range of spectroscopic techniques has been employed throughout this study and an overview is given below. In addition, microanalytical data have been collected for all isolated solids and electrospray mass spectrometry was utilised for the Mn(I) complexes discussed in Chapter 2.

1.4.1 Infra-red (IR) Spectroscopy

Previous studies have shown that the metal-halide stretching frequencies for the Group 4 metals occur in the region 400-250 cm^{-1}.[66] Therefore, IR spectra were recorded for all the Group 4 complexes formed here as nujol mulls (using sodium-dried Nujol) pressed between CsI plates in the range 1000-200 cm^{-1}. The number of metal-halide stretching frequencies observed has been useful for determining the geometry of the complexes by applying group theory.

The work described in Chapter 2 discusses manganese carbonyl adducts with thioether macrocycles. Here IR spectroscopy has been utilised to study changes in the manganese-carbonyl interaction *via* monitoring the C-O stretching frequencies (2200-1800 cm^{-1}). Thereby, an increase in Mn(I) π-backbonding into the σ^*(C-O) orbital of the carbonyl will result in decreased C-O interaction and therefore a decrease in the C-O stretching frequency. This has been used to indicate the influence of the coordinating thioether donor ligands on the electronic properties of the Mn(I) centre.

1.4.2 *Electronic (UV-visible) Spectroscopy*

For the d^0 Group 4 metal adducts studied here, electronic spectroscopy is simplified by the absence of d-d and metal to ligand charge transfer (MLCT) transitions. Therefore, with the exception of possible $\pi \rightarrow \pi^*$ transition from aryl substituents, all observed transitions can be defined as ligand to metal charge transfer (LMCT) transitions from lone pairs of electrons on the halides or Group 15 and 16 donor ligands.

Solution spectra are preferable due to the possibility of calculating the molar absorption coefficient ε_{max}. However, significant decomposition of the very moisture sensitive solutions was observed at the required low concentrations. Therefore, spectra were recorded by diffuse reflectance using anhydrous $BaSO_4$ as an inert diluent.

The position of electronic transitions can confirm the donor types present in a complex by comparing the optical electronegativities (χ_{opt}) of the respective metal and ligand.[67] Thus, the lowest energy LMCT transition can be predicted using the equation:[68]

$$\bar{\nu} \quad = \quad C\,[\,\chi_{opt}(\text{Ligand}) \quad - \quad \chi_{opt}(\text{Metal})\,]$$

For C = 30,000 cm^{-1}, the optical electronegativites are comparable to Pauling's values (χ_P),[69] and using these, it was possible to predict the lowest energy electronic transition.

1.4.3 *Nuclear Magnetic Resonance (NMR) Spectroscopy*

NMR spectroscopy has been used extensively throughout this study for the characterisation of the synthesised complexes. In many cases, multinuclear studies have been undertaken to provide complementary data relating to different aspects of the metal-ligand interaction. Furthermore, the utilisation of variable temperature NMR spectroscopy has permitted resolution of some of the dynamic processes occurring in solution, including pyramidal inversion for the Group 16 ligand complexes.

^{1}H NMR spectra were recording in 5 mm tubes using anhydrous $CDCl_3$ or CD_2Cl_2 solutions of the complexes. The lower sensitivity of the other studied nuclei necessitated the use of 10 mm tubes with anhydrous $CHCl_3$ or CH_2Cl_2 sample solutions containing 10-15% deuterated solvent. ^{1}H and $^{13}C\{^1H\}$ NMR spectroscopy are well established techniques and therefore will not be discussed in detail here.

1.4.3.1 *$^{31}P\{^1H\}$ NMR Spectroscopy*[70,71]

The ^{31}P nucleus is 100% naturally abundant and with spin $I = \frac{1}{2}$ and a relative receptivity of 6.6×10^{-2} compared to ^{1}H, is an excellent nucleus for NMR spectroscopy. The observed chemical shift for a PR_3 ligand is largely governed by the nature of the substituents R; electron rich R results in low frequency shifts, whereas electron withdrawing R gives rise to high frequency shifts. Similarly, on coordination to a metal centre, the dominating σ-donation of electrons away from the phosphine donor deshields the ^{31}P nucleus and results in a shift to higher frequency. This is known as the coordination shift (Δ), and is particularly significant for multidentate phosphines where chelate rings are formed on coordination to a metal centre. For these chelate rings, the observed shift has two components; the frequency shift due to the coordination of the two donor atoms (Δ_{donor}), and an additional contribution defined as the chelate-ring parameter (Δ_{ring}):

$$\Delta_{chelate} = \Delta_{donor} + \Delta_{ring}$$

The size of Δ_{ring} is dependent on the size of the chelate ring.[72] Generally, for 5-membered chelate rings, Δ_{ring} is large and positive, for 4- and 6-membered it is small and negative and is neglible for larger ring sizes. This is well illustrated in the series *cis*-$[PtMe_2\{Ph_2P(CH_2)_nPPh_2\}]$, where Δ_{ring} values −52.2, +24.1, −14.1 and −0.7 are observed for n = 1 to 4 and hence chelate ring sizes four to seven, respectively.[72]

1.4.3.2 $^{77}Se\{^{1}H\}$ *NMR Spectroscopy*[70,71]

Selenium has six naturally occurring isotopes, of which ^{77}Se, with natural abundance 7.6%, spin I = ½ and relative receptivity 5.26 x 10^{-4} compared to ^{1}H, is most suitable for NMR spectroscopy. While the abundance and receptivity appear low, they compare well in relation to ^{13}C, suggesting ^{77}Se is an accessible nucleus for NMR spectroscopy. However, long relaxation times necessitate slow pulse rates or the addition of a relaxation agent such as $Cr(acac)_3$, and therefore in practice, ^{77}Se is more difficult to observe than ^{13}C. As for ^{31}P, coordination of selenoether ligands to a metal centre through σ-donation deshields the ^{77}Se nuclei and the observed coordination shift is usually to high frequency.

1.4.3.3 ^{55}*Mn NMR Spectroscopy*[70,71]

The 100% abundance of ^{55}Mn and the relatively high receptivity of 0.175 compared with ^{1}H means the collection of ^{55}Mn NMR spectra is reasonably straightforward. However, ^{55}Mn nuclei have spin I = $^{5}/_{2}$ and a moderate quadrupolar moment Q = 0.55 x 10^{-28} m^{2}. Therefore, for complexes with less than octahedral (O_h) or tetrahedral (T_d) symmetry, the large electric field gradient generated by the quadrupole is expected to considerably broaden any ^{55}Mn resonances. For example, the C_{3v} cation $[Mn(CO)_3([9]aneS_3)]^+$ ($[9]aneS_3$ = 1,4,7-trithiacyclononance) gives a remarkably sharp ^{55}Mn resonance with half-height width $w_{½}$ = 120 Hz. However, on decreasing the symmetry to C_{2v} in $[Mn(CO)_3\{MeS(CH_2)_2S(CH_2)_2SMe\}]^+$ by using the equivalent open chain ligand, the observed ^{55}Mn resonance is considerably broadened, $w_{½}$ = 3500 Hz.[73] The significance of this broadening is reduced slightly due to the large chemical shift range of –3000 to +490 ppm observed for manganese adducts.

1.4.4 Single Crystal X-Ray Diffraction

The data for the single crystal X-ray diffraction studies were routinely collected on either a Rigaku AFC7S four-circle diffractometer or an Enraf-Nonius Kappa CCD diffractometer. The resulting reflections were sorted and the quality of data was gauged from the percentage of expected reflections that were observed. Also, comparison of data for equivalent reflections allows calculation of an internal residual factor R_{int}, with values less than 0.1 typically representative of a good data set.

The structures were solved using either direct methods[74] or Patterson synthesis[75] methods; the latter most suitable for structures containing heavy atoms, while the former can be used for all structures. For the coordination complexes studied here, the involvement of a transition metal justifies the use of Patterson synthesis, however in some cases both methods may have been attempted to gain the best structure solution. Also, the presence of heavy atoms necessitates the application of absorption corrections. Therefore, for the Rigaku data, psi-scans[76] were routinely recorded during data collection and for the Nonius data, absorption was calculated by comparison of symmetry equivalent reflections using SORTAV software.[77]

The resulting solutions were then refined using iterative cycles of full-matrix least-squares refinements[78] that attempt to minimise the difference between the Fourier transforms of the structure solution and the observed data. From this, a number of residual factors can be calculated to gauge the quality of the structure solution, including the R-factor (R) and the weighted R-factor (R_w). Again, values less than 0.1 typically represent a good structure solution. Another commonly quoted ratio is the number of observed reflections per parameter refined. Generally a reflection: parameter ratio of at least 8 is required for a satisfactory solution, though slightly lower values may be acceptable for high symmetry complexes. The reflection:parameter difference is also accounted for in the goodness of fit (*GOF*), which is a standardised comparison with optimal value equal to 1.

1.5 Overall Aims

The aims of this study were to investigate a selection of hard acid/soft base interactions, with a view to establish the influence of donor atom and ligand architecture on interaction stability. As an introduction to soft donor coordination chemistry, the ability of thioether macrocycles to stabilise Mn(I) centres has been studied. For manganese carbonyl adducts, soft donor coordination requires the removal of electron withdrawing carbonyl ligands, with the associated increase in electron density at Mn(I) destabilising the metal centre. Therefore, while coordination of high denticity thioether ligands is not expected due to the poor π-backbonding properties of the donor, this may be achieved *via* choice of ligand architecture, in this case by macrocyclic stabilisation.

To investigate hard/soft interactions, this study has concentrated on the chemistry of some of the hardest known metal centres, the d^0 M^{4+} cations of Group 4 ($M = Ti$, Zr, Hf). Using the halide precursors MX_4 ($X = Cl$, Br, I), the synthesis of a range of coordination complexes has been attempted using a variety of soft donor ligands from Groups 15 and 16. The metal-ligand interaction is expected to be weak and susceptible to dissociation in the presence of hard donors, hence the adducts are likely to be moisture sensitive. The stability of the interaction has been studied by numerous spectroscopic methods, with multinuclear NMR utilised to study the presence of dynamic processes in solution and therefore determine the relative acceptor and donor properties of MX_4 and the soft ligands. Single crystal X-ray diffraction studies have been employed to establish the influence of different ligand architectures on the coordination number and geometry observed at the metal centre.

Some of the Group 4 coordination complexes attempted within are potentially single source precursors to metal-chalcogenide materials used for various electronic applications. The formation of these materials *via* controlled thermal decomposition of the complexes has been discussed briefly.

1.6 References

[1] G. N. Lewis, *J. Am. Chem. Soc.*, 1913, **35**, 1448.

[2] S. Ahrland, J. Chatt, N. R. Davies, *Q. Rev. Chem. Soc.*, 1958, **12**, 265.

[3] R. G. Pearson, *J. Chem. Educ.*, 1968, **45**, 581 and 643.

[4] N. R. Champness, S. J. A. Pope, G. Reid, *J. Chem. Soc., Dalton Trans.*, 1997, 1639.

[5] S. C. Davies, M. C. Durrant, D. L. Hughes, C. Le Floc'h, S. J. A. Pope, G. Reid, R. L. Richards, J. R. Sanders, *J. Chem. Soc., Dalton Trans.*, 1998, 2191.

[6] R. J. H. Clark, in *Comprehensive Inorganic Chemistry*, J. C. Bailar, Jr., H. J. Emeleus, R. S. Nyholm, A. F. Trotman-Dickenson (eds.), Pergamon Press, Oxford, 1973, Vol. 3, Chapter 32.

[7] R. J. H. Clark, *The Chemistry of Titanium and Vanadium*, Elsevier, Amsterdam, 1968.

[8] D. S. Barratt, C. A. McAuliffe, in *Comprehensive Coordination Chemistry*, R. D. Gillard, J. A. McCleverty, G. Wilkinson (eds.), Pergamon Press, Oxford, 1987, Vol. 3, Chapter 31.

[9] D. L. Kepert, *The Early Transition Metals*, Academic Press, London, 1972.

[10] C. D. Garner, S. C. Wallwork, *J. Chem. Soc. (A)*, 1966, 1496.

[11] E. L. Muetterties, C. M. Wright, *J. Am. Chem. Soc.*, 1965, **87**, 4706.

[12] M. F. Lappert, *J. Chem. Soc.*, 1962, 542.

[13] R. J. H. Clark, W. Errington, J. Lewis, R. S. Nyholm, *J. Chem. Soc. (A)*, 1966, 989.

[14] R. C. Fay, in *Comprehensive Coordination Chemistry*, R. D. Gillard, J. A. McCleverty, G. Wilkinson (eds.), Pergamon Press, Oxford, 1987, Vol. 3, Chapter 32.

[15] D. C. Bradley, P. Thornton, in *Comprehensive Inorganic Chemistry*, J. C. Bailar, Jr., H. J. Emeleus, R. S. Nyholm, A. F. Trotman-Dickenson (eds.), Pergamon Press, Oxford, 1973, Vol. 3, Chapter 33.

[16] D. C. Bradley, M. H. Gitlitz, *J. Chem. Soc. (A)*, 1969, 1152.

[17] F. M. Chung, A. D. Westland, *Can. J. Chem.*, 1969, **47**, 195.

[18] A. W. Hofmann, *Justus Liebigs Annln Chem.*, 1857, **103**, 357.

[19] A. Cahours, H. Gal, *C. R. Hebd. Séanc. Acad. Sci., Paris*, 1870, **71**, 208.

[20] F. H. Jardine, J. A. Osborn, G. Wilkinson, J. F. Young, *J. Chem. Soc.*, 1966; 1711.

[21] A. M. Aguiar, D. Daigle, *J. Org. Chem.*, 1964, **29**, 1660.

[22] G. R. Van Hecke, W. deW. Horrocks, *Inorg. Chem.*, 1966, **5**, 1960.

[23] W. Lange, A. Tzschach, *Chem. Ber.*, 1962, **95**, 1360.

[24] A. M. Aguiar, H. J. Aguiar, T. G. Archibald, J. T. Mague, B. Preiean, *J. Org. Chem.*, 1968, **33**, 1681.

[25] P. Beck, L. Horner, V. G. Toscano, *Chem. Ber.*, 1961, **94**, 2122.

[26] H. C. E. McFarlane, W. McFarlane, *Polyhedron*, 1983, **2**, 303.

[27] R. J. H. Clark, R. H. U. Negrotti, R. S. Nyholm, *J. Chem. Soc., Chem. Commun.*, 1966, 468.

[28] R. L. Harris, E. P. Kyba, S.-T. Lui, *Organometallics*, 1983, **2**, 1877.

[29] R. D. Feltham, W. Silverthorn, *Inorg. Synth.*, 1967, **10**, 159.

[30] R. D. Feltham, A. Kasenally, R. S. Nyholm, *J. Organomet. Chem.*, 1967, **7**, 285.

[31] R. G. Cunningham, R. S. Nyholm, M. L. Tobe, *J. Chem. Soc.*, 1964, 580.

[32] J. Chatt, *Nature*, 1950, **165**, 637.

[33] N. G. Connelly, A. G. Orpen, *J. Chem. Soc., Chem. Commun.*, 1985, 1310.

[34] A. M. Arif, R. Hoffmann, C. Janiak, N. Kuhn, A. L. Rheingold, H. Schumann, *Inorg. Chem.*, 1991, **30**, 1618.

[35] C. A. Tolman, *J. Am. Chem. Soc.*, 1970, **92**, 2956.

[36] J. D. Oliver, J. D. Smith, *Inorg. Chem.*, 1978, **17**, 2585.

[37] M. S. Whittingham, *Prog. Solid State Chem.*, 1978, **12**, 41.

[38] F. R. Hartley, W. Levason, C. A. McAuliffe, S. G. Murray, H. E. Soutter, *Inorg. Chim. Acta*, 1979, **35**, 265.

[39] T. Kemmitt, W. Levason, *Organometallics*, 1989, **8**, 1303.

[40] D. J. Gulliver, E. G. Hope, W. Levason, G. L. Marshall, S. G. Murray, D. M. Potter, *J. Chem. Soc., Perkin Trans. II*, 1984, 429.

[41] E. G. Hope, T. Kemmitt, W. Levason, *J. Chem. Soc., Perkin Trans.*, 1987, 487.

[42] R. Ali, S. J. Higgins, W. Levason, *Inorg. Chim. Acta.*, 1984, **84**, 65.

[43] D. J. Gulliver, E. G. Hope, W. Levason, S. G. Murray, D. M. Potter, G. L. Marshall, *J. Chem. Soc., Perkin Trans., II*, 1984, 429.

[44] C-P. Mak, J. D. Michna, L. A. Ochrymowycz, *J. Org. Chem.*, 1974, **39**, 2079.

[45] D. Sellmann, L. Zapf, *Angew. Chem. Int. Ed. Engl.*, 1984, **23**, 807.

[46] D. Sellmann, L. Zapf, *J. Organomet. Chem.*, 1985, **289**, 57.

[47] D. L. Sales, J. Stokes, P. Woodward, *J. Chem. Soc. A*, 1968, 1852.

[48] E. N. Baker, N. G. Larsen, *J. Chem. Soc., Dalton Trans.*, 1976, 1769.

[49] P. J. Blower, G. E. D. Mullen, A. K. Powell, M. J. Went, S. Wocadlo, *Angew. Chem.*, 1997, **36**, 1205.

[50] P. M. Boorman, H. Jacobsen, H-B. Kraatz, T. Ziegler, *Organometallics*, 1993, **12**, 76.

[51] W. Levason, S. D. Orchard, G. Reid, *Organometallics*, 1999, **18**, 1275.

[52] W. Levason, S. D. Orchard, G. Reid, *J. Chem. Soc., Dalton Trans.*, 1999, 823.

[53] E. W. Abel, M. Booth, K. G. Orrell, *J. Chem. Soc., Dalton Trans.*, 1980, 1582.

[54] E. W. Abel, S. K. Bhargava, K. G. Orrell, *Prog. Inorg. Chem.*, 1984, **32**, 1.

[55] E. W. Abel, R. P. Bush, F. J. Hopton, C. R. Jenkins, *J. Chem. Soc., Chem. Commun.*, 1966, 58.

[56] K. G. Orrell, *Coord. Chem. Rev.*, 1989, **96**, 1.

[57] R. J. Cross, T. H. Green, R. Keat, *J. Chem. Soc., Dalton Trans.*, 1976, 1150.

[58] E. W. Abel, S. K. Bhargava, K. Kite, K. G. Orrell, V. Sik, B. L. Williams, *J. Chem. Soc., Dalton Trans.*, 1982, 583.

[59] E. W. Abel, A. R. Khan, K. Kite, K. G. Orrell, V. Sik, *J. Chem. Soc., Dalton Trans.*, 1980, 1175.

[60] E. W. Abel, T. Kemmitt, W. Levason, K. G. Orrell, S. P. Scanlan, D. Stephenson, *J. Chem. Soc., Dalton Trans.*, 1991, 591.

[61] E. W. Abel, S. K. Bhargava, K. Kite, K. G. Orrell, V. Sik, B. L. Williams, *Polyhedron*, 1982, **1**, 289.

[62] P. Haake, P. C. Turley, *J. Am. Chem. Soc.*, 1967, **89**, 4617.

[63] L. F. Lindoy, *The Chemistry of Macrocyclic Ligand Complexes*, Cambridge University Press, 1989.

[64] D. K. Cabbiness, D. W. Margerum, *J. Am. Chem. Soc.*, 1969, **91**, 6540.

[65] M. Micheloni, P. Peoletti, A. Sabatini, *J. Chem. Soc., Dalton Trans.*, 1983, 1189.

[66] I. R. Beattie, M. Webster, *J. Chem. Soc.*, 1964, 3507.

[67] A. B. P. Lever, *Inorganic Electronic Spectroscopy*, 2nd Edition, Elsevier, 1984.

[68] See P. W. Atkins, C. H. Langford, D. F. Shriver, *Inorganic Chemistry*, 2nd Edition, Oxford University Press, 1994, Chapter14.

[69] L. Pauling, *The Chemical Bond*, Oxford University Press, 1967.

[70] *Multinuclear NMR*, J. Mason (Editor), Plenum, New York, 1987.

[71] *NMR and the Periodic Table*, R. K. Harris, B. E. Mann (Editors), Academic Press, London, 1978.

[72] P. E. Garrou, *Chem. Rev.*, 1981, **81**, 229.

[73] J. Connolly, A. R. J. Genge, W. Levason, S. D. Orchard, S. J. A. Pope, G. Reid, *J. Chem. Soc., Dalton Trans.*, 1999, 2343.

[74] SHELXS-86, G. M. Sheldrick, *Acta Crystallogr., Sect. A*, 1990, **46**, 467.

[75] PATTY, The DIRDIF Program System, G. Admiraal, G. Beurskens, P. T. Beurskens, W. P. Bosman, S. Garcia-Granda, R. O. Gould, J. M. M. Smits, C. Smykallá, Technical Report of the Crystallography Laboratory, University of Nijmegen, 1992.

[76] F. S. Matthews, A. C. T. North, D. C. Phillips, *Acta Crystallogr., Sect. A*, 1968, **24**, 351.

[77] SORTAV, R. H. Blessing, *Acta Crystallogr., Sect. A*, 1995, **51**, 33.

[78] TeXsan, Crystal Structure Analysis Package, Molecular Structure Corporation, Houston, Texas, 1995.

Chapter 2

Stabilisation of Mn(I) Carbonyls by Thioether Macrocycles

2.1 Introduction

Unlike most other transition metals, the organometallic chemistry of manganese does not have an extensive history. Unconfirmed reports of phenylmanganese species date from 1937,[1,2] however it was over a decade later before dimanganese decacarbonyl, $[Mn_2(CO)_{10}]$, was isolated in 1949,[3] and subsequently characterised in 1954[4] as the first substantiated organomanganese compound. Significantly, this post-dated the discovery of ferrocene and hence much of the early work in organomanganese chemistry concentrated on the development of analogues to ferrocene derivatives.[5,6,7,8]

Other significant early discoveries include the *in situ* synthesis of $Na[Mn(CO)_5]$ and the carbonylation of MnI_2 to $[Mn(CO)_5I]$, with both pentacarbonyl adducts serving as important precursors to Mn^{-1} and Mn^{I} carbonyl complexes, respectively.[4] $[Mn(CO)_5Cl]$ and $[Mn(CO)_5Br]$ were subsequently prepared in 1959 through cleavage of the metal-metal bond in $[Mn_2(CO)_{10}]$ by the respective halogen,[9] and the accessibility of these manganese pentacarbonyl halides has led to their extensive use as synthetic precursors to a range of organomanganese compounds.[10,11]

Manganese in organometallic chemistry generally assumes the formal oxidation states −1, 0 or +1. Of these, Mn(I) is of particular interest due to the stability of the $3d^6$ electronic configuration presenting the basis for low-spin, kinetically inert, diamagnetic, octahedral complexes. However, such a low oxidation state requires the presence of π-acceptor ligands to reduce the high electron density associated with the manganese centre. Despite this, the ν(CO) stretching frequency of 2090 cm^{-1} for the parent Mn(I) carbonyl cation, $[Mn(CO)_6]^+$, (in THF) shows only a small deviation to that of free carbon monoxide at 2143 cm^{-1}. This suggests only a small extent of π-bonding between metal and ligand, in contrast to the strong π-bonding observed in the isoelectronic adducts $[Cr(CO)_6]$ and $[V(CO)_6]^-$, with respective ν(CO) frequencies 1996 cm^{-1} (in CCl_4) and 1859 cm^{-1} (in THF).[12]

The weak π-bonding observed for Mn(I) carbonyls presents the opportunity for substitution reactions *via* dissociation of carbonyl ligands. A large variety of complexes involving group 15 ligands have been synthesised this way, with carbonyl cations ranging from pentacarbonyl $[Mn(CO)_5L]^+$ adducts to monocarbonyl $[Mn(CO)(L)_5]^+$ species for phosphine ligands.[10,11] Indeed, the strongly π-backbonding phosphine ligands are also known to stabilise homoleptic Mn(I)-phosphine complexes.[13] Thus, $[Mn(dmpe)_3]^+$ [dmpe = 1,2-bis(dimethylphosphino)ethane] is synthesised *via* reaction of $[(syn\text{-}\eta^3\text{-pentadienyl})Mn(dmpe)_2]$ with dmpe and NH_4PF_6. Similar reaction in the presence of the trimethyl phosphite affords $[Mn(dmpe)_2\{P(OMe)_3\}_2]^+$, with the coordination sites vacated by the pentadienyl ligand now accommodated by the stronger π-acceptor phosphite ligand.

Until recently, complexes involving group 16 ligands have been much less studied, with work undertaken within this research group at Southampton addressing this situation over the last few years. Thus, a series of tricarbonyl complexes of the form *fac*-$[MnX(CO)_3(L_2)]$ (X = Cl, Br, I)[14,15,16] and *fac*-$[Mn(CO)_3(L_3)]^+$ [17,18,19] have been synthesised involving bi- and tri-dentate thio-, seleno- and telluro-ether ligands, respectively. Detailed multinuclear (^1H, $^{13}C\{^1H\}$, $^{77}Se\{^1H\}$, $^{125}Te\{^1H\}$ and ^{55}Mn) NMR spectroscopy, X-ray crystal structure determinations and IR ν(CO) frequency analyses have shown increasing σ-donation along the series $S < Se \ll Te$.

Of particular interest to this study are the cationic carbonyl thioether complexes *fac*-$[Mn(CO)_3(L_3)]^+$ for $L_3 = MeS(CH_2)_2S(CH_2)_2SMe$, $MeC(CH_2SMe)_3$ and $[10]aneS_3$ (1,4,7-trithiacyclododecane);[19] and *fac*-$[Mn(CO)_3([9]aneS_3)]^+$ ($[9]aneS_3$ = 1,4,7-trithiacyclononane) reported elsewhere.[20] The latter two complexes represent the only known Mn(I) macrocyclic thioether complexes and there are no reported examples with thioether ligands of higher denticity. However, coordination of the tetraselena macrocycle $[16]aneSe_4$ (1,5,9,13-tetraselenacyclohexadecane) with Mn(I) has been reported,[18] affording *fac*-$[Mn(CO)_3(\eta^3\text{-}[16]aneSe_4)]^+$. Attempts to complete macrocyclic coordination *via* decarbonylation provided limited spectroscopic data consistent with forming the dicarbonyl species *cis*-$[Mn(CO)_2(\eta^4\text{-}[16]aneSe_4)]^+$. However, difficulties encountered in isolating a pure sample of the unstable product prevented full characterisation of the dicarbonyl adduct.

This chapter investigates the coordination chemistry of macrocyclic thioether ligands of high denticity with the Mn(I) centre. Reported within is the synthesis and spectroscopic characterisation of a series of Mn(I) tricarbonyl cationic complexes of the form *fac*-$[Mn(CO)_3(\eta^3\text{-}L)][CF_3SO_3]$, incorporating the tetrathia- and pentathia-macrocyclic ligands, L = [12]-, [14]-, $[16]\text{-}aneS_4$ and $[15]aneS_5$ ($[12]aneS_4$ = 1,4,7,10-tetrathiacyclododecane, $[14]aneS_4$ = 1,4,8,11-tetrathiacyclotetradecane, $[16]aneS_4$ =

1,5,9,13-tetrathiacyclohexadecane, [15]aneS_5 = 1,4,7,10,13-pentathiacyclopentadecane). The subsequent decarbonylation of these complexes is investigated to afford the first characterised series of Mn(I) dicarbonyl cationic complexes incorporating thioether ligands, *cis*-$[Mn(CO)_2(\eta^4\text{-L})][CF_3SO_3]$.[21] The complexes are characterised by elemental analysis, IR and multinuclear (^1H, $^{13}C\{^1H\}$, ^{55}Mn) NMR spectroscopy, and electrospray mass spectrometry. Single crystal X-ray structure determinations are also reported for the complexes *fac*-$[Mn(CO)_3(\eta^3\text{-L})][CF_3SO_3]$ (L = [12]aneS_4, [15]aneS_5) and *cis*-$[Mn(CO)_2(\eta^4\text{-L})][CF_3SO_3]$ (L = [12]-, [16]-aneS_4, [15]aneS_5), to authenticate the geometry around the Mn(I) centre and to permit discussion on the consequences of increasing thioether coordination for the [12]aneS_4 and [15]aneS_5 complexes.

The only other reported examples of Mn(I) dicarbonyl cations incorporating the electron rich $[Mn(CO)_2]^+$ fragment involve strongly π-backbonding phosphine and phosphite ligands. Examples include both *cis*- and *trans*-$[Mn(CO)_2(L')_4]^+$ complexes for L′ = $PHPh_2$,[22] $PPh(OMe)_2$ and $P(OMe)_3$.[23] The synthesis of these complexes utilises the precursor *fac*-$[Mn(CO)_3(Me_2CO)_3]ClO_4$, formed *via* reaction of $[Mn(CO)_5Br]$ and $Ag[ClO_4]$ in acetone. Reaction of the precursor with phosphite ligands affords *cis*-dicarbonyl adducts that isomerise to the *trans*-adducts on reflux.[23] Whereas, the less strong π-acceptor phosphine ligands displace only the acetone groups to afford *fac*-tricarbonyl adducts. Subsequent decarbonylation presents *cis*-dicarbonyl species on reaction with Me_3NO, or *trans*-dicarbonyl species *via* photolytic routes.[22] A similar synthetic route was employed in this work, with the poor π-bonding properties of thioether ligands affording only *fac*-tricarbonyl adducts on reaction with the *fac*-$[Mn(CO)_3(Me_2CO)_3]^+$ precursor. Although the larger of the macrocycles used here could accommodate the *trans*-dicarbonyl adduct on decarbonylation, the highly electron-rich Mn(I) centre would be insufficiently stabilised by *trans* carbonyl ligands competing for electron density. Thus, the complexes exhibit exclusively *cis*-dicarbonyl geometry at Mn(I) in order to maximise the Mn-CO $d_\pi \rightarrow p_\pi$ backbonding.

2.2 Results and Discussion

2.2.1 *Mn(I) Tricarbonyl Thioether Macrocycle Complexes*

Reaction of *fac*-$[Mn(CO)_3(Me_2CO)_3]CF_3SO_3$[23] with one molar equivalent of thioether macrocycle L (L = [12]-, [14]-, [16]-aneS_4 or [15]aneS_5) in degassed acetone at room temperature afforded golden yellow solutions of *fac*-$[Mn(CO)_3(\eta^3\text{-}L)]CF_3SO_3$ (Figure 2.1). Reaction vessels were wrapped with aluminium foil to exclude light and reaction progress was monitored by solution IR spectroscopy of the carbonyl region. Reaction completion was evident through loss of bands at 2022 and 1932 cm^{-1} due to *fac*-$[Mn(CO)_3(Me_2CO)_3]CF_3SO_3$, together with the appearance of two or three new carbonyl stretching bands corresponding to the tricarbonyl product.

Figure 2.1 Reaction scheme for the synthesis of *fac*-$[Mn(CO)_3(\eta^3\text{-}L)][CF_3SO_3$.

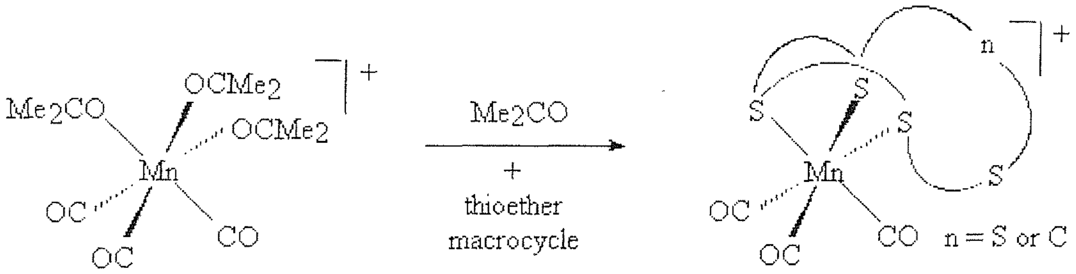

***fac*-$[Mn(CO)_3(Me_2CO)_3]CF_3SO_3$** ***fac*-$[Mn(CO)_3(\eta^3\text{-}L)]CF_3SO_3$**

The complexes were isolated as yellow solids by removal of Me_2CO *in vacuo*, dissolution of the residual yellow oils in $CHCl_3$ and precipitation with light petroleum ether (40-60°C). The solids showed a tendency to form oils on filtration, though washing with copious volumes of light petroleum ether gave air stable solids for L = [12]-, [14]-aneS_4 and [15]aneS_5. However, isolation of pure *fac*-$[Mn(CO)_3(\eta^3\text{-}[16]aneS_4)]CF_3SO_3$ proved unsuccessful and only limited characterisation was permissible using the residual orange oil formed on removal of solvent. Microanalytical data obtained for the isolated solids confirmed the formulation as $[Mn(CO)_3(L)]$-CF_3SO_3. Electrospray mass spectrometry showed the parent cation $[Mn(CO)_3(L)]^+$ as the most intense peak together with fragment peaks corresponding to loss of carbonyl ligands at much lower intensity (Figure 2.2).

Figure 2.2 Electrospray mass spectrum for *fac*-[Mn(CO)$_3$(η^3-[14]aneS$_4$)]$^+$ (MeCN).

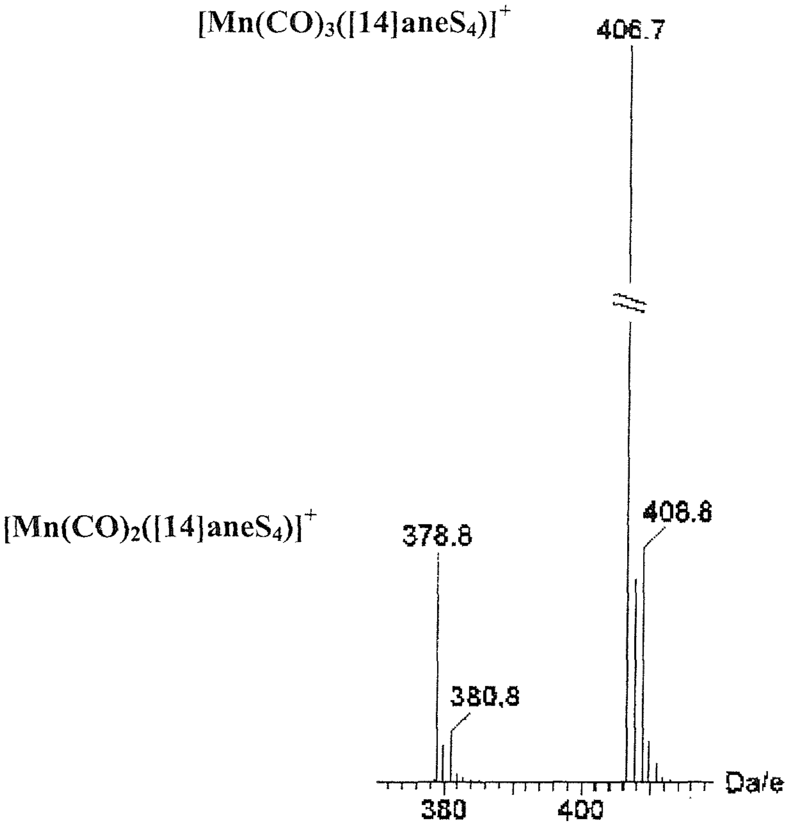

Solution IR spectroscopy (Me$_2$CO) of [Mn(CO)$_3$(η^3-[12]aneS$_4$)]$^+$ and [Mn(CO)$_3$-(η^3-[14]aneS$_4$)]$^+$ showed three stretching vibrations, (2A′ + A″), consistent with *fac*-tricarbonyl species with C$_s$ symmetry. This low symmetry can be attributed to the η^3-coordination of the macrocyclic rings presenting large chelate rings involving the uncoordinated donor atoms, thus precluding C$_3$ symmetry (Figure 2.3). However, the spectra for [Mn(CO)$_3$(η^3-[16]aneS$_4$)]$^+$ and [Mn(CO)$_3$(η^3-[15]aneS$_5$)]$^+$ showed only two carbonyl stretching vibrations in this region. This may be due to the polar Me$_2$CO medium in which the spectra were recorded resulting in broadening of the bands and preventing sufficient resolution of the carbonyl bands. Indeed, the spectra of these species did show broad bands and hence CsI disk IR spectroscopy was undertaken to provide greater resolution of the stretching frequencies. Thus, the spectra of [Mn(CO)$_3$(η^3-[12]aneS$_4$)]$^+$ and [Mn(CO)$_3$(η^3-[14]aneS$_4$)]$^+$ showed sharp bands (Figure 2.4), while the spectrum of [Mn(CO)$_3$(η^3-[15]aneS$_5$)]$^+$ revealed the splitting of the broad low frequency band observed in solution. While similar analysis was not possible for [Mn(CO)$_3$(η^3-[16]aneS$_4$)]$^+$, these results suggest the adducts exhibit C$_s$ symmetry.

Figure 2.3 C_s symmetry about the Mn(I) centre in *fac*-[$Mn(CO)_3(\eta^3$-L)]CF_3SO_3.

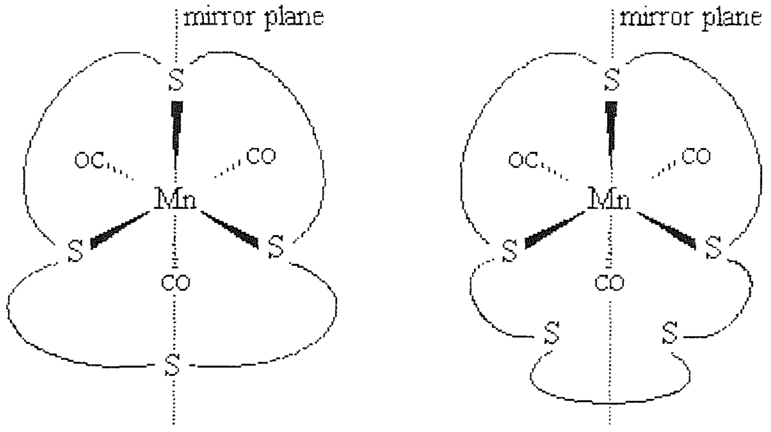

L = [12]-, [16]-aneS$_4$ **L = [15]aneS$_5$**

The observed carbonyl stretching frequencies (Table 2.1) compare well with other cationic Mn(I) tricarbonyl thioether complexes reported in the literature.[14,19,20] Notable examples are *fac*-[$Mn(CO)_3\{MeC(CH_2SMe)_3\}]CF_3SO_3$ (2048, 1968 cm^{-1} in $CHCl_3$) and *fac*-[$Mn(CO)_3\{MeS(CH_2)_2S(CH_2)_2SMe\}]CF_3SO_3$ (2047, 1968 cm^{-1} in Me_2CO).[19] Both complexes involve η^3-coordination of the thioether and form 6- and 5-membered chelate rings respectively. The observed bands showed the expected shift to low frequency compared with the parent Mn(I) cation [$Mn(CO)_6]^+$, due to the poor π-backbonding capacity of thioethers promoting strong π-backbonding into the C-O antibonding orbitals.

Table 2.1 Carbonyl stretching vibrations for *fac*-[$Mn(CO)_3(\eta^3$-L)]CF_3SO_3.

Complex	ν(CO) / cm^{-1} (CsI disk)	
	A′	A′ + A″
fac-[$Mn(CO)_3([12]aneS_4)]CF_3SO_3$	2061	1973, 1951
fac-[$Mn(CO)_3([14]aneS_4)]CF_3SO_3$	2042	1966, 1953
fac-[$Mn(CO)_3([16]aneS_4)]CF_3SO_3$ [a]	2042	1954(br)
fac-[$Mn(CO)_3([15]aneS_5)]CF_3SO_3$	2047	1974, 1951

[a] Solution IR spectroscopy data (Me_2CO)

Figure 2.4 Carbonyl region of $[Mn(CO)_3(\eta^3\text{-}[12]aneS_4)]^+$ IR spectrum (CsI disk)

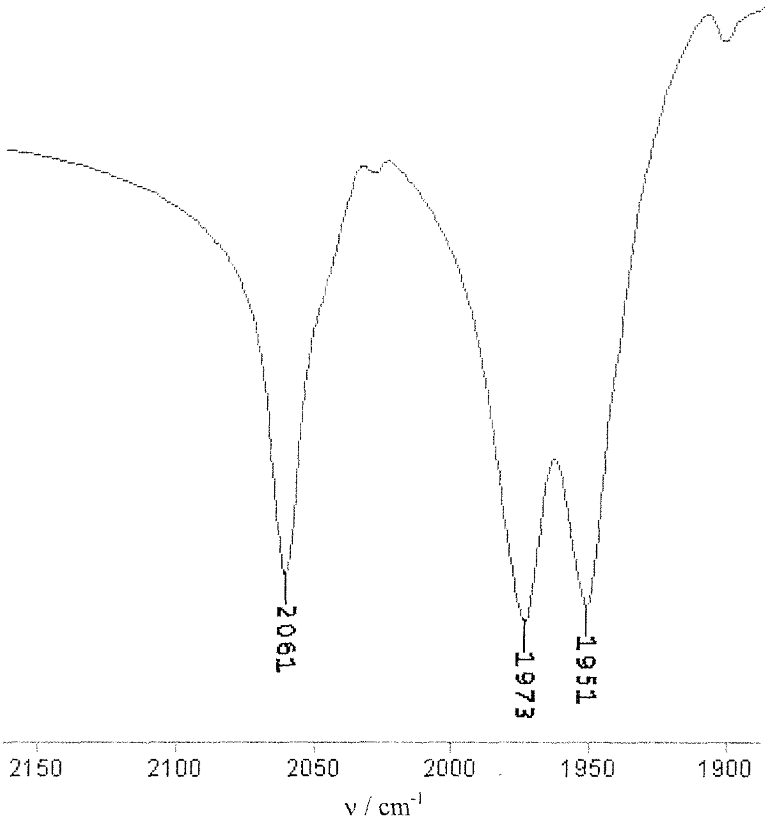

2.2.1.1 Multinuclear NMR Spectroscopy

As discussed in Chapter 1, coordination of chelating bidentate thioether ligands to metal centres leads to chirality at S, with pyramidal inversion giving rise to diastereoisomers (invertomers); two equivalent *meso* forms and a *DL* enantiomeric pair. In the case of the η^3-thioether macrocycles involved here, there are a number of possible invertomers as each coordinated thioether donor is capable of inverting independently. The nature of non-equivalent invertomers can be identified by multinuclear NMR spectroscopy, providing pyramidal inversion is slow on the NMR time-scale.

Other Mn(I) carbonyl complexes involving acyclic thioether ligands have shown inversion at S-donors to be close to the rapid inversion high-temperature limit at room temperature.[14,19] Thus, $[Mn(CO)_3\{MeC(CH_2SMe)_3\}]CF_3SO_3$ and $[MnX(CO)_3\text{-}\{MeS(CH_2)_3SMe\}]$ exhibit fast inversion, whereas $[MnX(CO)_3\{MeS(CH_2)_2SMe\}]$ (X =

Cl, Br, I) display slower inversion at room temperature and show the presence of invertomers. The constraints of the macrocyclic ring in the thioethers studied here will increase the energy barrier to inversion and present, in most cases, one invertomer at room temperature. Hence, multinuclear (^{1}H, ^{13}C{^{1}H}, ^{55}Mn) NMR spectroscopy has been employed to establish the properties of the invertomers formed for *fac*-[Mn(CO)$_3$-(η^3-L)]CF$_3$SO$_3$. Only ^{55}Mn NMR spectroscopy was possible for the reaction mixture residue of *fac*-[Mn(CO)$_3$(η^3-[16]aneS$_4$)]CF$_3$SO$_3$.

^{13}C{^{1}H} NMR spectroscopy proved the most informative of the NMR active nuclei available for investigating the nature of the invertomers formed. The spectrum for *fac*-[Mn(CO)$_3$(η^3-[12]aneS$_4$)]$^+$ showed three broad resonances in the methylene region, δ 30.7, 36.3 and 38.2, with approximate intensities 1:2:1. Such equivalence of carbon environments may be attributed to the presence of mirror plane symmetry, as shown in Figure 2.5a. Thus, the resonances reveal increasing shifts to high frequency from carbons adjacent to the uncoordinated donor (δ 30.7, **d**) to carbons adjacent to the donor involved in two 5-membered chelate rings (δ 38.2, **a**). The four carbons surrounding the remaining coordinating donor atoms are approximately equivalent and intermediate in frequency (δ 36.3, **b** ≈ **c**).

Figure 2.5 Representations of invertomers observed in ^{13}C{^{1}H} NMR spectroscopy of *fac*-[Mn(CO)$_3$(η^3-L)]CF$_3$SO$_3$ for L = a) [12]aneS$_4$, b) [15]aneS$_5$.

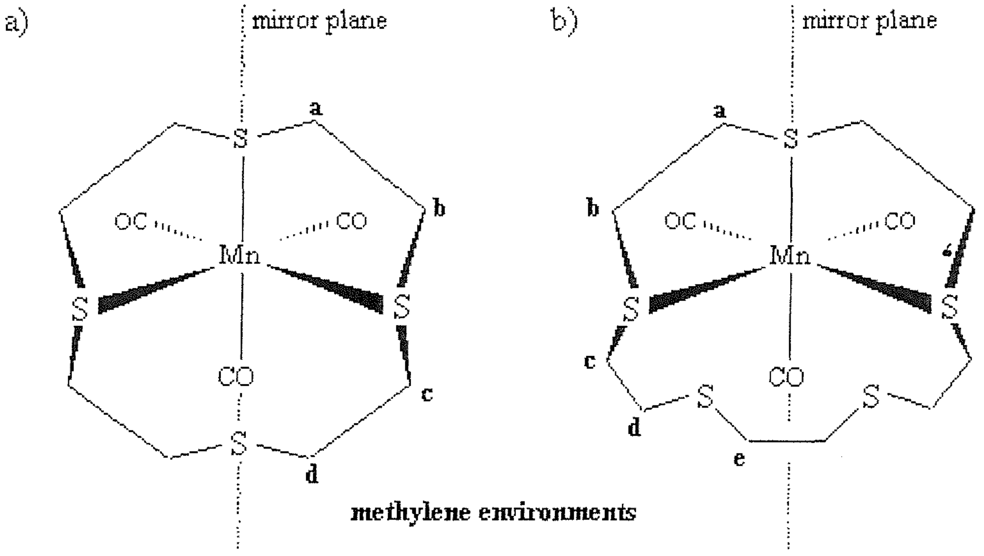

Likewise, the $^{13}C\{^{1}H\}$ NMR spectrum for *fac*-$[Mn(CO)_3(\eta^3\text{-}[15]aneS_5)]^+$ (Figure 2.6) showed only four resonances in this region, δ 31.1, 33.7, 35.0 and 37.8, with approximate intensities 2:1:1:1. Again, the equivalence of carbon environments may be attributed to the presence of a mirror plane (Figure 2.6b). As for *fac*-$[Mn(CO)_3(\eta^3\text{-}[12]aneS_4)]^+$, the resonances reveal increasing shifts to high frequency from carbons adjacent to the uncoordinated donors (δ 31.1, **d** ≈ **e**) to carbons adjacent to the donor involved in two 5-membered chelate rings (δ 37.8, **a**). However, the four carbons surrounding the remaining coordinating donor atoms are now no longer approximately equivalent, presumably due to the larger 11-membered chelate ring containing the uncoordinated donor atoms. Hence, the carbon atoms involved in 5-membered chelate rings are shifted to slightly higher frequency (δ 35.0, **b**) than the large chelate ring carbons (δ 33.7, **c**).

Figure 2.6 $^{13}C\{^{1}H\}$ NMR spectrum of $[Mn(CO)_3([15]aneS_5)]^+$ (methylene region).

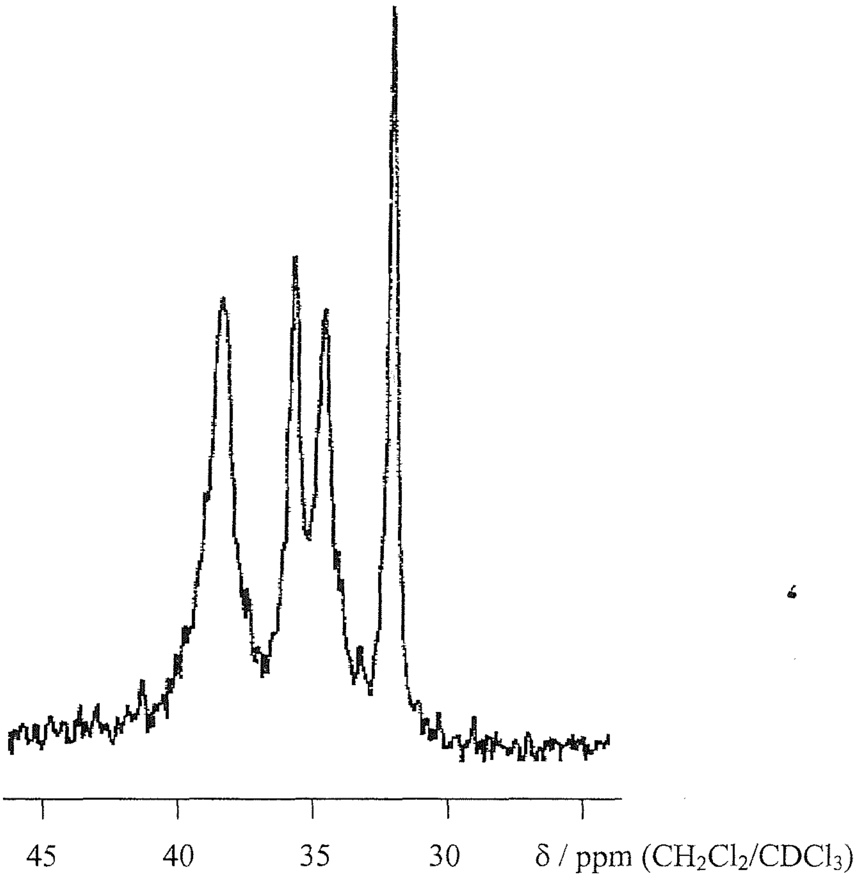

The spectrum for *fac*-[Mn(CO)$_3$(η^3-[14]aneS$_4$)]$^+$ was more complicated and showed six resonances, δ 24.4, 24.7, 27.4, 31.8, 36.2 and 36.4, with approximate intensities 1:1:2:2:2:2. This increase in complexity was expected as the asymmetry of η^3-coordinated [14]aneS$_4$ prevents equivalence of environments across a mirror plane, as above. Despite this, the trends in frequency shifts remain the same, with carbons involved in 5- or 6-membered chelate rings shifted to high frequency (δ 36.4, 36.2) and carbons adjacent to the uncoordinated donors least shifted to high frequency (δ 27.4) of the carbons adjacent to donor atoms. However, the propylene bridges in [14]aneS$_4$ present carbon environments isolated from thioether contact altogether, and hence even less shifted to high frequency (δ 24.4, 24.7).

The ^{13}C{^{1}H} NMR spectra also showed substantially broadened carbonyl resonances, with broadening attributed to the interaction with the directly bonded ^{55}Mn quadrupole. The data acquired were sufficient to define the carbonyl resonances for *fac*-[Mn(CO)$_3$(η^3-L)]$^+$, L = [12]aneS$_4$ (δ 214-219), [14]aneS$_4$ (δ 215-224) and [15]aneS$_5$ (δ 212-219). These values compare well with other cationic Mn(I) tricarbonyl thioether complexes reported in the literature,[14,19] notably with *fac*-[Mn(CO)$_3${MeC-(CH$_2$SMe)$_3$}]$^+$ (δ 214-217) and *fac*-[Mn(CO)$_3${MeS(CH$_2$)$_2$S(CH$_2$)$_2$SMe}]$^+$ (δ 212-220).

Also of note, the ^{13}C{^{1}H} NMR spectra of *fac*-[Mn(CO)$_3$(η^3-[12]aneS$_4$)]CF$_3$SO$_3$ and *fac*-[Mn(CO)$_3$(η^3-[14]aneS$_4$)]CF$_3$SO$_3$ showed several weak resonances in both carbonyl and methylene regions, later confirmed to be due to the dicarbonyl species, *cis*-[Mn(CO)$_2$(η^4-L)]CF$_3$SO$_3$ (Section 2.2.2.1). This spontaneous decarbonylation in solution can be attributed to the energetic stabilisation proffered by the macrocyclic effect *via* complete coordination of the tetrathia macrocycles. Consequently, *fac*-[Mn(CO)$_3$(η^3-[15]aneS$_5$)]CF$_3$SO$_3$ showed no such evidence of decarbonylation, as macrocyclic coordination is not completed in the dicarbonyl species.

Room temperature ^{1}H NMR spectroscopy proved rather uninformative as the resonances observed were considerably broadened by the ^{55}Mn quadrupole. Similar broadening has been observed for other Mn(I) carbonyl thioether complexes, where low temperature (200 K) spectra showed only a minimal sharpening of the resonances.[14] Although the broadening has prevented conclusive assignment of proton environments, the observed chemical shift ranges are as expected.

Work undertaken within this research group has shown the importance of ^{55}Mn NMR spectroscopy in investigating changes in electron density at the manganese centre.[14–19] The studies relating to thioether donors have shown that the manganese nucleus becomes less shielded as thioether coordination is changed from macrocyclic to acyclic.[18] Thus, the complexes *fac*-[Mn(CO)$_3$([9]aneS$_3$)]$^+$, *fac*-[Mn(CO)$_3$([10]aneS$_3$)]$^+$ and *fac*-[Mn(CO)$_3${MeS(CH$_2$)$_2$S(CH$_2$)$_2$SMe}]$^+$ show resonances at δ -963 (120), -764 (550) and -696 (3500), respectively [linewidths in parentheses (Hz)].

In *fac*-[Mn(CO)$_3$(η^3-L)]CF$_3$SO$_3$, the macrocyclic thioether ligand acts essentially as a chelating tridentate ligand. However, the constraints of the macrocyclic ring lead to strained metal-ligand interactions. The observed ^{55}Mn NMR spectra reflect this, with all complexes exhibiting resonances to high frequency of both the macrocyclic and acyclic coordinated examples above (Table 2.2). Indeed, only *fac*-[Mn(CO)$_3$(η^3-[15]aneS$_5$)]$^+$, with a large macrocyclic ring that can accommodate η^3-coordination with less strain, displays a ^{55}Mn resonance even comparable with *fac*-[Mn(CO)$_3${MeS(CH$_2$)$_2$-S(CH$_2$)$_2$SMe}]$^+$. The observed linewidths, ranging from 1700-3000 Hz, are moderately large, but comparable with the acyclic trithioether example above. The broadness can be attributed to the unsymmetrical nature of the η^3-macrocyclic coordination reducing the local symmetry at Mn(I) to C$_s$, and giving rise to a large electric field gradient.

Table 2.2 ^{55}Mn NMR data for selected Mn(I) tricarbonyl thioether complexes.

Complex	δ ^{55}Mn [a]	$w_{1/2}$ / Hz [a]
fac-[Mn(CO)$_3$([12]aneS$_4$)]CF$_3$SO$_3$	-334	3000
fac-[Mn(CO)$_3$([14]aneS$_4$)]CF$_3$SO$_3$	-471	1700
fac-[Mn(CO)$_3$([16]aneS$_4$)]CF$_3$SO$_3$	-276	3000
fac-[Mn(CO)$_3$([15]aneS$_5$)]CF$_3$SO$_3$	-658	2200
fac-[Mn(CO)$_3$([9]aneS$_3$)]Br [b,c]	-963	120
fac-[Mn(CO)$_3$([10]aneS$_3$)]Br [b,c]	-764	550
fac-[Mn(CO)$_3${MeS(CH$_2$)$_2$S(CH$_2$)$_2$SMe}]CF$_3$SO$_3$ [c]	-696	3500

[a] Spectra recorded in CH$_2$Cl$_2$/CDCl$_3$ unless otherwise stated; [b] In dmf; [c] Data taken from reference[19].

2.2.1.2 X-ray Crystallographic Studies

Previous work on Mn(I) trithioether tricarbonyl complexes include crystallographic studies on *fac*-$[Mn(CO)_3(L^3)]^+$, L^3 = [9]aneS_3,[20] [10]aneS_3, $MeC(CH_2SMe)_3$ and MeS-$(CH_2)S(CH_2)SMe$.[19] To allow comparison with these examples, single crystal X-ray diffraction studies were undertaken on two of the complexes formed here. Thus, single crystals of *fac*-$[Mn(CO)_3([12]aneS_4)]CF_3SO_3$ and *fac*-$[Mn(CO)_3([15]aneS_5)]CF_3SO_3$ were grown by vapour diffusion of diethyl ether into CH_2Cl_2 solutions of the adducts.

The structure of $[Mn(CO)_3([12]aneS_4)]^+$ (Figure 2.7, Tables 2.3, 2.4) shows the Mn(I) centre coordinated to three mutually *fac* carbonyl ligands and three thioether donors from the tetrathia macrocycle. The constraints within the small macrocyclic ring results in a distortion of the octahedral environment around Mn(I). Thus, S-Mn-S bond angles deviate from the expected 90°, with 5-membered chelating thioether bite angles contracted [87.10(3) and 86.47(2)°] and the 8-membered ring angle augmented [104.87(3)]. Such large distortion suggests the flexibility within the small macrocyclic ring is insufficient to alleviate strain associated with η^3-coordination.

Figure 2.7 View of the structure of *fac*-$[Mn(CO)_3([12]aneS_4)]^+$ with numbering scheme adopted. Ellipsoids drawn at 40%, H-atoms omitted for clarity.

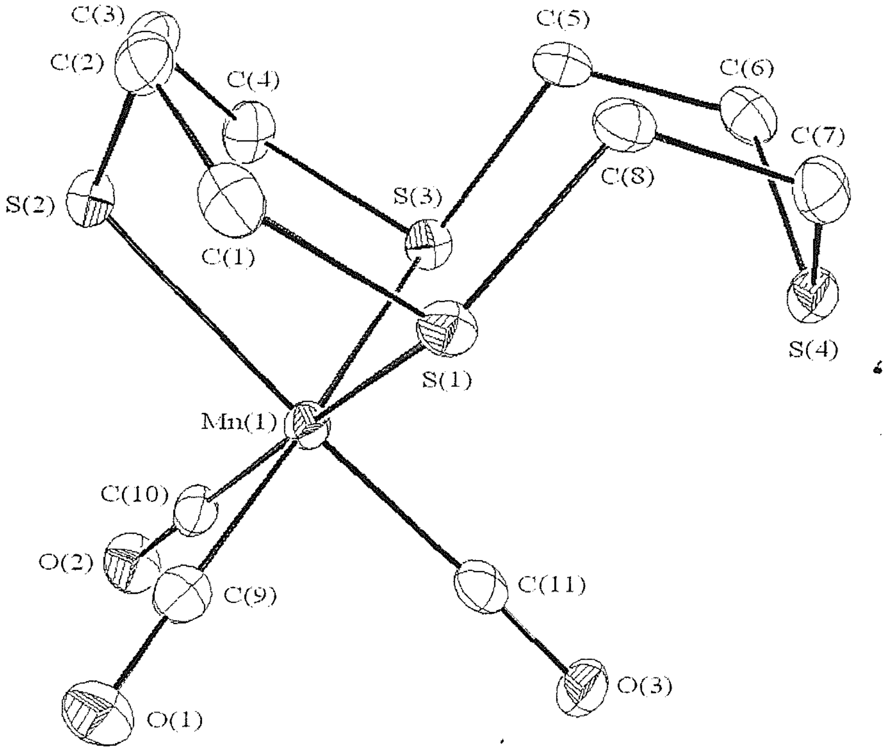

Table 2.3 Selected bond lengths for *fac*-$[Mn(CO)_3([12]aneS_4)]^+$.

Atom	Atom	Distance / Å	Atom	Atom	Distance / Å
Mn(1)	S(1)	2.3881(7)	Mn(1)	S(2)	2.3461(7)
Mn(1)	S(3)	2.3728(7)	Mn(1)	C(9)	1.809(3)
Mn(1)	C(10)	1.815(3)	Mn(1)	C(11)	1.837(3)
C(9)	O(1)	1.146(3)	C(10)	O(2)	1.147(3)
C(11)	O(3)	1.135(3)			

Table 2.4 Selected bond angles for *fac*-$[Mn(CO)_3([12]aneS_4)]^+$.

Atom	Atom	Atom	Angle / °	Atom	Atom	Atom	Angle / °
S(1)	Mn(1)	S(2)	87.10(3)	S(1)	Mn(1)	S(3)	104.87(3)
S(1)	Mn(1)	C(9)	82.76(8)	S(1)	Mn(1)	C(10)	170.65(8)
S(1)	Mn(1)	C(11)	91.84(8)	S(2)	Mn(1)	S(3)	86.47(2)
S(2)	Mn(1)	C(9)	93.35(8)	S(2)	Mn(1)	C(10)	92.76(8)
S(2)	Mn(1)	C(11)	176.44(8)	S(3)	Mn(1)	C(9)	172.34(8)
S(3)	Mn(1)	C(10)	84.45(8)	S(3)	Mn(1)	C(11)	90.53(8)
C(9)	Mn(1)	C(10)	87.9(1)	C(9)	Mn(1)	C(11)	89.9(1)
C(10)	Mn(1)	C(11)	88.8(1)				

The Mn-S bond lengths reflect the strained coordination, with thioether donor atoms associated with the 8-membered chelate ring showing slightly longer bonds to the Mn(I) centre [Mn-S(1) 2.3881(7), Mn-S(3) 2.3728(7) Å] than the donor involved in two 5-membered chelate rings [Mn-S(2) 2.3461(7) Å]. Hence, the observed Mn-S bond lengths are slightly longer than those reported in the literature.[14,19,20] Notably *fac*-$[Mn(CO)_3\{MeS(CH_2)S(CH_2)SMe\}]^+$ shows similar trends in trithioether coordination, with one short bond to the donor involved in two 5-membered chelate rings [2.320(3) Å] and longer bonds to the terminal donor atoms [2.352(3), 2.402(4) Å].[19]

The fourth thioether donor remains uncoordinated, though is approximately coplanar with the coordinated donor atoms. Interestingly, this configuration places the uncoordinated thioether donor directly above one of the carbonyl ligands suggesting macrocyclic coordination of the thioether might be completed *via* decarbonylation.

The crystals obtained for $[Mn(CO)_3([15]aneS_5)]CF_3SO_3$ were not as strongly diffracting as for the $[12]aneS_4$ analogue, hence the final residuals were correspondingly higher (Figure 2.8, Tables 2.5, 2.6). Nevertheless, the structure obtained shows similar distorted octahedral geometry around Mn(I) to that above, comprising three mutually-*fac* carbonyl ligands and three thioether donor atoms from the pentathia macrocycle. Again, S-Mn-S bond angles in the 5-membered chelate rings are contracted [85.7(1) and 87.3(1)°], however the larger 11-membered chelate ring angle is only slightly augmented [92.00(10)]. This reflects the capacity of the large macrocyclic ring to relieve the strain associated with η^3-coordination of the pentathia macrocycle. The release of strain is also reflected in shorter Mn-S bond lengths [Mn-S(1) 2.329(3), Mn-S(2) 2.329(3), and Mn-S(3) 2.368(3) Å], now more comparable with those reported in the literature.[14,19,20] The remaining donor atoms remain uncoordinated.

Figure 2.8 View of the structure of *fac*-$[Mn(CO)_3([15]aneS_5)]^+$ with numbering scheme adopted. Ellipsoids drawn at 40%, H-atoms omitted for clarity.

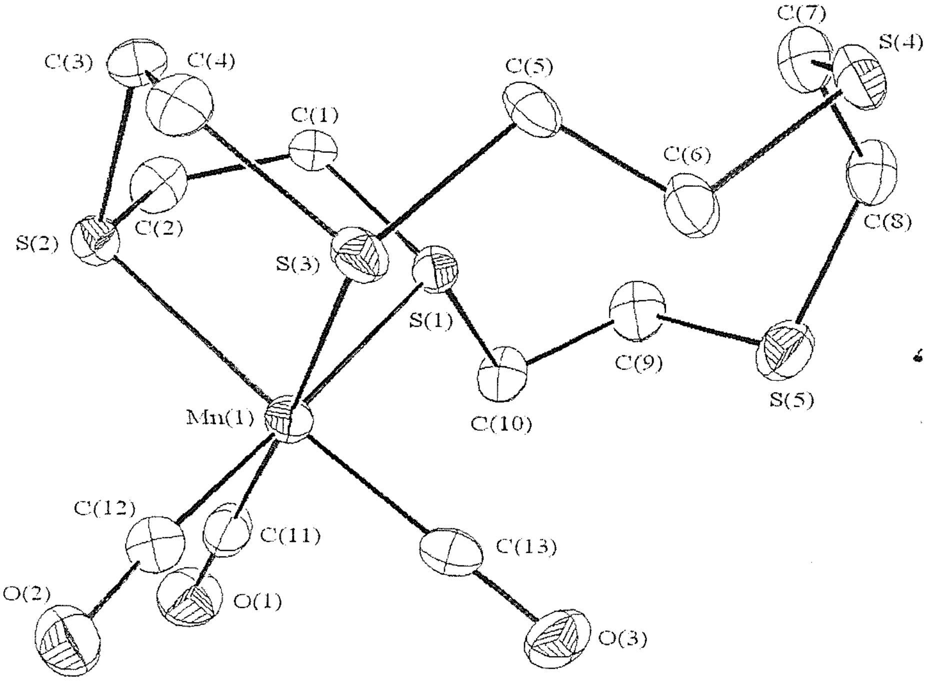

Table 2.5 Selected bond lengths for *fac*-$[Mn(CO)_3([15]aneS_5)]^+$.

Atom	Atom	Distance / Å	Atom	Atom	Distance / Å
Mn(1)	S(1)	2.329(3)	Mn(1)	S(2)	2.329(3)
Mn(1)	S(3)	2.368(3)	Mn(1)	C(11)	1.82(1)
Mn(1)	C(12)	1.81(1)	Mn(1)	C(13)	1.81(1)
C(11)	O(1)	1.13(1)	C(12)	O(2)	1.14(1)
C(13)	O(3)	1.16(1)			

Table 2.6 Selected bond angles for *fac*-$[Mn(CO)_3([15]aneS_5)]^+$.

Atom	Atom	Atom	Angle / °	Atom	Atom	Atom	Angle / °
S(1)	Mn(1)	S(2)	85.7(1)	S(1)	Mn(1)	S(3)	92.00(10)
S(1)	Mn(1)	C(11)	92.1(4)	S(1)	Mn(1)	C(12)	178.3(3)
S(1)	Mn(1)	C(13)	91.8(3)	S(2)	Mn(1)	S(3)	87.3(1)
S(2)	Mn(1)	C(11)	90.6(3)	S(2)	Mn(1)	C(12)	92.6(3)
S(2)	Mn(1)	C(13)	176.9(3)	S(3)	Mn(1)	C(11)	175.2(4)
S(3)	Mn(1)	C(12)	88.1(3)	S(3)	Mn(1)	C(13)	91.0(3)
C(11)	Mn(1)	C(12)	87.7(5)	C(11)	Mn(1)	C(13)	91.3(4)
C(12)	Mn(1)	C(13)	90.0(5)				

Both structures include a non-coordinating $CF_3SO_3^-$ anion to maintain electro-neutrality. Also of note, the invertomer observed in the solid state for *fac*-$[Mn(CO)_3([12]aneS_4)]CF_3SO_3$ correlates well with the predictions from $^{13}C\{^1H\}$ NMR analysis. Figure 2.7 clearly shows the approximate mirror plane present in $[Mn(CO)_3([12]aneS_4)]^+$, leading to the near equivalence of carbon environments either side of the plane. Figure 2.8 shows such a mirror plane is not present in *fac*-$[Mn(CO)_3([15]aneS_5)]CF_3SO_3$, however the larger macrocyclic ring may present greater degrees of freedom in solution and lead to the equivalence of carbon environments observed by $^{13}C\{^1H\}$ NMR spectroscopy.

2.2.2 Mn(I) Dicarbonyl Thioether Macrocycle Complexes

Following decarbonylation of the tetrathia macrocyclic tricarbonyl complexes during acquisition of $^{13}C\{^1H\}$ NMR data (Section 2.2.1.1), attempts were made to isolate the dicarbonyl species $[Mn(CO)_2(\eta^4\text{-}L)]CF_3SO_3$. Thus, $[Mn(CO)_3(\eta^3\text{-}L)]CF_3SO_3$ (L = [12]-, [14]-aneS$_4$ or [15]aneS$_4$) was treated with one molar equivalent of Me_3NO in dry, degassed MeCN solution at room temperature. An immediate colour change occurred to give orange solutions of $[Mn(CO)_2(\eta^4\text{-}L)]CF_3SO_3$. Reaction completion was evident through solution IR spectroscopy, with loss of carbonyl bands due to the *fac*-tricarbonyl species and the appearance of two new bands from the dicarbonyl products.

The complexes *cis*-$[Mn(CO)_2(\eta^4\text{-}L)]CF_3SO_3$ were isolated as air stable orange solids by removal of MeCN *in vacuo*, washing with Et_2O to remove Me_3NO, dissolution of the residual orange oils in $CHCl_3$ and recrystallisation *via* vapour diffusion of light petroleum ether (40-60 °C). Attempts to isolate solids *via* precipitation led to the formation of oils. Microanalytical data and electrospray mass spectrometry confirmed the formulation as $[Mn(CO)_2(L)]CF_3SO_3$, with mass spectra showing the parent cation $[Mn(CO)_2(L)]^+$ as the most intense peak. Fragment peaks corresponding to the loss of a carbonyl ligand were only observed for *cis*-$[Mn(CO)_2(\eta^4\text{-}[15]aneS_5)]$ (Figure 2.9).

Figure 2.9 Electrospray mass spectrum for *fac*-$[Mn(CO)_2(\eta^4\text{-}[15]aneS_5)]^+$ (MeCN).

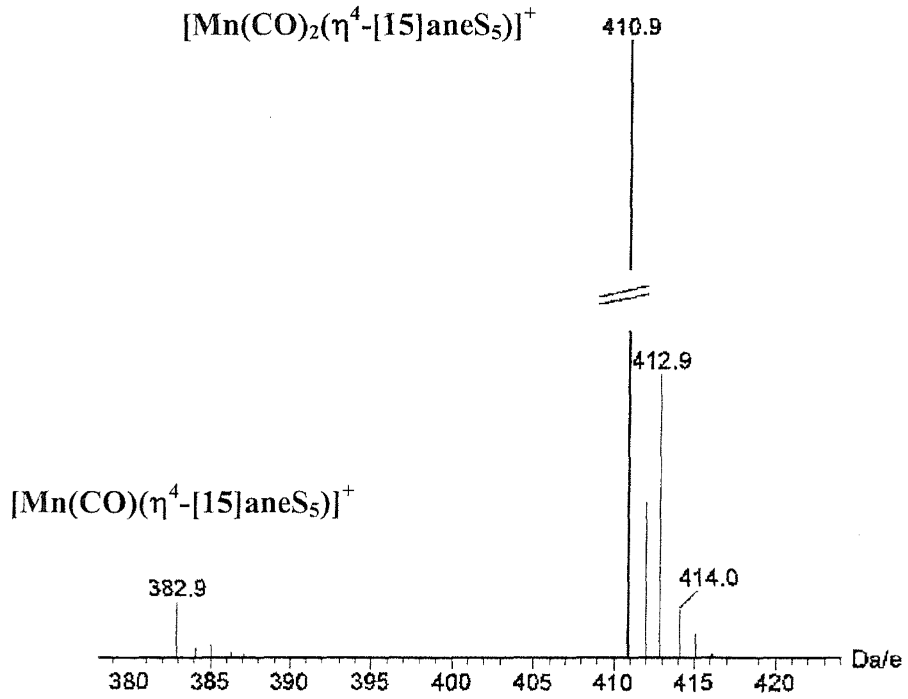

Reaction of the *fac*-[Mn(CO)$_3$(η^3-[16]aneS$_4$)]CF$_3$SO$_3$ crude oil with Me$_3$NO also showed carbonyl bands corresponding to the dicarbonyl species by solution IR spectroscopy. However recrystallisation attempts afforded only very few crystals of *cis*-[Mn(CO)$_2$(η^4-[16]aneS$_4$)]CF$_3$SO$_3$ and thus characterisation was limited to mass spectrometry, IR spectroscopy and X-ray crystallography.

These are the first thioether complexes incorporating the [Mn(CO)$_2$]$^+$ fragment, and their formation is thought to be attributable to the strong binding capabilities of macrocyclic thioethers. Solution IR spectroscopy (Me$_2$CO) showed two carbonyl stretching vibrations, consistent with *cis*-dicarbonyl species. The η^4-coordination of the tetrathia ligands may present pseudo-C_{2v} local symmetry at Mn(I) (Figure 2.10), with the two bands observed corresponding to A_1 + B_1 stretching vibrations. For [Mn(CO)$_2$(η^4-[15]aneS$_5$)]CF$_3$SO$_3$, the presence of the 8-membered chelate ring containing the uncoordinated thioether donor, may reduce the local symmetry at Mn(I) to C_1, though two bands are still observed (2A).

CsI disk IR spectroscopy showed a sharpening of the bands, together with the appearance of fine structure on one of the two bands (Figure 2.11). This is attributed to solid-state effects, whereby the close packing of neighbouring molecules can lead to small differences in the observed carbonyl stretching frequencies. Interestingly, the fine structure was observed on the low frequency carbonyl band for the pseudo-C_{2v} tetrathia macrocycle complexes, whereas C_1 [Mn(CO)$_2$(η^4-[15]aneS$_5$)]CF$_3$SO$_3$ shows fine structure on the higher frequency band. Presumably, this is due to the different symmetry of the pentathia macrocyclic adduct.

Figure 2.10 Symmetry around the Mn(I) centre in *cis*-[Mn(CO)$_2$(η^4-L)]CF$_3$SO$_3$.

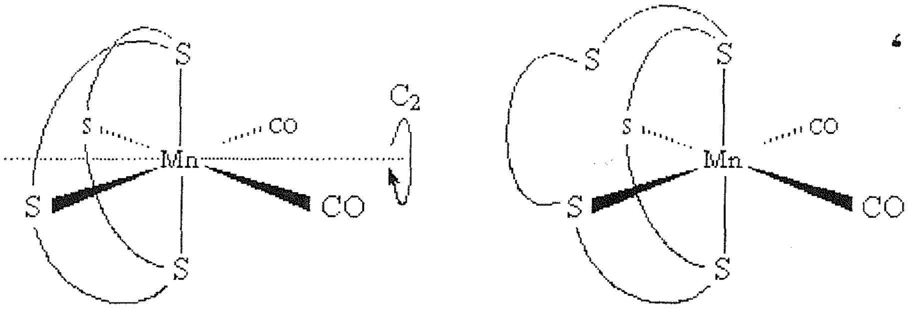

L = tetrathia macrocycle **L = pentathia macrocycle**

Due to the absence of other Mn(I) dicarbonyl thioether complexes, comparison of the carbonyl stretching frequencies observed is restricted to the small number of such complexes incorporating P-donor ligands.[10,11] Thus, *cis*-$[Mn(CO)_2(PHPh_2)_4]^+$, formed as above by treatment of the tricarbonyl adduct with Me_3NO, exhibits carbonyl stretching frequencies at 1964 and 1909 cm^{-1}.[22] Other dicarbonyl species have been formed *via* direct reaction with the *fac*-$[Mn(CO)_3(Me_2CO)_3]^+$ precursor using 4 : 1 ratios of strong π-acceptor ligands. Examples include *cis*-$[Mn(CO)_2(L')_4]^+$ for L′ = $PPh(OMe)_2$ (1992, 1938 cm^{-1}) and $P(OMe)_3$ (2000, 1944 cm^{-1}).[23]

Figure 2.11 Carbonyl region of $[Mn(CO)_2(\eta^4\text{-}[12]aneS_4)]^+$ IR spectrum (CsI disk)

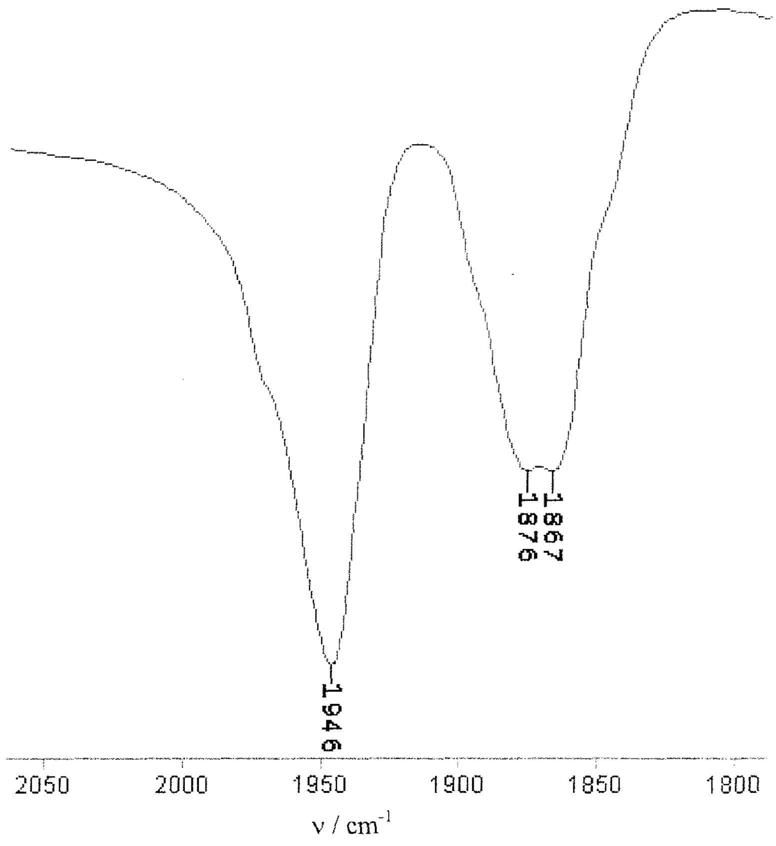

The carbonyl stretching frequencies reported for the P-donor adducts above are significantly higher than those observed for the thioether complexes formed here (Table 2.7). This is consistent with a concentration of electron density on the Mn(I) centre from σ-donation of the thioethers. This promotes strong π-backbonding into the CO antibonding orbitals and hence reduces the carbonyl stretching frequency, as observed.

The large extent of this π-backbonding suggests the thioethers are not competing for electron density and that π-acceptance by the donor atoms in these species is negligible. This is despite reports in the literature that suggest π-backbonding plays an important part in metal-ligand bonding for homoleptic thioether complexes.[24,25] However, the strong π-acceptor carbonyl ligands in the complexes formed here are expected to dominate the π-backbonding and make any such contribution by the much poorer π-acceptor thioether ligands insubstantial.

Table 2.7 Carbonyl stretching vibrations for *cis*-$[Mn(CO)_2(\eta^4\text{-}L)]CF_3SO_3$.

Complex	ν(CO) / cm^{-1} (CsI disk)	
	$A_1 + B_1$	
cis-$[Mn(CO)_2([12]aneS_4)]CF_3SO_3$	1946	1876, 1867
cis-$[Mn(CO)_2([14]aneS_4)]CF_3SO_3$	1952	1886, 1878, 1866
cis-$[Mn(CO)_2([16]aneS_4)]CF_3SO_3$ [a]	1956	1885
cis-$[Mn(CO)_2([15]aneS_5)]CF_3SO_3$ [b]	1967, 1961	1884

[a] Solution IR spectroscopy data (Me_2CO) [b] C_1 symmetry (2A)

Attempts to isolate the monocarbonyl complex $[Mn(CO)(\eta^5\text{-}[15]aneS_5)]CF_3SO_3$ *via* reaction of the dicarbonyl complex with excess Me_3NO or by photochemical routes proved unsuccessful. This is not surprising since the IR data from the dicarbonyl adducts suggest negligible π-acceptance by the thioether donors, hence further removal of strongly π-accepting carbonyl ligands would destabilise the already highly electron-rich Mn(I) centre. This contrasts the coordination chemistry of strong π-acceptor P-donor ligands with Mn(I), where monocarbonyl adducts are known. For example, the cationic complexes $[Mn(CO)\{P(OR)_3\}_5]PF_6$ (R = Me, Et, Pr^I, Ph) can be formed *via* reaction of the hydride species $[Mn(H)(CO)\{P(OR)_3\}_4]$ with Ph_3CPF_6 and phosphite ligand.[26] Indeed, as mentioned earlier, homoleptic phosphine coordination can also be attained, as in $[Mn(dmpe)_3]^+$ and $[Mn(dmpe)_2\{P(OMe)_3\}_2]$.[13] Clearly, the strong π-acceptor properties of the P-donor ligands involved in these complexes are sufficient to stabilise the highly electron-rich Mn(I) centre even in the absence of carbonyl ligands.

2.2.2.1 Multinuclear NMR Spectroscopy

As for the dicarbonyl adducts, multinuclear (^1H, $^{13}C\{^1H\}$, ^{55}Mn) NMR spectroscopy was employed to establish the properties of the invertomers formed for *fac*-$[Mn(CO)_2(\eta^4\text{-}L)]CF_3SO_3$. $^{13}C\{^1H\}$ NMR spectroscopy again proved the most informative of the NMR active nuclei available for investigating the nature of the invertomers formed. The spectrum for *fac*-$[Mn(CO)_2(\eta^4\text{-}[12]aneS_4)]CF_3SO_3$ showed four resonances of approximately equal intensity in the methylene region, δ 31.6, 37.6, 42.1 and 45.7 (Figure 2.12). $[12]aneS_4$ is a highly symmetric macrocycle and can potentially bind symmetrically to present C_{2v} adducts with only two non-equivalent carbon environments. This is not observed here, presumably due to the strain associated with attaining tetrathia coordination from the small macrocycle resulting in distorted geometry around the Mn(I) centre. The observed equivalence of the carbon environments may however be attributed to one of two invertomers, differing in the orientation of one donor atom (Figure 2.13). The resulting C_2 or C_s forms both present four carbon environments (each 2C), consistent with the observed four resonances of approximately equal intensity.

Figure 2.12 $^{13}C\{^1H\}$ NMR spectrum of $[Mn(CO)_2([12]aneS_4)]^+$ (methylene region).

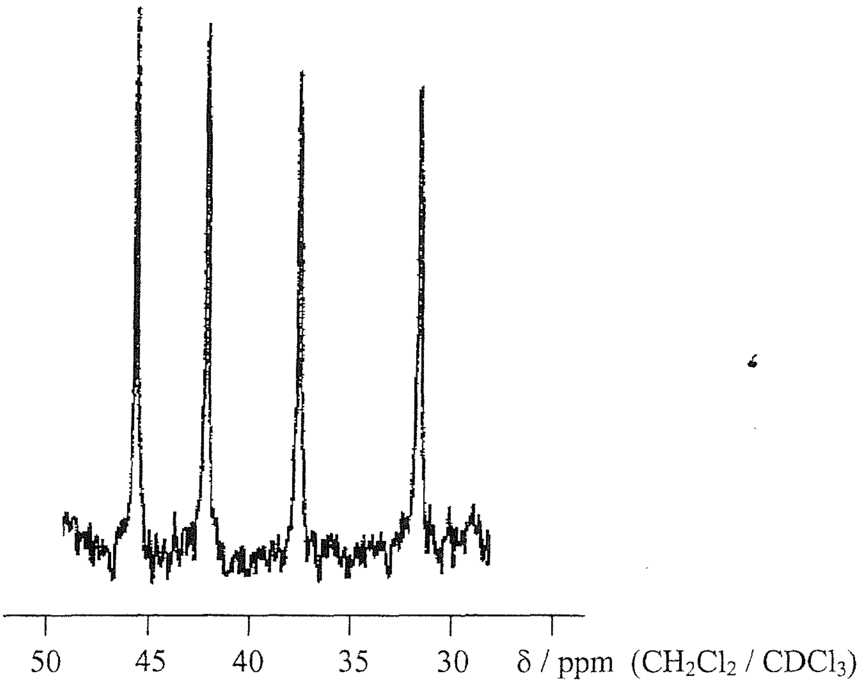

Figure 2.13 Representations of the possible invertomers observed in $^{13}C\{^1H\}$ NMR spectroscopy of *cis*-[Mn(CO)$_2$(η^4-[12]aneS$_4$)]CF$_3$SO$_3$.

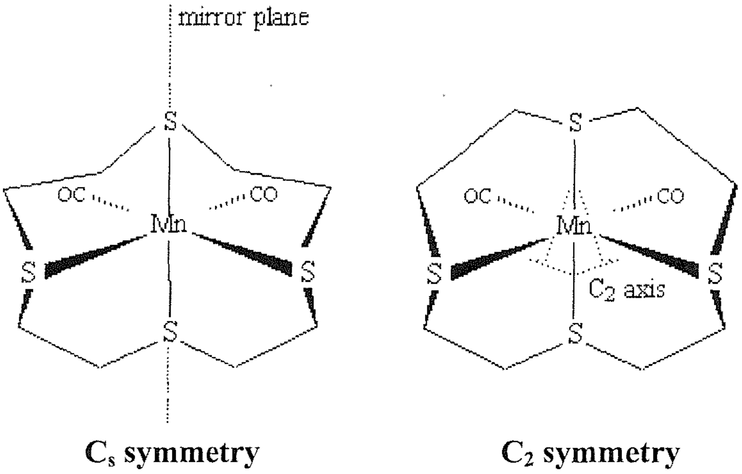

The $^{13}C\{^1H\}$ NMR spectrum for *fac*-[Mn(CO)$_3$(η^3-[14]aneS$_4$)]CF$_3$SO$_3$ showed five resonances of approximately equal intensity in the methylene region, δ 31.0, 33.0, 34.0, 37.0 and 44.5. Here the equivalence of environments could not be attributed to a mirror plane because of the alternating methylene and propylene bridges in [14]aneS$_4$. However, similar equivalence can be attained through C$_2$ symmetry. The spectrum for *fac*-[Mn(CO)$_2$(η^4-[15]aneS$_5$)]CF$_3$SO$_3$ was much more complicated and showed ten resonances of equal intensity in the methylene region, δ 32.4, 33.1, 33.7, 36.7, 37.9, 38.0, 38.5, 39.6, 40.9 and 43.2, suggesting no symmetry in the cation. As for the tricarbonyl adducts, the carbons adjacent to the coordinated donor atoms are shifted to high frequency and those adjacent to the uncoordinated donor least shifted.

Also of note, the above resonances for *cis*-[Mn(CO)$_2$(η^4-[12]aneS$_4$)]CF$_3$SO$_3$ and *cis*-[Mn(CO)$_2$(η^4-[14]aneS$_4$)]CF$_3$SO$_3$ confirm the spontaneous formation of the dicarbonyl adduct during acquisition of $^{13}C\{^1H\}$ NMR data for the tricarbonyl species (Section 2.2.1.1). The dicarbonyl resonances observed here correlate exactly with the weak resonances observed in the tricarbonyl spectra.

The $^{13}C\{^1H\}$ NMR spectra also showed substantially broadened carbonyl resonances for *cis*-[Mn(CO)$_2$(η^4-L)]CF$_3$SO$_3$, L = [12]aneS$_4$ (δ 220-222), [14]aneS$_4$ (δ 218-226) and [15]aneS$_5$ (δ 220-225). These values are to high frequency of those observed for the tricarbonyl species by ca. 6 ppm, corresponding to the stronger π-backbonding of the carbonyls with the more electron rich Mn(I) centre.

The ^{55}Mn NMR spectra of *cis*-[Mn(CO)$_2$(η^4-L)]CF$_3$SO$_3$ also showed the effects of the increased electron density on Mn(I) in the dicarbonyl species, with a significant shift to low frequency by several hundred ppm (Table 2.8). The resonances observed are also considerably broader and required longer acquisition times than the tricarbonyl adducts (Figure 2.14). This is consistent with the decrease in local-symmetry at Mn(I) on formation of the *cis*-dicarbonyl species, resulting in increased electric field gradient and therefore increased line broadening. Again, room temperature ^{1}H NMR spectroscopy proved rather uninformative as the resonances observed were considerably broadened by the ^{55}Mn quadrupole. However, the observed chemical shift ranges are as expected.

Table 2.8 ^{55}Mn NMR data for *cis*-[Mn(CO)$_2$(η^4-L)]CF$_3$SO$_3$.

Complex	δ ^{55}Mn [a]	$w_{1/2}$ / Hz [a]
cis-[Mn(CO)$_2$([12]aneS$_4$)]CF$_3$SO$_3$	-1540	18000
cis-[Mn(CO)$_2$([14]aneS$_4$)]CF$_3$SO$_3$	-1350	30000
cis-[Mn(CO)$_2$([15]aneS$_5$)]CF$_3$SO$_3$	-980	12000

[a] Spectra recorded in CH$_2$Cl$_2$/CDCl$_3$.

Figure 2.14 Comparison of the ^{55}Mn NMR spectra of a) *fac*-[Mn(CO)$_3$(η^3-[15]aneS$_5$)]$^+$ and b) *cis*-[Mn(CO)$_2$(η^4-[15]aneS$_5$)]$^+$ (CH$_2$Cl$_2$ / CDCl$_3$).

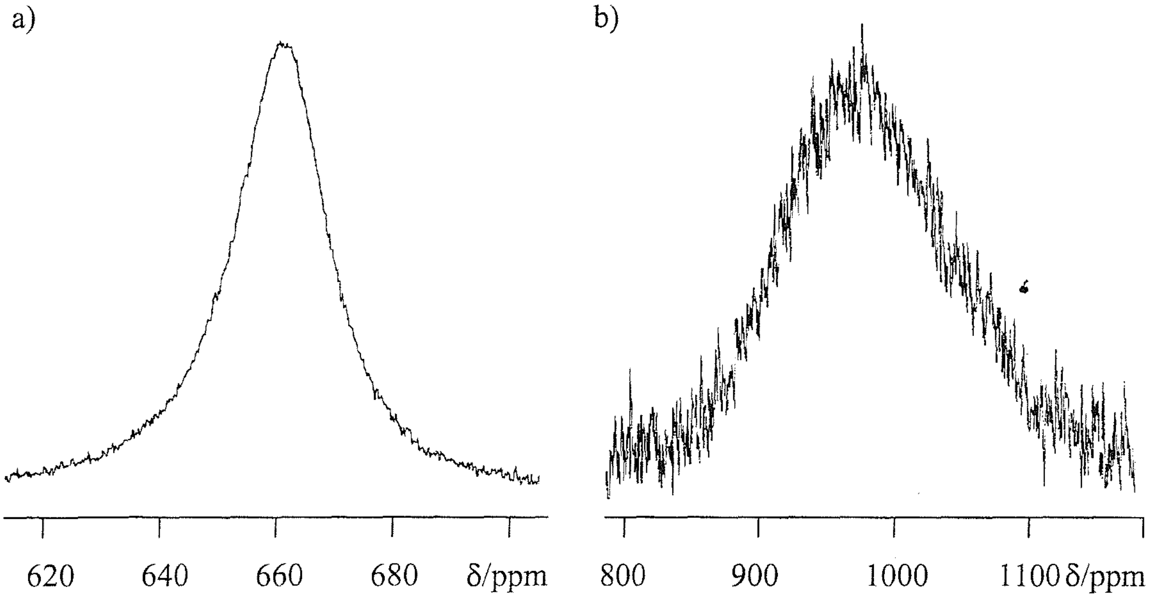

2.2.2.2 X-ray Crystallographic Studies

To ascertain the consequences of decarbonylation of the tricarbonyl adducts and subsequent tetrathia coordination of the macrocycles, single crystal X-ray diffraction studies were undertaken on the dicarbonyl complexes formed here. Thus, single crystals of *cis*-$[Mn(CO)_2([12]aneS_4)]CF_3SO_3$ and *cis*-$[Mn(CO)_2([15]aneS_5)]CF_3SO_3$ were grown by vapour diffusion of light petroleum ether (40-60°C) into $CHCl_3$ solutions of the adducts. A small number of moderate quality single crystals of *cis*-$[Mn(CO)_2$-$([16]aneS_4)]CF_3SO_3$ were also acquired during attempts to isolate the bulk sample.

The structure of $[Mn(CO)_2([12]aneS_4)]CF_3SO_3$ shows two independent Mn(I) carbonyl cations, two non-coordinating $CF_3SO_3^-$ anions maintaining charge neutrality and one molecule of $CHCl_3$ in the asymmetric unit. Both $[Mn(CO)_2([12]aneS_4)]^+$ cations show the Mn(I) centre coordinated to two mutually-*cis* carbonyl ligands and all four S-donors from the tetrathia macrocycle. However, one of the cations exhibited disorder around the thioether donor atoms *trans* to the two carbonyl ligands. This was adequately modelled to reveal the presence of two different conformations occupying the same space within the crystal lattice. Although this disorder model provides an adequate solution to the diffraction data, it precludes meaningful discussion of bond parameters, and hence the disordered cation will be ignored in the following discussion.

The ordered $[Mn(CO)_2([12]aneS_4)]^+$ cation exhibits a distorted octahedral environment around the Mn(I) centre, resulting from strained tetrathia coordination of the $[12]aneS_4$ macrocycle (Figure 2.15, Tables 2.9, 2.10). Thus, S-Mn-S bond angles deviate from the expected 90°, with those associated with the 5-membered chelate rings even more contracted [83.12(9), 83.47(9), 85.98(9), 87.20(9)°] than those observed in the tricarbonyl adduct [86.47(2) and 87.10(3)°]. The extent of strain associated with macrocyclic coordination can be determined from the bond angle between the mutually-*trans* non-chelating donors. Thus, the S(1)-Mn(1)-S(3) bond angle [164.80(9)°] shows severe contraction from the idealised 180° geometry. Such large distortion suggests the relatively small 12-membered macrocycle is poorly matched to the ionic size of Mn(I).

Despite such strain on the macrocycle, the Mn-S bond distances are shorter [2.311(2), 2.316(3), 2.326(3), 2.338(3) Å] than in the tricarbonyl adduct [2.3461(7), 2.3728(7), 2.3881(7) Å]. This may be attributed to the superior stabilisation proffered by the macrocyclic effect (see Chapter 1). Indeed, the observed bond distances are comparable with those of the macrocyclic adducts $[Mn(CO)_3([X]aneS_3)]^+$ [X = 9, 2.314(4) – 2.341(4) Å, three independent cations in the asymmetric unit;[20] X = 10, 2.303(5) – 2.405(6) Å, two independent cations in the asymmetric unit].[19]

Figure 2.15 View of the structure of the ordered *cis*-$[Mn(CO)_2([12]aneS_4)]^+$ cation in the asymmetric unit, with numbering scheme adopted. Ellipsoids drawn at 40% probability, H-atoms omitted for clarity.

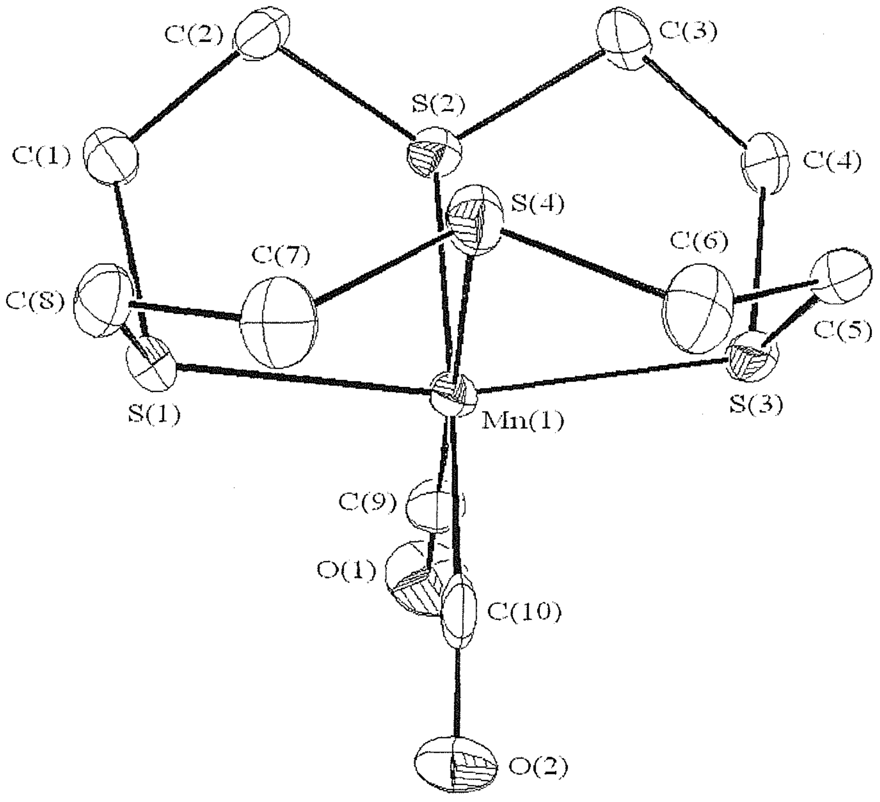

Table 2.9 Selected bond lengths for the ordered *cis*-$[Mn(CO)_2([12]aneS_4)]^+$ cation.

Atom	Atom	Distance / Å	Atom	Atom	Distance / Å
Mn(1)	S(1)	2.311(2)	Mn(1)	S(2)	2.338(3)
Mn(1)	S(3)	2.316(3)	Mn(1)	S(4)	2.326(3)
Mn(1)	C(9)	1.795(10)	Mn(1)	C(10)	1.795(10)
C(9)	O(1)	1.147(11)	C(10)	O(2)	1.158(11)

Table 2.10 Selected bond angles for the ordered *cis*-$[Mn(CO)_2([12]aneS_4)]^+$ cation.

Atom	Atom	Atom	Angle / °	Atom	Atom	Atom	Angle / °
S(1)	Mn(1)	S(2)	85.98(9)	S(1)	Mn(1)	S(3)	164.80(9)
S(1)	Mn(1)	S(4)	83.12(9)	S(1)	Mn(1)	C(9)	96.3(3)
S(1)	Mn(1)	C(10)	93.0(3)	S(2)	Mn(1)	S(3)	87.20(9)
S(2)	Mn(1)	S(4)	91.30(9)	S(2)	Mn(1)	C(9)	87.2(3)
S(2)	Mn(1)	C(10)	172.7(3)	S(3)	Mn(1)	S(4)	83.47(9)
S(3)	Mn(1)	C(9)	96.9(3)	S(3)	Mn(1)	C(10)	95.4(3)
S(4)	Mn(1)	C(9)	178.5(3)	S(4)	Mn(1)	C(10)	95.7(3)
C(9)	Mn(1)	C(10)	85.7(4)				

The observed bond lengths also show the bonding characteristics of the carbonyl ligands in the cation. The Mn-S bond distances for the thioether donor atoms *trans* to carbonyls are significantly longer than those of the mutually-*trans* thioethers. This can be attributed to strong π-acceptor capabilities of the carbonyls removing electron density from the electron rich Mn(I) centre, thus reducing the metal-donor interaction of the *trans* thioether donors. This increase in carbonyl π-bonding correlates with shorter Mn-C bond distances and longer C-O distances than the tricarbonyl adduct. However, the large estimated standard deviations (σ) associated with the disordered structure prevents conclusive comparison of the carbonyl bond distances, as the differences remain marginally below the required level of significance (3σ).

The conformation of the ordered $[Mn(CO)_2([12]aneS_4)]^+$ cation also correlates well with the conclusions from IR and $^{13}C\{^1H\}$ NMR spectroscopy. Figure 2.15 shows the S(4) donor is orientated in the opposite direction to the other donor atoms, thus precluding C_2 symmetry. However, a non-crystallographic mirror plane is clearly evident, with the Mn(I) centre, both carbonyl ligands and S(2) and S(4) positioned within the plane. This presents C_s symmetry as inferred earlier.

The crystals obtained for $[Mn(CO)_2([15]aneS_5)]CF_3SO_3$ were not as strongly diffracting as for the $[12]aneS_4$ analogue, hence the carbon atoms were refined only isotropically and the final residuals were correspondingly higher (Figure 2.16, Tables 2.11, 2.12). Nevertheless, the structure obtained shows similar distorted octahedral geometry around Mn(I) to that above, comprising two mutually-*cis* carbonyl ligands and four thioether donor atoms from the pentathia macrocycle.

Figure 2.16 View of the structure of *cis*-$[Mn(CO)_2([15]aneS_5)]^+$ with numbering scheme adopted. Carbon atoms refined isotropically, ellipsoids drawn at 40% probability and H-atoms omitted for clarity.

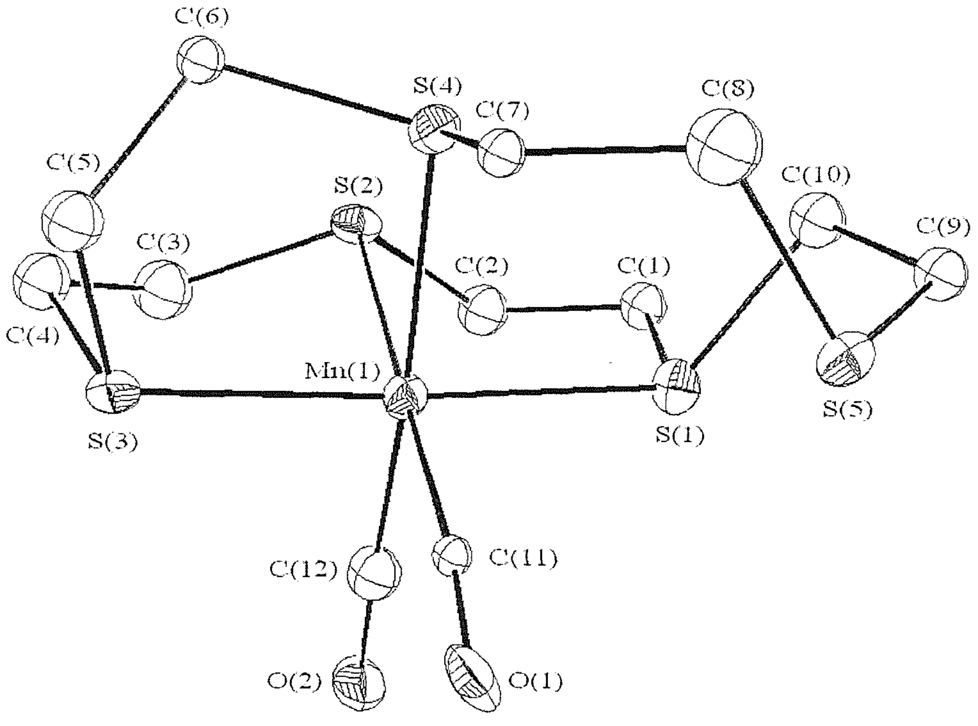

Table 2.11 Selected bond lengths for *cis*-$[Mn(CO)_2([15]aneS_5)]^+$.

Atom	Atom	Distance / Å	Atom	Atom	Distance / Å
Mn(1)	S(1)	2.334(5)	Mn(1)	S(2)	2.325(6)
Mn(1)	S(3)	2.285(5)	Mn(1)	S(4)	2.387(6)
Mn(1)	C(11)	1.82(2)	Mn(1)	C(12)	1.79(2)
C(11)	O(1)	1.12(2)	C(12)	O(2)	1.14(2)

Table 2.12 Selected bond angles for *cis*-$[Mn(CO)_2([15]aneS_5)]^+$.

Atom	Atom	Atom	Angle / °	Atom	Atom	Atom	Angle / °
S(1)	Mn(1)	S(2)	85.2(2)	S(1)	Mn(1)	S(3)	171.1(2)
S(1)	Mn(1)	S(4)	93.6(2)	S(1)	Mn(1)	C(11)	93.8(5)
S(1)	Mn(1)	C(12)	88.8(6)	S(2)	Mn(1)	S(3)	86.3(2)
S(2)	Mn(1)	S(4)	85.0(2)	S(2)	Mn(1)	C(11)	178.3(6)
S(2)	Mn(1)	C(12)	92.9(7)	S(3)	Mn(1)	S(4)	88.5(2)
S(3)	Mn(1)	C(11)	94.6(5)	S(3)	Mn(1)	C(12)	88.7(6)
S(4)	Mn(1)	C(11)	96.4(6)	S(4)	Mn(1)	C(12)	176.6(7)
C(11)	Mn(1)	C(12)	85.7(8)				

Again, S-Mn-S bond angles in the 5-membered chelate rings are contracted [85.0(2), 85.2(2), 86.3(2) and 88.5(2)°], however the angles are still comparable with those in the tricarbonyl adduct [85.7(1) and 87.3(1)]. This reflects the capacity of the large macrocyclic ring to accommodate η^4-coordination of the pentathia macrocycle with little increase in strain over η^3-coordination. This can also be ascertained from the bond angle between the two mutually-*trans* donor atoms, where distortion from idealised 180° geometry is reduced [$\angle$S(1)-Mn(1)-S(3) = 171.1(2)°] in comparison to the severely strained $[Mn(CO)_2([12]aneS_4)]^+$ cation [164.80(9)°].

The Mn-S bond distances [2.285(5), 2.325(6), 2.334(5), 2.387(6) Å] are also comparable with those in the tricarbonyl adduct [2.329(3), 2.329(3), 2.368(3) Å]. This again differs from the $[12]aneS_4$ complexes, where Mn-S bond distances shorten significantly upon η^4-coordination. This can be attributed to the absence of the macrocyclic effect for $[Mn(CO)_2([15]aneS_5)]^+$, where coordination of the pentathia macrocycle is still not complete.

The conformation of the $[Mn(CO)_2([15]aneS_5)]^+$ cation again correlates well with the conclusions from IR and $^{13}C\{^1H\}$ NMR spectroscopy. Figure 2.16 clearly shows the presence of the uncoordinated donor precludes C_2 or mirror symmetry and reduces the symmetry of the cation to C_1, as inferred earlier.

The crystals obtained for $[Mn(CO)_2([16]aneS_4)]CF_3SO_3$ were even less strongly diffracting than the $[15]aneS_5$ analogue, hence again the carbon atoms were refined only isotropically and the final residuals were significantly higher (Figure 2.17, Tables 2.13, 2.14). The structure obtained does however show a similar distorted octahedral geometry around Mn(I) to that above, comprising two mutually-*cis* carbonyl ligands and all four thioether donor atoms from the tetrathia macrocycle. The size of the estimated standard deviations associated with the bond distances and angles precludes any detailed comparisons, though these do indicate much less distortion than in the $[12]aneS_4$ and $[15]aneS_5$ analogues. Thus, the angle between the two mutually-*trans* donor atoms is close to the idealised 180° [$\angle$S(1)-Mn(1)-S(3) = 178.6(2)°], suggesting the propylene bridges provide sufficient flexibility to retain near octahedral geometry upon η^4-coordination of the macrocycle.

Figure 2.17 View of the structure of *cis*-$[Mn(CO)_2([16]aneS_4)]^+$ with numbering scheme adopted. Carbon atoms refined isotropically, ellipsoids drawn at 40% probability and H-atoms omitted for clarity.

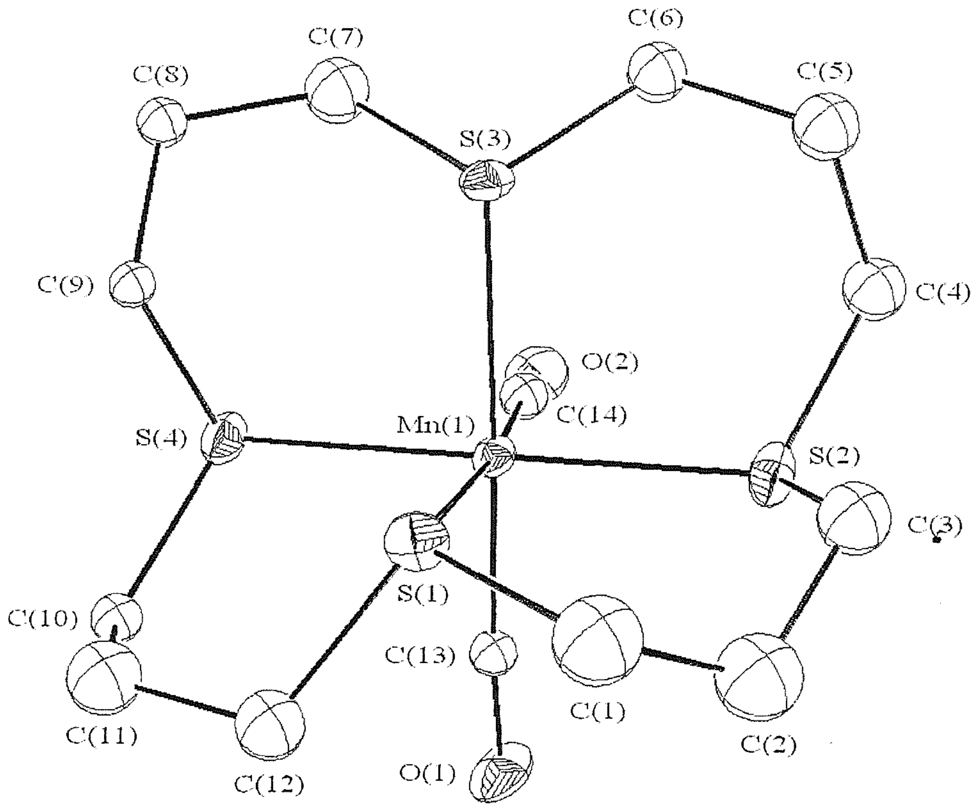

Table 2.13 Selected bond lengths for *cis*-$[Mn(CO)_2([16]aneS_4)]^+$.

Atom	Atom	Distance / Å	Atom	Atom	Distance / Å
Mn(1)	S(1)	2.37(4)	Mn(1)	S(2)	2.31(2)
Mn(1)	S(3)	2.38(6)	Mn(1)	S(4)	2.34(2)
Mn(1)	C(13)	1.78(5)	Mn(1)	C(14)	1.76(4)
C(13)	O(1)	1.14(4)	C(14)	O(2)	1.16(3)

Table 2.14 Selected bond angles for *cis*-$[Mn(CO)_2([16]aneS_4)]^+$.

Atom	Atom	Atom	Angle / °	Atom	Atom	Atom	Angle / °
S(1)	Mn(1)	S(2)	96(2)	S(1)	Mn(1)	S(3)	85.5(3)
S(1)	Mn(1)	S(4)	85(2)	S(1)	Mn(1)	C(13)	92.9(7)
S(1)	Mn(1)	C(14)	173.9(7)	S(2)	Mn(1)	S(3)	93(2)
S(2)	Mn(1)	S(4)	178.6(2)	S(2)	Mn(1)	C(13)	89(2)
S(2)	Mn(1)	C(14)	90(2)	S(3)	Mn(1)	S(4)	88(2)
S(3)	Mn(1)	C(13)	177.9(7)	S(3)	Mn(1)	C(14)	92.8(8)
S(4)	Mn(1)	C(13)	91(2)	S(4)	Mn(1)	C(14)	89(2)
C(13)	Mn(1)	C(14)	89(1)				

2.3 Conclusions

The complexes *fac*-$[Mn(CO)_3(\eta^3\text{-}L)]CF_3SO_3$ (L = [12]-, [14]-, [16]-aneS_4 and [15]aneS_5) have been prepared *via* the reaction of *fac*-$[Mn(CO)_3(Me_2CO)_3]CF_3SO_3$ with L in acetone. Microanalyses, electrospray mass spectrometry and ^1H NMR spectroscopy have confirmed the identity of these complexes. IR spectroscopy has confirmed the presence of three mutually *fac*-carbonyl ligands and together with $^{13}C\{^1H\}$ NMR spectroscopy has shown the complexes exhibit C_s symmetry. ^{55}Mn NMR spectroscopy has shown the electron density at the Mn(I) centre is less than for other reported trithioether Mn(I) tricarbonyl cationic complexes. This was attributed to strained η^3-coordination of the tetrathia macrocycles, with the larger pentathia macrocyclic complex exhibiting a ^{55}Mn resonance more comparable with the literature.

X-ray crystallography of the [12]aneS_4 and [15]aneS_5 tricarbonyl adducts has confirmed the above conclusions showing *fac*-$[Mn(CO)_3(\eta^3\text{-}L)]CF_3SO_3$, with pseudo-$C_s$ symmetry clearly evident for the [12]aneS_4 adduct. Longer Mn-S bond distances than for other reported trithioether Mn(I) tricarbonyl cationic complexes supports the conclusions from ^{55}Mn NMR spectroscopy, and the observed bond angles clearly show greater strain associated with η^3-coordination of the tetrathia macrocycle compared to the pentathia macrocycle.

$^{13}C\{^1H\}$ NMR spectroscopy of the isolated tetrathia macrocyclic adducts also showed spontaneous decarbonylation in solution to afford small quantities of the dicarbonyl adducts, $[Mn(CO)_2(\eta^4\text{-}L)]CF_3SO_3$. This was attributed to the stabilisation proffered by the macrocyclic effect upon η^4-coordination. Thus, the [15]aneS_5 tricarbonyl adduct showed no signs of spontaneous decarbonylation, as the macrocyclic effect would not be a driving force here.

The complexes *cis*-$[Mn(CO)_2(\eta^4\text{-}L)]CF_3SO_3$ have been prepared *via* the reaction of *fac*-$[Mn(CO)_3(\eta^3\text{-}L)]CF_3SO_3$ with Me_3NO in MeCN, and present the first examples of thioether stabilisation of the highly electron-rich $[Mn(CO)_2]^+$ fragment. Microanalyses, electrospray mass spectrometry and ^1H NMR spectroscopy again confirmed the identity of these complexes. IR spectroscopy has confirmed the presence of two mutually *cis*-carbonyl ligands, and the anomalously low carbonyl stretching frequencies show the thioethers are acting principally as σ-donors, with negligible π-bonding. $^{13}C\{^1H\}$ NMR spectroscopy ruled out the possibility of C_{2v} symmetry for the tetrathia macrocycle adducts, suggesting the ligands must bind unsymmetrically, giving complexes with C_2 or C_s symmetry. ^{55}Mn NMR spectroscopy showed an increase in electron density at the Mn(I) centre corresponding to the increased thioether coordination together with the loss of the strong π-acceptor carbonyl ligand. The observed resonances were also significantly broadened compared to the tricarbonyl adducts, reflecting the reduced local symmetry at the Mn(I) centre.

X-ray crystallography of the [12]aneS_4, [16]aneS_4 and [15]aneS_5 dicarbonyl adducts has confirmed the above conclusions showing *cis*-[Mn(CO)$_2$(η^4-L)]CF_3SO_3, with pseudo-C_s symmetry clearly evident for the [12]aneS_4 adduct. The bond angles for the *cis*-[Mn(CO)$_2$(η^4-[12]aneS_4)]$^+$ also show severe strain associated with η^4-coordination of the small macrocyclic ring around the Mn(I) centre. Despite this, the Mn-S bond distances are significantly shorter than the tricarbonyl adduct, presumably due to stabilisation by the macrocyclic effect. Indeed, the [15]aneS_5 dicarbonyl adduct shows no significant changes in bond distances compared to the tricarbonyl adduct due to the absence of the macrocyclic effect. The bond angles also change little from the tricarbonyl adduct, suggesting [15]aneS_5 is sufficiently large to accommodate η^4-coordination with little increase in strain over η^3-coordination. The [16]aneS_4 dicarbonyl structure continues this trend, with the propylene bridges between donor atoms permitting near octahedral coordination, although the high estimated standard deviations associated with the bond angles prevent conclusive analysis.

The above syntheses have demonstrated the ability of thioether macrocycles to stabilise the highly electron-rich [Mn(CO)$_2$]$^+$ fragment, despite negligible π-backbonding from the thioether donor atoms. Presumably, the stabilisation is attained through the macrocyclic effect from the η^4-coordination of the tetrathia macrocycles. However, the isolation of the pentathia macrocyclic dicarbonyl complex suggests the macrocyclic effect is not the sole factor. Attempts to utilise the macrocyclic effect to stabilise the monocarbonyl species [Mn(CO)(η^5-[15]aneS_5)]CF_3SO_3 proved unsuccessful. This is not surprising considering the negligible participation of the thioethers in π-bonding, thus removal of strongly π-accepting carbonyl ligands would only further destabilise the already highly electron-rich Mn(I) centre.

2.4 Experimental

The compounds $[Mn(CO)_5Cl]$[27] and *fac*-$[Mn(CO)_3(Me_2CO)_3]CF_3SO_3$[23] were prepared *via* the literature procedures and the ligands [12]-, [14]-, [16]-aneS_4 and [15]aneS_5 purchased from Aldrich Chemical Company. Dry MeCN required for Mn(I) the decarbonylation reactions was distilled over P_2O_5 and all solvents were degassed with dry N_2 for 15 minutes prior to use. Reactions were performed under an N_2 atmosphere with reaction vessels wrapped in aluminium foil to exclude light, and isolated products were stored in foil covered vials.

fac-$[Mn(CO)_3(\eta^3\text{-}[12]aneS_4)]CF_3SO_3$

[12]aneS_4 (48 mg, 0.2 mmol) was added to a solution of *fac*-$[Mn(CO)_3(Me_2CO)_3]$-CF_3SO_3 (0.2 mmol) in Me_2CO in a foil covered flask. The solution was stirred under an N_2 atmosphere at room temperature for ~2 hours. Solution IR spectra were taken at regular intervals to observe the loss of carbonyl stretching frequencies at 2022 and 1932 cm^{-1} corresponding to *fac*-$[Mn(CO)_3(Me_2CO)_3]CF_3SO_3$. The resulting solution was reduced to dryness *in vacuo*, the orange oil formed dissolved in $CHCl_3$ (5 cm^3) and petroleum ether (40-60 °C, 10 cm^3) added to give a yellow precipitate. This solid was filtered, washed with petroleum ether (40-60 °C, 3 x 25 cm^3) and dried *in vacuo* to give the required *fac*-$[Mn(CO)_3(\eta^3\text{-}[12]aneS_4)]CF_3SO_3$ (yield 80 mg, 76 %). Required for $[C_{12}H_{16}F_3MnO_6S_5]$. ½ $CHCl_3$: C = 25.6, H = 2.8 %; found: C = 26.0, H = 2.8 %. Electrospray mass spectrum (MeCN): found *m/z* = 379, 351; calculated for $[Mn(CO)_3([12]aneS_4)]^+$ *m/z* = 379, $[Mn(CO)_2([12]aneS_4)]^+$ *m/z* = 351. ^1H NMR: δ 2.5-4.0 (br, *m*, CH_2). $^{13}C\{^1H\}$ NMR: δ 214-219 (br, CO), 38.2 (CH_2, 2C), 36.3 (CH_2, 4C), 30.7 (CH_2, 2C). ^{55}Mn NMR: δ -334, $w_{½}$ ~3000 Hz. ν(CO) (Me_2CO): 2061s; 1972s, 1958s; (CsI disk): 2061s, 1973s, 1951s cm^{-1}.

fac-$[Mn(CO)_3(\eta^3\text{-}[14]aneS_4)]CF_3SO_3$

As above, but using [14]aneS_4 (54 mg, 0.2 mmol). A yellow solid was isolated as the required *fac*-$[Mn(CO)_3(\eta^3\text{-}[14]aneS_4)]CF_3SO_3$ (yield 90 mg, 81 %). Required for $[C_{14}H_{20}F_3MnO_6S_5]$: C = 30.2, H = 3.6 %; found: C = 29.9, H = 3.3 %. Electrospray mass spectrum (MeCN): found *m/z* = 407, 379; calculated for $[Mn(CO)_3([14]aneS_4)]^+$

m/z = 407, $[Mn(CO)_2([14]aneS_4)]^+$ *m/z* = 379. ^1H NMR: δ 2.1-4.0 (br, *m*, CH_2). $^{13}C\{^1H\}$ NMR: δ 215-224 (br, CO), 36.4, 36.2, 31.8, 27.4 (CH_2, each 2C), 24.7 and 24.4 (CH_2, both 1C). ^{55}Mn NMR: δ -471, $w_{½}$ ~1700 Hz. ν(CO) (Me_2CO): 2043s 1965s, 1955s; (CsI disk): 2042s, 1966s, 1953s cm^{-1}.

fac-$[Mn(CO)_3(\eta^3$-$[16]aneS_4)]CF_3SO_3$

As above, but using $[16]aneS_4$ (60 mg, 0.2 mmol). A solid was not isolated, however characterisation performed on the orange oil formed by removal of solvent *in vacuo* allowed identification of the product to be the required *fac*-$[Mn(CO)_3(\eta^3$-$[16]aneS_4)]CF_3SO_3$. Electrospray mass spectrum (MeCN): found *m/z* = 435, 407; calculated for $[Mn(CO)_3([16]aneS_4)]^+$ *m/z* = 435, $[Mn(CO)_2([16]aneS_4)]^+$ *m/z* = 407. ^{55}Mn NMR: δ -276, $w_{½}$ ~3000 Hz. ν(CO) (Me_2CO): 2042s, 1954s cm^{-1}.

fac-$[Mn(CO)_3(\eta^3$-$[15]aneS_5)]CF_3SO_3$

As above, but using $[15]aneS_5$ (60 mg, 0.2 mmol). A yellow solid was isolated as the required *fac*-$[Mn(CO)_3(\eta^3$-$[15]aneS_5)]CF_3SO_3$ (yield 100 mg, 85 %). Required for $[C_{14}H_{20}F_3MnO_6S_6]$: C = 28.6, H = 3.4 %; found: C = 28.2, H = 3.1 %. Electrospray mass spectrum (MeCN): found *m/z* = 439; calculated for $[Mn(CO)_3([15]aneS_5)]^+$ *m/z* = 439. ^1H NMR: δ 2.6-3.7 (br, *m*, CH_2). $^{13}C\{^1H\}$ NMR: δ 212-219 (br, CO), 37.8, 35.0, 33.7 (CH_2, each 2C), 31.1 (CH_2, 4C). ^{55}Mn NMR: δ -658, $w_{½}$ ~2200 Hz. ν(CO) (Me_2CO): 2046s, 1966s; (CsI disk): 2047s, 1974s, 1951s cm^{-1}.

cis-$[Mn(CO)_2(\eta^4$-$[12]aneS_4)]CF_3SO_3$

fac-$[Mn(CO)_3(\eta^3$-$[12]aneS_4)]CF_3SO_3$ (53 mg, 0.1 mmol) was dissolved in dry degassed MeCN (40 cm^3) under an N_2 atmosphere in a foil covered flask. Me_3NO (8 mg, 0.1 mmol) was added resulting in an immediate solution colour change from yellow to orange. The solution was stirred under N_2 for ~1 hour and solution IR spectra were taken at regular intervals to observe a loss in the *fac*-carbonyl stretching frequencies. The resulting solution was reduced to dryness *in vacuo* and the orange oil formed washed with Et_2O (3 x 25 cm^3). The remaining residue was dissolved in $CHCl_3$ (5 cm^3)

and recrystallised *via* slow vapour diffusion of petroleum ether (40-60 °C) into this solution. The resulting yellow brown solid was filtered, washed with petroleum ether (40-60 °C, 3 x 15 cm^3) and dried *in vacuo* to give the required *cis*-$[Mn(CO)_2(\eta^4$-[12]ane$S_4)]CF_3SO_3$ (yield 45 mg, 90 %). Required for $[C_{11}H_{16}F_3MnO_5S_5]$. ½ $CHCl_3$: C = 24.8, H = 3.0 %; found: C = 25.2, H = 3.3 %. Electrospray mass spectrum (MeCN): found *m/z* = 351 calculated for $[Mn(CO)_2([12]aneS_4)]^+$ *m/z* = 351. ^1H NMR: δ 2.5-4.1 (br, *m*, CH_2). $^{13}C\{^1H\}$ NMR: δ 220-222 (br, CO), 45.7, 42.1, 37.6, 31.6 (CH_2, each 2C). ^{55}Mn NMR: δ -1540, $w_{½}$ ~18000 Hz. ν(CO) (Me_2CO) 1964s, 1892s; (CsI disk): 1946s, 1876s, 1867s cm^{-1}.

cis-$[Mn(CO)_2(\eta^4$-[14]ane$S_4)]CF_3SO_3$

As above, but using *fac*-$[Mn(CO)_3(\eta^3$-[14]ane$S_4)]CF_3SO_3$ (56 mg, 0.1 mmol). An orange brown solid was isolated as the required *cis*-$[Mn(CO)_2(\eta^4$-[14]ane$S_4)]CF_3SO_3$ (yield 31 mg, 60 %). Required for $[C_{13}H_{20}F_3MnO_5S_5]$: C = 29.5, H = 3.8 %; found: C = 29.3, H = 3.6 %. Electrospray mass spectrum (MeCN): found *m/z* = 379; calculated for $[Mn(CO)_2([14]aneS_4)]^+$ *m/z* = 379. ^1H NMR: δ 2.3-3.9 (br, *m*, CH_2). $^{13}C\{^1H\}$ NMR: δ 218-226 (br, CO), 44.5, 37.0, 34.0, 33.0, 31.0 (CH_2, each 2C). ^{55}Mn NMR: δ -1350, $w_{½}$ ~30000 Hz. ν(CO) (Me_2CO) 1960s, 1888s; (CsI disk): 1952s, 1886s, 1878s, 1866s cm^{-1}.

cis-$[Mn(CO)_2(\eta^4$-[16]ane$S_4)]CF_3SO_3$

As above, but using residual oil from above synthesis of *fac*-$[Mn(CO)_3(\eta^3$-[14]ane$S_4)]CF_3SO_3$ (0.1 mmol). A low yield of orange crystals were isolated and provided limited characterisation as the required *cis*-$[Mn(CO)_2(\eta^4$-[14]ane$S_4)]CF_3SO_3$ (yield 10 mg, 18 %). Electrospray mass spectrum (MeCN): found *m/z* = 407; calculated for $[Mn(CO)_2([16]aneS_4)]^+$ *m/z* = 407. ν(CO) (Me_2CO) 1956s, 1885s.

cis-$[Mn(CO)_2(\eta^4$-[15]ane$S_5)]CF_3SO_3$

As above, but using *fac*-$[Mn(CO)_3(\eta^3$-[15]ane$S_5)]CF_3SO_3$ (59 mg, 0.1 mmol). A brown solid was isolated as the required *cis*-$[Mn(CO)_2(\eta^4$-[15]ane$S_5)]CF_3SO_3$ (yield 35 mg, 68 %). Required for $[C_{13}H_{20}F_3MnO_5S_6]$: C = 27.9, H = 3.6 %; found: C = 27.5, H =

3.4 %. Electrospray mass spectrum (MeCN): found m/z = 411, 383; calculated for $[Mn(CO)_2([15]aneS_5)]^+$ m/z = 411, $[Mn(CO)([15]aneS_5)]^+$ m/z = 383. ^1H NMR: δ 2.3-3.9 (br, *m*, CH_2). $^{13}C\{^1H\}$ NMR: δ 220-225 (br, CO), 43.2, 40.9, 39.6, 38.5, 38.0, 37.9, 36.7, 33.7, 33.1, 31.1 (CH_2, each 1C). ^{55}Mn NMR: δ -980, $w_{½}$ ~12000 Hz. ν(CO) (Me_2CO) 1962s, 1885s; (CsI disk): 1967s, 1961s, 1884s cm^{-1}.

Crystallographic Studies

Details of the crystallographic data collection and refinement parameters are given in Table 2.15. Crystals of $[Mn(CO)_3(\eta^3\text{-}L)]CF_3SO_3$ (L = $[12]aneS_4$ and $[15]aneS_5$) were grown by vapour diffusion of diethyl ether into solutions of the complexes in CH_2Cl_2. Whereas crystals of $[Mn(CO)_2(\eta^4\text{-}L)]CF_3SO_3$ (L = $[12]aneS_4$, $[16]aneS_4$ and $[15]aneS_5$) were grown by vapour diffusion of light petroleum ether (40-60 °C) into solutions of the complexes in $CHCl_3$. Data collection used a Rigaku AFC7S four-circle diffractometer except for $[Mn(CO)_2([15]aneS_5)]CF_3SO_3$, for which data collection used an Enraf Nonius Kappa CCD diffractometer. Both diffractometers used graphite-monochromated Mo-Kα X-radiation (λ = 0.71073 Å) and each was equipped with an Oxford Systems open-flow cryostat operating at 150 K.

The solution[28] and refinement[29] of the structures of $[Mn(CO)_3([12]aneS_4)]CF_3SO_3$ and $[Mn(CO)_3([15]aneS_5)]CF_3SO_3$ were routine. The crystals of $[Mn(CO)_2([16]aneS_4)]$-CF_3SO_3 and $[Mn(CO)_2([15]aneS_5)]CF_3SO_3$ were rather weakly diffracting and this reflected in the relatively low number of observed reflections. The structures were solved routinely by heavy atom methods,[28] but there was insufficient data of good quality to refine all atoms anisotropically. Hence carbon atoms were refined isotropically[29] and H atoms were included in calculated positions. The structure solution of $[Mn(CO)_3([15]aneS_5)]CF_3SO_3$ was sufficient to compare geometric parameters, whereas the solution of $[Mn(CO)_3([16]aneS_4)]CF_3SO_3$ only allowed confirmation of the gross coordination architecture around the Mn(I) centre.

The crystals of $[Mn(CO)_2([12]aneS_4)]CF_3SO_3$ were also weakly diffracting and this was reflected in slightly higher than normal residuals. The structure was solved by heavy atom methods[28] and developed with iterative cycles of full-matrix least squares refinement[30] to reveal two independent cations, two independent $CF_3SO_3^-$ anions and one $CHCl_3$ solvent molecule in the asymmetric unit. One of the cations showed disorder within the macrocyclic ring, giving two ligand conformations in a 70:30 ratio. The conformations are related by C_2 rotation about an axis passing through the Mn(I) centre and bisecting the carbonyl ligands. The two components do not superimpose due to the unsymmetrical coordination of the [12]aneS_4 macrocycle, where one thioether donor is oriented in the opposite direction to the others (Section 2.2.2.2). Thus, the thioether donor atoms *trans* to the carbonyl ligands, and the carbons adjacent to these donors, have alternative positions. In order to model this disorder, it was necessary to constrain the Mn-S bond distances for the disordered donor atoms to 2.32 Å, otherwise some of the observed bond distances were unrealistically short, with others unrealistically long. All non-H atoms, except for those in the minor component, were refined anisotropically and H atoms were included in calculated positions. Although the disorder model was adequate, the structural information available from the disordered cation was of limited value, other than to support the notion of unsymmetrical coordination of the [12]aneS_4 ligand. The second cation showed no signs of disorder and therefore structural discussion and comparison of geometric parameters for this complex were based on the ordered cation alone.

Table 2.15 Crystallographic data collection and refinement parameters for $[Mn(CO)_3(L)]CF_3SO_3$ and $[Mn(CO)_2(L)]CF_3SO_3$.

	$[Mn(CO)_3([12]aneS_4)]^+$	$[Mn(CO)_3([15]aneS_5)]^+$	$[Mn(CO)_2([12]aneS_4)]^+$	$[Mn(CO)_2([15]aneS_5)]^+$	$[Mn(CO)_2([16]aneS_4)]^+$
Formula	$C_{12}H_{16}F_3MnO_6S_5$	$C_{14}H_{20}F_3MnO_6S_6$	$C_{11.5}H_{16.5}Cl_{1.5}F_3MnO_5S_5$	$C_{13}H_{20}F_3MnO_5S_6$	$C_{15}H_{24}F_3MnO_5S_5$
Formula weight	528.49	588.60	560.16	560.59	556.58
Crystal system	Triclinic	Monoclinic	Triclinic	Monoclinic	Orthorhombic
Space group	$P\bar{1}$ (# 2)	$P2_1/n$ (# 14)	$P\bar{1}$ (# 2)	$P2_1/n$ (# 14)	Pbca (# 61)
a / Å	9.4610(9)	11.420(4)	14.095(2)	10.125(2)	11.674(8)
b / Å	11.593(2)	14.642(3)	15.267(3)	8.641(2)	17.046(9)
c / Å	9.372(1)	13.605(3)	9.641(2)	24.554(5)	22.434(6)
α / °	93.56(1)	90	90.983(17)	90	90
β / °	96.581(10)	96.55(2)	90.332(14)	99.55(3)	90
γ / °	72.653(9)	90	86.531(13)	90	90
U / Å^3	974.3(2)	2260.0(9)	2070.6(6)	2118.5(8)	4464(3)
Z	2	4	4	4	8
μ(Mo-K$_\alpha$) / cm^{-1}	12.68	11.91	13.83	12.63	11.08
No. of unique reflections	3427	4168	7306	4418	6461
R_{int} (based on F^2)	0.023	0.030	0.068	0.254	0.105
No. of obs. reflections [a]	2650	2847	3708	1233	2214
No. of parameters	244	271	511	188	187
R [b]	0.027	0.072	0.066 ($R1$) [d]	0.082	0.083
R_w [c]	0.039	0.101	0.1643 (w$R2$) [e]	0.073	0.129

[a] Observed if $[I_o > 2\sigma(I_o)]$ [b] $R = \sum (|F_{obs}|_i - |F_{calc}|_i) / \sum |F_{obs}|_i$ [c] $R_w = \sqrt{[\sum w_i(|F_{obs}|_i - |F_{calc}|_i)^2 / \sum w_i|F_{obs}|_i^2}$ [d] $R1 = \sum (|F_{obs}| - |F_{calc}|) / \sum |F_{obs}|$ [e] $wR2 = \sqrt{[\sum w(|F^2_{obs}| - |F^2_{calc}|)^2 / \sum w|F^2_{obs}|^2}$

2.5 References

[1] H. Gilman, J. C. Bailie, *J. Org. Chem.*, 1937, **2**, 84.

[2] H. Gilman, R. H. Kirby, *J. Am. Chem. Soc.*, 1941, **63**, 2046.

[3] D. T. Hurd, G. W. Sentell Jr., F. J. Norton, *J. Am. Chem. Soc.*, 1949, **71**, 1899.

[4] E. O. Brimm, M. A. Lynch Jr, W. J. Sensy, *J. Am. Chem. Soc.*, 1954, **76**, 3831.

[5] F. A. Cotton, G. Wilkinson, *Chem. Ind. (London)*, 1954, 307.

[6] E. O. Fischer, R. Jira, *Z. Naturforsch., Teil B*, 1954, **9**, 618.

[7] F. A. Cotton, T. S. Piper, G. Wilkinson, *J. Inorg. Nucl. Chem.*, 1955, **1**, 165.

[8] J. M. Birmingham, F. A. Cotton, G. Wilkinson, *J. Inorg. Chem.*, 1956, **2**, 95.

[9] E. W. Abel, G. Wilkinson, *J. Chem. Soc.*, 1959, 1501.

[10] P. M. Treichel, in *Comprehensive Organometallic Chemistry*, E. W. Abel, F. G. A. Stone, G. Wilkinson (eds.), 1st edition, Pergamon, Oxford, 1982, Vol. 4, Chapter 29.

[11] P. M. Treichel, in *Comprehensive Organometallic Chemistry II*, E. W. Abel, F. G. A. Stone, G. Wilkinson (eds.), 1st edition, Pergamon, Oxford, 1995, Vol. 6, Chapter 1.

[12] W. Beck, R. E. Nitzschmann, *Z. Naturforsch., Teil B*, 1962, **17**, 577.

[13] J. R. Bleeke, J. J. Kotyk, *Organometallics*, 1985, **4**, 194.

[14] J. Connolly, G. W. Goodban, G. Reid, A. M. Z. Slawin, *J. Chem. Soc., Dalton Trans.*, 1998, 2225.

[15] J. Connolly, M. K. Davies, G. Reid, *J. Chem. Soc., Dalton Trans.*, 1998, 3833.

[16] W. Levason, S. D. Orchard, G. Reid, *Organometallics*, 1999, **18**, 1275.

[17] W. Levason, S. D. Orchard, G. Reid, *J. Chem. Soc., Dalton Trans.*, 1999, 823.

[18] M. K. Davies, M. C. Durrant, W. Levason, G. Reid, R. L. Richards, *J. Chem. Soc., Dalton Trans.*, 1999, 1077.

[19] J. Connolly, A. R. J. Genge, W. Levason, S. D. Orchard, S. J. A. Pope, G. Reid, *J. Chem. Soc., Dalton Trans.*, 1999, 2343.

[20] H. Elias, H.–J. Küppers, B. Nuber, M. Saher, G. Schmidt, J. Weiss, K. Wieghardt, *Inorg. Chem.*, 1989, **28**, 3021.

[21] B. Patel, G. Reid, *J. Chem. Soc., Dalton Trans.*, 2000, 1303.

[22] G. A. Carriedo, V. Riera, M. L. Rodríguez, J. J. Sainz-Velicia, *Polyhedron*, 1987, **6**, 1879.

[23] M. P. Gamasa, J. Gimeno, M. Laguna, V. Riera, R. Usón, *J. Chem. Soc., Dalton Trans.*, 1979, 996.

[24] S. R. Cooper, S. C. Rawle, *Struct. Bonding (Berlin)*, 1990, **72**, 1.

[25] P. J. Blower, G. E. D. Mullen, A. K. Powell, M. J. Went, S. Wocadlo, *Angew. Chem., Int. Ed. Engl.*, 1997, **36**, 1205.

[26] H. Berke, G. Weiler, *Z. Naturforsch, Teil B*, 1984, **39**, 431.

---

[27] R. J. Angelici, K. J. Reimer, A. Shaver, M. H. Quick, *Inorg. Synth.*, 1978, **19**, 159.

[28] PATTY, The DIRDIF Program System, G. Admiraal, G. Beurskens, P. T. Beurskens, W. P. Bosman, S. Garcia-Granda, R. O. Gould, J. M. M. Smits, C. Smykalla, Technical Report of the Crystallography Laboratory, University of Nijmegen, 1992.

[29] TeXsan, Crystal Structure Analysis Package, Molecular Structure Corporation, Houston, Texas, 1995.

[30] SHELXL 97, G. M. Sheldrick, University of Göttingen, 1997.

Chapter 3

Titanium (IV) Halide Complexes with Bidentate Thio- and Seleno-ether Ligands

3.1 Introduction

The small ionic radius and high positive charge associated with the Ti(IV) centre makes for an extremely hard Lewis acid. Thus, the coordination chemistry of Ti(IV) is dominated by that involving hard Lewis bases, such as N- and O-donor ligands.[1,2] Consequently, one would expect coordination with soft donor ligands such as thioethers to be unfavoured. Indeed, a thermodynamic study of the stability of $TiCl_4$ adducts with tetrahydrofuran (THF) and tetrahydrothiophene (THT) showed stronger coordination of the O-donor compared to the S-donor,[3] although the small difference in coordination strengths suggests Ti(IV) is a softer acceptor than its position in the periodic table would imply. Other examples of thioether coordination with Ti(IV) have also presented some rather unexpected conclusions. Thus, a series of complexes $[TiX_4(L)]$ and $[TiX_4(L)_2]$ (X = Cl, Br) have been synthesised involving the potentially bidentate cyclic ligands, L = 1,4-dioxan ($C_4H_8O_2$), 1,4-thioxan (C_4H_8OS) and 1,4-dithian ($C_4H_8S_2$).[4,5] IR spectroscopy of the $[TiX_4(L)]$ complexes suggests the ligands bridge two Ti(IV) centres to give a polymeric structure with 6-coordinate titanium (Figure 3.1). However, IR spectra of the $[TiX_4(L)_2]$ complexes show only monodentate coordination of the ligand to present monomeric 6-coordinate Ti(IV) (Figure 3.1). Notably, the spectra of the bis-1,4-thioxan complexes show C-O-C stretching modes unaltered from the free ligand, whereas the C-S-C stretching modes are shifted to low frequency. This, together with ^1H NMR spectroscopic data showing a greater shift to high frequency for protons adjacent to the S-donor compared to those adjacent to the O-donor, shows thioether coordination is preferred over ether coordination for these ligands. Similarly, selenoether coordination is observed in the 1,4-selenoxan adduct $[TiCl_4(C_4H_8SeO)_2]$.[6]

Figure 3.1 Predicted structures of $[TiCl_4(L)]$ and $[TiCl_4(L)_2]$ for L = 1,4-dioxan, 1,4-thioxan and 1,4-dithian (E = S, Se; taken from refs. 4 and 5).

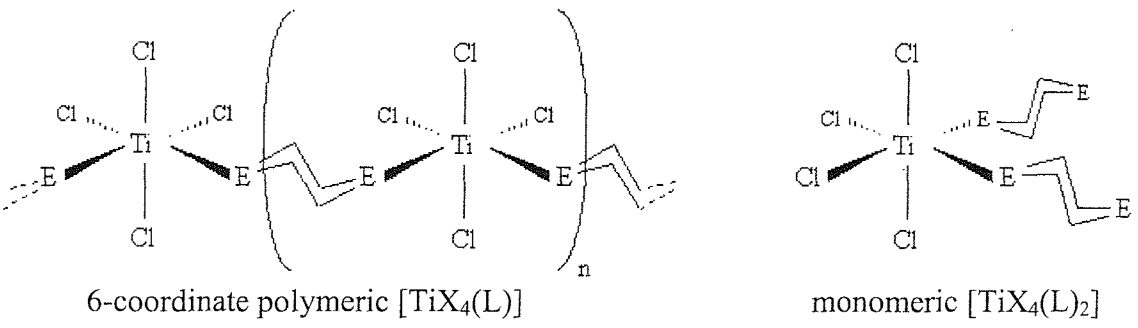

6-coordinate polymeric $[TiX_4(L)]$

monomeric $[TiX_4(L)_2]$

Further examples showing preferential coordination of thioethers over ethers with Ti(IV) are presented in the series of $TiCl_4$ adducts involving the potentially tridentate ligands MeC(X)(Y)(Z) [X = Y = Z = CH_2OMe; X = Y = CH_2OMe, Z = CH_2SMe or CH_2NMe_2; X = CH_2OMe, Y = CH_2SMe, Z = CH_2NMe_2].[7] ^1H VT-NMR spectroscopy shows the presence of an uncoordinated donor, suggesting the ligands act as bidentates only to give 6-coordinate $[TiCl_4\{\eta^2\text{-}MeC(X)(Y)(Z)\}]$. When all three donor types are present, the major product observed shows the expected coordination of the hard N- and O-donor atoms, with the thioether remaining uncoordinated. However, a second product is also observed in significant proportion, with thioether coordinated in preference to the O-donor. Furthermore, the complex involving $MeC(CH_2OMe)_2(CH_2SMe)$ shows coordinated S-donor and a free O-donor as the major product. These results suggest thioether coordination may be preferred over ether coordination for these ligands, however the absence of structural characterisation prevents conclusive determination.

The above examples suggest there is little disparity between the coordination of thioethers, selenoethers and ethers with TiX_4 (X = Cl, Br) for certain ligand types, indicating Ti(IV) may be of softer character than implied by the hard-soft acid-base (HSAB) principle (see Chapter 1).[8] Thus, there was immediate interest in investigating the coordination of S-donor ligands with Ti(IV) following the synthesis of the above 1,4-thioxan and 1,4-dithian complexes in 1964. Examples of the early reported complexes include $[TiX_4(L')_2]$ for L′ = monodentate thiols (EtSH, ^{n}PrSH, ^{n}BuSH and PhSH, X = Cl);[9] monodentate thioethers (Me_2S and Et_2S, X = Cl);[10] and cyclic thioethers $\{(CH_2)_nS$ for n = 3-5, X = Cl, Br$\}$.[11] However, characterisation of these complexes was restricted to melting points, elemental analyses and IR spectroscopy only. Various $[TiX_4(L'')]$ complexes have also been reported for L″ = bidentate thiols (ethane-1,2-dithiol, propane-1,2-dithiol and propane-1,3-dithiol, X = Cl);[9] bidentate thioethers $\{RS(CH_2)_2SR$ for R = Me, Et and Ph, X = Cl, Br$\}$;[12] and monodentate cyclic thioethers $\{(CH_2)_nS$ for n = 3-5, X = Cl, Br$\}$.[11] Again, spectroscopic characterisation of these complexes is very limited, with no detailed solution or structural studies reported. Complexes involving Se-donor coordination are much less common, with $[TiCl_4(L)]$ (L = Et_2Se,[10] $Me_2Se(CH_2)_2SeMe$ and $Me_2Se(CH_2)_3SeMe$[13]) among the few early examples.

The above complexes are all extremely moisture sensitive, brightly coloured (red-yellow) complexes, most involving 6-coordinate Ti(IV). This moisture sensitivity may be responsible for the very limited spectroscopic characterisation reported for these early complexes. It was 1987 before the first multinuclear NMR studies were reported, providing confirmation of the *cis* coordination of $[TiX_4(L)_2]$ (L = Me_2E, E = S, Se, X = Cl, Br).[14] Kinetic studies investigating the *cis-trans* isomerisation of these complexes suggest the halide ligands preferentially reside *trans* to the chalcogenoether ligands, whereas the equivalent Sn(IV) adducts form both *cis* and *trans* isomers. It was proposed that the determining factor for *cis*-TiX_4 adducts was the possibility X–Ti $p_\pi \rightarrow d_\pi$ bonding, utilising empty Ti(IV) *d*-orbitals. Thus, as chalcogenoethers do not strongly participate in π-bonding (Chapter 1), the *trans* halides experience no competition for the *d*-orbitals. For d^{10} Sn(IV), X–Sn $p_\pi \rightarrow d_\pi$ bonding is not significant and hence both *cis* and *trans* isomers are observed. The chemistry of Sn(IV) provides a good comparison to Ti(IV) as both are hard Lewis acids with very similar covalent and ionic radii.

Only recently have a limited number of Ti(IV) halide adducts with thio- or seleno-ether ligands been structurally characterised, with $[TiCl_2(NBu^t)([9]aneS_3)]$ reported as the first such macrocyclic complex.[15] The structure shows octahedral geometry at Ti(IV), with Ti-S bond lengths *trans* to NBu^t significantly longer than the *cis* Ti-S distances, consistent with the well known *trans* influence of the imido ligand.[16] Octahedral geometry at Ti(IV) has also been observed for the complexes $[TiCl_4(L)_2]$ (L = $C_6H_{11}SH$,[17] C_4H_8S,[18] Me_2Se and Et_2Se).[19] The structures confirm the adducts are monomeric with *cis* coordination of the monodentate donor ligands, as assigned *via* IR spectroscopy in the early reported syntheses. Accompanying these structures was the reported synthesis of $TiCl_4$ adducts with MeSSMe,[18] MeSeSeMe and EtSeSeEt.[19] Structural characterisation of two of these complexes (Figure 3.2) show the ligands bridge two Ti(IV) centres with 6-coordination accomplished *via* bridging chloride ligands to give $[\{Cl_3Ti\}_2(\mu\text{-}Cl)_2(\mu\text{-}L')]$ (L′ = MeSSMe, EtSeSeEt). This bridging geometry may be attributed to the inability of the dichalcogenide ligand to chelate.

These dichalcogenide Ti(IV) adducts are examples of a relatively new class of compounds used as single source precursors to titanium dichalcogenide materials. Pure, crystallographically orientated thin films of these materials are desirable due to their potential as high-energy cathode materials in rechargeable lithium batteries.[20,21,22,23] Conventional routes to TiS_2 include the vapour phase reaction of $TiCl_4$ with organo-thiols, -sulfides and -disulfides *via* high temperature and/or high pressure chemical vapour deposition (CVD).[24,25] Single source precursors have pre-formed Ti-E (E = S, Se) interactions, hence eliminating the need for two-phase CVD and the problems associated with mixing gases at low pressures. Indeed, TiS_2 thin films have been formed by this method at atmospheric pressure and at reduced temperatures.[26] Similarly $TiSe_2$ films, previously unattainable *via* two-phase CVD, have been formed by this method.

Figure 3.2 View of the structure of [$(TiCl_4)_2$(MeSSMe)] (taken from ref. 18)

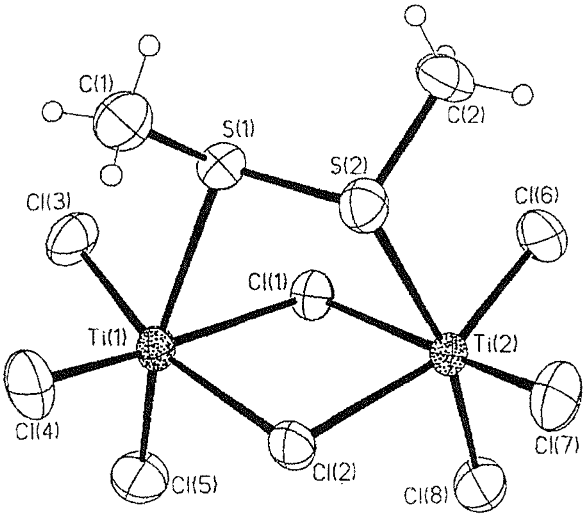

This chapter investigates the coordination chemistry of bidentate thio- and seleno-ether ligands with titanium halides, with a view to producing new single source precursors to titanium dichalcogenide materials. The volatility of these adducts and the deposition orientations of the TiE_2 (E = S, Se) films formed *via* thermal decomposition are expected to vary with the halogen and ligand structure. Thus, reported within is the synthesis and spectroscopic characterisation of a series of TiX_4 (X = Cl, Br and I) complexes with various bidentate thio- and seleno-ether ligands [$MeE(CH_2)_nEMe$, $PhE(CH_2)_2EPh$ and *o*-$C_6H_4(EMe)_2$ for E = S or Se, n = 2 or 3].[27] The complexes are characterised by elemental analysis and IR, UV-visible and multinuclear (^1H, $^{13}C\{^1H\}$, $^{77}Se\{^1H\}$) NMR spectroscopy. X-ray single crystal structure determinations are reported for the complexes [$TiCl_4(L)$] {L = $MeS(CH_2)_2SMe$, $MeS(CH_2)_3SMe$, $MeSe(CH_2)_3SeMe$ and *o*-$C_6H_4(SeMe)_2$} in order to establish the effects of changing the donor atom and ligand backbone on the metal-donor interaction. A brief discussion on the decomposition of these complexes is also reported, including the structural characterisation of the partially hydrolysed oxo-bridged binuclear adduct, [$(\{MeS(CH_2)_2SMe\}Cl_3Ti)_2(\mu\text{-}O)$].

3.2 Results and Discussion

Reaction of $TiCl_4$ with one molar equivalent of bidentate thio- or seleno-ether ligand, L_2 [L_2 = $MeE(CH_2)_nEMe$, $PhE(CH_2)_2EPh$, *o*-$C_6H_4(EMe)_2$ for E = S or Se, n = 2 or 3] in rigorously anhydrous *n*-hexane at room temperature resulted in the immediate precipitation of bright yellow, orange or red solids, [$TiCl_4(L_2)$], in high yield (Figure 3.3). Similarly, dissolution of $TiBr_4$ in rigorously anhydrous CH_2Cl_2 followed by addition of one molar equivalent of L_2' [L_2' = $MeE(CH_2)_nEMe$, *o*-$C_6H_4(EMe)_2$ for E = S or Se, n = 2 or 3] afforded deep orange and red solutions of [$TiBr_4(L_2')$]. Again, intensely coloured solids were isolated in high yield *via* precipitation with *n*-hexane. As expected, reactions of TiI_4 were less straightforward due to its poor solubility in non-coordinating solvents and much poorer acceptor properties. Hence, deep purple TiI_4 solutions were prepared *via* partial dissolution in comparatively large volumes of mildly refluxing CH_2Cl_2 and subsequent filtration to remove any undissolved material. Addition of one molar equivalent of L_2'' [L_2'' = $MeE(CH_2)_2EMe$, *o*-$C_6H_4(EMe)_2$ for E = S or Se] resulted in significant colour changes to give dark red/brown solutions of [$TiI_4(L_2'')$]. The products proved particularly difficult to isolate as solids, with the thioether complexes affording only oily residues unsuitable for characterisation. The selenoether adducts were isolated as deep red powdered solids *via* precipitation with *n*-hexane, though in considerably lower yields than the $TiCl_4$ and $TiBr_4$ adducts.

Figure 3.3 Reaction scheme for the synthesis of [$TiX_4(L_2)$], X = Cl, Br, I.

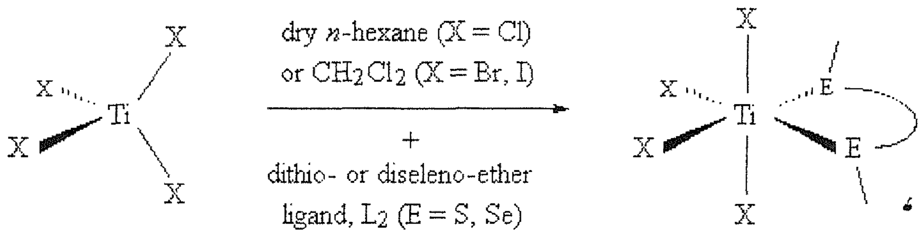

All of the isolated complexes are extremely moisture sensitive, liberating the free ligand and rapidly decolourising almost immediately upon exposure to moist air. Similarly rapid hydrolysis has been observed for the related class of Ti(IV) complexes, [$TiCl_3Me(L)$] for L = $MeO(CH_2)_2OMe$, $MeS(CH_2)_2SMe$ and $Me_2N(CH_2)_2NMe_2$.[28] Here the O- and S-donor adducts are hydrolysed almost immediately on exposure to moist air. Even reaction with the more stable group 15 N-donor adduct is fast, with hydrolysis becoming apparent within one minute. Therefore, the compounds isolated here were routinely handled and stored in a dry, continuously N_2-purged glove box, under which conditions, the solids remained stable and showed no signs of decomposition over a few months. $[TiCl_4\{PhSe(CH_2)_2SePh\}]$ was the sole exception and decolourised within one month, thus its decomposition behaviour was further investigated (Section 3.2.4).

The formulation of the complexes as $[TiCl_4(L_2)]$, $[TiBr_4(L_2')]$ and $[TiI_4(L_2'')]$ was confirmed *via* microanalytical data. With five naturally abundant titanium isotopes providing a distinctive signature for titanium adducts, mass spectrometry was conducted on a number of representative complexes to confirm the molecularity of the products. However, electrospray mass spectrometry resulted only in ligand displacement by the MeCN carrier solution. While various vapour phase techniques (chemical ionisation, electron ionisation and MALDI) afforded only peaks corresponding to ionised free ligand, TiX_4^+ (X = Cl, Br) and sequential loss of halide. These results are consistent with the expected weak interaction between soft chalcogenoether ligands and the hard Ti(IV) centre being insufficient to withstand either dissolution in coordinating solvents or the high energy ionisation conditions of the vapour phase techniques. Similarly unsuccessful electron ionisation mass spectroscopy have been reported for the Ti(IV) adducts $[TiCl_4(RSH)]$ (R = Et, ^{n}Pr, ^{n}Bu, Ph) and $[TiCl_4\{HS(CH_2)_nSH\}]$ (n = 2, 3).[9]

The successful isolation of the above titanium halide thio- and seleno-ether complexes prompted a study of telluroether coordination with Ti(IV). Thus, $TiCl_4$ was added to a solution of $MeTe(CH_2)_3TeMe$ and o-$C_6H_4(TeMe)_2$ in *n*-hexane at 0 °C, resulting in the immediate precipitation of brown solids. However, microanalytical data indicated a complicated mixture of titanium chloride and chlorinated telluroether ligand, similar to that reported during the attempted synthesis of $[TiCl_4(Et_2Te)_2]$.[10] These results are not surprising as the poor interaction between the contracted orbitals of the hard Ti(IV) centre and the diffuse orbitals of the soft Te donor may prevent the formation of Ti-Te interactions. Telluroether coordination with Ti(IV) has been reported recently, with reaction of $TiCl_4$ with the tellurium-bridged chelating bis(aryloxo) ligand, L_3 = 2,2′-Te(4-Me-6-^{t}Bu-$C_6H_2O)_2$ affording chloride bridged $[\{Cl(L_3)Ti(\mu\text{-}Cl)\}_2]$.[29] Structural characterisation (Figure 3.4) shows coordination of the peripheral O-donors places the Te-donor in close proximity to the Ti(IV) centre, thus promoting interaction.

Figure 3.4 View of the structure of [{Cl(L_3)Ti(μ-Cl)}$_2$] (taken from ref. 29)

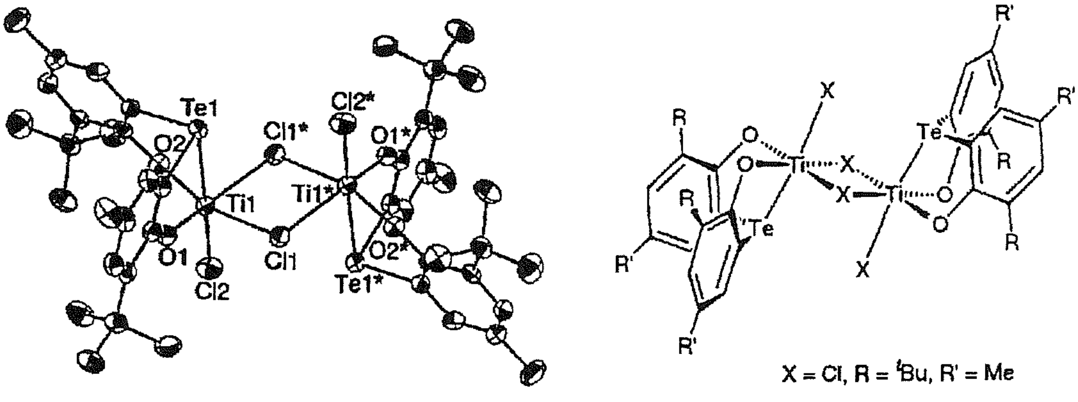

3.2.1 *IR and UV-visible spectroscopy*

Although the small chain lengths of the ligands used dictates only *cis* coordination when chelating, *trans* coordination of two bridging ligand molecules may be observed in a polymeric structure (Figure 3.5). In the latter, the D_{4h} local symmetry around the Ti(IV) centre would present only one IR active titanium-halide stretching vibration, E_u. For *cis* coordination, the complex has C_{2v} symmetry and hence exhibits four such vibrations, $2A_1 + B_1 + B_2$. The number of Ti-X stretching vibrations observed should therefore determine which molecular structure is formed. However, as *cis* coordination at Ti(IV) could also be attained *via* bridging ligand molecules, for example [Cl_4Ti{μ-L_2}$_2TiCl_4$], X-ray crystallographic studies have been undertaken to unequivocally confirm the coordination geometry at Ti(IV) (Section 3.2.3).

Figure 3.5 View of two of the possible binding modes of the bidentate ligands.

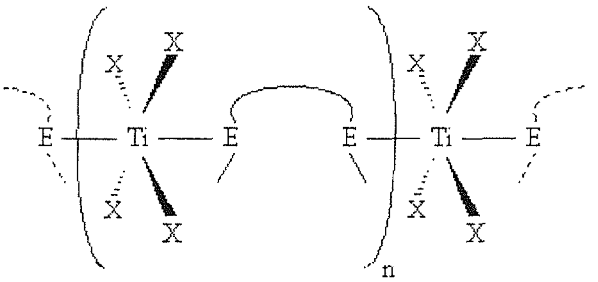

polymeric *trans*-[$TiX_4(L_2)$]

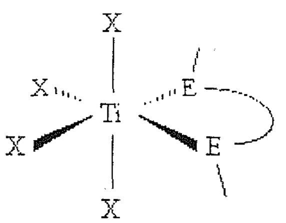

monomeric *cis*-[$TiX_4(L_2)$]

Far IR data were collected for the [$TiX_4(L_2)$] (X = Cl, Br) adducts, with the high sensitivity of the complexes dictating the use of sodium dried-Nujol mulls pressed between CsI plates. All of the spectra showed four overlapping Ti-X stretching vibrations (Figure 3.6), thus confirming the formulation as *cis*-[$TiX_4(L_2)$]. The observed stretching frequencies of 420-370 cm^{-1} for ν(Ti-Cl) and 330-290 cm^{-1} for ν(Ti-Br) compare well with those reported for similar thioether complexes [$TiX_4(L)_2$], L = $(CH_2)_nS$, n = 3-5 [420-380 and 318-306 cm^{-1} for X = Cl, Br respectively].[11] IR spectroscopy of the TiI_4 adducts showed no metal-halogen stretching vibrations down to 220 cm^{-1}, though this is not surprising as the far IR spectrum of TiI_4 shows all but one of the Ti-I stretching and bending modes occur below 200 cm^{-1}.[30]

Figure 3.6 ν(Ti-Cl) region of [$TiCl_4\{MeSe(CH_2)_2SeMe\}$] IR spectrum (Nujol mull).

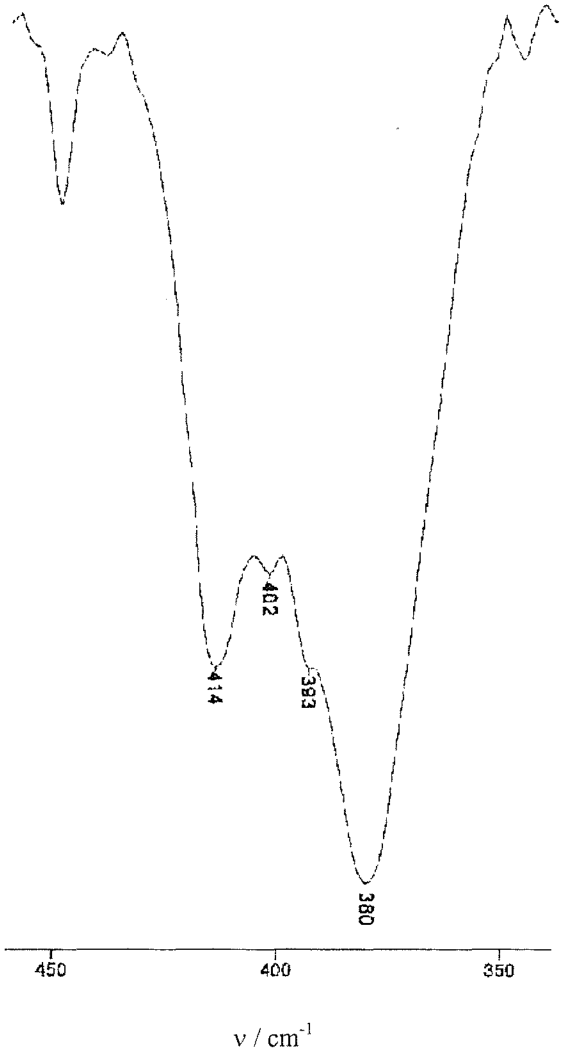

The intense colours of the solids isolated as [$TiX_4(L_2)$] indicate the presence of strong electronic transitions within the complexes. As Ti(IV) is d^0, metal-ligand and *d-d* transitions are not possible, hence any observed transitions can be unambiguously defined as ligand-metal charge transfer (LMCT) transitions. Attempts to collect solution phase electronic spectra using Schlenk quartz cells and rigorously anhydrous CH_2Cl_2 resulted only in the rapid hydrolysis of the small concentrations of compounds necessary. Thus, spectra were recorded by diffuse reflectance, using anhydrous $BaSO_4$ as the inert diluent. The resulting spectra for the chloro-adducts showed several broad, but resolved intense LMCT transitions, whereas those of the bromo-adducts were ill defined and overlapping. This is not surprising since on electronegativity grounds the electronic transition $\pi(Cl) \rightarrow Ti(t_{2g})$ is likely to be quite different from $\pi(S \text{ or } Se) \rightarrow Ti(t_{2g})$, whereas $\pi(Br) \rightarrow Ti(t_{2g})$ is probably more comparable with the S and Se transitions. Thus, the data shows $\pi(Cl) \rightarrow Ti(t_{2g})$ transitions at *ca.* 28500 cm^{-1}, $\pi(Br) \rightarrow Ti(t_{2g})$ at *ca.* 22500 cm^{-1}, $\pi(S) \rightarrow Ti(t_{2g})$ at *ca.* 22000 cm^{-1} and $\pi(Se) \rightarrow Ti(t_{2g})$ at *ca.* 21000 cm^{-1}. Although these values are subject to large errors (± 1000 cm^{-1}) due to the broad nature of the observed bands, the halide transitions do compare well with the lowest energy $\pi(X) \rightarrow Ti(t_{2g})$ LMCT transitions in similar Ti(IV) adducts $[TiX_6]^{2-}$ [*ca.* 28000 cm^{-1}, X = Cl; 22000 cm^{-1}, X = Br].[31] Furthermore, comparison of the data with the transitions predicted using the Pauling scale of optical electronegativities,[32] shows good correlation within the errors of the Pauling values and hence confirms the donor types present. These data, together with the above IR spectroscopic and microanalytical data, confirm the formulation of the products as *cis*-[$TiX_4(L_2)$].

3.2.2 Multinuclear NMR spectroscopy

As discussed in Chapters 1 and 2, pyramidal inversion at the chalcogen leads to diastereoisomers (invertomers) for chalcogenoether ligands that chelate to metal centres. Multinuclear NMR spectroscopy can provide valuable information regarding the two NMR distinguishable sets of invertomers (*meso* and *DL* pair, Figure 3.7), provided pyramidal inversion and dissociation of the ligand are slow on the NMR time scale. Thus, ^1H, $^{13}C\{^1H\}$ and where appropriate, $^{77}Se\{^1H\}$ NMR spectroscopic studies were undertaken for the complexes [$TiX_4(L_2)$] for X = Cl, Br, I.

Figure 3.7 View of the possible invertomers for *cis*-[$TiX_4(L_2)$] (E = S, Se).

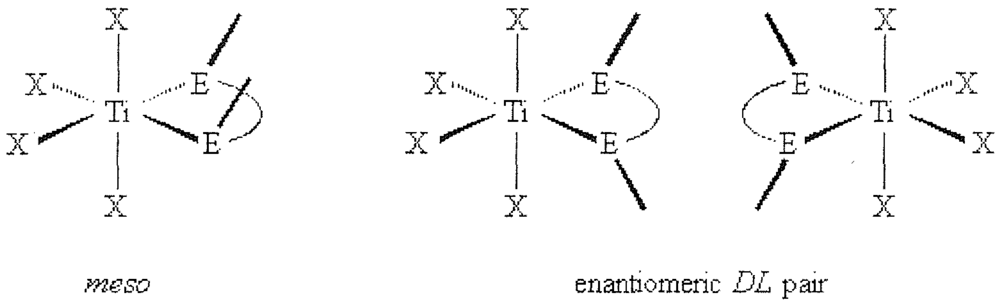

The room temperature ^{1}H NMR spectra of the $TiCl_4$/dithioether adducts showed sharp resonances with the expected coupling patterns corresponding to H-environments of the respective ligands (Figure 3.8). Analysis of the chemical shifts reveals a high frequency shift upon ligand coordination, consistent with the reduced electron density at the thioether following σ-donation to the Ti(IV) centre (see Chapter 1). The absence of resonances due to different invertomers may be attributed to one of three factors. Either one invertomer is energetically favoured to the exclusion of the other, the system is exhibiting fast ligand exchange or fast pyramidal inversion is occurring. The reported variable temperature ^{1}H NMR studies of the Ti(IV) complex [$MeTiCl_3\{MeS(CH_2)_2$-SMe}] has shown sharp resonances at room temperature that resolve to reveal individual invertomers at low temperatures (−100 °C).[28] This suggests the room temperature system is probably exhibiting rapid inversion at the thioether. The $TiCl_4$/dithioether adducts formed here are expected to show similar behaviour, consistent with the low-energy barrier to inversion for coordinated thioether donors (see Chapter 1).[33] The ^{1}H NMR spectra for the selenoether adducts support this, showing similar shifts to high frequency upon coordination, though with significantly broader resonances than for the thioether adducts (Figure 3.8). This suggests pyramidal inversion is slower than the high temperature limiting case, consistent with the higher activation energies for inversion at selenoethers compared to thioethers.[33]

The ^{1}H NMR spectra for the bromo-adducts showed much broader resonances with less resolved splitting patterns (Figure 3.8). This broadening may be attributed to the increased activation energy for inversion at the chalcogen due to the poorer acceptor ability of $TiBr_4$, as shown by the reduced shift to high frequency shift compared with the above chloro-adducts. Thus the planar transition state is less stabilised (see Chapter 1) and may slow pyramidal inversion below the high temperature limiting case to present broad coalesced resonances from the different invertomers. Furthermore, the weaker interaction between the chalcogenoether and the poorer $TiBr_4$ acceptor may also lead to resonance broadening *via* ligand dissociation.

The ^1H NMR spectra for the iodo-adducts revealed resonances even less shifted to high frequency compared with the chloro- and bromo-adducts. This is again consistent with the even poorer acceptor properties of TiI_4 removing less electron density from the chalcogenoether donors. Indeed, the observed resonances were reasonably sharp, which may indicate that the H-environments from the coordinated and uncoordinated ligand are averaged due to rapid ligand exchange, and thus rendering comparison of chemical shifts for these adducts meaningless.

Figure 3.8 Comparison of RT ^1H NMR spectra for a) $[TiCl_4\{MeS(CH_2)_3SMe\}]$, b) $[TiBr_4\{MeS(CH_2)_3SMe\}]$ and c) $[TiCl_4\{MeSe(CH_2)_3SeMe\}]$ ($CDCl_3$).

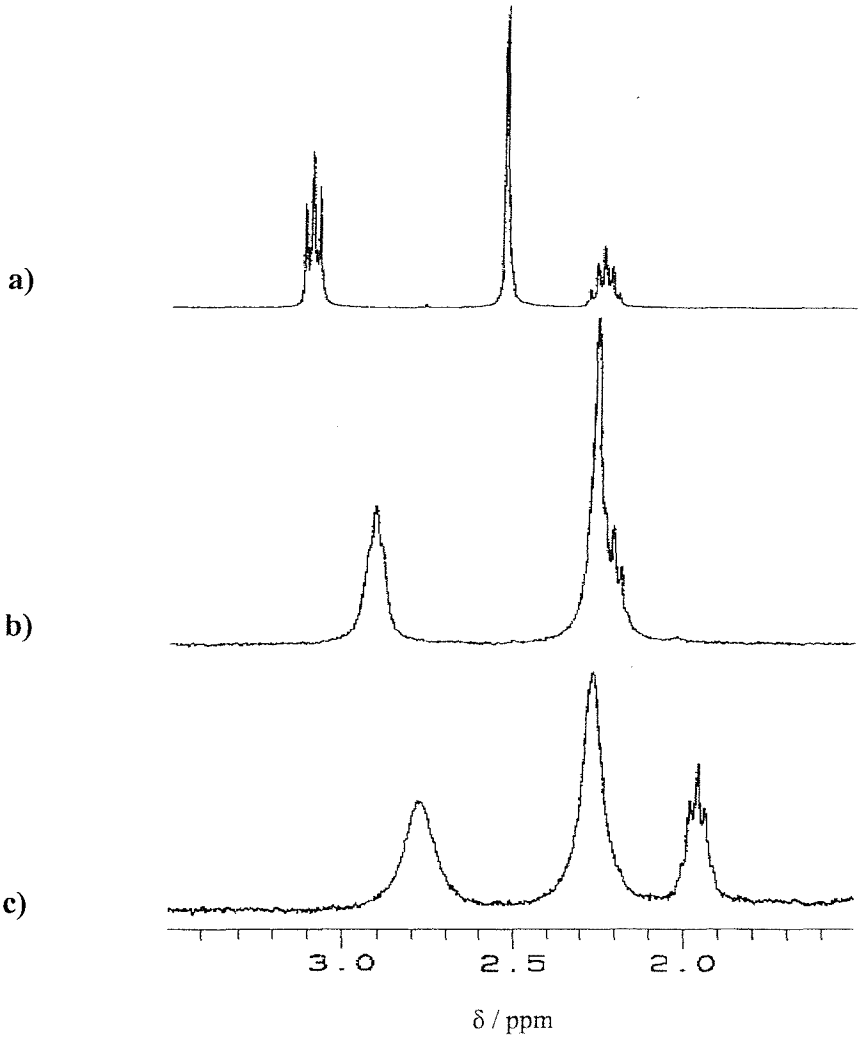

Although low temperature ^{1}H NMR spectroscopy can show the relative contributions of pyramidal inversion and/or ligand dissociation in the above $[TiX_4(L_2)]$ adducts, this was not employed due to the expected increased complexity and possible overlapping of coupled resonances at low temperatures. Thus, variable temperature $^{13}C\{^{1}H\}$ and $^{77}Se\{^{1}H\}$ NMR spectroscopy were employed to further investigate these dynamic processes. NMR spectroscopy of the metal centre nucleus has been informative in previously reported studies of the SnX_4 adducts with Group 16 ligands.[34,35] Hence, $^{47/49}Ti$ NMR spectroscopy was attempted in order to probe the bonding characteristics of the thio- and seleno-ether ligands in the Ti(IV) complexes formed here. $^{47/49}Ti$ NMR spectroscopy has been previously reported in the study of *cis-trans* isomerisation of $[TiCl_4\{(MeO)_3PO\}_2]$ at room temperature.[14] However, the quadrupolar spin states and low relative receptivities of the NMR active nuclei, ^{47}Ti (7.28 %, $I = {}^{5}/_{2}$, $D_p = 1.5 \times 10^{-4}$) and ^{49}Ti (5.51 %, $I = {}^{7}/_{2}$, $D_p = 2.1 \times 10^{-4}$), make acquisition of these data difficult. Thus, although both ^{47}Ti and ^{49}Ti resonances were observed at room temperature for a test solution of $[(\eta^{5}\text{-}C_5H_5)_2TiCl_2]$ in $CH_2Cl_2/CDCl_3$, cooling led to a broadening and eventual loss of the signal, presumably due to the quadrupole. Furthermore, no resonances were observed either at room temperature or on cooling for the thio- and seleno-ether $[TiX_4(L_2)]$ complexes formed here. This unfortunately rendered $^{47/49}Ti$ NMR spectroscopy of no use for these Ti(IV) adducts.

3.2.2.1 Dithio- and diseleno-ether adducts of $TiCl_4$

The room temperature $^{13}C\{^{1}H\}$ NMR spectra of the $TiCl_4$/dithioether adducts reveal sharp resonances corresponding to only one conformation of the ligand (Figure 3.9), consistent with the high temperature limiting case of pyramidal inversion. The resonances are significantly shifted to high frequency indicating the reduced electron density at the thioether following σ-donation to the Ti(IV) centre. The equivalent spectra for the diselenoether adducts show similar shifts to high frequency, though with significant broadening of the resonances. This indicates that pyramidal inversion is slower in the diselenoether adducts, consistent with the higher activation energy for inversion at coordinated selenoethers compared with thioethers.[33] These data parallel the conclusions from the room temperature ^{1}H NMR spectroscopy of these adducts.

Figure 3.9 VT $^{13}C\{^1H\}$ NMR spectroscopy of $[TiCl_4\{MeS(CH_2)_2SMe\}]$

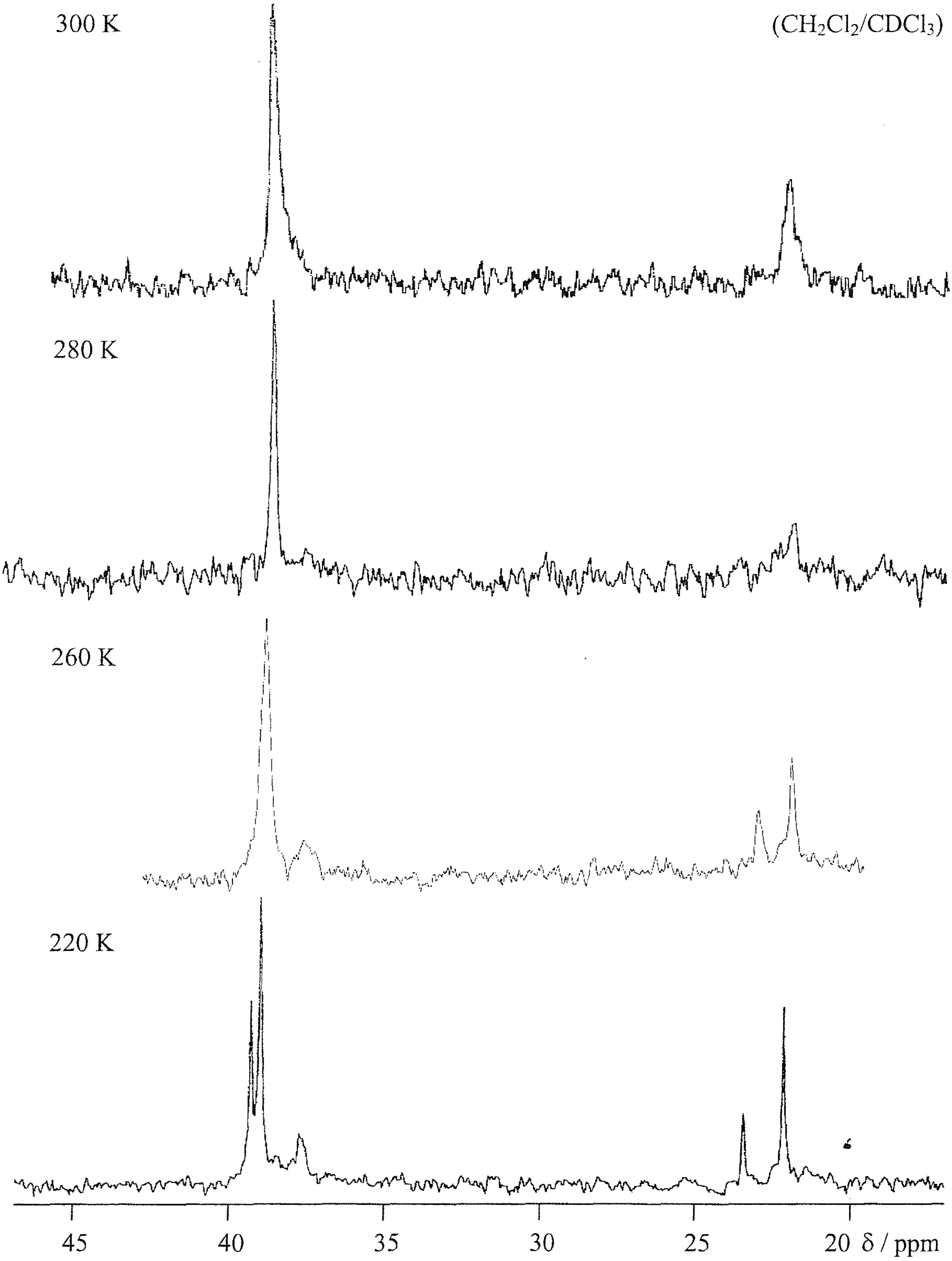

Lowering the temperature slows the pyramidal inversion process and gradually reveals resonances due to the individual invertomers. Figure 3.9 shows the variable temperature $^{13}C\{^1H\}$ NMR spectra for $[TiCl_4\{MeS(CH_2)_2SMe\}]$. Thus, at room temperature, two resonances are observed corresponding to the methyl (δ 23.2) and methylene (δ 38.9) carbon environments. Cooling down to 260 K shows pyramidal inversion has slowed sufficiently to show broad resonances due to the individual invertomers. While cooling further to 220 K stops pyramidal inversion on the NMR time scale and shows four sharp resonances due to the *meso* and *DL* forms of the methyl (δ 22.2, 23.5) and methylene (δ 39.1, 39.4) carbon environments. Similarly, variable temperature ^{77}Se{^{1}H} NMR spectroscopy also revealed the presence of individual invertomers on cooling. Thus, the room temperature ^{77}Se{^{1}H} NMR spectra for the $TiCl_4$/selenoether adducts showed no ^{77}Se resonances due to fast pyramidal inversion; whereas spectra at 200 K revealed two ^{77}Se resonances of varying intensity (Figure 3.10). The low temperature spectra of all the $TiCl_4$ adducts have also revealed a large variation in the ratio of *meso/DL* invertomers, ranging from almost 1 : 1 for [$TiCl_4${*o*-$C_6H_4(EMe)_2$}] (E = S, Se) to *ca.* 8 : 1 for [$TiCl_4${$MeSe(CH_2)_3SeMe$}].

The role of ligand dissociation in solution for the $TiCl_4$ adducts was also investigated *via* ^{13}C{^{1}H} NMR spectroscopy. Thus, a solution of $MeS(CH_2)_2SMe$ and [$TiCl_4${$MeS(CH_2)_2SMe$}] showed broad ^{13}C{^{1}H} resonances corresponding to coordinated [δ 22 (Me), 39 (CH_2)] and uncoordinated [δ 18 (Me), 35 (CH_2)] ligand at room temperature. The fact that resonances were observed for both free and coordinated ligand suggests ligand exchange is slow at room temperature on the NMR time-scale. Cooling to 250 K results in the resolution of *meso/DL* invertomers for the coordinated ligand [δ 22.0, 23.5 (Me), 39.0, 39.3 (CH_2)] and reveals no significant frequency shift for the free ligand [δ 16.0 (Me), 33.0 (CH_2)]. There was also no evidence for the formation of the 8-coordinate species [$TiCl_4${$MeS(CH_2)_2SMe$}$_2$] *via in situ* reaction with excess ligand. Although similar addition of free ligand was not performed for all complexes, most of the low temperature spectra show an absence of resonances due to uncoordinated ligand, suggesting ligand exchange is not significant in these adducts. However, the low temperature (200 K) ^{13}C{^{1}H} NMR spectra of the adducts involving $MeE(CH_2)_3EMe$, E = S, Se, did show very weak resonances corresponding to free ligand. Presumably, the less favoured 6-membered chelate ring formed on the coordination of these ligands presents more labile ligands capable of room temperature ligand dissociation.

Figure 3.10 LT ^{77}Se{^{1}H} NMR spectrum of [$TiCl_4${$MeSe(CH_2)_3SeMe$}]

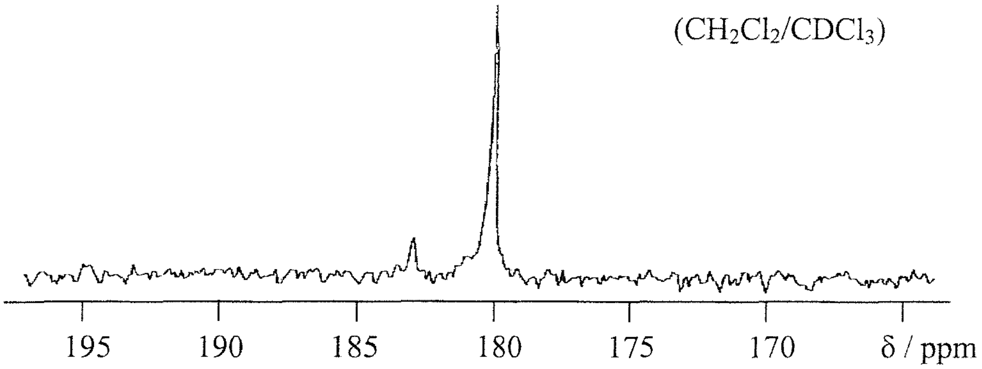

3.2.2.2 Dithio- and diseleno-ether adducts of $TiBr_4$

Following the observed trends from ^{1}H NMR spectroscopy, it was expected that the Ti(IV) adducts would show increasingly dynamic behaviour in solution with decreasing Lewis acidity of the TiX_4 adduct. Indeed, the room temperature ^{13}C{^{1}H} and ^{77}Se{^{1}H} NMR spectra of the $TiBr_4$ thio- and seleno-ether adducts gave no observable resonances corresponding to either free or coordinated ligand, suggesting the presence of dynamic processes in solution. Cooling to 200 K slowed these processes sufficiently to observe weak ^{13}C{^{1}H} resonances shifted to high frequency corresponding to coordinated ligand, with the individual invertomers observed in most cases. In addition, the spectra also showed strong resonances corresponding to uncoordinated ligand. For example, the ^{13}C{^{1}H} NMR spectrum of [$TiBr_4${o-$C_6H_4(SeMe)_2$}] (Figure 3.11) shows resonances corresponding to free o-$C_6H_4(SeMe)_2$ [δ 8.1 (Me); 126.7, 129.2 (o-C_6H_4)] and the *meso* and *DL* invertomers of the coordinated ligand [δ25.5, 25.9 (Me); 131.3, 134.5 (o-C_6H_4, invertomers not resolved)]. This suggests that fast ligand exchange is occurring at room temperature, giving rise to an equilibrium between [$TiBr_4(L_2)$] and $TiBr_4$ + free L_2. On cooling to 200 K, ligand exchange stops on the NMR time scale, and so the spectrum shows the equilibrium mixture present while ligand exchange was still fast. ^{77}Se{^{1}H} NMR spectroscopy showed only resonances little shifted from free ligand even at 200 K, suggesting ligand exchange is still fast on the ^{77}Se{^{1}H} NMR time scale.

3.2.2.3 Diselenoether adducts of TiI_4

The room temperature ^{1}H NMR spectra for the TiI_4/diselenoether adducts suggested that fast ligand exchange was occurring in solution as a result of weak metal-ligand interactions with the poor Lewis acid TiI_4. Variable temperature $^{13}C\{^1H\}$ and $^{77}Se\{^1H\}$ NMR spectroscopy of these adducts has confirmed these observations. Thus, the room temperature $^{13}C\{^1H\}$ NMR spectrum (Figure 3.11) of $[TiI_4\{o\text{-}C_6H_4(SeMe)_2]$ showed sharp resonances only slightly shifted to high frequency [δ 9.8 (Me); 128.6, 131.5 ($o\text{-}C_6H_4$)] with respect to free $o\text{-}C_6H_4(SeMe)_2$ [δ 8.1 (Me); 126.7, 129.2 ($o\text{-}C_6H_4$)]. Cooling to 200 K resulted in an increased shift to high frequency [δ 12.8 (Me); 129.5, 131.0 ($o\text{-}C_6H_4$)], though no resonances corresponding to free $o\text{-}C_6H_4(SeMe)_2$ were observed. This indicates ligand exchange has been slowed, but is still fast on the NMR time scale at 200 K, consistent with the poor acceptor ability of TiI_4 presenting only weak interactions with the selenoether donors. The $^{77}Se\{^1H\}$ NMR spectra parallel these observations, showing a single resonance slightly shifted to high frequency at room temperature [δ 214, cf. 200 in free $o\text{-}C_6H_4(SeMe)_2$]. Again the 200 K spectrum showed an increased high frequency shift [δ 239], but no free ligand resonance.

Figure 3.11 LT $^{13}C\{^1H\}$ NMR spectra of $[TiX_4\{o\text{-}C_6H_4(SeMe)_2\}]$ for X = Cl, Br, I ($CH_2Cl_2/CDCl_3$)

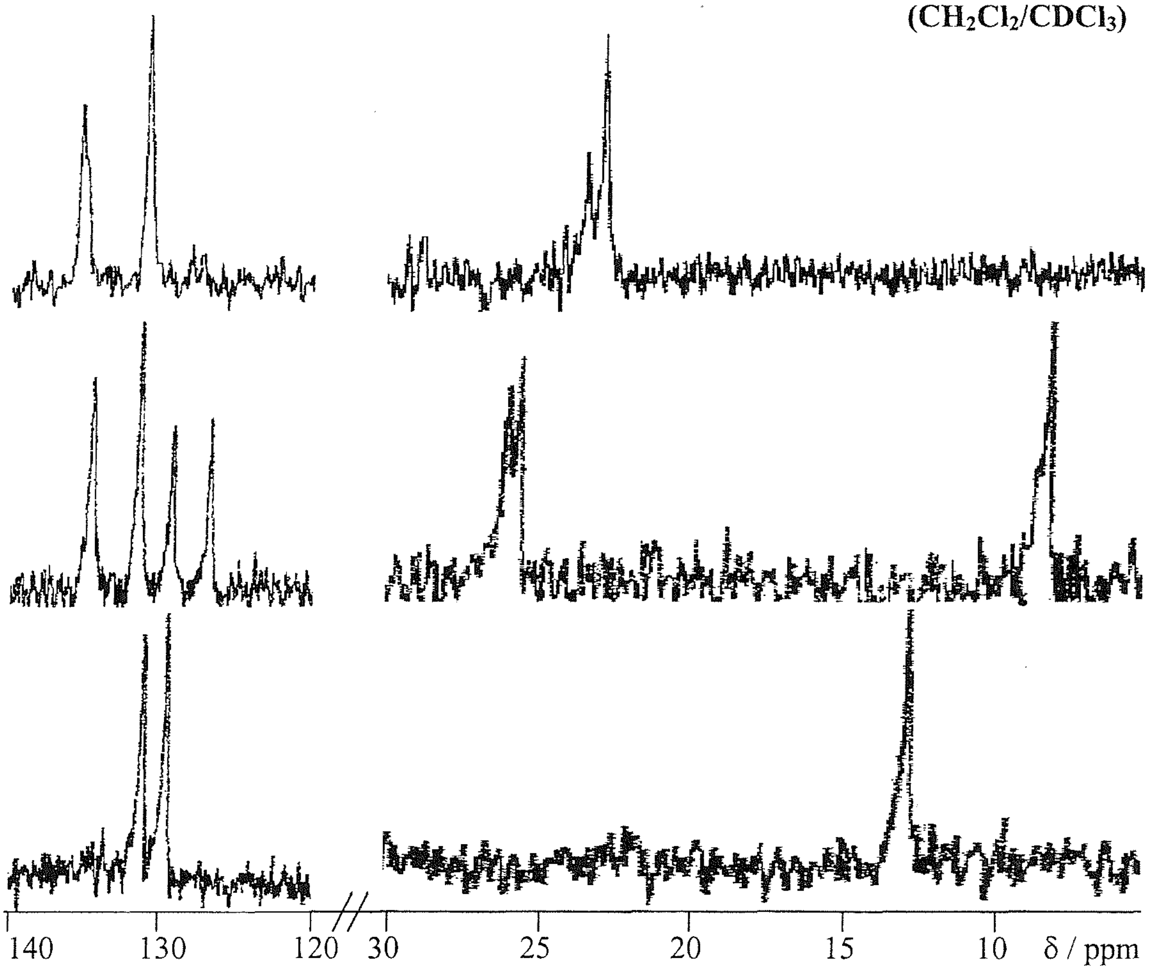

3.2.3 *X-ray crystallographic studies*

In view of the paucity of structurally characterised thio- and seleno-ether complexes of Ti(IV) and in order to confirm the coordination geometry at Ti(IV), single crystal X-ray diffraction studies were undertaken on four of the complexes formed here. Thus, single crystals of [$TiCl_4\{MeS(CH_2)_2SMe\}$], [$TiCl_4\{MeS(CH_2)_3SMe\}$], [$TiCl_4$-$\{MeSe(CH_2)_3SeMe\}$] and [$TiCl_4\{o\text{-}C_6H_4(SeMe)_2\}$] were grown by slow evaporation of CH_2Cl_2 solutions of the complexes in a dry N_2-purged glove box.

The structures of all four complexes (Figures 3.12 – 3.15, Tables 3.1 – 3.4) show a distorted octahedral environment at Ti(IV) comprising four chloro ligands and two mutually *cis* thio- or seleno-ether donors from the chelating ligand. The bond angles between any two mutually *cis* chloride ligands are greater than that expected for octahedral geometry, with the greatest distortion observed between the two chlorides *trans* to the thio- or seleno-ether donor atoms. These angles range from 102.8(1)° in [$TiCl_4\{MeS(CH_2)_3SMe\}$] to 109.28(7)° in [$TiCl_4\{o\text{-}C_6H_4(SeMe)_2\}$], a deviation of almost 20° from the expected 90° in the latter. Indeed, these angles are more consistent with the tetrahedral geometry of the originating $TiCl_4$ adduct, with the angles distorted slightly to accommodate the incoming dithio- and diseleno-ether ligands. Thus, the bond angles between the two mutually *trans* chloride ligands are most distorted, ranging from 165.1(1)° in [$TiCl_4\{MeS(CH_2)_3SMe\}$] to 162.91(3) in [$TiCl_4\{MeS(CH_2)_2SMe\}$]. Such large deviations from the expected octahedral geometry may be attributed to the spatial requirements of the chlorides, with electronic repulsion from three lone pairs of electrons on each chloride ligand. Similar distortions have been observed for the equivalent Sn(IV) dichalcogenoether complexes, [$SnX_4(L)$] for L = dithio-, diseleno- or ditelluro-ether ligand.[34,35] For example, the equivalent $SnCl_4$ adducts to those structurally characterised here show bond angles between the two chlorides *trans* to the thio- or seleno-ether donor atoms in the range 96.32(8) – 101.7(1)° and mutually *trans* chloride bond angles in the range 169.7(1) – 172.04(8)°. These distortions are less severe than for the Ti(IV) complexes formed here and this can be attributed to reduced steric crowding in the Sn(IV) adducts due to longer M-Cl bond distances in the latter.

The Ti-Cl bond distances have also been informative for these complexes. The bond distances for the chlorides *trans* to the thio- or seleno-ether donor atoms range from 2.2253(9) and 2.2358(8) Å in [$TiCl_4${MeS(CH_2)$_2$SMe}] to 2.247(4) Å in [$TiCl_4${MeSe(CH_2)$_3$SeMe}]. These are significantly shorter than the mutually *trans* chloride bond distances, ranging from 2.278(3) Å in [$TiCl_4${MeSe(CH_2)$_3$SeMe}] to 2.2907(8) and 2.2926(8) Å in [$TiCl_4${MeS(CH_2)$_2$SMe}]. These data suggest a *trans* influence order on Ti(IV) of Cl > S, Se, consistent with the preference of hard chloro ligands by the hard Ti(IV) centre. However, this order is opposite to that observed for more commonly studied soft Pt(II) complexes, indicating that the *trans* influence of ligands is dependent on the hardness of the metal centre. Indeed, equivalent dithio- and diseleno-ether complexes of the hard Sn(IV) centre also show a similar disparity in M-Cl bond distances [$d(Sn\text{-}Cl_{trans\ S/Se}) = 2.360(3) - 2.378(2)$ Å, $d(Sn\text{-}Cl_{trans\ Cl}) = 2.389(3) - 2.426(3)$ Å] to the Ti(IV) complexes formed here, again indicating a *trans* influence order of Cl > S, Se for hard Lewis acid centres. The distances also agree with the reported observation that halide ligands will preferentially reside *trans* to chalcogenoether ligands to maximise any X–Ti $p_\pi \rightarrow d_\pi$ bonding.[14]

Figure 3.12 View of the structure of [$TiCl_4${MeS(CH_2)$_2$SMe}] with numbering scheme adopted. Ellipsoids drawn at 40%, H-atoms omitted for clarity.

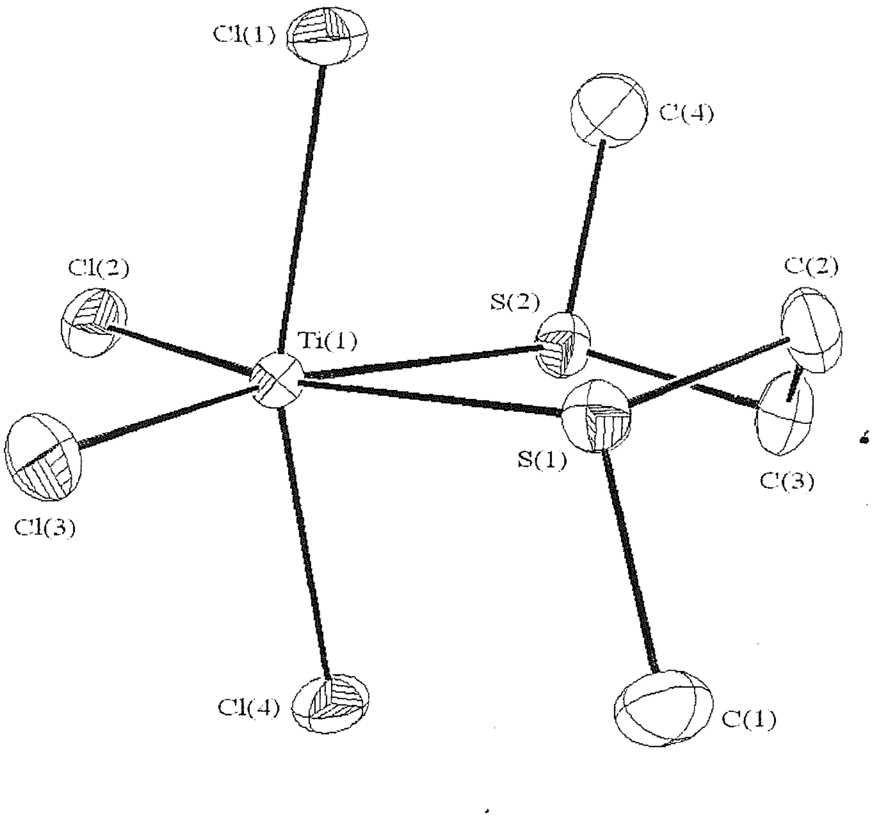

Table 3.1 Selected bond lengths for [$TiCl_4L$], L = $MeS(CH_2)_2SMe$, *o*-$C_6H_4(SeMe)_2$.

	Distance / Å	
Bond (E = S, Se)	[$TiCl_4\{MeS(CH_2)_2SMe\}$]	[$TiCl_4\{o\text{-}C_6H_4(SeMe)_2\}$]
Ti(1) – E(1)	2.6106(9)	2.727(1)
Ti(1) – E(2)	2.6010(8)	2.744(1)
Ti(1) – Cl(1)	2.2907(8)	2.267(2)
Ti(1) – Cl(2)	2.2253(9)	2.231(2)
Ti(1) – Cl(3)	2.2358(8)	2.239(2)
Ti(1) – Cl(4)	2.2926(8)	2.308(2)

Table 3.2 Selected bond angles for [$TiCl_4L$], L = $MeS(CH_2)_2SMe$, *o*-$C_6H_4(SeMe)_2$.

	Angle / °	
Bond (E = S or Se)	[$TiCl_4\{MeS(CH_2)_2SMe\}$]	[$TiCl_4\{o\text{-}C_6H_4(SeMe)_2\}$]
E(1) – Ti(1) – E(2)	80.34(3)	74.42(3)
E(1) – Ti(1) – Cl(1)	80.02(3)	87.20(5)
E(1) – Ti(1) – Cl(2)	167.45(3)	162.48(6)
E(1) – Ti(1) – Cl(3)	86.30(3)	87.69(5)
E(1) – Ti(1) – Cl(4)	87.58(3)	80.74(5)
E(2) – Ti(1) – Cl(1)	86.98(3)	84.41(5)
E(2) – Ti(1) – Cl(2)	88.03(3)	88.46(5)
E(2) – Ti(1) – Cl(3)	165.73(3)	162.05(6)
E(2) – Ti(1) – Cl(4)	79.33(3)	81.00(4)
Cl(1) – Ti(1) – Cl(2)	94.75(3)	94.94(6)
Cl(1) – Ti(1) – Cl(3)	95.68(3)	96.42(7)
Cl(1) – Ti(1) – Cl(4)	162.91(3)	163.11(7)
Cl(2) – Ti(1) – Cl(3)	105.66(3)	109.28(7)
Cl(2) – Ti(1) – Cl(4)	94.95(3)	93.14(6)
Cl(3) – Ti(1) – Cl(4)	95.20(3)	94.87(6)

The structures show that the ligands adopt a *DL* conformation in all cases except for *o*-$C_6H_4(SeMe)_2$, which adopts a *meso* conformation with both methyl groups residing on the same side of the $TiCl_2Se_2$ plane. Presumably, the reduced flexibility of the aromatic backbone in the latter disfavours the twisted *DL* conformation observed for the more flexible aliphatic ligands. This is also reflected in the *cis* coordinated ligand bite angles, with that of the *o*-$C_6H_4(SeMe)_2$ adduct [∠Se(1)-Ti-Se(2) = 74.42(3)°] significantly smaller than those of the aliphatic ligand complexes, [$TiCl_4(L_2)$] [L_2 = $MeS(CH_2)_2SMe$: ∠S(1)-Ti-S(2) = 80.34(3)°, $MeS(CH_2)_3SMe$: ∠S(1)-Ti-S(1*) = 80.8(1)°, $MeSe(CH_2)_3SeMe$: ∠Se(1)-Ti-Se(1*) = 81.12(12)°].

Figure 3.13 View of the structure of [$TiCl_4\{o\text{-}C_6H_4(SeMe)_2\}$] with numbering scheme adopted. Ellipsoids drawn at 40%, H-atoms omitted for clarity.

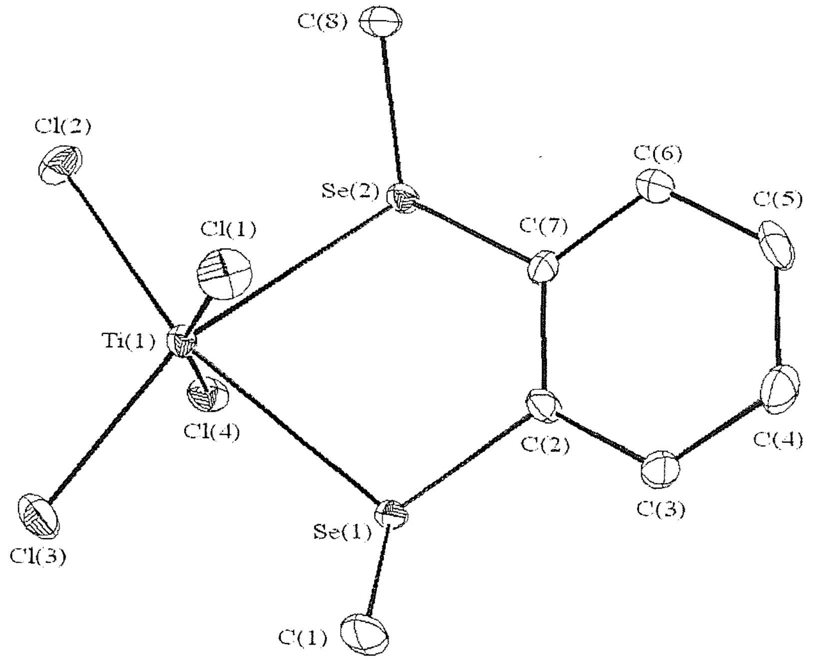

Ti-E (E = S, Se) bond distances from the structures have permitted some comparison of the σ-donor properties of the various ligands types used. Thus, the dithioether complexes [$TiCl_4\{MeS(CH_2)_nSMe\}$] show shorter distances for the methylene (n = 2) bridged donors [Ti-S(1) = 2.6106(9), Ti-S(2) = 2.6010(8) Å] compared with propylene (n = 3) bridged donors [Ti-S(1) = 2.664(2) Å]. This is consistent with the multinuclear NMR spectroscopy of these complexes, which showed greater ligand dissociation for the $MeE(CH_2)_3EMe$ adducts in solution at room temperature. Comparison of the Ti-E bond distances in the complexes [$TiCl_4$-{$MeE(CH_2)_3EMe$}] shows the expected longer bond distance for the selenoether donors [Ti-Se(1) = 2.755(3) Å], consistent with the larger covalent radius and softer nature of Se over S donor atoms. Finally, the Ti-Se bond distances in [$TiCl_4${*o*-$C_6H_4(SeMe)_2$}] are significantly shorter [Ti-Se(1) = 2.727(1), Ti-Se(2) = 2.744(1) Å] than those in the $MeSe(CH_2)_3SeMe$ adduct. This suggests the stabilisation offered by the 5-membered chelate ring in the former is sufficient to withstand the strain associated with the restricted bite angle from the less flexible *o*-$C_6H_4(SeMe)_2$ aromatic ligand.

Figure 3.14 View of the structure of [$TiCl_4${$MeS(CH_2)_3SMe$}] with numbering scheme adopted. Ellipsoids drawn at 40%, H-atoms omitted for clarity.

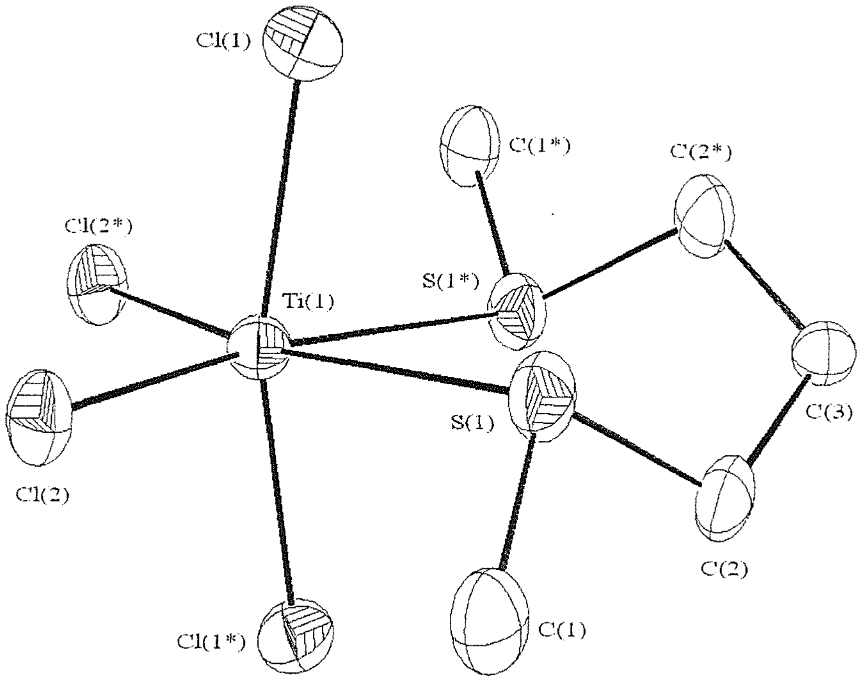

Table 3.3 Selected bond lengths for [$TiCl_4L$], L = $MeE(CH_2)_3EMe$, E = S, Se.

	Distance / Å	
Bond (E = S, Se)	[$TiCl_4${$MeS(CH_2)_3SMe$}]	[$TiCl_4${$MeSe(CH_2)_3SeMe$}]
Ti(1) – E(1)	2.644(2)	2.755(3)
Ti(1) – Cl(1)	2.285(2)	2.278(3)
Ti(1) – Cl(2)	2.235(2)	2.247(4)

Table 3.4 Selected bond angles for [$TiCl_4L$], L = $MeE(CH_2)_3EMe$, E = S, Se.

	Angle / °	
Bond (E = S or Se)	[$TiCl_4${$MeS(CH_2)_3SMe$}]	[$TiCl_4${$MeSe(CH_2)_3SeMe$}]
E(1) – Ti(1) – E(1*)	80.8(1)	81.12(12)
E(1) – Ti(1) – Cl(1)	82.24(9)	81.58(11)
E(1) – Ti(1) – Cl(2)	88.37(7)	87.50(11)
E(1) – Ti(1) – Cl(1*)	86.44(9)	86.07(11)
E(1) – Ti(1) – Cl(2*)	168.3(1)	168.09(14)
Cl(1) – Ti(1) – Cl(2)	96.53(9)	94.19(14)
Cl(1) – Ti(1) – Cl(1*)	165.1(1)	163.7(2)
Cl(1) – Ti(1) – Cl(2*)	92.73(9)	95.79(13)
Cl(2) – Ti(1) – Cl(2*)	102.8(1)	104.1(2)

Figure 3.15 View of the structure of [$TiCl_4${$MeSe(CH_2)_3SeMe$}] with numbering scheme adopted. Ellipsoids drawn at 40%, H-atoms omitted for clarity.

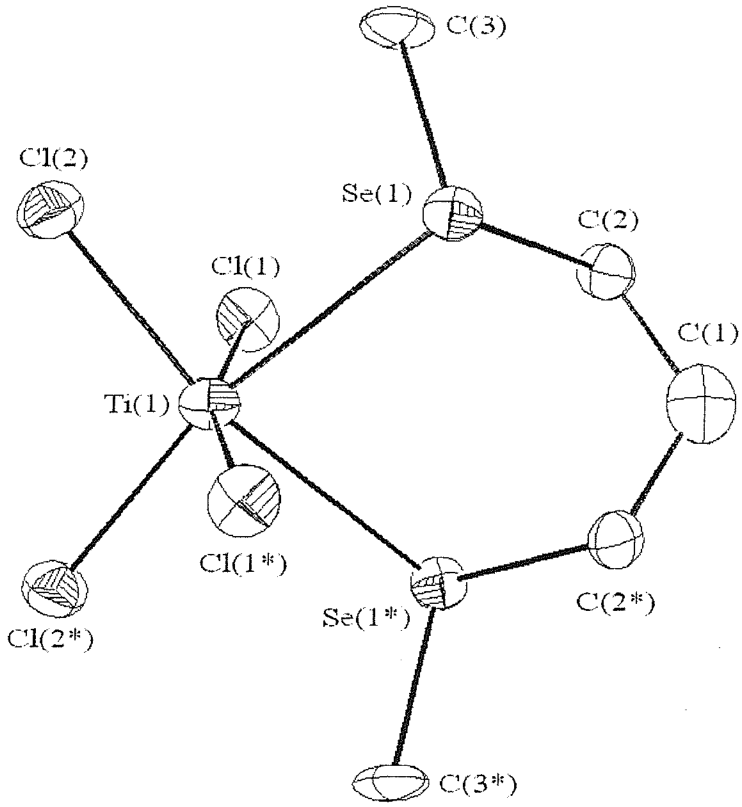

The above Ti-E bond distances all compare well with those reported in the literature for similar Ti(IV) complexes. Thus, the Ti-S bond distances observed here [2.6010(8) – 2.664(2) Å] are comparable with those in the monodentate thiol [2.663(2), 2.646(2) Å]^{17} and thioether [2.625(7), 2.626(7) Å]^{18} complexes, $[TiCl_4(C_6H_{11}SH)_2]$ and $[TiCl_4(C_4H_8S)_2]$ respectively. The distances are significantly shorter than the bridged binuclear disulfide adduct $[\{Cl_3Ti\}_2(\mu\text{-}Cl)_2(\mu\text{-}MeSSMe)]$ [2.712(3), 2.742(3) Å],^{18} possibly due to the strain associated with the bridging ligand in this example. Similarly, the Ti-Se bond distances observed in the complexes formed here [2.727(1) – 2.755(3) Å] are significantly shorter than the bridged binuclear diselenide adduct $[\{Cl_3Ti\}_2(\mu\text{-}Cl)_2(\mu\text{-}MeSeSeMe)]$ [2.796(2) Å].^{19} The distances are much more comparable however, with the monodentate selenoether complexes $[TiCl_4(R_2Se)]$, for R = Me [2.743(4), 2.777(4) Å] and R = Et [2.740(2), 2.763(2) Å].^{19}

3.2.4 Decomposition studies

As mentioned earlier, the $[TiX_4(L_2)]$ complexes formed here are extremely moisture sensitive, decomposing almost immediately in the presence of moist air. Thus, the complexes were stored in sealed vials in a dry N_2 purged glove box where the complexes remained stable over a period of a few months. However, the complex $[TiCl_4\{PhSe(CH_2)_2SePh\}]$ decomposed even under these conditions, changing colour from dark red to pale yellow within one month. $^{77}Se\{^1H\}$ NMR spectroscopy was utilised in order to establish the behaviour of the diselenoether ligand during this decomposition. Thus, a deep red solution of freshly prepared $[TiCl_4\{PhSe(CH_2)_2SePh\}]$ gave no spectrum at 300 K, however exhibited $^{77}Se\{^1H\}$ resonances corresponding to the *meso* and *DL* forms of the coordinated ligand [δ 417, 406] at 200 K. Slow decomposition of this solution within the glove box afforded a yellow solution in *ca.* 3 days. $^{77}Se\{^1H\}$ NMR spectroscopy of this showed a strong resonance at δ 457 at 300 K, corresponding to neither coordinated nor free $PhSe(CH_2)_2SePh$ ligand [δ 340]. The resonance at δ 457 (referenced to neat Me_2Se) suggests the presence of PhSeSePh [δ 464 referenced to $Me_2Se/CDCl_3$]. Indeed, addition of PhSeSePh to this solution results only in a strengthening of the resonance at δ 457, with no additional resonances. This is supported by $^{13}C\{^1H\}$ NMR spectroscopy of the complex, which showed resonances corresponding to both methylene [δ 31.0] and phenyl [δ 128-134] carbon environments for the freshly prepared sample, but only more clearly resolved phenyl resonances [δ 128, 130, 133] after decomposition. This suggests the decolourisation of $[TiCl_4\{PhSe(CH_2)_2SePh\}]$ may be attributable to the dealkylation of the ligand to afford yellow PhSeSePh. Similar diselenide ligands have been reported to undergo reaction with $TiCl_4$ and form complexes of the form $[\{Cl_3Ti\}_2(\mu\text{-}Cl)_2(\mu\text{-}L')]$, L′ = MeSeSeMe, EtSeSeEt.[19] Thus, the PhSeSePh formed here may be expected to react *in situ* to form the equivalent complex, $[\{Cl_3Ti\}_2(\mu\text{-}Cl)_2(\mu\text{-}PhSeSePh)]$. Indeed, the $^{77}Se\{^1H\}$ NMR spectrum of the decomposed sample does show a weak resonance at δ 478, slightly to high frequency of free PhSeSePh and hence consistent with the coordinated ligand.

The moisture sensitivity of the complexes in solution was also investigated. Thus, $^{13}C\{^1H\}$ NMR spectroscopy of a bright yellow solution of $[TiCl_4\{MeS(CH_2)_2SMe\}]$ in rigorously anhydrous $CH_2Cl_2/CDCl_3$ exhibited $^{13}C\{^1H\}$ resonances corresponding to the coordinated ligand [δ 39.0 (CH_2), 22.5 (CH_3)]. Subsequent addition of non-anhydrous CH_2Cl_2 resulted in an immediate and complete decolourisation of the solution and showed only $^{13}C\{^1H\}$ resonances corresponding to free ligand [δ 33.0 (CH_2), 16.0 (CH_3)]. This indicates the ligand dissociates without decomposition upon hydrolysis of these $[TiX_4(L_2)]$ complexes, consistent with weak interactions between the hard Ti(IV) centre and soft thio- and seleno-ether donor ligands.

Partial hydrolysis of these complexes has also been observed *via* X-ray crystallography. Thus, single crystals were grown by layering a solution of $[TiCl_4\{MeS(CH_2)_2SMe\}]$ in anhydrous CH_2Cl_2 with non-anhydrous *n*-hexane. Subsequent crystallographic studies showed the crystals were not of $[TiCl_4\{MeS(CH_2)_2SMe\}]$, but of a partially hydrolysed species $[(\{MeS(CH_2)_2SMe\}Cl_3Ti)_2(\mu\text{-}O)]$. The structure shows (Figure 3.16, Tables 3.5, 3.6) two distorted octahedral Ti(IV) centres linked by a bridging oxo-ligand, with the O-donor displacing one chloride ligand from each of the metal centres. The oxo-ligand occupies a crystallographic inversion centre, thus imposing a Ti(1)-O(1)-Ti(1*) bond angle of 180°. Other structurally characterised partially hydrolysed Ti(IV) adducts have been reported with the bridging O-donor occupying an inversion centre or near 180° Ti-O-Ti bond angles. Thus, the structure of *cis*-$[\{(MeCN)Cl_4Ti\}_2(\mu\text{-}O)]^{2-}$, an inadvertent hydrolysis product from the attempted crystallisation of $[\{(MeCN)Cl_4Ti\}_2(\mu\text{-}Se)]^{2-}$, shows the O-donor occupies an inversion centre.[36] Whereas, isomeric *trans*-$[\{(MeCN)Cl_4Ti\}_2(\mu\text{-}O)]^{2-}$ formed *via* the controlled hydrolysis of $TiCl_4$ in $MeCN/H_2O$, shows a Ti-O-Ti bond angle of 174.7(3)°.[37] The structure of $[\{(THF)_2Cl_3Ti\}_2(\mu\text{-}O)]$ shows similar geometry around Ti(IV) as the complex formed here, with one THF donor ligand *trans* to the bridging oxo-ligand and a Ti-O-Ti bond angle approximately linear at 176.7°.[38] Interestingly the equivalent chelating diether complex $[(\{MeO(C_{11}H_{22})OMe\}Cl_3Ti)_2(\mu\text{-}O)]$, formed *via* inadvertent hydrolysis during the attempted crystallisation of $[TiCl_4\{MeO(C_{11}H_{22})OMe\}]$, shows a much more distorted Ti-O-Ti bond angle of 163.4(4)°.[39]

A direct comparison can be made between the structure of $[(\{MeS(CH_2)_2SMe\}\text{-}Cl_3Ti)_2(\mu\text{-}O)]$ (**1**) reported here and that of $[TiCl_4\{MeS(CH_2)_2SMe\}]$ (**2**) discussed earlier. Both show similarly distorted octahedral geometry at Ti(IV), with the chelating dithioether ligands adopting the *DL* form and showing near identical bite angles of 80.34(3) **1** and 80.54(6)° **2**. The bond angles around Ti(IV) again show significant distortion towards the dithioether ligand, with the oxo-ligand behaving similar to the chloride ligand in the mononuclear adduct. Thus, the structure of the binuclear species shows distorted bond angles between the ligands *trans* to the S-donors [$\angle$Cl(2)-Ti(1)-O(1) = 102.77(6)° **1**, c.f. $\angle$Cl(2)-Ti(1)-Cl(4) = 105.66(3)° **2**] and between the mutually *trans* chloride ligands [$\angle$Cl(1)-Ti(1)-Cl(3) = 160.80(7)° **1**, c.f. 162.91(3)° **2**]. The Ti-Cl bond length *trans* to one of the S-donors [2.255(2) Å] is again significantly shorter than the mutually *trans* chlorides [2.295(2), 2.300(2) Å], indicating the *trans* influence order of Cl > S. However, the Ti-S bond distances do show some disparity to the mononuclear adduct, with the bond length for the S-donor *trans* to the oxo-ligand [2.653(3) Å] significantly longer than that of the other S-donor [2.624(2) Å] and those of the mononuclear adduct [2.6010(8), 2.6106(9) Å]. This may be due to the preference of the hard Ti(IV) centre for the hard oxo-ligand over soft S-donors. EI mass spectrometry of the isolated crystals showed major peaks with the correct isotopic distributions corresponding to the dicationic species $[(\{MeS(CH_2)_2SMe\}Cl_3Ti)(\mu\text{-}O)(TiCl_2\{MeS\text{-}(CH_2)_2SMe\})]^{2+}$, together with fragment peaks showing further loss of chloride ligands. These data, together with microanalytical data, confirm the formulation of the complex isolated in this way to be $[(\{MeS(CH_2)_2SMe\}Cl_3Ti)_2(\mu\text{-}O)]$.

Figure 3.16 View of the structure of [({MeS$(CH_2)_2$SMe}$Cl_3Ti)_2$(μ-O)] with numbering scheme adopted. Ellipsoids drawn at 40%.

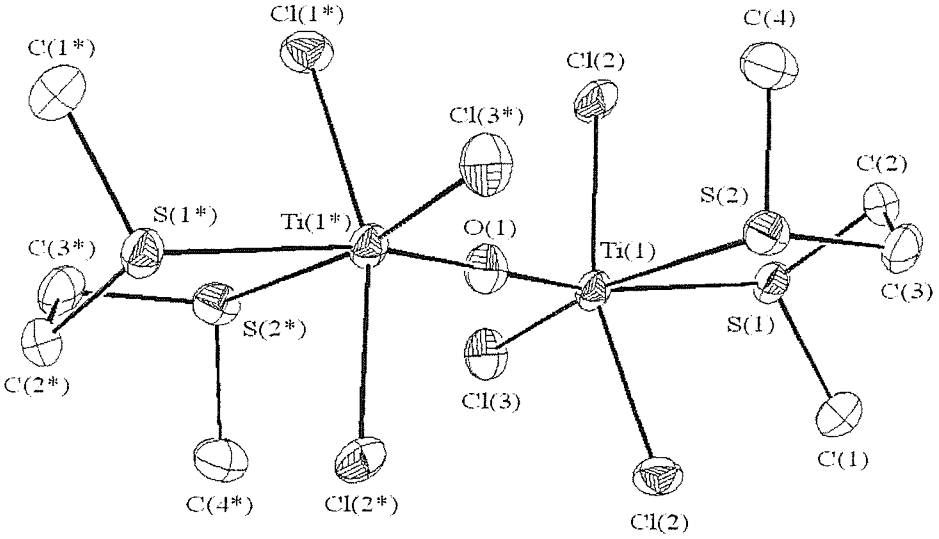

Table 3.5 Selected bond lengths for [({MeS$(CH_2)_2$SMe}$Cl_3Ti)_2$(μ-O)].

Bond	Distance / Å	Bond	Distance / Å
Ti(1) – S(1)	2.624(2)	Ti(1) – S(2)	2.653(2)
Ti(1) – Cl(1)	2.295(2)	Ti(1) – Cl(2)	2.255(2)
Ti(1) – Cl(3)	2.300(2)	Ti(1) – O(1)	1.788(1)

Table 3.6 Selected bond angles for [({MeS$(CH_2)_2$SMe}$Cl_3Ti)_2$(μ-O)].

Bond	Angle / °	Bond	Angle / °
S(1) – Ti(1) – S(2)	80.54(6)	S(1) – Ti(1) – Cl(1)	78.80(6)
S(1) – Ti(1) – Cl(2)	169.18(7)	S(1) – Ti(1) – Cl(3)	87.94(6)
S(1) – Ti(1) – O(1)	86.40(5)	S(2) – Ti(1) – Cl(1)	86.28(6)
S(2) – Ti(1) – Cl(2)	90.92(6)	S(2) – Ti(1) – Cl(3)	77.82(6)
S(2) – Ti(1) – O(1)	165.39(7)	Cl(1) – Ti(1) – Cl(2)	94.12(7)
Cl(1) – Ti(1) – Cl(3)	160.80(7)	Cl(1) – Ti(1) – O(1)	97.66(6)
Cl(2) – Ti(1) – Cl(3)	96.79(7)	Cl(2) – Ti(1) – O(1)	102.77(6)
Cl(3) – Ti(1) – O(1)	95.27(6)	Ti(1) – O(1) – Ti(1*)	180.00

The potential of these complexes as single source precursors to titanium sulfide and selenide materials was also briefly investigated. Thus, the complexes [$TiCl_4${MeE-$(CH_2)_2$EMe}] (E = S, Se) were heated *in vacuo* (0.1 mmHg) in a Schlenk glass tube *via* an external furnace. The complexes sublimed through the heated area at temperatures as low as 100 °C, though the resulting yellow and orange deposits were identified as the unchanged complexes *via* powder X-ray diffraction. This suggests that although the complexes are mobile at low temperatures, they are sufficiently stable to withstand decomposition. Thus, the furnace temperature was increased to 300 °C and 600 °C and under these conditions the complexes immediately sublimed through the heated area. Powder X-ray diffraction of the resulting materials again showed the presence of only unchanged complexes suggesting the increased mobility of the adducts results in an insufficient exposure to the heated area for thermal decomposition to take place. Repeating the experiments under reduced vacuum (2 mmHg) made little observable change and it is expected that furnace conditions need to be optimised before thermal decomposition of these mobile complexes can be observed. Unfortunately, as finding these optimum furnace conditions for each complex would be time consuming, further sublimation experiments were not undertaken in this particular study. However the observations from the above experiments do indicate that the complexes are sufficiently mobile for *in vacuo* thermal decomposition and may merit future investigation.

3.3 Conclusions

The complexes [$TiX_4(L_2)$] {L_2 = $MeE(CH_2)_nEMe$ and o-$C_6H_4(EMe)_2$, X = Cl, Br and L_2 = $PhE(CH_2)_2EPh$, X = Cl for E = S, Se, n = 2, 3} and [$TiI_4(L_2)$] {L_2 = $MeSe(CH_2)_2SeMe$ and o-$C_6H_4(SeMe)_2$} have been prepared *via* the reaction of TiX_4 with the respective bidentate ligand, L_2 in anhydrous *n*-hexane (X = Cl) or CH_2Cl_2 (X = Br, I). Similar reactions with bidentate telluroether ligands proved unsuccessful, indicating the poor interaction between the contracted Ti(IV) orbitals and the diffuse Te orbitals. Microanalytical data have established the formulation of [$TiX_4(L_2)$] for the thio- and seleno-ether adducts while electronic spectroscopy has confirmed the donor atoms around the Ti(IV) centre. IR spectroscopy has shown the ligands adopt a *cis* conformation, though the sensitivity of the complexes to ligand dissociation prevented confirmation of the nuclearity of the complexes *via* mass spectrometry.

Variable temperature multinuclear (^1H, $^{13}C\{^1H\}$ and $^{77}Se\{^1H\}$) NMR spectroscopy has permitted detailed investigation of the solution behaviour of these [$TiX_4(L_2)$] complexes. Thus, the chloro-adducts show fast pyramidal inversion at room temperature, with the selenoether adducts exhibiting slower pyramidal inversion, consistent with the higher activation energy for inversion at Se compared with S. Cooling slows pyramidal inversion sufficiently to resolve resonances due to the *meso* and *DL* invertomers in varying ratios. Weak resonances corresponding to free ligand are only observed for the $MeE(CH_2)_3EMe$ adducts, suggesting ligand exchange is detectable, but not fast at room temperature for these less favoured 6-membered chelate ring complexes. The bromo-adducts undergo both fast pyramidal inversion and fast ligand exchange at room temperature, with both processes slowing significantly at low temperatures to give a mixture of [$TiBr_4(L_2)$], $TiBr_4$ and free L_2 in varying amounts. The iodo-adducts show even greater ligand dissociation, with ligand exchange still fast even at 200 K. These data are consistent with the decreasing Lewis acidity of the Ti(IV) centre for $TiCl_4$ > $TiBr_4$ > TiI_4, leading to increasingly weak interactions with the thio- and seleno-ether donor ligands and hence increasing ligand dissociation in solution.

X-ray crystallography of [$TiCl_4(L_2)$], L_2 = $MeS(CH_2)_2SMe$, $MeS(CH_2)_3SMe$, $MeSe(CH_2)_3SeMe$ and o-$C_6H_4(SeMe)_2$ has confirmed the *cis* coordination of the thio- and seleno-ether ligands, with bite angles contacted by *ca.* 10° from the expected 90° upon ligand chelation. The structures show severe distortions from octahedral geometry with mutually *cis* and mutually *trans* chloride angles distorted as much as 20°. The longer Ti-Cl bond lengths observed between chlorides *trans* to Cl compared to those *trans* to S/Se show a *trans* influence of Cl > S, Se on Ti(IV), consistent with the preference for the harder Cl donor. The Ti-E (E = S, Se) bond lengths show shorter distances for ligands that adopt 5-membered chelate rings compared to those giving 6-membered rings, consistent with the increased stabilisation proffered by the former. Also, the Ti-Se bond lengths are longer than the Ti-S bond lengths in accord with the larger covalent radius and softer nature of Se over S.

The $[TiX_4(L_2)]$ complexes have shown extreme sensitivity to moisture, decomposing almost immediately in moist air. The complex $[TiCl_4\{PhSe(CH_2)_2SePh\}]$ even decomposed under the inert conditions of a N_2 purged glove box, with the ligand dealkylating and dissociating to afford free PhSeSePh. Ligand dissociation was observed without decomposition upon addition of non-anhydrous CH_2Cl_2 to a solution of the complex $[TiCl_4\{MeS(CH_2)_2SMe\}]$ in anhydrous CH_2Cl_2. However, on layering with non-anhydrous *n*-hexane, a partially hydrolysed adduct was isolated, with spectroscopic and structural characterisation confirming the formulation $[(\{MeS(CH_2)_2SMe\}Cl_3Ti)_2(\mu\text{-}O)]$. The structure shows the bridging oxo-ligand resides on a crystallographic inversion centre and replaces one chloride from each titanium centre to give a similar geometry at Ti(IV) as in the unhydrolysed adduct. Thus, the Ti-Cl bond length of the chloride *trans* to S is again longer than those *trans* to Cl, while the Ti-S bond lengths are non-equivalent, with those *trans* to the oxo-ligand significantly longer, indicating the preference of the hard O-donor by the hard Ti(IV) centre.

Attempts to generate titanium disulfide and diselenide materials from the $[TiX_4(L_2)]$ complexes have been unsuccessful. Although the complexes are mobile *in vacuo*, decomposition was not observed at low temperatures and at higher temperatures, the vapour sublimed through the heated area too rapidly under vacuum. Optimisation of furnace conditions may slow sublimation sufficiently at high temperatures to allow thermal decomposition to TiS_2 and $TiSe_2$ prior to deposition.

3.4 Experimental

The bidentate thio- and seleno-ether ligands were prepared *via* the literature procedures[40,41,42,43,44] and TiX_4 used as received from Aldrich Chemical Company. Rigorously anhydrous *n*-hexane and CH_2Cl_2 were freshly distilled over sodium/ benzophenone and CaH_2 respectively, and degassed with dry N_2. All reactions and sample preparations were performed under an N_2 atmosphere using standard Schlenk techniques and products were transferred and stored in a dry, N_2-purged glove box.

[TiCl$_4${MeS(CH$_2$)$_2$SMe}]

$TiCl_4$ (0.10 cm^3, 0.91 mmol) was added *via* degassed syringe to a solution of $MeS(CH_2)_2SMe$ (0.11 g, 0.91 mmol) in dry, degassed *n*-hexane (20 cm^3), affording the immediate precipitation of a bright yellow solid. This was filtered, washed with *n*-hexane (5 cm^3) and dried *in vacuo* to give the required [$TiCl_4${$MeS(CH_2)_2SMe$}] (yield 0.26 g, 91 %). Required for [$C_4H_{10}Cl_4S_2Ti$]: C = 15.4, H = 3.2 %; found: C = 15.3, H = 3.2 %. ^{1}H NMR: δ 2.92 (br, *s*, CH_2, 4H), 2.38 (br, *s*, CH_3, 6H). $^{13}C\{^1H\}$ NMR (300 K): δ 38.9 (CH_2), 23.2 (CH_3); (200 K): 39.4, 39.1 (CH_2), 23.5, 22.2 (CH_3). IR ν(TiCl): 420, 406, 397, 383 cm^{-1}. Electronic spectrum (10^{-3} ν_{max}): 23.8, 29.5(sh), 33.3(sh) cm^{-1}.

[TiCl$_4${MeS(CH$_2$)$_3$SMe}]

As above, but using $MeS(CH_2)_3SMe$ (0.13 g, 0.91 mmol). An orange solid was isolated as the required [$TiCl_4${$MeS(CH_2)_3SMe$}] (yield 0.29 g, 88 %). Required for [$C_5H_{12}Cl_4S_2Ti$]: C = 18.4, H = 3.7 %; found: C = 17.9, H = 3.6 %. ^{1}H NMR: δ 3.10 (*t*, SCH_2, 4H), 2.53 (*s*, CH_3, 6H), 2.24 (*qn*, CH_2, 2H). $^{13}C\{^1H\}$ NMR (300 K): δ 36.4 (SCH_2), 24.0 (CH_2), 22.0 (CH_3); (200 K): 37.5, 35.1 (SCH_2), 32.7 (w, CH_2 free dithioether), 27.6 (w, SCH_2 free dithioether), 24.4 (CH_2), 22.8, 21.8 (CH_3), 15.4 (w, CH_3 free dithioether). IR ν(TiCl): 408, 398, 387, 378 cm^{-1}. Electronic spectrum (10^{-3} ν_{max}): 22.5, 27.0(sh), 31.3(sh) cm^{-1}.

[TiCl$_4${PhS(CH$_2$)$_2$SPh}]

As above, but using $PhS(CH_2)_2SPh$ (0.23 g, 0.91 mmol). A red solid was isolated as the required [$TiCl_4$\{PhS(CH_2)$_2$SPh\}] (yield 0.37 g, 85 %). Required for [$C_{14}H_{14}Cl_4S_2Ti$]: C = 38.6, H = 3.2 %; found: C = 38.2, H = 3.5 %. ^{1}H NMR: δ 7.32-7.46 (*m*, Ph, 10H), 3.58 (*s*, CH_2, 4H). ^{13}C\{^{1}H\} NMR (300 K): δ 127-130 (Ph), 34.6 (CH_2); (200 K): 126-132 (Ph), 35.9, 33.0 (CH_2). IR ν(TiCl): 413, 400, 386, 378 cm^{-1}. Electronic spectrum (10^{-3} ν_{max}): 20.5(br), 28.5(sh) cm^{-1}.

[$TiCl_4$\{*o*-C_6H_4(SMe)$_2$\}]

As above, using *o*-C_6H_4(SMe)$_2$ (0.16 g, 0.91 mmol). An orange solid was isolated as the required [$TiCl_4$\{*o*-C_6H_4(SMe)$_2$\}] (yield 0.20 g, 55 %). Required for [$C_8H_{10}Cl_4$-S_2Ti]: C = 26.7, H = 2.8 %; found: C = 26.5, H = 3.0 %. ^{1}H NMR: δ 7.14-7.25 (*m*, *o*-C_6H_4, 4H), 2.47 (*s*, CH_3, 6H). ^{13}C\{^{1}H\} NMR (300 K): δ 134, 129 (*o*-C_6H_4), 26.8 (CH_3); (200 K): 134, 128 (*o*-C_6H_4), 28.0, 27.0 (CH_3). IR ν(TiCl): 405, 396, 387, 382 cm^{-1}.

[$TiCl_4$\{MeSe(CH_2)$_2$SeMe\}]

As above, but using MeSe(CH_2)$_2$SeMe (0.20 g, 0.91 mmol). An orange solid was isolated as the required [$TiCl_4$\{MeSe(CH_2)$_2$SeMe\}] (yield 0.37 g, 90 %). Required for [$C_4H_{10}Cl_4Se_2Ti$]: C = 11.8, H = 2.5 %; found: C = 11.5, H = 2.0 %. ^{1}H NMR: δ 3.30 (br, *s*, CH_2, 4H), 2.60 (br, *s*, CH_3, 6H). ^{13}C\{^{1}H\} NMR (300 K): δ 34.2 (CH_2), 14.5 (CH_3); (200 K): 34.4, 34.2 (CH_2), 14.9, 14.6 (CH_3). ^{77}Se\{^{1}H\} NMR (300 K): no spectrum; (200 K) δ 313, 307. IR ν(TiCl): 414, 402, 393, 380 cm^{-1}. Electronic spectrum (10^{-3} ν_{max}): 23.0, 24.0, 29.5(sh), 34.0 cm^{-1}.

[$TiCl_4$\{MeSe(CH_2)$_3$SeMe\}]

As above, but using MeSe(CH_2)$_3$SeMe (0.21 g, 0.91 mmol). A bright red solid was isolated as the required [$TiCl_4$\{MeSe(CH_2)$_3$SeMe\}] (yield 0.35 g, 84 %). Required for [$C_5H_{12}Cl_4Se_2Ti$]: C = 14.3, H = 2.9 %; found: C = 14.2, H = 3.0 %. ^{1}H NMR: δ 2.90 (*s*, SeCH_2, 4H), 2.28 (*s*, CH_3, 6H), 2.22 (*qn*, CH_2, 2H). ^{13}C\{^{1}H\} NMR (300 K): no spectrum; (200 K): 34.3, 32.1 (SeCH_2), 30.3 (w, CH_2 free diselenoether), 25.2 (w, SeCH_2 free diselenoether), 24.4 (CH_2), 17.0, 15.8 (CH_3), 4.0 (w, CH_3 free diselenoether). ^{77}Se\{^{1}H\} NMR (300 K): no spectrum; (200 K) δ 183, 180. IR ν(TiCl): 396, 384, 378, 373 cm^{-1}. Electronic spectrum (10^{-3} ν_{max}): 20.1, 24.5, 29.0(sh), 32.2(sh) cm^{-1}.

[$TiCl_4\{PhSe(CH_2)_2SePh\}$]

As above, but using $PhSe(CH_2)_2SePh$ (0.31 g, 0.91 mmol). A dark red solid was isolated as the required [$TiCl_4\{PhSe(CH_2)_2SePh\}$] (yield 0.42 g, 79 %). Required for [$C_{14}H_{14}Cl_4Se_2Ti$]: C = 31.7, H = 2.7 %; found: C = 32.0, H = 2.8 %. ^1H NMR: δ 7.9-8.2 (*m*, Ph, 10H), 3.7 (br, *s*, CH_2, 4H). $^{13}C\{^1H\}$ NMR (300 K): δ 128-134 (Ph), 31.0 (CH_2); (200 K): 129-133 (Ph), 32.6, 32.2 (CH_2). $^{77}Se\{^1H\}$ NMR (300 K): no spectrum; (200 K) δ 417, 406. IR ν(TiCl): 405, 385, 377, 373 cm^{-1}. Electronic spectrum (10^{-3} ν_{max}): 20.4, 31.6(br) cm^{-1}.

[$TiCl_4\{o\text{-}C_6H_4(SeMe)_2\}$]

As above, but using $o\text{-}C_6H_4(SeMe)_2$ (0.24 g, 0.91 mmol). An orange solid was isolated as the required [$TiCl_4\{o\text{-}C_6H_4(SeMe)_2\}$] (yield 0.35 g, 76 %). Required for [$C_8H_{10}Cl_4Se_2Ti$]: C = 21.2, H = 2.2 %; found: C = 21.0, H = 2.3 %. ^1H NMR: δ 7.28-7.46 (*m*, $o\text{-}C_6H_4$, 4H), 2.58 (*s*, CH_3, 6H). $^{13}C\{^1H\}$ NMR (300 K): δ 134.9, 131.0 ($o\text{-}C_6H_4$), 21.7 (CH_3); (200 K): 135.3, 130.8 ($o\text{-}C_6H_4$), 23.5, 22.9 (CH_3). $^{77}Se\{^1H\}$ NMR (300 K): no spectrum; (200 K) δ 399, 390. IR ν(TiCl): 390, 386, 382, 379 cm^{-1}. Electronic spectrum (10^{-3} ν_{max}): 21.6, 28.5(sh), 34.6(sh) cm^{-1}.

[$(\{MeS(CH_2)_2SMe\}Cl_3Ti)_2(\mu\text{-}O)$]

A solution of [$TiCl_4\{MeS(CH_2)_2SMe\}$] (0.05 g, 0.16 mmol) in dry, degassed CH_2Cl_2 (5 cm^3) was layered with non-anhydrous *n*-hexane (5 cm^3) and allowed to slowly diffuse and evaporate over *ca.* 3 days in a N_2 purged glove box. The resulting yellow crystals were isolated as the required [$(\{MeS(CH_2)_2SMe\}Cl_3Ti)_2(\mu\text{-}O)$]. Required for [$C_8H_{20}Cl_6OS_4Ti_2$]: C = 12.7, H = 2.7 %; found: C = 13.0, H = 2.8 %. EI mass spectrum: found *m/z* 342, 325, 267, 249; calc. for [$^{48}Ti_2{}^{35}Cl_3O\{MeS(CH_2)_2SMe\}$]$^+$ *m/z* 339, [$^{48}Ti_2{}^{35}Cl_6O$]$^+$ *m/z* 322, [$^{48}Ti_2{}^{35}Cl_5O\{MeS(CH_2)_2SMe\}_2$]$^{2+}$ *m/z* 265.5, [$^{48}Ti_2{}^{35}Cl_4O\{MeS(CH_2)_2SMe\}_2$]$^{2+}$ *m/z* 248.

[$TiBr_4\{MeS(CH_2)_2SMe\}$]

$MeS(CH_2)_2SMe$ (0.10 g, 0.82 mmol) in dry, degassed CH_2Cl_2 (10 cm^3) was added to a solution of $TiBr_4$ (0.30 g, 0.82 mmol) in CH_2Cl_2 (30 cm^3). The resulting red solution was stirred for 30 min. then concentrated *in vacuo* to 5 cm^3. Addition of dry, degassed *n*-hexane (20 cm^3) afforded an orange solid that was filtered, washed with *n*-hexane (5 cm^3) and dried *in vacuo* to give the required $[TiBr_4\{MeS(CH_2)_2SMe\}]$ (yield 0.28 g, 58 %). Required for $[C_4H_{10}Br_4S_2Ti]$: C = 9.8, H = 2.1 %; found: C = 10.1, H = 2.0 %. ^1H NMR: δ 2.8 (*s*, CH_2, 4H), 2.2 (*s*, CH_3, 6H). $^{13}C\{^1H\}$ NMR (300 K): no spectrum; (200 K): 37.9 (w, CH_2), 33.5 (CH_2 free dithioether), 20.1 (w, CH_3), 15.9 (CH_3 free dithioether). IR ν(TiBr): 332, 325, 319, 311 cm^{-1}. Electronic spectrum (10^{-3} ν_{max}): 22.2(v br), 33.0(sh) cm^{-1}.

$[TiBr_4\{MeS(CH_2)_3SMe\}]$

As above, but using $MeS(CH_2)_3SMe$ (0.11 g, 0.82 mmol). A bright red solid was isolated as the required $[TiBr_4\{MeS(CH_2)_3SMe\}]$ (yield 0.31 g, 61 %). Required for $[C_5H_{12}Br_4S_2Ti]$: C = 11.9, H = 2.4 %; found: C = 12.2, H = 2.5 %. ^1H NMR: δ 2.76 (*s*, SCH_2, 4H), 2.27 (*s*, CH_3, 6H), 1.95 (*m*, CH_2, 2H). $^{13}C\{^1H\}$ NMR (300 K): δ 35.5 (SCH_2), 25.3 (CH_2), 21.0 (CH_3); (200 K): 38.0, 35.0 (SCH_2), 32.3 (CH_2 free dithioether), 27.4 (SCH_2 free dithioether), 26.2 (CH_2), 22.8, 21.5 (CH_3), 15.1 (CH_3 free dithioether). IR ν(TiBr): 325, 321, 317, 311 cm^{-1}. Electronic spectrum (10^{-3} ν_{max}): 20.4, 22.5(sh), 31.5(sh) cm^{-1}.

$[TiBr_4\{o\text{-}C_6H_4(SMe)_2\}]$

As above, but using *o*-$C_6H_4(SMe)_2$ (0.14 g, 0.82 mmol). An orange solid was isolated as the required $[TiBr_4\{o\text{-}C_6H_4(SMe)_2\}]$ (yield 0.34 g, 64 %). Required for $[C_8H_{10}Br_4S_2Ti]$: C = 17.9, H = 1.9 %; found: C = 18.2, H = 2.2 %. ^1H NMR: δ 7.29-7.44 (*m*, *o*-C_6H_4, 4H), 2.73 (*s*, CH_3, 6H). $^{13}C\{^1H\}$ NMR (300 K) no spectrum; (200 K): 123-127 (*o*-C_6H_4 free dithioether), 15.6 (CH_3 free dithioether). IR ν(TiBr): 327, 317, 310, 304 cm^{-1}. Electronic spectrum (10^{-3} ν_{max}): 23.3 cm^{-1}.

$[TiBr_4\{MeSe(CH_2)_2SeMe\}]$

As above, but using $MeSe(CH_2)_2SeMe$ (0.18 g, 0.82 mmol). A red solid was isolated as the required $[TiBr_4\{MeSe(CH_2)_2SeMe\}]$ (yield 0.30 g, 51 %). Required for

[$C_4H_{10}Br_4Se_2Ti$]: C = 8.2 H = 1.7 %; found: C = 8.6, H = 1.9 %. ^1H NMR: δ 2.86 (*s*, CH_2, 4H), 2.10 (*s*, CH_3, 6H). $^{13}C\{^1H\}$ NMR (300 K): no spectrum; (200 K): 35.2, 35.0 (CH_2), 24.3 (CH_2 free diselenoether), 14.8, 14.6 (CH_3), 4.0 (CH_3 free diselenoether). $^{77}Se\{^1H\}$ NMR (300 K): no spectrum; (200 K) δ 118 (w, Se free diselenoether). IR ν(TiBr): 317, 312, 300, 294 cm^{-1}. Electronic spectrum (10^{-3} ν_{max}): 20.5, 26.0, 39.2 cm^{-1}.

[$TiBr_4\{MeSe(CH_2)_3SeMe\}$]

As above, but using $MeSe(CH_2)_3SeMe$ (0.19 g, 0.82 mmol). A dark red solid was isolated as the required [$TiBr_4\{MeSe(CH_2)_3SeMe\}$] (yield 0.31 g, 52 %). Required for [$C_5H_{12}Br_4Se_2Ti$]: C = 10.5, H = 2.0 %; found: C = 10.3, H = 2.2 %. ^1H NMR: δ 2.68 (*s*, $SeCH_2$, 4H), 2.05 (*s*, CH_3, 6H), 2.00 (*s*, CH_2, 2H). $^{13}C\{^1H\}$ NMR (300 K): no spectrum; (200 K): 35.6, 34.0 ($SeCH_2$), 29.8 (CH_2 free diselenoether), 24.5 ($SeCH_2$ free diselenoether), 24.4 (CH_2), 20.0, 18.5 (CH_3), 4.0 (CH_3 free diselenoether). $^{77}Se\{^1H\}$ NMR (300 K): no spectrum; (200 K) δ 69 (Se free diselenoether). IR ν(TiBr): 327, 317, 308, 300 cm^{-1}. Electronic spectrum (10^{-3} ν_{max}): 21.8(br) cm^{-1}.

[$TiBr_4\{o\text{-}C_6H_4(SeMe)_2\}$]

As above, but using $o\text{-}C_6H_4(SeMe)_2$ (0.22 g, 0.82 mmol). A brown solid was isolated as the required [$TiBr_4\{o\text{-}C_6H_4(SeMe)_2\}$] (yield 0.36 g, 57 %). Required for [$C_8H_{10}Br_4Se_2Ti$]: C = 15.2, H = 1.6 %; found: C = 15.8, H = 1.8 %. ^1H NMR: δ 7.20-7.42 (*m*, $o\text{-}C_6H_4$, 4H), 2.47 (*s*, CH_3, 6H). $^{13}C\{^1H\}$ NMR (300 K): no spectrum; (200 K): 134.5, 131.3 ($o\text{-}C_6H_4$), 129.2, 126.7 ($o\text{-}C_6H_4$ free diselenoether) 25.9, 25.5 (CH_3), 8.4, 8.1 (CH_3 free diselenoether). $^{77}Se\{^1H\}$ NMR : no spectrum. IR ν(TiBr): 326, 321, 305, 299 cm^{-1}. Electronic spectrum (10^{-3} ν_{max}): 20.5(br), 29.0(sh) cm^{-1}.

[$TiI_4\{MeSe(CH_2)_2SeMe\}$]

TiI_4 (0.20 g, 0.36 mmol) was dissolved in mildly refluxing dry CH_2Cl_2 (80 cm^3), with subsequent removal of undissolved solids *via* filtration affording a deep purple solution. Addition of $MeSe(CH_2)_2SeMe$ (0.09 g, 0.36 mmol) in dry, degassed CH_2Cl_2 (10 cm^3) gave an immediate colour change and the resulting red solution was stirred for 30 min., then concentrated *in vacuo* to 5 cm^3. Dry, degassed *n*-hexane (20 cm^3) was added and CH_2Cl_2 was removed *in vacuo* to afford a dark purple *n*-hexane solution with some dark precipitate. This was filtered to give the required $[TiI_4\{MeSe(CH_2)_2SeMe\}]$, though the partial solubility of the complex in *n*-hexane gave only a reduced yield (0.15 g, 19 %). Required for $[C_4H_{10}I_4S_2Ti]$: C = 6.2, H = 1.3 %; found: C = 6.5, H = 1.5 %. ^1H NMR: δ 3.02 (*s*, CH_2, 4H), 2.28 (*s*, CH_3, 6H). $^{13}C\{^1H\}$ / $^{77}Se\{^1H\}$ NMR : no spectrum.

$[TiI_4\{o\text{-}C_6H_4(SeMe)_2\}]$

As above, using $o\text{-}C_6H_4(SeMe)_2$ (0.10 g, 0.36 mmol). A brown solid was isolated as the required $[TiI_4\{o\text{-}C_6H_4(SeMe)_2\}]$ (yield 0.24 g, 30 %). Required for $[C_8H_{10}I_4Se_2\text{-}Ti]$: C = 11.7, H = 1.2 %; found: C = 11.3, H = 1.1 %. ^1H NMR: δ 7.20-7.38 (*m*, $o\text{-}C_6H_4$ 4H), 2.40 (*s*, CH_3, 6H). $^{13}C\{^1H\}$ NMR (300 K): δ 131.5, 128.6 ($o\text{-}C_6H_4$), 9.8 (CH_3); (200 K): 131.0, 129.5 ($o\text{-}C_6H_4$), 12.8 (CH_3). $^{77}Se\{^1H\}$ NMR (300 K): δ 214; (200 K) 240.

Crystallographic Studies

Details of the crystallographic data collection and refinement parameters are given in Table 3.7. Crystals of $[TiCl_4(L_2)]$, L_2 = $MeS(CH_2)_2SMe$, $MeS(CH_2)_3SMe$, $MeSe(CH_2)_3SeMe$ and $o\text{-}C_6H_4(SeMe)_2$ were grown by slow evaporation of the complexes in dry CH_2Cl_2 within a N_2 purged glove box. Crystals of $[(\{MeS(CH_2)_2SMe\}Cl_3Ti)_2(\mu\text{-}O)]$ were grown by slow diffusion of non-anhydrous *n*-hexane into a solution of $[TiCl_4\{MeS(CH_2)_2SMe\}]$ in dry CH_2Cl_2, followed by slow evaporation of the solution within a N_2 purged glove box. Data collection used a Rigaku AFC7S four-circle diffractometer using graphite-monochromated Mo-Kα X-radiation (λ = 0.71073 Å) and equipped with an Oxford Systems open-flow cryostat operating at 150 K. Structure solution[45,46] and refinement[47,48] were routine, except for $[TiCl_4\{MeSe(CH_2)_3SeMe\}]$, where data were collected in the Laue group 4/*mmm*, however the resulting systematic absences excluded all possible space groups with this Laue group. Thus, the structure was solved in the alternative tetragonal Laue group, 4/*m*, with twinning evident from two components of equal population leading to the incorrect assignment of Laue group during data collection. This was modelled using the program TWIN 010 100 00-1 in SHELXL 97[49], with the systematic absences indicating the space group $I4_1/a$ (# 88) and allowing routine refinement of the structure.

Table 3.7 Crystallographic data collection and refinement parameters for $[TiCl_4(L_2)]$ and $[(\{MeS(CH_2)_2SMe\}Cl_3Ti)_2(\mu\text{-}O)]$.

	$[TiCl_4\{MeS(CH_2)_2SMe\}]$	$[TiCl_4\{MeS(CH_2)_3SMe\}]$	$[TiCl_4\{MeSe(CH_2)_3SeMe\}]$	$[TiCl_4\{o\text{-}C_6H_4(SeMe)_2\}]$	$[(\{MeS(CH_2)_2SMe\}Cl_3Ti)_2O]$
Formula	$C_4H_{10}Cl_4S_2Ti$	$C_5H_{12}Cl_4S_2Ti$	$C_5H_{12}Cl_4Se_2Ti$	$C_8H_{10}Cl_4Se_2Ti$	$C_8H_{20}Cl_6OS_4Ti_2$
Formula weight	311.95	325.98	449.77	453.80	569.00
Crystal system	Monoclinic	Tetragonal	Tetragonal	Triclinic	Monoclinic
Space group	$P2_1/n$ (# 14)	$I\bar{4}2d$ (# 122)	$I4_1/a$ (# 88)	$P\bar{1}$ (# 2)	$P2_1/n$ (# 14)
a / Å	6.922(2)	10.071(1)	10.029(6)	8.2588(9)	8.963(1)
b / Å	13.335(1)	10.071(1)	10.029(6)	11.091(2)	10.672(2)
c / Å	12.678(1)	24.542(3)	25.698(14)	8.232 (1)	11.196(1)
α / °	90	90	90	90.74(1)	90
β / °	95.17(1)	90	90	97.72(1)	90.36(1)
γ / °	90	90	90	108.93(1)	90
U / Å^3	1165.4(3)	2489.1(7)	2585(3)	705.5(2)	1070.8(3)
Z	4	8	8	2	2
μ(Mo-K$_\alpha$) / cm^{-1}	19.51	18.41	70.74	64.42	18.77
No. of unique reflections	2151	683	1145	2478	2013
R_{int} (based on F^2)	0.019	-	-	0.056	0.039
No. of obs. reflections [a]	1764	525	792	1972	1412
No. of parameters	100	56	56	136	97
R [b]	0.023	0.041	0.054 [d]	0.031	0.049
R_w [c]	0.029	0.041	0.142 [e]	0.035	0.060

[a] Observed if $[I_o > 2\sigma(I_o)]$ [b] $R = \sum (|F_{obs}|_i - |F_{calc}|_i) / \sum |F_{obs}|_i$ [c] $R_w = \sqrt{[\sum w_i(|F_{obs}|_i - |F_{calc}|_i)^2 / \sum w_i|F_{obs}|_i^2}$ [d] $R1 = \sum (|F_{obs}| - |F_{calc}|) / \sum |F_{obs}|$ [e] $wR2 = \sqrt{[\sum w(|F^2_{obs}| - |F^2_{calc}|)^2 / \sum w|F^2_{obs}|^2}$

3.5 References

[1] R. J. H. Clark, in *Comprehensive Inorganic Chemistry*, J. C. Bailar, Jr., H. J. Emeleus, R. S. Nyholm, A. F. Trotman-Dickenson (eds.), Pergamon Press, Oxford, 1973, Vol. 3, Chapter 32.

[2] D. C. Bradley, *Adv. Inorg. Chem. Radiochem.*, 1972, **15**, 259.

[3] B. Hessett, P. G. Perkins, *J. Chem. Soc. (A)*, 1970, 3229.

[4] G. W. A. Fowles, R. A. Walton, *J. Chem. Soc.*, 1964, 4330.

[5] E. C. Alyea, E. G. Torrible, *Can. J. Chem.*, 1965, **43**, 3468.

[6] K. L. Baker, G. W. A. Fowles, *J. Chem. Soc. (A)*, 1968, 801.

[7] A. J. McAlees, R. McCrindle, A. R. Woon-Fat, *Inorg. Chem.*, 1976, **15**, 1065.

[8] R. G. Pearson, *J. Chem. Educ.*, 1968, **45**, 581 and 643.

[9] J. A. Douek, J. T. Spickett, *J. Inorg. Nucl. Chem.*, 1973, **35**, 511.

[10] A. D. Westland, L. Westland, *Can. J. Chem.*, 1965, **43**, 426.

[11] H. S. Ahuja, S. C. Jain, R. Rivest, *J. Inorg. Nucl. Chem.*, 1968, **30**, 2459.

[12] R. J. H. Clark, W. Errington, *Inorg. Chem.*, 1966, **5**, 650.

[13] E. E. Aynsley, N. N. Greenwood, J. B. Leach, *Chem. Ind.*, 1966, 379.

[14] A. E. Merbach, R. M. Nielson, E. Turin, *Inorg. Chim. Acta*, 1987, **134**, 67 and 79.

[15] A. J. Blake, P. Mountford, M. Schröder, P. J. Wilson, *J. Chem. Soc., Chem. Commun.*, 1998, 1007.

[16] W. A. Nujent, J. M. Mayer, *Metal-Ligand Multiple Bonds*, Wiley-Interscience, New York, 1988.

[17] T. S. Lewkebandara, J. W. Proscia, A. L. Rheingold, C. H. Winter, *Inorg. Chem.*, 1993, **32**, 3807.

[18] B. S. Haggerty, T. S. Lewkebandara, P. J. McKarns, A. L. Rheingold, C. H. Winter, G. P. A. Yap, *Polyhedron*, 1998, **17**, 1.

[19] T. S. Lewkebandara, L. M. Liable-Sands, P. J. McKarns, A. L. Rheingold, C. H. Winter, G. P. A. Yap, *Inorg. Chem.*, 1998, **37**, 418.

[20] M. S. Whittingham, *Prog. Solid State Chem.*, 1978, **12**, 41.

[21] B. Scrosati, *Electrochim. Acta*, 1981, **26**, 1559.

[22] J. P. Gabane, *Lithium Batteries*, Academic Press, London, 1983.

[23] R. H. Friend, A. D. Yoffe, *Adv. Phys.*, 1987, **36**, 1.

[24] Y. Ito, K. Kanehori, F. Kirino, T. Kudo, K. Miyauchi, *J. Electrochem. Soc.*, 1989, **136**, 1265.

[25] H. S. W. Chang, D. M. Schleich, *J. Solid State Chem.*, 1992, **100**, 62.

[26] T. S. Lewkebandara, J. W. Proscia, C. H. Winter, *Chem. Mater.*, 1992, **4**, 1144.

[27] W. Levason, B. Patel, G. Reid, V.-A. Tolhurst, M. Webster, *J. Chem. Soc., Dalton*

Trans., 2000, 3001.

[28] R. J. H. Clark, A. J. McAlees, *J. Chem. Soc. (A)*, 1970, 2026.

[29] A. Harada, A. Nakamura, Y. Nakayama, N. Ueyama, K. Watanabe, *Organometallics*, 2000, **19**, 2498.

[30] R. J. H. Clark, C. J. Willis, *J. Chem. Soc. (A)*, 1971, 838.

[31] B. J. Brisdon, T. E. Lester, R. A. Walton, *Spectrochim. Acta*, 1967, **23A**, 1969.

[32] A. B. P. Lever, *Inorganic Electronic Spectroscopy*, 2nd Edition, Elsevier, 1984.

[33] R. J. Cross, T. H. Green, R. Keat, *J. Chem. Soc., Chem. Commun.*, 1974, 207; *J. Chem. Soc., Dalton Trans.*, 1976, 1150.

[34] S. E. Dann, A. R. J. Genge, W. Levason, G. Reid, *J. Chem. Soc., Dalton Trans.*, 1996, 4471; 1997, 2207.

[35] A. R. J. Genge, W. Levason, G. Reid, *J. Chem. Soc., Dalton Trans.*, 1997, 4479 and 4549.

[36] V. V. Krug, U. Müller, *Acta Crystallogr., Sect. C*, 1990, **46**, 547.

[37] M. G. B. Drew, J. Palin, G. R. Willey, *J. Chem. Soc., Dalton Trans.*, 1994, 1799.

[38] B. M. Bulichev, V. K. Bel'skii, L. V. Ivakina, P. A. Storozhenko, N. R. Strel'tsova, *Koord. Khim.*, 1988, **14**, 421.

[39] M. Ahlgren, E. Iiskola, H. J. Kakkonen, T. A. Pakkanen, A. Pelkonen, J. Pursiainen, *Acta Crystallogr., Sect. C*, 1993, **49**, 1607.

[40] F. R. Hartley, W. Levason, C. A. McAuliffe, S. G. Murray, H. E. Soutter, *Inorg. Chim. Acta*, 1979, **35**, 265.

[41] D. J. Gulliver, E. G. Hope, W. Levason, G. L. Marshall, S. G. Murray, D. M. Potter, *J. Chem. Soc., Perkin Trans. II*, 1984, 429.

[42] E. G. Hope, T. Kemmitt, W. Levason, *J. Chem. Soc., Perkin Trans. II*, 1987, 487.

[43] E. G. Hope, T. Kemmitt, W. Levason, *Organometallics*, 1988, **7**, 78.

[44] T. Kemmitt, W. Levason, *Organometallics*, 1989, **8**, 1303.

[45] PATTY, The DIRDIF Program System, G. Admiraal, G. Beurskens, P. T. Beurskens, W. P. Bosman, S. Garcia-Granda, R. O. Gould, J. M. M. Smits, C. Smykalla, Technical Report of the Crystallography Laboratory, University of Nijmegen, 1992.

[46] SHELXS-86, G. M. Sheldrick, *Acta Crystallogr., Sect. A*, 1990, **46**, 467.

[47] TeXsan, Crystal Structure Analysis Package, Molecular Structure Corporation, Houston, Texas, 1995.

[48] H. D. Flack, *Acta Crystallogr., Sect. A*, 1983, **39**, 876.

[49] SHELXL 97, Program for crystal structure refinement, G. M. Sheldrick, University of Göttingen, 1997.

Chapter 4

Titanium (IV) Halide Complexes with Bidentate Phosphine and Arsine Ligands

4.1 Introduction

The work discussed in Chapter 3 has established that despite a considerable mismatch between the extreme hardness of Ti(IV) and softness of Group 16 donor ligands, complexes of the form $[TiX_4(L_2)]$ are readily isolated *via* reaction of TiX_4 (X = Cl, Br, I) and bidentate thio- and seleno-ether ligands (L_2). As the donor ligands of Group 15 are considered stronger σ-donors than the respective Group 16 ligands, the interaction between Ti(IV) and phosphine and arsine ligands (L_2') is expected to be sufficiently strong to observe the equivalent $[TiX_4(L_2')]$ complexes. Indeed, reaction of $TiCl_4$ with the monodentate phosphine PH_3 to afford $[TiCl_4(PH_3)]$ was reported as early as 1832,[1] while reaction with the monodentate arsine $AsPh_3$ was reported in 1924[2] and later identified as $[TiCl_4(AsPh_3)]$.[3] Subsequently, a number of Ti(IV) complexes involving monodentate phosphine and arsine ligands have been reported, including 1:1 metal : ligand adducts $[TiCl_4(L)]$ (L = PR_3, R = Me,[4] Ph,[5] Cy;[6] AsH_3[7]) and 6-coordinate 1:2 adducts $[TiCl_4(PR_3)_2]$ (R = H,[8] Et, Ph[9]). Similar 6-coordinate complexes have been isolated upon reaction with certain bidentate phosphine and arsine ligands, affording $[TiCl_4(L\text{-}L)]$ (L-L = $R_2P(CH_2)_2PR_2$, R = Me, Et,[9] Ph;[3] $Me_2AsCH{=}CHAsMe_2$,[10] *o*-C_6H_4-$(PEt_2)_2$[9] and *o*-$C_6H_4(AsR_2)_2$, R = Me,[11,12] Et[13]). However, possibly due to sensitivity to moisture, the characterisation of the above Ti(IV) phosphine and arsine complexes has been in general limited to analytical data, melting points and electronic and vibrational spectroscopy. Only one significant solution NMR spectroscopic study has been reported[6] and only very recently has structural characterisation been performed for $[TiCl_4\{R_2P(CH_2)_2PR_2\}]$ (R = Me, Et),[14] confirming *cis*-coordination geometry at Ti(IV). The attempted synthesis of a small number of $TiBr_4$ adducts has revealed some disparity with the $TiCl_4$ adducts. Thus, although the 6-coordinate complexes involving bidentate arsine ligands ($Me_2AsCH{=}CHAsMe_2$,[10] *o*-$C_6H_4(AsR_2)_2$, R = Me,[12] Et[13]) are readily formed, reaction with $AsPh_3$ affords only the 1:1 adduct,[3] presumably due to the poorer Lewis acidity of $TiBr_4$ compared with $TiCl_4$.

In contrast to the observations in Chapter 3 that bidentate thio- and seleno-ether ligands form only 6-coordinate complexes with TiX_4, bidentate phosphines and arsines have been reported to stabilise increased coordination numbers at Ti(IV). Thus, reaction of $TiCl_4$ with excess ligand (L-L = $Ph_2E(CH_2)_2EPh_2$, E = P, As) affords 2:3 adducts $[(TiCl_4)_2\{Ph_2E(CH_2)_2EPh_2\}_3]$,[5] although no structural characterisation has been performed on these adducts. Moreover, a small number of bidentate Group 15 ligands have been reported to form 8-coordinate complexes with Ti(IV). The structural characterisation of [$TiCl_4\{o\text{-}C_6H_4(AsMe_2)_2\}_2$][11,12] presented the first example of an 8-coordinate first row transition metal complex, with the structure showing dodecahedral geometry at Ti(IV). The analogous bromo and phosphine adducts [$TiBr_4\{o\text{-}C_6H_4(AsMe_2)_2\}_2$][12] and [$TiCl_4\{o\text{-}C_6H_4(PMe_2)_2\}_2$],[15] have also been assigned as 8-coordinate by comparison of the X-ray powder diffraction data with the arsine chloro adduct, however spectroscopic characterisation is again limited to analytical data, melting points and electronic and vibrational spectroscopy. There are no reported solution NMR spectroscopic studies for any of the 8-coordinate complexes, despite the clear potential for dynamic ligand exchange processes at the crowded Ti(IV) centre to afford the 6-coordinate 1:1 adducts and free ligand. Reaction of $TiCl_4$ with 1,8-bis(dimethylarsino)naphthalene has also been reported to form a 1:2 8-coordinate complex, however this assignment is on the basis of microanalytical data and IR spectroscopy only.[16]

A number of studies have been conducted to establish why 8-coordinate Ti(IV) complexes are formed almost exclusively for the ligands $o\text{-}C_6H_4(EMe_2)_2$, E = P, As; and not for other bidentate ligands. Thus, addition of $o\text{-}C_6H_4(AsMe_2)(NMe_2)$ to $TiCl_4$ affords only the 6-coordinate 1:1 adduct,[17] suggesting the amine donor does not lead to 8-coordination despite the increased hardness and σ-donating ability of N-donor atoms compared to P or As. Indeed similar reaction with excess $o\text{-}C_6H_4(NMe_2)_2$ yields only a black oily solid of indefinite composition.[18] Much smaller perturbations in the ligand σ-donor properties have also resulted in the loss of 8-coordination, with both $o\text{-}C_6H_4(PEt_2)_2$[9] and $o\text{-}C_6H_4(AsEt_2)_2$[13] affording only 1:1 adducts with $TiCl_4$. This reduced coordination *via* replacing methyl groups with ethyl groups may be attributed to a combination of the lower σ-donor ability and the increased size of the ethyl-substituted ligands. However, 8-coordinate 1:2 adducts are formed for another slightly modified arsine ligand, $o\text{-}C_6H_4\{As(CD_3)_2\}$,[17] despite having σ-donor properties comparable with $o\text{-}C_6H_4(AsEt_2)_2$. This suggests the determining factor for 8-coordination here is the similarity in size between the deuterated ligand and $o\text{-}C_6H_4(AsMe_2)_2$. Indeed, the similar methyl-substituted phosphine $Me_2P(CH_2)_2PMe_2$ also forms 8-coordinate complexes with $TiCl_4$,[19] with the structure of the complex showing similar dodecahedral geometry at Ti(IV) with that observed in the arsine complex, [$TiCl_4${*o*-$C_6H_4(AsMe_2)_2$}$_2$]. Surprisingly though, the methyl-substituted arsine $Me_2AsCH{=}CHAsMe_2$ forms only a 1:1 adduct with $TiCl_4$ and $TiBr_4$,[10] despite the steric similarity with *o*-$C_6H_4(AsMe_2)_2$. This may due to the differing electronic properties of the two ligands, suggesting the formation of 8-coordinate Ti(IV) adducts is dependent on a combination of both steric and electronic properties of the coordinating ligands.

This chapter investigates the coordination chemistry of bidentate phosphine and arsine ligands with titanium halides, with a view to establishing both the solution and solid state properties of these complexes. While Ti(IV) complexes with phosphine and arsine ligands have been known for some time, only a few NMR spectroscopic studies or structurally characterised complexes have been reported. Also, while 8-coordinate Ti(IV) complexes are known, there is only one example where both 6- and 8-coordinate complexes have been isolated and structurally characterised. Thus, reported within is the synthesis and spectroscopic characterisation of a series of 6- and 8-coordinate TiX_4 (X = Cl, Br and I) complexes with various bidentate phosphine and arsine ligands [$Ph_2As(CH_2)_2AsPh_2$, $Ph_2P(CH_2)_nPPh_2$ (n = 1, 2 or 3), *o*-$C_6H_4(PPh_2)_2$ and *o*-$C_6H_4(EMe)_2$ (E = P or As)].[20] The complexes are characterised by elemental analysis and IR, UV-visible and multinuclear (^1H, $^{13}C\{^1H\}$, $^{31}P\{^1H\}$) NMR spectroscopy. X-ray single crystal structure determinations are reported for the complexes [$TiCl_4${*o*-$C_6H_4(PMe_2)_2$}], [$TiCl_4${*o*-$C_6H_4(PMe_2)_2$}$_2$], [$TiBr_4${*o*-$C_6H_4(PMe_2)_2$}$_2$] and [$TiBr_4${*o*-$C_6H_4(AsMe_2)_2$}$_2$] in order to establish the consequences of changing the coordination number, donor atom and halide on the metal-donor interaction. The structural characterisation of an unusual zwitter-ionic adduct [$TiCl_5(Ph_2PCH_2PHPh_2)$] formed by partial decomposition of [$TiCl_4(Me_2PCH_2PMe_2)$] is also reported, along with structures of the Fe(II) and Fe(III) complexes [FeI_2{*o*-$C_6H_4(AsMe_2)_2$}$_2$] and [FeI_2{*o*-$C_6H_4(AsMe_2)_2$}$_2$][I_3], formed during the synthesis of [TiI_4{*o*-$C_6H_4(AsMe_2)_2$}$_2$] *via* iron impurities in TiI_4.

UNIVERSITY OF SOUTHAMPTON LIBRARY

4.2 Results and Discussion

Reaction of $TiCl_4$ with one molar equivalent of bidentate phosphine or arsine ligand, L_2 [$L_2 = Ph_2As(CH_2)_2AsPh_2$, $Ph_2P(CH_2)_nPPh_2$ ($n = 1$, 2 or 3), *o*-$C_6H_4(PPh_2)_2$ and *o*-$C_6H_4(EMe_2)_2$ (E = P, As)] in rigorously anhydrous *n*-hexane at room temperature resulted in the immediate precipitation of bright yellow, orange and red solids, [$TiCl_4(L_2)$], in high yield (Figure 4.1). Similarly, dissolution of $TiBr_4$ in rigorously anhydrous CH_2Cl_2 followed by addition of one molar equivalent of L_2' [$L_2' = Ph_2As(CH_2)_2AsPh_2$, $Ph_2P(CH_2)_nPPh_2$ ($n = 2$ or 3), *o*-$C_6H_4(PPh_2)_2$ and *o*-$C_6H_4(EMe_2)_2$ (E = P, As)] afforded deep orange and red coloured solutions of [$TiBr_4(L_2')$]. Intensely coloured solids were isolated in high yield *via* precipitation with *n*-hexane. As with the thio- and seleno-ether complexes discussed in Chapter 3, reactions with TiI_4 required comparatively large volumes of CH_2Cl_2 due to the poor solubility of TiI_4 in non-coordinating solvents. Subsequent addition of one molar equivalent of L_2'' [$L_2'' =$ *o*-$C_6H_4(EMe_2)_2$ (E = P, As)] resulted in a colour change to give dark red/purple solutions of [$TiI_4(L_2'')$]. The products were isolated as deep purple solids *via* precipitation with *n*-hexane, though in considerably lower yields than the $TiCl_4$ and $TiBr_4$ adducts.

Reaction of TiX_4 (X = Cl, Br, I) with three molar equivalents of bidentate ligand L_2'' [$L_2'' =$ *o*-$C_6H_4(EMe_2)_2$ (E = P, As)] afforded yellow, orange and purple Ti(IV) complexes, [$TiX_4(L_2'')_2$] (Figure 4.1). Analogous reactions with three molar equivalents of the phenyl-substituted arsine and phosphine bidentate ligands L_2''' [$L_2''' = Ph_2As(CH_2)_2AsPh_2$, $Ph_2P(CH_2)_nPPh_2$ ($n = 1$, 2 or 3) and *o*-$C_6H_4(PPh_2)_2$] resulted only in the isolation of 1:1 metal : ligand adducts, [$TiX_4(L_2''')$]. This is consistent with previous studies of Ti(IV) complexes that show 8-coordination at Ti(IV) is only achieved with a very small number of ligands possessing specific electronic and steric properties.[13,15,17]

All of the isolated complexes are extremely moisture sensitive, liberating free ligand and rapidly decolourising on exposure to moist air. However, the complexes are noticeably more stable than the thio- and seleno-ether Ti(IV) complexes reported in Chapter 3, consistent with the stronger σ-donor properties of Group 15 ligands over those of Group 16. The formulation of the complexes as [$TiCl_4(L_2)$], [$TiBr_4(L_2')$], [$TiI_4(L_2'')$] and [$TiX_4(L_2'')_2$] (X = Cl, Br, I) was confirmed *via* microanalytical data while, as for the Ti(IV) complexes reported in Chapter 3, mass spectrometry proved of little value.

Figure 4.1 Reaction scheme for the synthesis of [TiX_4(L-L)] and [$TiX_4(L-L)_2$].

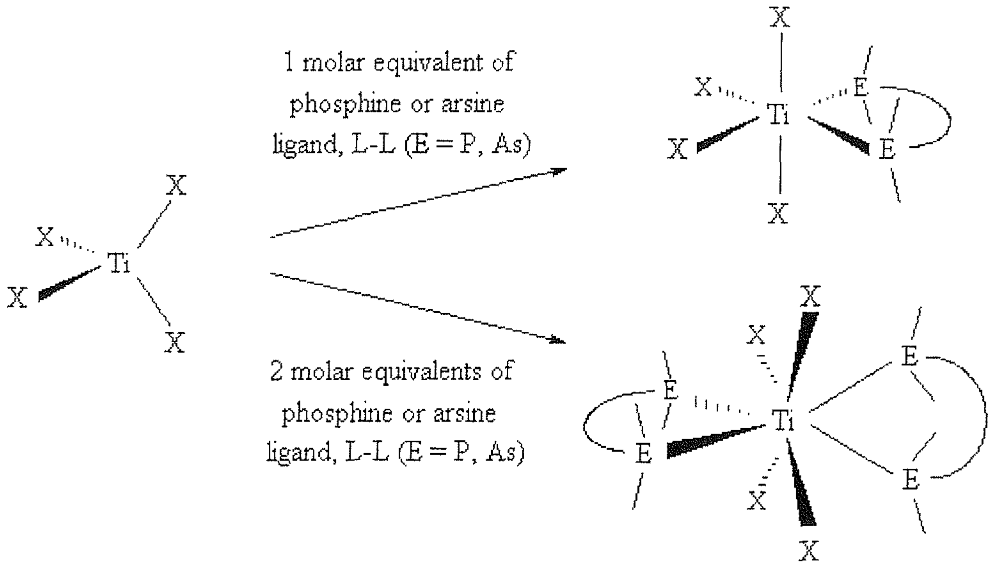

The successful isolation of titanium halide complexes with bidentate phosphine and arsine ligands prompted a study of the coordination chemistry of distibine ligands with Ti(IV). Thus, $TiCl_4$ was added to a solution of $Ph_2Sb(CH_2)_nSbPh_2$ (n = 1, 3) in anhydrous CH_2Cl_2 at 0 °C, resulting in an immediate deep purple coloration. Precipitation with anhydrous *n*-hexane afforded brown solids, however microanalytical data indicated chlorination of the distibine ligand, similar to that reported during the attempted synthesis of [$TiCl_4(Ph_3Sb)_2$][5]. These results are not surprising as the weak interaction between the contracted orbitals of the hard Ti(IV) centre and the diffuse orbitals of the soft Sb donor prevents the formation of strong Ti-Sb interactions.

4.2.1 IR and UV-visible spectroscopy

As with the thio- and seleno-ether ligands used in Chapter 3, the small chain lengths of the phosphine and arsine ligands used here dictates only *cis* coordination when chelating. Thus, the 1:1 metal : ligand complexes are expected to show C_{2v} symmetry and exhibit four IR active titanium-halide stretching vibrations, $2A_1 + B_1 + B_2$. Far IR data were recorded for the [$TiX_4(L_2)$] (X = Cl, Br) adducts, with the high sensitivity of the complexes dictating the use of sodium dried-Nujol mulls pressed between CsI plates and prepared within a N_2 purged glove box. In addition to peaks corresponding to the coordinated phosphine and arsine ligands, the spectra showed four Ti-X stretching vibrations (Figure 4.2) in the range of 420-350 cm^{-1} for ν(Ti-Cl) and 320-280 cm^{-1} for ν(Ti-Br). These data compare well with those reported for similar Ti(IV) phosphine/arsine complexes[3,5,13,10,21,22] [e.g. *cis*-[$TiX_4(PPh_3)_2$]: 381-325 and 308-256 cm^{-1} for X = Cl, Br respectively][21] and with those of the thio- and seleno-ether complexes reported in Chapter 3 [420-370 cm^{-1} for ν(Ti-Cl) and 330-290 cm^{-1} for ν(Ti-Br)]. Again IR spectroscopy of the TiI_4 adducts showed no metal-halogen stretching vibrations down to 220 cm^{-1}, as expected.[23]

Figure 4.2 ν(Ti-Cl) IR spectra of [$TiCl_4\{o\text{-}C_6H_4(PMe_2)_2\}_n$] for n = 1, 2 (Nujol mull).

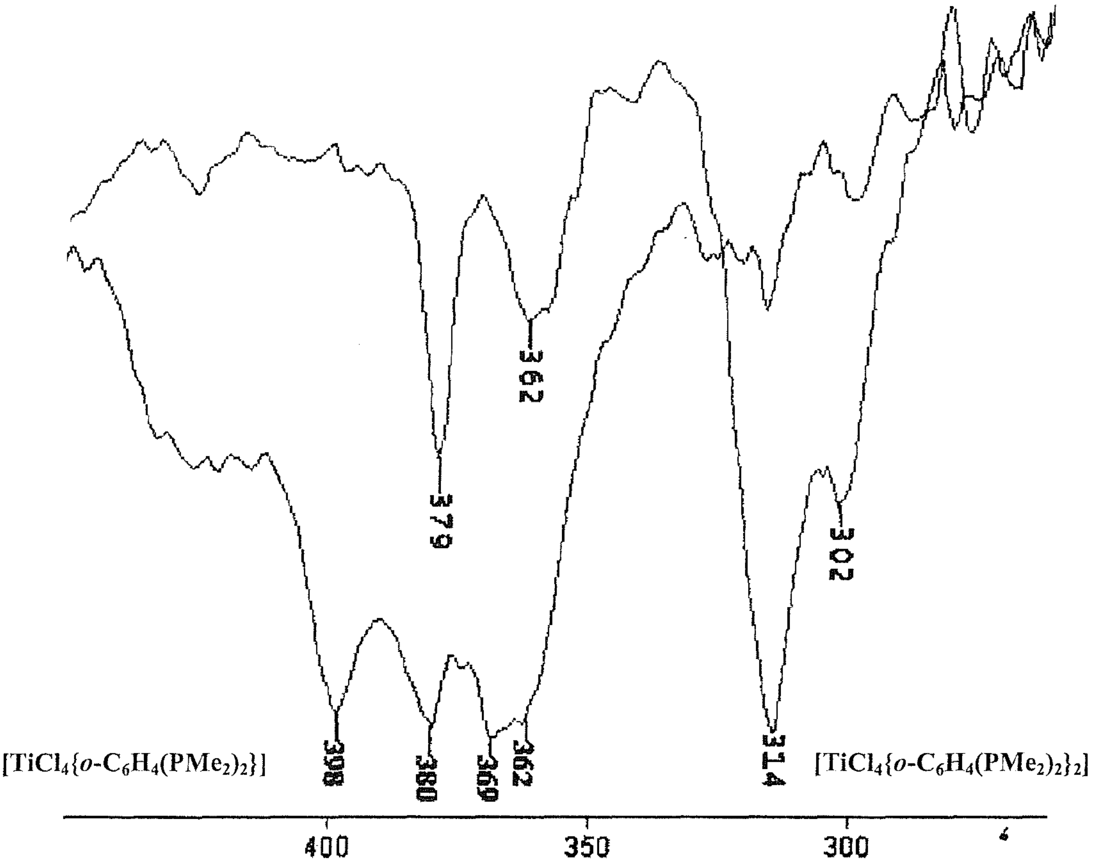

Previous reports on 8-coordinate Ti(IV) complexes have shown that adducts of the form [$TiX_4(L\text{-}L)_2$] (L-L = bidentate donor ligand) invariably adopt distorted dodecahedral structures. Thus, the 1:2 metal : ligand [$TiX_4(L_2'')_2$] (X = Cl, Br) complexes formed here are expected to show similar D_{2d} symmetry and exhibit two IR active titanium-halide stretching vibrations, $B_2 + E$. The far IR data for these adducts agree with this geometry, showing two Ti-X stretching vibrations (Figure 4.2) at *ca.* 315 cm^{-1} for ν(Ti-Cl) and *ca.* 290 cm^{-1} for ν(Ti-Br). These frequencies are significantly lower than those of the corresponding 6-coordinate 1:1 complexes above. This is consistent with a lengthening of the Ti-X bonds as a result of increased steric crowding around the small Ti(IV) centre in the 8-coordinate complexes. The Ti-X stretching frequencies for the chloro-adducts $[TiCl_4\{o\text{-}C_6H_4(EMe_2)_2\}_2]$ (E = As: 317 cm^{-1}, E = P: 312 cm^{-1}) have been reported previously[15,24] and show good agreement with those reported here (E = As: 323, 317 cm^{-1}, E = P: 314, 302 cm^{-1}).

The intense colours of the solids isolated as $[TiCl_4(L_2)]$, $[TiBr_4(L_2')]$, $[TiI_4(L_2'')]$ and $[TiX_4(L_2'')_2]$ (X = Cl, Br, I) indicate the presence of strong ligand-metal charge transfer (LMCT) transitions within the d^0 Ti(IV) complexes. As with the thio- and seleno-ether Ti(IV) adducts reported in Chapter 3, attempts to obtain solution phase electronic spectra were hindered by the moisture sensitivity of the complexes, thus spectra were recorded by diffuse reflectance, using anhydrous $BaSO_4$ as the diluent. The resulting spectra for the 6-coordinate 1:1 chloro-adducts, $[TiCl_4(L_2)]$, showed two broad, but resolved LMCT transitions at *ca.* 22,000 and 28,000 cm^{-1}, assigned to π(As or P) → Ti(t_{2g}) and π(Cl) → Ti(t_{2g}) transitions respectively. Although the actual symmetry at Ti(IV) is C_{2v} and not octahedral as implied by these assignments, the lifting of the degeneracy of the Ti(t_{2g}) orbitals in the former symmetry did not result in resolved splittings by diffuse reflectance spectroscopy. However, this unresolved *d*-orbital splitting may be partly responsible for the broad nature of the observed bands. The spectra of the 1:1 bromo-adducts showed less well resolved absorption bands at *ca.* 20,000 and 23,000 cm^{-1} similarly assigned to π(As or P) → Ti(t_{2g}) and π(Br) → Ti(t_{2g}) transitions respectively. This slightly lower energy π(As or P) → Ti(t_{2g}) transition for the bromo-adduct compared to the chloro-adduct has been similarly observed with later transition metals, such as Os(IV) in $[OsX_4(L)_2]$ for various monodentate tertiary phosphine and arsine ligands (L).[25]

The electronic spectra for the 8-coordinate 1:2 adducts, $[TiX_4(L_2)]$, showed similar broad absorption bands corresponding to the LMCT transitions from the donor ligands. For the now D_{2d} Ti(IV) centre, defining the principal S_4 inversion axis to be along the z-axis allows the assignment of these transitions as π(As or P) → Ti(b_1) and π(X) →

Ti(b_1). The energy of the halide transitions appears to be unaffected by the increase in coordination number at Ti(IV), however the phosphine/arsine transitions are slightly lower in energy (by *ca.* 2000 cm^{-1}) than those in the 6-coordinate analogues, possibly due to differing metal-ligand interactions in the two adducts. Despite the difference in the energy of these LMCT transitions in the 1:1 and 1:2 adducts, the broadness of the observed bands result in spectra of similar appearance. Hence, although the stoichiometry of the complexes can be deduced by comparison of both diffuse reflectance spectra, the differences are not sufficiently large to allow confident assignment of coordination number from one spectrum alone.

Although all of the above values are subject to large errors ($\geq \pm$ 500 cm^{-1}) due to the broad nature of the observed bands, the halide transitions do compare well with those observed in the thio- and seleno-ether Ti(IV) adducts reported in Chapter 3 and those in the similar Ti(IV) adducts $[TiX_6]^{2-}$.[26] Furthermore, the data correlate well with the transitions predicted using the Pauling scale of optical electronegativities,[27] and hence confirm the donor types present. These data, together with the above IR spectroscopic and microanalytical data, confirm the formulation of the products as *cis*-$[TiX_4(L_2)]$ and $[TiX_4(L_2)_2]$.

4.2.2 Multinuclear NMR spectroscopy

Unlike the thio- and seleno-ether Ti(IV) complexes discussed in Chapter 3, pyramidal inversion is not relevant for the phosphine and arsine complexes formed here. Nevertheless, variable temperature multinuclear NMR spectroscopy of these adducts can be useful for monitoring the presence of ligand dissociation and hence relative stability of these complexes in solution. Furthermore, the lability of the ligands in solution may allow exchange between the various 1:1 and 1:2 metal : ligand adducts isolated. Thus, ^1H and where possible, $^{13}C\{^1H\}$ or $^{31}P\{^1H\}$ NMR spectroscopic studies were undertaken for the complexes $[TiX_4(L_2)]$ and $[TiX_4(L_2)_2]$ for X = Cl, Br and I, though the studies were on the whole hindered by the limited solubility of the adducts in non-coordinating solvents.

4.2.2.1 Ti(IV) adducts with $Ph_2E(CH_2)_nEPh_2$ and o-$C_6H_4(PPh_2)_2$

Room temperature ^1H NMR spectra of [$TiCl_4${o-$C_6H_4(PPh_2)_2$}] and [$TiCl_4${Ph_2P-$(CH_2)_nPPh_2$}] (n = 1, 2, 3) showed sharp resonances with the expected coupling patterns corresponding to the H-environments of the respective ligands. Whereas the spectrum of [$TiCl_4${$Ph_2As(CH_2)_2AsPh_2$}] showed broad resonances, possibly due to decomposition even in anhydrous solvents. This may be attributed to weaker interactions between the hard Ti(IV) centre and the softer arsine ligand compared to phosphines. $^{31}P\{^1H\}$ NMR spectroscopy of the phosphine adducts generally showed sharp resonances to high frequency compared with the free ligand, however the spectrum of [$TiCl_4${$Ph_2PCH_2PPh_2$}] showed a series of resonances indicating decomposition in solution. The ^1H and $^{31}P\{^1H\}$ NMR spectra of the bromo complexes revealed broad resonances, consistent with rapid ligand dissociation in solution at room temperature.

4.2.2.2 Ti(IV) adducts with o-$C_6H_4(PMe_2)_2$

$^{31}P\{^1H\}$ NMR spectroscopy proved an excellent probe for comparing the solution behaviour of the various *o*-$C_6H_4(PMe_2)_2$-Ti(IV) adducts formed here. Thus, the room temperature spectra of the chloro-adducts [$TiCl_4${*o*-$C_6H_4(PMe_2)_2$}] and [$TiCl_4${*o*-$C_6H_4(PMe_2)_2$}$_2$] showed single sharp $^{31}P\{^1H\}$ resonances at δ 29.5 and 31.5 respectively. The spectra remained essentially unchanged on cooling, with an absence of additional resonances for free *o*-$C_6H_4(PMe_2)_2$ or differing metal:ligand ratios indicating ligand dissociation is not extensive at room temperature. The corresponding ^1H NMR data support this, showing second order multiplets for the PMe_2 groups at δ 1.90 and 1.83 for the 1:1 and 1:2 adducts respectively at room temperature, with little change on cooling to −90 °C.

The $^{31}P\{^1H\}$ NMR spectrum of [$TiBr_4${*o*-$C_6H_4(PMe_2)_2$}] revealed a sharp singlet at δ 24.5, with an absence of additional resonances on cooling again showing ligand dissociation is not extensive at room temperature (Figure 4.3). Addition of *o*-$C_6H_4(PMe_2)_2$ to this solution resulted in the *in situ* formation of the 1:2 adduct showing a sharp singlet $^{31}P\{^1H\}$ resonance at δ 22.2, along with the expected free ligand resonance at δ -55 (Figure 4.3). The $^{31}P\{^1H\}$ NMR spectrum of the isolated complex

[TiBr$_4${*o*-C$_6$H$_4$(PMe$_2$)$_2$}$_2$] showed resonances corresponding to both the 1:2 adduct (δ 22.2) and the 1:1 adduct (δ 24.5), along with free *o*-C$_6$H$_4$(PMe$_2$)$_2$. This suggests the complex partially dissociates in solution to the 1:1 adduct and free ligand, demonstrating the increased lability of the ligand and hence the weaker interaction with the poorer Lewis acid TiBr$_4$. These conclusions are again supported by ^{1}H NMR data, with the room temperature spectrum of [TiBr$_4${*o*-C$_6$H$_4$(PMe$_2$)$_2$}$_2$] showing broad resonances consistent with rapid ligand exchange. Cooling to –90 °C slows ligand exchange and the solution exhibits both methyl (δ 1.31, *s*) and *o*-C$_6$H$_4$ (δ 7.8 – 7.9, *m*) ^{1}H resonances for free *o*-C$_6$H$_4$(PMe$_2$)$_2$, together with resonances corresponding to the coordinated ligand in the 1:1 (δ 2.04, *d*, Me; 7.7 – 7.8, *m*, *o*-C$_6$H$_4$) and 1:2 (δ 1.97, *d*, Me; 7.6 – 7.7, *m*, *o*-C$_6$H$_4$) Ti(IV) adducts. The spectrum for [TiBr$_4${*o*-C$_6$H$_4$(PMe$_2$)$_2$}] showed only resonances due to the 1:1 coordinated phosphine even on cooling, confirming ligand dissociation is not extensive at room temperature.

Figure 4.3 ^{31}P{^{1}H} NMR spectrum of [TiBr$_4${*o*-C$_6$H$_4$(PMe$_2$)$_2$}] and subsequent addition of free ligand (CH$_2$Cl$_2$/CDCl$_3$).

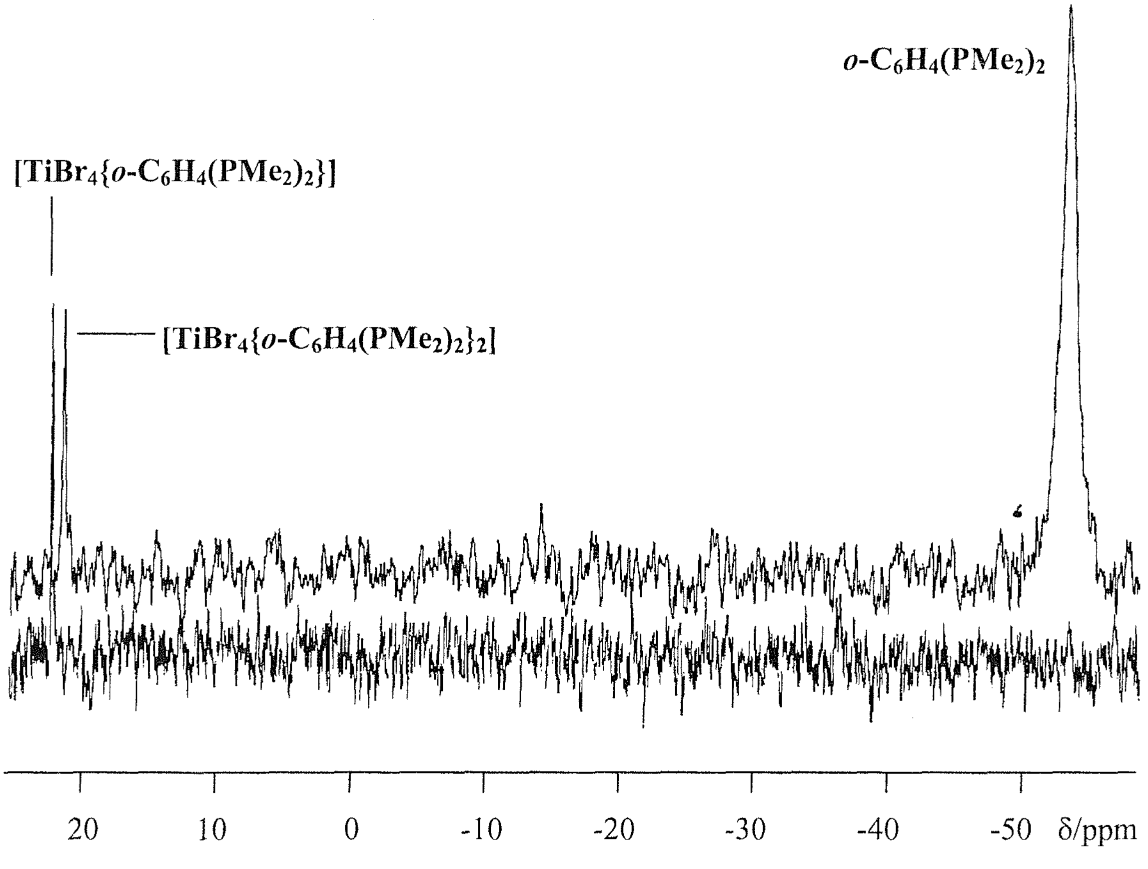

^{1}H NMR spectroscopy of [TiI_4\{o-$C_6H_4(PMe_2)_2$\}] showed only resonances due to the coordinated phosphine even on cooling (δ 2.28, *d*, Me, 7.7 – 7.8 *o*-C_6H_4), confirming the 1:1 complex is not undergoing extensive dissociation at room temperature. The $^{31}P\{^1H\}$ NMR spectrum revealed a sharp singlet even less shifted to high frequency (δ 18.0) with respect to free *o*-$C_6H_4(PMe_2)_2$ (Figure 4.4), consistent with the even poorer Lewis acid TiI_4 forming even weaker interactions with the phosphine ligand. This again confirms the expected Lewis acidity trend of $TiCl_4$ > $TiBr_4$ > TiI_4, as observed for the thio- and seleno-ether Ti(IV) complexes discussed in Chapter 3. Addition of *o*-$C_6H_4(PMe_2)_2$ to a solution of [TiI_4\{*o*-$C_6H_4(PMe_2)_2$\}] resulted in an immediate change from purple to yellow, with the resulting $^{31}P\{^1H\}$ NMR spectrum showing only a broad resonance corresponding to free ligand (δ -54), possibly indicating decomposition of the complex in presence of excess phosphine. Unfortunately ^{1}H and $^{31}P\{^1H\}$ NMR spectroscopy of isolated [TiI_4\{*o*-$C_6H_4(PMe_2)_2$\}$_2$] revealed resonances corresponding to a mixture of adducts (see Section 4.2.3) and thus further interpretation was not possible.

Figure 4.4 $^{31}P\{^1H\}$ NMR spectra of [TiX_4\{*o*-$C_6H_4(PMe)_2$\}] ($CH_2Cl_2/CDCl_3$).

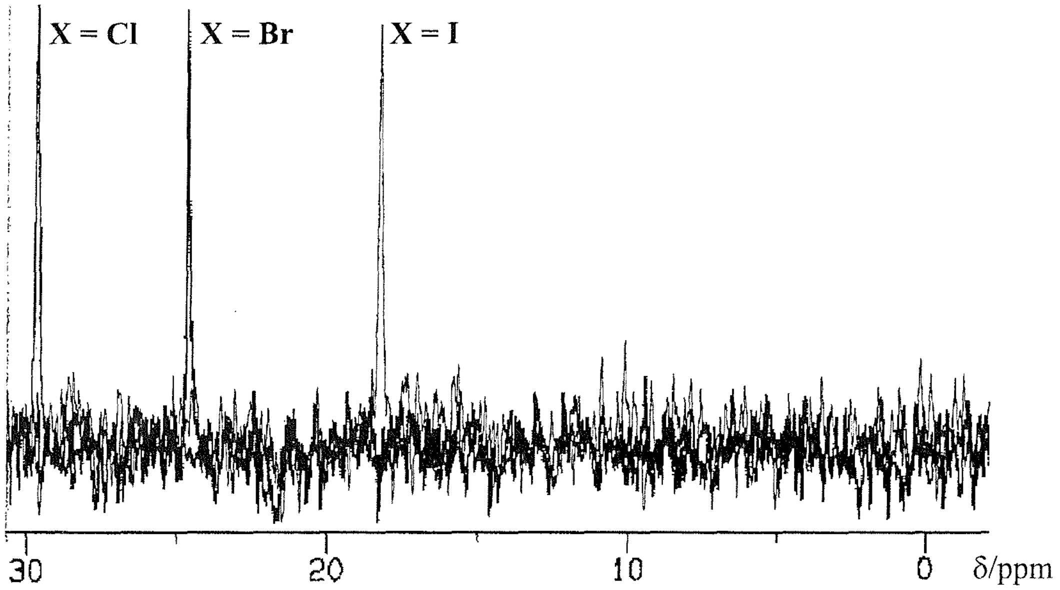

4.2.2.3 *Ti(IV) adducts with o-$C_6H_4(AsMe_2)_2$*

For the *o*-$C_6H_4(AsMe_2)_2$-Ti(IV) adducts, $^{13}C\{^1H\}$ NMR spectroscopy was utilised for comparing the solution behaviour of the TiX_4 adducts formed here, with spectra recorded at low temperature (–80 °C) to slow any exchange processes. Thus, $^{13}C\{^1H\}$ NMR spectra of the chloro-adducts [$TiCl_4\{o$-$C_6H_4(AsMe_2)_2\}$] and [$TiCl_4\{o$-$C_6H_4(AsMe_2)_2\}_2$] showed single sharp $AsMe_2$ resonances at δ 13.7 and 14.9 respectively (Figure 4.5). Resonances corresponding to the *o*-phenylene carbons were observed for all the TiX_4 (X = Cl, Br) adducts in the region δ 131-133, with little difference irrespective of complex. The absence of additional resonances for free *o*-$C_6H_4(AsMe_2)_2$ or differing metal : ligand ratios again suggest ligand dissociation is not extensive at room temperature. The ^1H NMR data support this, showing sharp singlets for the $AsMe_2$ groups at δ 1.90 and 1.78 for the 1:1 and 1:2 adducts respectively at room temperature, with little change on cooling to –90 °C. Again, the *o*-phenylene resonances showed little variance (δ 7.55-7.65) and will not be discussed further.

The lower solubilities of the bromo-adducts hindered the acquisition of good quality NMR data, with the spectra invariably revealing weak resonances corresponding to decomposition of the complexes either on dissolution or during the longer NMR experiments. Nevertheless, the low temperature $^{13}C\{^1H\}$ NMR spectrum of [$TiBr_4\{o$-$C_6H_4(AsMe_2)_2\}$] revealed a sharp $AsMe_2$ singlet at δ 17.3, with an absence of additional methyl resonances suggesting that ligand dissociation is not extensive at ambient temperatures. Unfortunately, the low solubility of the 1:2 adduct prevented analysis by $^{13}C\{^1H\}$ NMR spectroscopy. However, ^1H NMR spectroscopy did prove sufficiently sensitive to compare the solution behaviour of the bromo-adducts. Thus, the ^1H NMR spectrum of 1:1 complex [$TiBr_4\{o$-$C_6H_4(AsMe_2)_2\}$] showed a sharp singlet for the $AsMe_2$ groups at δ 1.90, with little change on cooling. Whereas, the spectrum for the 1:2 adduct [$TiBr_4\{o$-$C_6H_4(AsMe_2)_2\}_2$] showed broad resonances corresponding to free and coordinated *o*-$C_6H_4(AsMe_2)_2$ at room temperature, indicating the presence of dynamic processes in solution. Cooling to –90 °C slows the exchange process and the solution exhibits $AsMe_2$ ^1H resonances corresponding to the coordinated ligand in both the 1:1 (δ 1.93) and 1:2 (δ 1.79) Ti(IV) adducts. The absence of resonances due to free ligand in the low temperature spectrum may be attributed to a shift in the equilibrium between the 1:1 and 1:2 adducts in solution towards the latter.

These results are consistent with the conclusions from the o-$C_6H_4(PMe_2)_2$-Ti(IV) adducts, showing the chloro- and 1:1-adducts do not exhibit extensive ligand dissociation at room temperature, whereas the bromo-1:2-adduct reveals dissociation of ligand at ambient temperatures to present an equilibrium between the 1:1 and 1:2 adducts and free ligand. Unfortunately, $^{13}C\{^1H\}$ NMR spectroscopy of the iodo-adducts were not obtained due to a combination of poor solubility of the complexes in non-coordinating solvents and extensive ligand dissociation from the poor Lewis acid TiI_4.

Figure 4.5 Methyl region of $^{13}C\{^1H\}$ NMR spectra of $[TiCl_4\{o\text{-}C_6H_4(AsMe)_2\}_n]$ for $n = 1, 2$ ($CH_2Cl_2/CDCl_3$).

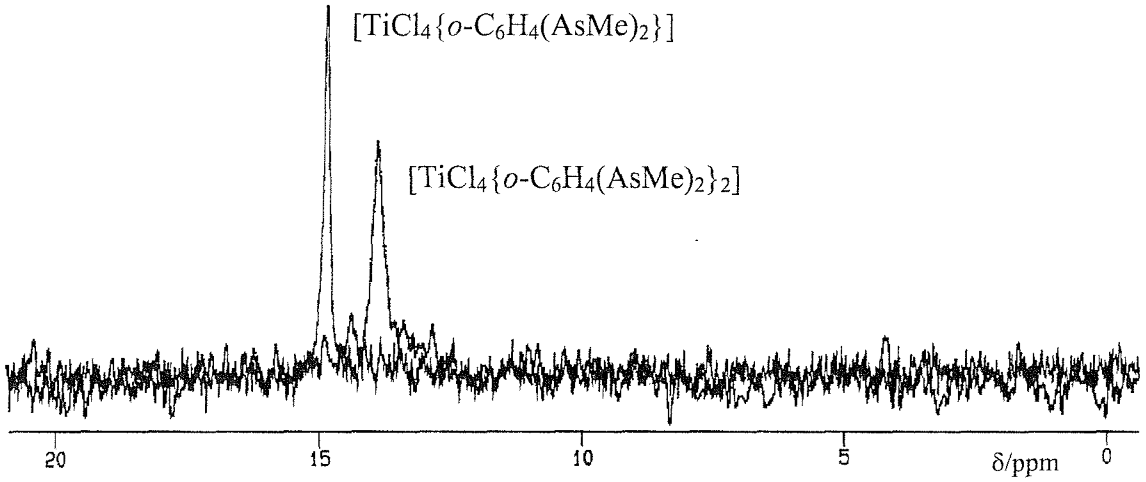

4.2.3 *X-ray crystallographic studies*

In view of the paucity of structurally characterised Ti(IV) phosphine and arsine complexes and in order to establish unequivocally the coordination geometry at Ti(IV), single crystal X-ray diffraction studies were undertaken on four of the complexes formed here. Thus, single crystals of $[TiCl_4\{o\text{-}C_6H_4(PMe_2)_2\}_n]$ ($n = 1, 2$) and $[TiBr_4\{o\text{-}C_6H_4(EMe_2)_2\}_2]$ (E = P, As) were grown by slow evaporation of CH_2Cl_2 solutions of the complexes in a dry N_2-purged glove box. In addition to the previously reported structure of $[TiCl_4\{o\text{-}C_6H_4(AsMe_2)_2\}_2]$, these diffraction studies present a near complete set of crystallographic data for the complexes $[TiX_4\{o\text{-}C_6H_4(EMe_2)_2\}_n]$ for X = Cl, Br; E = P, As; $n = 1, 2$. Consequently, the data provide an opportunity for comparing the effects of changing donor atom, halide or coordination number on the geometry about Ti(IV).

The structure of [$TiCl_4\{o\text{-}C_6H_4(PMe_2)_2\}$] (Figure 4.6, Tables 4.1, 4.2) shows a distorted octahedral environment at Ti(IV) comprising four chloro ligands and two mutually *cis* phosphine donor atoms from the chelating ligand. The bond angles between any two mutually *cis* chloride ligands are greater than octahedral 90°, with the greatest distortion observed between the two chlorides *trans* to the phosphine ligand, as observed for the thio- or seleno-ether Ti(IV) complexes discussed in Chapter 3. Thus the phosphine adduct exhibits $\angle Cl(2)_{trans\ P} - Ti(1) - Cl(3)_{trans\ P} = 114.58(5)^\circ$, which compares well with the equivalent angle in similar 6-coordinate Ti(IV) phosphine adducts [$TiCl_4$(L-L)], L-L = $Me_2P(CH_2)_2PMe_2$ [113.43(7)°] and $Et_2P(CH_2)_2PEt_2$ [111.03(5)°].[14] Consequently, the chloride ligands lean towards the phosphine ligand to give distorted bond angles between the mutually *trans* chlorides, $\angle Cl(1)_{trans\ Cl} - Ti(1) - Cl(4)_{trans\ Cl} = 164.25(5)^\circ$ and the chelating phosphine donor atoms, $\angle P(1) - Ti(1) - P(2) = 76.05(3)^\circ$. This bidentate phosphine bite angle compares well with those in similar Ti(IV) phosphine adducts with C_2 bridges between the P-donors, [$TiCl_4$(L-L)], L-L = $Me_2P(CH_2)_2PMe_2$ [75.95(6)°] and $Et_2P(CH_2)_2PEt_2$ [76.71(4)°].[14] Similarly, the Ti-P bond distances [2.5608(10), 2.5745(11) Å] also compare well with those in [$TiCl_4$(L-L)], L-L = $Me_2P(CH_2)_2PMe_2$ [2.577(2), 2.582(2) Å] and $Et_2P(CH_2)_2PEt_2$ [2.5981(9) Å].[14] The Ti-Cl bond distances show a similar trend to that observed for the Ti(IV) thio- and seleno-ether complexes, with bond distances for the chlorides *trans* to the donor ligand [2.2522(11), 2.2746(10) Å] significantly shorter than those of the mutually *trans* chlorides [2.2956(11), 2.2980(11) Å]. This indicates a *trans* influence of Cl > P, illustrating the preference of the hard Ti(IV) centre for the hard chloride ligands over softer phosphine donor atoms.

Table 4.1 Selected bond lengths for [$TiCl_4\{o\text{-}C_6H_4(PMe_2)_2\}$].

Bond	Distance / Å	Bond	Distance / Å
Ti(1) – P(1)	2.5745(11)	Ti(1) – P(2)	2.5608(10)
Ti(1) – Cl(1)	2.2980(11)	Ti(1) – Cl(2)	2.2522(11)
Ti(1) – Cl(3)	2.2746(10)	Ti(1) – Cl(4)	2.2956(11)

Table 4.2 Selected bond angles for [$TiCl_4\{o\text{-}C_6H_4(PMe_2)_2\}$].

Bond	Angle / °	Bond	Angle / °
P(1) – Ti(1) – P(2)	76.05(3)	P(1) – Ti(1) – Cl(1)	82.77(4)
P(1) – Ti(1) – Cl(2)	160.99(4)	P(1) – Ti(1) – Cl(3)	84.40(4)
P(1) – Ti(1) – Cl(4)	84.60(4)	P(2) – Ti(1) – Cl(1)	82.38(4)
P(2) – Ti(1) – Cl(2)	84.94(4)	P(2) – Ti(1) – Cl(3)	160.40(4)
P(2) – Ti(1) – Cl(4)	85.48(4)	Cl(1) – Ti(1) – Cl(2)	94.40(4)
Cl(1) – Ti(1) – Cl(3)	93.83(4)	Cl(1) – Ti(1) – Cl(4)	164.25(5)
Cl(2) – Ti(1) – Cl(3)	114.58(5)	Cl(2) – Ti(1) – Cl(4)	94.49(5)
Cl(3) – Ti(1) – Cl(4)	94.26(4)		

Figure 4.6 View of the structure of [$TiCl_4\{o\text{-}C_6H_4(PMe_2)_2\}$] with numbering scheme adopted. Ellipsoids drawn at 40%, H-atoms omitted for clarity.

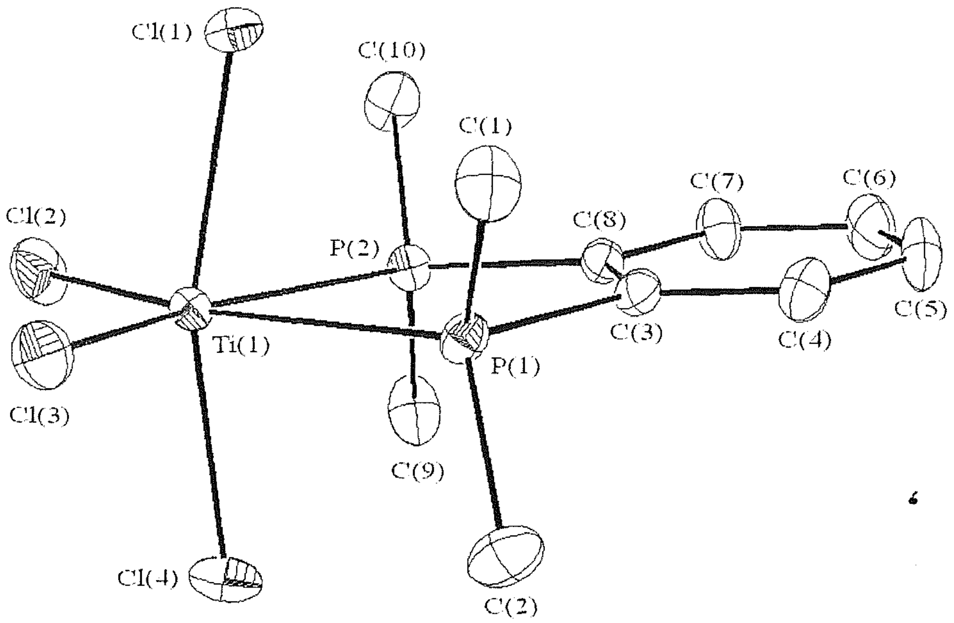

Crystals obtained for the directly comparable 1:2 adduct [$TiCl_4\{o\text{-}C_6H_4(PMe_2)_2\}_2$] were of slightly poorer quality and hence the final structure solution led to higher residuals than the 1:1 structure. Nevertheless, the observed structure (Figure 4.7, Tables

4.3, 4.4) shows dodecahedral geometry at Ti(IV), resulting from crystallographic $\bar{4}$ symmetry. The 8-coordinate structure comprises four symmetry equivalent P-donor atoms occupying the A-type vertices and four equivalent chloro ligands occupying B vertices (see Coordination Geometry, Chapter 1). Similar arrangements of the donor atoms have been observed for the only other structurally characterised 8-coordinate Ti(IV) complexes, $[TiCl_4\{o\text{-}C_6H_4(AsMe_2)_2\}_2]$[11,12] and $[TiCl_4\{Me_2P(CH_2)_2PMe_2\}_2]$,[19] though the early report of the former provided little crystallographic data concerning the geometry at Ti(IV). The Ti-P bond lengths [2.654(4) Å] in $[TiCl_4\{o\text{-}C_6H_4(PMe_2)_2\}_2]$ are significantly longer (*ca.* 0.1 Å) than those in the 1:1 adduct [2.5608(10), 2.5745(11) Å], consistent with increased steric crowding upon increasing the coordination number at Ti(IV). However, the Ti-Cl bond lengths [2.503(3) Å] show approximately twice this increase in bond length (*ca.* 0.2 – 0.25 Å) compared to the 1:1 adduct [2.2522(11) – 2.2980(11) Å]. This disparity between the effect of increasing coordination number on the respective bond lengths may at least in part be due to the differing *trans* influences in the respective adducts. Thus, in the 1:1 adduct, the P-donor atoms reside approximately *trans* to chloro ligands [$\angle Cl_{trans\ P} - Ti - P = 160.40(4), 160.99(4)°$], whereas in the 1:2 adduct the $Cl_{trans\ P} - Ti - P$ angle is 143.93(10)° and therefore there are no formally *trans* ligands. Hence the *trans* influence in the former is high, leading to shortened $Ti\text{-}Cl_{trans\ P}$ bond distances. Whereas, the absence of a *trans* influence in the 1:2 adduct results in a greater increase in Ti-Cl bond lengths compared with Ti-P upon increasing coordination number at Ti(IV). The increased Ti-P bond lengths in the 1:2 adduct also lead to a more acute bite-angle for the chelating ligand [$\angle$ P(1) – Ti(1) – P(2) = 72.7(2)°, cf. 76.05(3)° in 1:1 adduct], with the short ligand backbone enforcing distortion of the dodecahedral geometry. These bond parameters all compare well with those previously reported for $[TiCl_4\{Me_2P(CH_2)_2PMe_2\}_2]$,[19] which exhibited only 2-fold symmetry at Ti(IV) [Ti-P = 2.648(1), 2.654(1) Å, Ti-Cl = 2.445(1), 2.451(1) Å, chelating $\angle$ P-Ti-P = 73.12(3)°]. Comparison of this structure with the analogous 1:1 adduct $[TiCl_4\{Me_2P(CH_2)_2PMe_2\}]$ shows similar trends to those observed here,[14] with the Ti-Cl bonds [av. 2.290(2) Å] reduced to a greater extent than the Ti-P bond distances [av. 2.580(2) Å] in the 1:1 adduct. These structures represent the only other case where directly comparable 6- and 8-coordinate Ti(IV) complexes with phosphine or arsine ligands have been structurally characterised.

Figure 4.7 View of the structure of [$TiCl_4\{o\text{-}C_6H_4(PMe_2)_2\}_2$] with numbering scheme adopted. Ellipsoids drawn at 40%, H-atoms omitted for clarity.

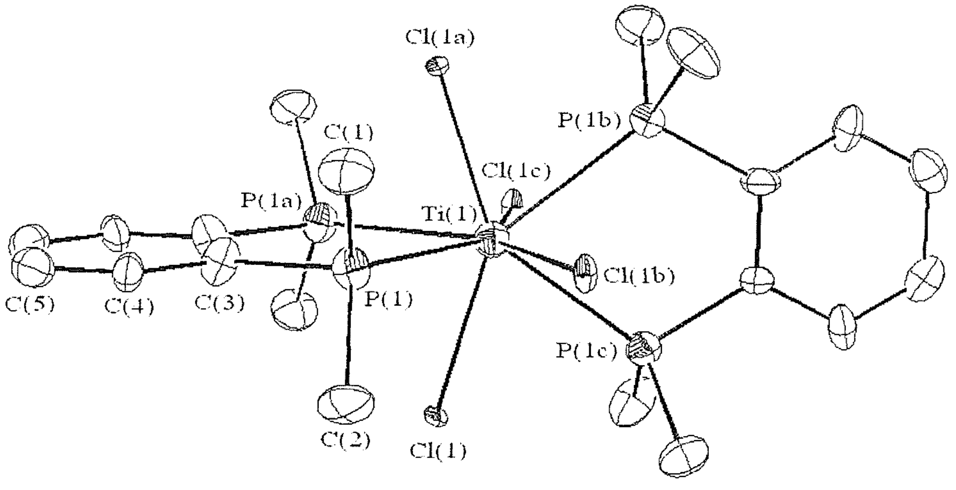

The crystals of [$TiBr_4\{o\text{-}C_6H_4(PMe_2)_2\}_2$] (Figure 4.8, Tables 4.3, 4.4) are isostructural with the above [$TiCl_4\{o\text{-}C_6H_4(PMe_2)_2\}_2$] adduct and hence comparison of these structures shows the effect of the halide (X) on the geometry at Ti(IV). However, while the Ti-P bond lengths [2.672(2) Å] increased slightly (*ca.* 0.02 Å) on changing halide from Cl to Br, the higher than normal residuals associated with the chloro-structure prevented conclusive determination as to the effect of changing halide. Nevertheless, an increase in Ti-P bond length would be consistent with the expected weaker interactions between the phosphine ligand and the poorer Lewis acid $TiBr_4$.

Figure 4.8 View of the structure of [$TiBr_4\{o\text{-}C_6H_4(PMe_2)_2\}_2$] with numbering scheme adopted. Ellipsoids drawn at 40%, H-atoms omitted for clarity.

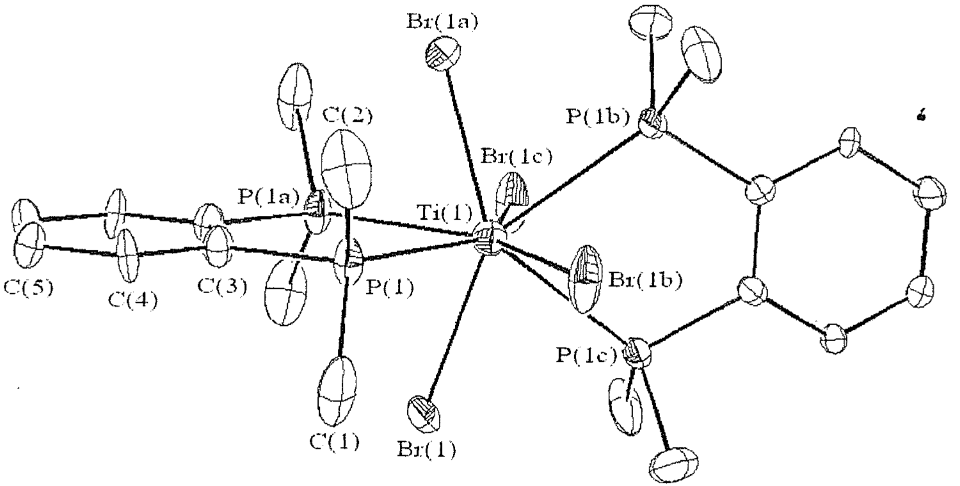

Table 4.3 Selected bond lengths for [$TiX_4\{o\text{-}C_6H_4(EMe_2)_2\}_2$].

		Distance / Å	
Bond	X = Cl, E =P	X = Br, E =P	X = Br, E =As
Ti(1) – E(1)	2.654(4)	2.672(2)	2.7324(13)
Ti(1) – X(1)	2.503(3)	2.5776(9)	2.5869(12)

Table 4.4 Selected bond angles for [$TiX_4\{o\text{-}C_6H_4(EMe_2)_2\}_2$].

		Angle / °	
Bond	X = Cl, E =P	X = Br, E =P	X = Br, E =As
E(1) – Ti(1) – E(1a)	72.7(2)	72.86(10)	73.35(5)
E(1) – Ti(1) – E(1b/c)	130.44(11)	130.34(6)	130.03(3)
E(1) – Ti(1) – X(1)	75.97(12)	75.89(7)	75.98(5)
E(1) – Ti(1) – X(1a)	75.88(12)	75.86(7)	75.92(5)
E(1) – Ti(1) – X(1b)	71.22(10)	71.22(6)	70.94(4)
E(1) – Ti(1) – X(1c)	143.93(10)	144.08(5)	144.29(4)
X(1) – Ti(1) – X(1a)	144.85(11)	144.70(4)	144.77(6)
X(1) – Ti(1) – X(1b/c)	95.23(3)	95.276(13)	95.26(2)

The crystals of [$TiBr_4\{o\text{-}C_6H_4(AsMe_2)_2\}_2$] (Figure 4.9, Tables 4.3, 4.4) are also isostructural with the other 1:2 adducts and show nearly identical bond angles at the Ti(V) centre. The Ti-As bond lengths [2.7324(13) Å] are consistent with those reported for [$TiCl_4\{o\text{-}C_6H_4(AsMe_2)_2\}_2$] [2.71(2) Å], [11,12] although the large estimated standard deviations (e.s.d's) associated with the reported structure prevents detailed comparison of the bond parameters. The Ti-As bond lengths in [$TiBr_4\{o\text{-}C_6H_4(AsMe_2)_2\}_2$] are longer than the Ti-P bond lengths in the analogous phosphine adduct [$TiBr_4\{o\text{-}C_6H_4(PMe_2)_2\}_2$], again consistent with the larger size and softer nature of the of the As-donor compared to P. However, the observed difference of *ca.* 0.06 Å is smaller than that observed for other transition metal halide complexes involving the ligands $o\text{-}C_6H_4(EMe_2)_2$ (E = P, As). For example, the M-E bond distances in [$NiCl_2\{o\text{-}C_6H_4\text{-}(EMe_2)_2\}_2$]$^+$ differ by *ca.* 0.09 Å [E = P, 2.255(3) Å; E = As, 2.339(3), 2.345(3) Å][28,29].

Figure 4.9 View of the structure of $[TiBr_4\{o\text{-}C_6H_4(AsMe_2)_2\}_2]$ with numbering scheme adopted. Ellipsoids drawn at 40%, H-atoms omitted for clarity.

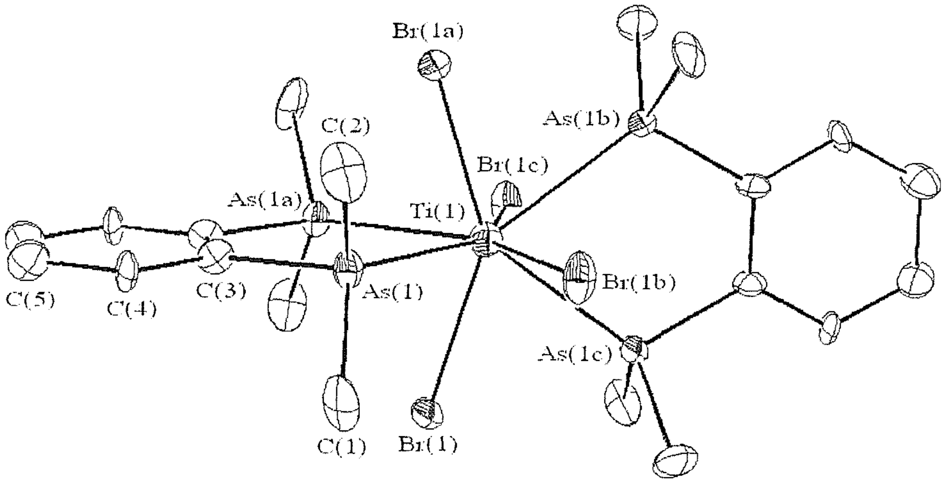

During attempts to grow crystals of $[TiCl_4(Ph_2PCH_2PPh_2)]$ *via* slow evaporation of a CH_2Cl_2 solution of the complex in a dry N_2-purged glove box, a small number of single crystals of the partially decomposed complex $[TiCl_5(Ph_2PCH_2PHPh_2)]$ were isolated. One possible *in situ* route to this adduct may arise through the lability of the phosphine ligand in solution due to the highly strained 4-membered chelate ring present in the original $[TiCl_4(Ph_2PCH_2PPh_2)]$. Thus, chelate ring opening may lead to an equilibrium between $[TiCl_4(Ph_2PCH_2PPh_2)]$, $[TiCl_4(\eta^1\text{-}Ph_2PCH_2PPh_2)]$, $TiCl_4$ and $Ph_2PCH_2PPh_2$. As free $TiCl_4$ hydrolyses in the presence of trace moisture to give TiO_2 and HCl,[30] it is possible that HCl may undergo addition with the coordinatively unsaturated species $[TiCl_4(\eta^1\text{-}Ph_2PCH_2PPh_2)]$ to afford the observed complex.

The structure shows (Figure 4.10, Tables 4.5, 4.6) the phosphine coordinated as a monodentate ligand to the $TiCl_5$ fragment, with the uncoordinated P-donor protonated to give a phosphonium functionality. The P-bound proton was located during the structure solution and its presence provides charge neutrality with the $[TiCl_5]^-$ fragment. The geometry of this unusual zwitter-ionic species shows similarities with other 6-coordinate Ti(IV) phosphine complexes, with the chloride ligands again leaning towards the phosphine donor [$\angle$ P-Ti-$Cl_{cis\ P}$ = 82.16(11) – 87.60(12)°]. The *trans* influence again accounts for a shorter Ti-Cl bond distance for the chloride *trans* to the donor ligand [2.276(3) Å] compared with the mutually *trans* chlorides [2.283(3) – 2.333(3) Å], however the disparity is surprisingly small considering the near linear P-Ti-$Cl_{trans\ P}$

bond angle [176.53(13)°]. This may reflect that the phosphine is not strongly coordinating and therefore does not compete with the *trans* chloride. Indeed, the Ti-P bond distance [2.731(4) Å] is considerably longer than those observed in other 6-coordinate Ti(IV) phosphine complexes, [$TiCl_4\{o\text{-}C_6H_4(PMe_2)_2\}$] [2.5608(10), 2.5745(11) Å] and [$TiCl_4\{Ph_2P(CH_2)_2PPh_2\}$] [2.577(2), 2.582(2) Å].[14] This may be attributed to the deactivation of the P-based lone pair upon quaternisation of the adjacent P centre in [$TiCl_5(Ph_2PCH_2PHPh_2)$]. The small yield of crystals prevented further characterisation except for IR spectroscopy, which showed three Ti-Cl stretching vibrations ($2A_1$ + E) consistent with the local C_{4v} symmetry at Ti(IV).

Figure 4.10 View of the structure of [$TiCl_5(Ph_2PCH_2PHPh_2)$] with numbering scheme adopted. Ellipsoids drawn at 40%, H-atoms omitted for clarity.

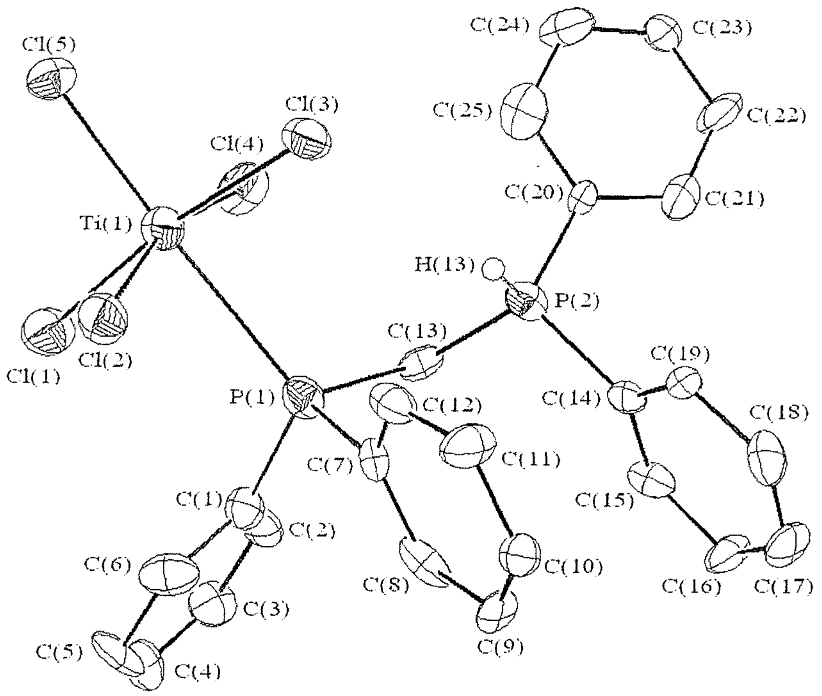

Table 4.5 Selected bond lengths for [$TiCl_5(Ph_2PCH_2PHPh_2)$].

Bond	Distance / Å	Bond	Distance / Å
Ti(1) – P(1)	2.731(4)	Ti(1) – Cl(1)	2.283(3)
Ti(1) – Cl(2)	2.290(3)	Ti(1) – Cl(3)	2.333(3)
Ti(1) – Cl(4)	2.320(3)	Ti(1) – Cl(5)	2.276(2)

Table 4.6 Selected bond angles for [$TiCl_5(Ph_2PCH_2PHPh_2)$].

Bond	Angle / °	Bond	Angle / °
P(1) – Ti(1) – Cl(1)	87.60(12)	P(1) – Ti(1) – Cl(2)	82.23(10)
P(1) – Ti(1) – Cl(3)	83.67(11)	P(1) – Ti(1) – Cl(4)	82.15(11)
P(1) – Ti(1) – Cl(5)	176.53(13)	Cl(1) – Ti(1) – Cl(2)	89.1(1)
Cl(1) – Ti(1) – Cl(3)	171.2(1)	Cl(1) – Ti(1) – Cl(4)	87.88(13)
Cl(1) – Ti(1) – Cl(5)	95.69(12)	Cl(2) – Ti(1) – Cl(3)	90.96(12)
Cl(2) – Ti(1) – Cl(4)	164.21(13)	Cl(2) – Ti(1) – Cl(5)	98.90(12)
Cl(3) – Ti(1) – Cl(4)	89.67(13)	Cl(3) – Ti(1) – Cl(5)	93.02(13)
Cl(4) – Ti(1) – Cl(5)	96.83(12)		

Other unusual structures were also observed during attempts to grow crystals of the 1:2 iodo complex [$TiI_4\{o\text{-}C_6H_4(AsMe_2)_2\}_2$]. Thus, deep purple solutions of two independently synthesised samples of the complex were allowed to slowly evaporate in a dry N_2-purged glove box. Although both solutions showed signs of decomposition through the deposition of a pale coloured precipitate, a small number of dark red/purple coloured crystals were isolated from each solution. The resulting structure solutions clearly showed the coordination of two chelating $o\text{-}C_6H_4(AsMe_2)_2$ ligands to the metal centre, however both structures were only 6-coordinate with two of the iodo ligands apparently displaced by arsine coordination. Surprisingly both structures suggested reduction of the Ti(IV) centre, with the first structure (**1**) showing only one tri-iodo counter-anion $[I_3]^-$ indicating Ti(III), and the second (**2**) showing no counter-anions and thus indicating a rare example of Ti(II). However, unusually large thermal parameters associated with the metal centres and considerably shorter M-As bond distances [*ca.* 2.38 Å (**1**), *ca.* 2.34 Å (**2**)] compared to [$TiX_4\{o\text{-}C_6H_4(AsMe_2)_2\}_2$] [X = Cl, 2.71(2) Å;[11,12] X = Br 2.7324(13) Å] suggested the metal centre was not actually titanium. Comparison with published collective bond length tables[31] suggested that the crystals were actually of Fe(III) and Fe(II) adducts and final structure solutions modelling these iron metal centres exhibited much more sensible thermal parameters (Figures 4.11, 4.12, Tables 4.7, 4.8). Indeed the observed bond distances [Fe-As: 2.3804(8), 2.3818(9) Å

(**1**), 2.3377(8), 2.3380(9) Å (**2**); Fe-I: 2.6018(6) Å (**1**), 2.6825(6) Å (**2**)] compare reasonably well with those ascertained *via* Fe K-edge EXAFS (extended X-ray absorption fine structure) spectroscopy of the previously reported adducts [FeI_2{*o*-$C_6H_4(AsMe_2)_2$}$_2$][BF_4] {Fe-As: 2.365(4) Å, Fe-I: 2.535(6) Å} and [FeI_2{*o*-$C_6H_4(AsMe_2)_2$}$_2$] {Fe-As: 2.341(2) Å, Fe-I: 2.701(3) Å}. The structures show the expected increase in Fe-As bond distances and decrease in Fe-I bond distances with increasing oxidation state of the metal centre. This is consistent with the harder Fe(III) centre forming weaker interactions with the soft arsine ligands and stronger interactions with the hard iodo ligands. This unusual observation of iron complexes from solutions of titanium samples may be attributed to iron impurities in TiI_4. Indeed, reported attempts to purify TiI_4 have shown the largest metallic impurity to be iron.[32,33] While the synthetic origin of the TiI_4 used in this study is unknown, the presence of an iron impurity is perhaps not surprising considering one of the principal ores for the production of titanium is the iron-containing mineral ilmenite ($FeTiO_3$). The presence of Fe metal centres was unambiguously confirmed *via* Energy Dispersive Analysis X-ray (EDAX) spectroscopy of the crystalline samples. Similar analysis of the bulk [TiI_4{*o*-$C_6H_4(AsMe_2)_2$}$_2$] sample confirmed that the isolated complex was indeed the Ti(IV) adduct with a small impurity of iron corresponding to the structurally characterised Fe(III) and Fe(II) complexes. This may explain the complicated spectra observed during NMR spectroscopy of the iodo phosphine and arsine adducts.

Figure 4.11 View of the structure of [FeI_2{*o*-$C_6H_4(AsMe_2)_2$}$_2$] with numbering scheme adopted. Ellipsoids drawn at 40%, H-atoms omitted for clarity.

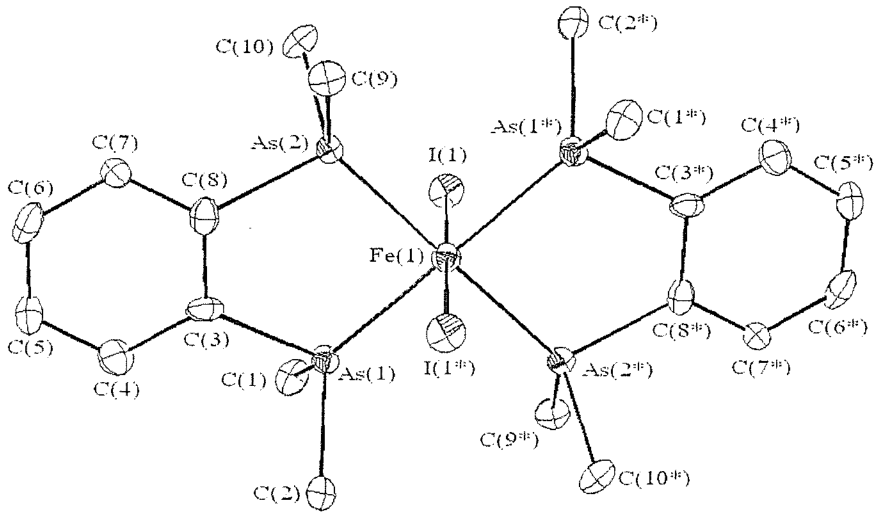

Figure 4.12 View of the structure of [$FeI_2\{o\text{-}C_6H_4(AsMe_2)_2\}_2$][$I_3$] with numbering scheme adopted. Ellipsoids drawn at 40%, H-atoms omitted for clarity.

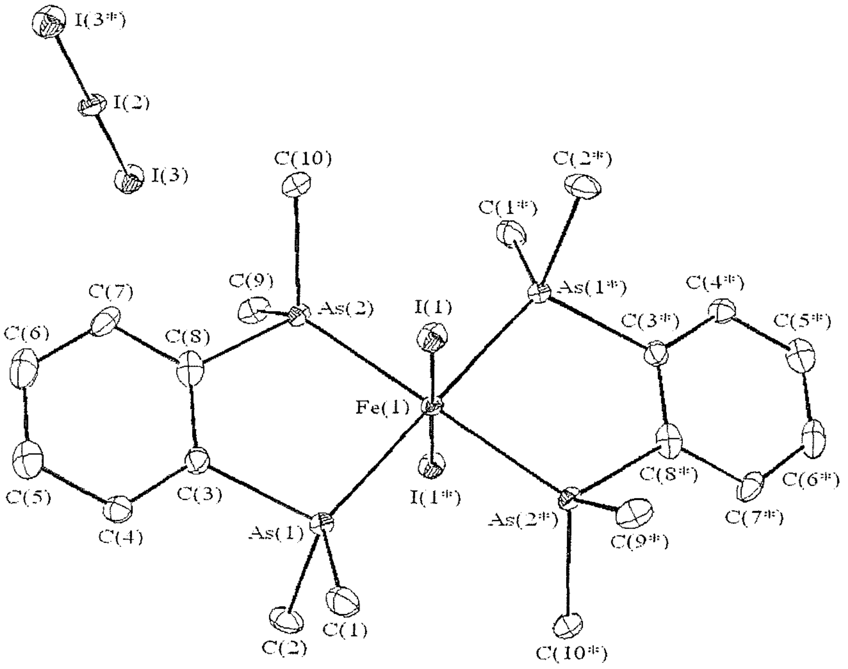

Table 4.7 Selected bond angles for [$FeI_2\{o\text{-}C_6H_4(AsMe_2)_2\}_2$] and [$FeI_2\{o\text{-}C_6H_4\text{-}(AsMe_2)_2\}_2$][$I_3$].

Bond	Angle / °	
	[$FeI_2\{o\text{-}C_6H_4(AsMe_2)_2\}_2$]	[$FeI_2\{o\text{-}C_6H_4(AsMe_2)_2\}_2$][$I_3$]
As(1) – Fe(1) – As(2)	86.34(3)	84.53(3)
As(1) – Fe(1) – As(1*)	180	180
As(1) – Fe(1) – As(2*)	93.66(3)	95.47(3)
As(1) – Fe(1) – I(1)	92.05(3)	87.30(3)
As(1) – Fe(1) – I(1*)	87.95(3)	92.70(3)
As(2) – Fe(1) – As(2*)	180	180
As(2) – Fe(1) – I(1)	92.24(2)	87.48(3)
As(2) – Fe(1) – I(1*)	87.76(2)	92.52(3)
I(1) – Fe(1) – I(1*)	180	180
I(3) – I(2) – I(3*)	-	180

Table 4.8 Selected bond lengths for [FeI$_2${*o*-C$_6$H$_4$(AsMe$_2$)$_2$}$_2$] and [FeI$_2${*o*-C$_6$H$_4$(AsMe$_2$)$_2$}$_2$][I$_3$].

Bond	Distance / Å	
	[FeI$_2${*o*-C$_6$H$_4$(AsMe$_2$)$_2$}$_2$]	[FeI$_2${*o*-C$_6$H$_4$(AsMe$_2$)$_2$}$_2$][I$_3$]
Fe(1) – As(1)	2.3377(8)	2.3818(9)
Fe(1) – As(2)	2.3380(9)	2.3804(8)
Fe(1) – I(1)	2.6825(6)	2.6018(6)

4.3 Conclusions

The complexes [TiX$_4$(L$_2$)] {X = Cl, Br; L$_2$ = Ph$_2$As(CH$_2$)$_2$AsPh$_2$, Ph$_2$P(CH$_2$)$_n$PPh$_2$ (n = 1, 2 or 3), *o*-C$_6$H$_4$(PPh$_2$)$_2$ and X = Cl, Br, I; *o*-C$_6$H$_4$(EMe)$_2$ (E = P or As)} have been prepared *via* the reaction of TiX$_4$ with the respective bidentate ligand, L$_2$ in anhydrous *n*-hexane (X = Cl) or CH$_2$Cl$_2$ (X = Br, I). Similar reactions with bidentate stibine ligands proved unsuccessful, indicating the poor interaction between the contracted Ti(IV) orbitals and the diffuse Sb orbitals. The complexes [TiX$_4$(L$_2'$)$_2$] {X = Cl, Br, I; L$_2'$ = *o*-C$_6$H$_4$(EMe)$_2$ (E = P or As)} have been similarly prepared using three equivalents of the respective ligands and present rare examples of 8-coordinate Ti(IV).

IR spectroscopy showed the 1:1 and 1:2 adducts adopt C$_{2v}$ and D$_{2d}$ local symmetry at Ti(IV) respectively, while electronic spectroscopy confirmed the donor atoms around Ti(IV). ^{1}H, ^{13}C{^{1}H} and ^{31}P{^{1}H} NMR spectroscopy revealed the solution behaviour of [TiX$_4$(L$_2$)] and [TiX$_4$(L$_2'$)$_2$], with the phenyl-substituted phosphine and arsine adducts showing increased ligand dissociation for bromo- compared to chloro-adducts. Furthermore, the 1:1 *o*-C$_6$H$_4$(EMe)$_2$ (E = P or As) adducts showed reduced high frequency shifts and hence reduced metal-ligand interactions with decreasing Ti(IV) Lewis acidity, TiCl$_4$ > TiBr$_4$ > TiI$_4$. Ligand dissociation was not extensive at room temperature for these 6-coordinate complexes, however the 8-coordinate 1:2 adducts showed increasing ligand dissociation with decreasing Ti(IV) Lewis acidity, with the bromo-adducts revealing dynamic equilibria between 1:1 and 1:2 adducts and free *o*-$C_6H_4(EMe)_2$. Spectra of the iodo adducts revealed the presence of impurities.

X-ray crystallography of $[TiCl_4\{o\text{-}C_6H_4(PMe_2)_2\}]$ confirmed *cis* coordination of the phosphine ligand, with chloride ligands leaning towards the bidentate ligand, as observed for the thio- and seleno-ether Ti(IV) complexes reported in Chapter 3. Longer Ti-Cl bond lengths between chlorides *trans* to Cl compared to those *trans* to P revealed a *trans* influence of Cl > P on Ti(IV), illustrating preference for the harder Cl donor. The 8-coordinate complexes $[TiX_4\{o\text{-}C_6H_4(EMe_2)_2\}_2]$ (E = P, X = Cl, Br; E = As, X = Br) are all isostructural and show dodecahedral geometry at Ti(IV). Comparison of the structures of $[TiCl_4\{o\text{-}C_6H_4(EMe_2)_2\}_n]$ (n = 1, 2) showed the expected increase in bond lengths with increased coordination number, with greatest increase observed for Ti-Cl, consistent with the absence of any *trans* influence in the 1:2 adduct.

Attempts to crystallise $[TiCl_4(Ph_2PCH_2PPh_2)]$ afforded the partially decomposed complex $[TiCl_5(Ph_2PCH_2PHPh_2)]$, with the uncoordinated P-donor protonated to give a phosphonium unit. Comparison of the structure with that of $[TiCl_4\{o\text{-}C_6H_4(PMe_2)_2\}]$ showed similar geometry at Ti(IV), with chlorides leaning towards the phosphine ligand. The Ti-P bond length is significantly longer in the phosphonium adduct, consistent with deactivation of the lone pair by quaternisation of the adjacent P-atom.

Crystals of the Fe(II) and Fe(III) complexes $[FeI_2\{o\text{-}C_6H_4(AsMe_2)_2\}_2]$ and $[FeI_2\{o\text{-}C_6H_4(AsMe_2)_2\}_2][I_3]$ were obtained from solutions of $[TiI_4\{o\text{-}C_6H_4(AsMe_2)_2\}_2]$. This has been attributed to Fe impurity in TiI_4, with subsequent reaction with *o*-$C_6H_4(AsMe_2)_2$ forming a mixture of Ti and Fe containing complexes. The structures showed increased Fe-As bond lengths and decreased Fe-I bond lengths with increasing oxidation state, consistent with the preference of the charged iodo ligands by the harder Fe(III) centre.

4.4 Experimental

The bidentate ligands *o*-$C_6H_4(PPh_2)_2$, *o*-$C_6H_4(PMe_2)_2$, *o*-$C_6H_4(AsMe_2)_2$ and $Ph_2As(CH_2)_2AsPh_2$ were prepared *via* the literature procedures,[34,35,36,37] while the other phosphine ligands and TiX_4 were used as received from Aldrich Chemical Company. Rigorously anhydrous *n*-hexane and CH_2Cl_2 were freshly distilled over sodium/ benzophenone and CaH_2 respectively and degassed with dry N_2, while deuterated solvents were dried over molecular sieves. All reactions were performed under an N_2 atmosphere using standard Schlenk techniques. The products were transferred and stored in a dry, continuously N_2-purged glove box, as were all sample preparations.

[TiCl$_4$(Ph$_2$PCH$_2$PPh$_2$)]

$TiCl_4$ (0.10 cm^3, 0.91 mmol) was added *via* degassed syringe to a solution of $Ph_2PCH_2PPh_2$ (0.35 g, 0.91 mmol) in dry, degassed *n*-hexane (20 cm^3). The immediately precipitated bright orange solid was filtered, washed with *n*-hexane (5 cm^3) and dried *in vacuo* to give the required [$TiCl_4(Ph_2PCH_2PPh_2)$] (yield 0.45 g, 88 %). Required for [$C_{25}H_{22}Cl_4P_2Ti$]: C = 52.3, H = 3.8 %; found: C = 52.0, H = 3.7 %. ^{1}H NMR (300 K): δ 7.0-8.0 (*m*, Ph, 20H), 4.0 (*t*, CH_2, 2H, $^2J_{H\text{-}P}$ = 10 Hz). IR ν(TiCl): 419, 398, 385, 375 cm^{-1}. Electronic spectrum (10^{-3} ν_{max}): 20.7, 28.5(sh), 34.8 cm^{-1}.

[TiCl$_4$(Ph$_2$P(CH$_2$)$_2$PPh$_2$)]

As above, but using $Ph_2P(CH_2)_2PPh_2$ (0.36 g, 0.91 mmol). An orange solid was isolated as the required [$TiCl_4(Ph_2P(CH_2)_2PPh_2)$] (yield 0.43 g, 80 %). Required for [$C_{26}H_{24}Cl_4P_2Ti$]: C = 53.0, H = 4.1 %; found: C = 53.7, H = 4.4 %. ^{1}H NMR (300 K): δ 7.1-7.9 (*m*, Ph, 20H), 3.0 (*d*, CH_2, 4H). ^{31}P{^{1}H} NMR (300 K): δ 24.6. IR ν(TiCl): 420, 398, 385, 376 cm^{-1}. Electronic spectrum (10^{-3} ν_{max}): 20.7, 26.1(sh), 34.8 cm^{-1}.

[TiCl$_4${Ph$_2$P(CH$_2$)$_3$PPh$_2$}]

As above, using $Ph_2P(CH_2)_3PPh_2$ (0.38 g, 0.91 mmol). An orange solid was isolated as the required [$TiCl_4(Ph_2P(CH_2)_2PPh_2)$] (yield 0.49 g, 91 %). Required for [$C_{27}H_{26}Cl_4$-P_2Ti]: C = 53.8, H = 4.3 %; found: C = 53.6, H = 4.4 %. ^{1}H NMR (300 K): δ 7.2-7.8 (*m*, Ph, 20H), 2.7 (*t*, CH_2, 4H), 2.2 (*q*, CH_2, 2H). ^{31}P{^{1}H} NMR (300 K): δ 2.3(br). IR ν(TiCl):

417, 394, 369, 372 cm^{-1}. Electronic spectrum (10^{-3} ν_{max}): 20.7, 27.8(sh), 37.7 cm^{-1}.

[TiCl$_4${o-C$_6$H$_4$(PPh$_2$)$_2$}]

As above, but using o-C$_6$H$_4$(PPh$_2$)$_2$ (0.41 g, 0.91 mmol). An orange solid was isolated as the required [TiCl$_4${o-C$_6$H$_4$(PPh$_2$)$_2$}] (yield 0.69 g, 81 %). Required for [$C_{30}H_{24}Cl_4P_2Ti$]: C = 56.6, H = 3.8 %; found: C = 56.3, H = 3.9 %. ^{1}H NMR (300 K): δ 7.0-8.2 (*m*, *o*-C$_6$H$_4$, Ph). ^{31}P{^{1}H} NMR (300 K): δ 34.1. IR ν(TiCl): 420, 408, 386, 375 cm^{-1}. Electronic spectrum (10^{-3} ν_{max}): 21.3, 26.0(sh), 32.3 cm^{-1}.

[TiCl$_4${o-C$_6$H$_4$(PMe$_2$)$_2$}]

As above, but using o-C$_6$H$_4$(PMe$_2$)$_2$ (0.18 g, 0.91 mmol). A pale yellow solid was isolated as the required [TiCl$_4${o-C$_6$H$_4$(PMe$_2$)$_2$}] (yield 0.10 g, 57 %). Required for [$C_{10}H_{16}Cl_4P_2Ti$]: C = 31.0, H = 4.2 %; found: C = 31.2, H = 4.3 %. ^{1}H NMR (300 K): δ 7.75-7.80 (*m*, *o*-C$_6$H$_4$), 1.90 (*d*, Me). ^{31}P{^{1}H} NMR (300 K): δ 29.5. IR ν(TiCl): 426, 398, 381, 365 cm^{-1}. Electronic spectrum (10^{-3} ν_{max}): 22.7, 28.6, 33.0 cm^{-1}.

[TiCl$_4${Ph$_2$As(CH$_2$)$_2$AsPh$_2$}]

As above, but using Ph$_2$As(CH$_2$)$_2$AsPh$_2$ (0.44 g, 0.91 mmol). A red solid was isolated as the required [TiCl$_4${Ph$_2$As(CH$_2$)$_2$AsPh$_2$}] (yield 0.26 g, 86 %). Required for [$C_{26}H_{24}As_2Cl_4Ti$]: C = 46.2, H = 3.6 %; found: C = 46.0, H = 3.7 %. ^{1}H NMR (300 K): δ 7.7-7.3 (*m*, Ph, 20H), 3.1 (*s*, CH$_2$, 4H). IR ν(TiCl): 401, 385, 377, 370 cm^{-1}. Electronic spectrum (10^{-3} ν_{max}): 20.0, 21.7, 25.0, 32.3 cm^{-1}.

[TiCl$_4${o-C$_6$H$_4$(AsMe$_2$)$_2$}]

As above, but using o-C$_6$H$_4$(AsMe$_2$)$_2$ (0.26 g, 0.91 mmol). A pale orange solid was isolated as the required [TiCl$_4${o-C$_6$H$_4$(AsMe$_2$)$_2$}] (yield 0.16 g, 62 %). Required for [$C_{10}H_{16}As_2Cl_4Ti$]: C = 25.2, H = 3.4 %; found: C = 25.4, H = 3.4 %. ^{1}H NMR (300 K): δ 7.65-7.75 (*m*, *o*-C$_6$H$_4$), 1.90 (*s*, Me). ^{13}C{^{1}H} NMR (193 K): δ 131-132 (*o*-C$_6$H$_4$), 13.7 (AsMe$_2$). IR ν(TiCl): 412, 396, 366, 357 cm^{-1}. Electronic spectrum (10^{-3} ν_{max}): 21.9, 29.1, 33.0 cm^{-1}.

[$TiCl_4\{o$-$C_6H_4(PMe_2)_2\}_2$]

As above, but using $TiCl_4$ (0.05 cm^3, 0.46 mmol) and 3 molar equivalents of *o*-$C_6H_4(PMe_2)_2$ (0.27 g, 1.37 mmol). A golden yellow solid was isolated as the required [$TiCl_4\{o$-$C_6H_4(PMe_2)_2\}_2$] (yield 0.23 g, 85 %). Required for [$C_{20}H_{32}Cl_4P_4Ti$]: C = 41.0, H = 5.5 %; found: C = 40.6, H = 5.3 %. ^1H NMR (300 K): δ 7.70-7.75 (*m*, *o*-C_6H_4), 1.83 (*d*, Me). $^{31}P\{^1H\}$ NMR (300 K): δ 31.5. IR ν(TiCl): 314, 302 cm^{-1}. Electronic spectrum (10^{-3} ν_{max}): 20.8, 22.5, 24.0, 28.0 cm^{-1}.

[$TiCl_4\{o$-$C_6H_4(AsMe_2)_2\}_2$]

As above, but using $TiCl_4$ (0.05 cm^3, 0.46 mmol) and 3 molar equivalents of *o*-$C_6H_4(AsMe_2)_2$ (0.39 g, 1.37 mmol). A bright orange solid was isolated as the required [$TiCl_4\{o$-$C_6H_4(AsMe_2)_2\}_2$] (yield 0.31 g, 89 %). Required for [$C_{20}H_{32}As_4Cl_4Ti$]: C = 31.5, H = 4.2 %; found: C = 31.4, H = 4.0 %. ^1H NMR (300 K): δ 7.55-7.65 (*m*, *o*-C_6H_4), 1.78 (*s*, Me). $^{13}C\{^1H\}$ NMR (193 K): δ 132-133 (*o*-C_6H_4), 14.9 ($AsMe_2$). IR ν(TiCl): 323, 317 cm^{-1}. Electronic spectrum (10^{-3} ν_{max}): 21.6, 27.6 cm^{-1}.

[$TiBr_4\{Ph_2P(CH_2)_2PPh_2\}$]

$Ph_2P(CH_2)_2PPh_2$ (0.16 g, 0.41 mmol) in dry, degassed CH_2Cl_2 (10 cm^3) was added to a solution of $TiBr_4$ (0.15 g, 0.41 mmol) in CH_2Cl_2 (30 cm^3). The resulting red solution was stirred for 30 min. then concentrated *in vacuo* to 5 cm^3. Addition of dry, degassed *n*-hexane (20 cm^3) afforded an orange solid that was filtered, washed with *n*-hexane (5 cm^3) and dried *in vacuo* to give the required [$TiBr_4\{Ph_2P(CH_2)_2PPh_2\}$] (yield 0.26 g, 65 %). Required for [$C_{26}H_{24}Br_4P_2Ti$]: C = 40.8, H = 3.2 %; found: C = 40.4, H = 3.2 %. ^1H NMR (300 K): δ 6.8-7.9 (*m*, Ph, 20H), 4.4-4.8 (*m*, CH_2, 4H). $^{31}P\{^1H\}$ NMR (300 K): δ 13.0 (*s*); (200 K): δ 15.4. IR ν(TiBr): 309, 299, 292, 284 cm^{-1}. Electronic spectrum (10^{-3} ν_{max}): 20.6, 25.5, 34.5 cm^{-1}.

[$TiBr_4\{Ph_2P(CH_2)_3PPh_2\}$]

As above, but using $Ph_2P(CH_2)_3PPh_2$ (0.17 g, 0.41 mmol). An orange/red solid was isolated as the required [$TiBr_4(Ph_2P(CH_2)_2PPh_2)$] (yield 0.23 g, 73 %). Required for [$C_{27}H_{26}Br_4P_2Ti$]: C = 41.5, H = 3.3 %; found: C = 42.0, H = 3.5 %. ^1H NMR (300 K): δ

7.2-8.3 (*m*, Ph, 20H), 3.0-3.6 (br, CH_2, 6H). $^{31}P\{^1H\}$ NMR (300 K): δ 3.5(br). IR ν(TiBr): 313, 298, 293, 285 cm^{-1}. Electronic spectrum (10^{-3} ν_{max}): 22.5, 32.7 cm^{-1}.

[$TiBr_4\{o\text{-}C_6H_4(PPh_2)_2\}$]

As above, but using $o\text{-}C_6H_4(PPh_2)_2$ (0.18 g, 0.41 mmol). A red/orange solid was isolated as the required [$TiBr_4\{o\text{-}C_6H_4(PPh_2)_2\}$] (yield 0.26 g, 72 %). Required for [$C_{30}H_{24}Br_4P_2Ti$]: C = 44.2, H = 2.9 %; found: C = 44.6, H = 3.0 %. ^1H NMR (300 K): δ 7.0-8.3 (*m*, Ph, $o\text{-}C_6H_4$). $^{31}P\{^1H\}$ NMR (300 K): δ -10.3(br). IR ν(TiBr): 315, 310, 304, 301 cm^{-1}. Electronic spectrum (10^{-3} ν_{max}): 20.5, 21.8, 24.6 cm^{-1}.

[$TiBr_4\{o\text{-}C_6H_4(PMe_2)_2\}$]

As above, but using $o\text{-}C_6H_4(PMe_2)_2$ (0.08 g, 0.41 mmol). An orange/brown solid was isolated as the required [$TiBr_4\{o\text{-}C_6H_4(PMe_2)_2\}$] (yield 0.16 g, 55 %). Required for [$C_{10}H_{16}Br_4P_2Ti$]: C = 21.2, H = 2.8 %; found: C = 21.6, H = 2.9 %. ^1H NMR (300 K): δ 7.60-7.70 (*m*, $o\text{-}C_6H_4$), 2.03 (*d*, Me). $^{31}P\{^1H\}$ NMR (300 K): δ 24.5. IR ν(TiBr): 321, 317(sh), 308(sh), 300 cm^{-1}. Electronic spectrum (10^{-3} ν_{max}): 21.0, 23.3, 27.7 cm^{-1}.

[$TiBr_4\{Ph_2As(CH_2)_2AsPh_2\}$]

As above, but using $Ph_2As(CH_2)_2AsPh_2$ (0.20 g, 0.41 mmol). A red solid was isolated as the required [$TiBr_4\{Ph_2As(CH_2)_2AsPh_2\}$] (yield 0.33 g, 78 %). Required for [$C_{26}H_{24}As_2Br_4Ti$]: C = 36.6, H = 2.8 %; found: C = 36.3, H = 3.0 %. ^1H NMR (300 K): δ 7.7-7.4 (*m*, 20H, Ph), 3.1 (s, 4H, CH_2). IR ν(TiCl): 304, 295, 291, 285 cm^{-1}. Electronic spectrum (10^{-3} ν_{max}): 18.9, 22.2, 28.6, 32.3 cm^{-1}.

[$TiBr_4\{o\text{-}C_6H_4(AsMe_2)_2\}$]

As above, but using $o\text{-}C_6H_4(AsMe_2)_2$ (0.12 g, 0.41 mmol). A bright red solid was isolated as the required [$TiBr_4\{o\text{-}C_6H_4(AsMe_2)_2\}$] (yield 0.17 g, 53 %). Required for [$C_{10}H_{16}As_2Cl_4Ti$]: C = 18.4, H = 2.5 %; found: C = 18.4, H = 2.5 %. ^1H NMR (300 K): δ 7.55-7.65 (*m*, $o\text{-}C_6H_4$), 1.90 (*s*, Me). $^{13}C\{^1H\}$ NMR (193 K): δ 131-132 ($o\text{-}C_6H_4$), 17.3 ($AsMe_2$). IR ν(TiBr): 330(sh), 326, 322, 318(sh) cm^{-1}. Electronic spectrum (10^{-3} ν_{max}): 20.0, 22.6, 27.2 cm^{-1}.

[TiBr$_4${*o*-C$_6$H$_4$(PMe$_2$)$_2$}$_2$]

As above, but using TiBr$_4$ (0.10 g, 0.27 mmol) and 3 molar equivalents of *o*-C$_6$H$_4$(PMe$_2$)$_2$ (0.16 g, 0.82 mmol). A bright orange solid was isolated as the required [TiBr$_4${*o*-C$_6$H$_4$(PMe$_2$)$_2$}$_2$] (yield 0.11 g, 55 %). Required for [C$_{20}$H$_{32}$Br$_4$P$_4$Ti]: C = 31.4, H = 4.2 %; found: C = 31.2, H = 4.0 %. ^{1}H NMR (300 K): δ 7.6-7.8 (*m*, *o*-C$_6$H$_4$), 2.05 (*d*, Me, 1:1), 1.33 (*s*, Me, free ligand); (183 K): 7.6-7.9 (*m*, *o*-C$_6$H$_4$), 2.05 (*m*, Me, 1:1), 1.97 (*d*, Me, 1:2), 1.32 (*s*, Me, free ligand). ^{31}P{^{1}H} NMR (300 K): δ 22.2 [TiBr$_4${*o*-C$_6$H$_4$(PMe$_2$)$_2$}$_2$], 24.5 [TiBr$_4${*o*-C$_6$H$_4$(PMe$_2$)$_2$}] and -54 *o*-C$_6$H$_4$(PMe$_2$)$_2$. IR ν(TiBr): 288, 280 cm^{-1}. Electronic spectrum (10^{-3} ν_{max}): 18.9, 21.5, 25.8, 29.0 cm^{-1}.

[TiBr$_4${*o*-C$_6$H$_4$(AsMe$_2$)$_2$}$_2$]

As above, but using TiBr$_4$ (0.10 g, 0.27 mmol) and 3 molar equivalents of *o*-C$_6$H$_4$(AsMe$_2$)$_2$ (0.24 g, 0.82 mmol). An orange/red solid was isolated as the required [TiBr$_4${*o*-C$_6$H$_4$(AsMe$_2$)$_2$}$_2$] (yield 0.19 g, 76 %). Required for [C$_{20}$H$_{32}$As$_4$Br$_4$Ti]: C = 25.6, H = 3.4 %; found: C = 25.2, H = 3.5 %. ^{1}H NMR (300 K): δ 7.5-7.7 (*m*, *o*-C$_6$H$_4$), 1.90 (*d*, Me, 1:1), 1.34 (*s*, Me, free ligand); (183 K): 7.6-7.7 (*m*, *o*-C$_6$H$_4$), 1.94 (*d*, Me, 1:1), 1.79 (*d*, Me, 1:2). ^{13}C{^{1}H} NMR (193 K): δ 130-132 (*o*-C$_6$H$_4$, 1:1), 17.4 (AsMe$_2$, 1:1). IR ν(TiBr): 280, 277 cm^{-1}. Electronic spectrum (10^{-3} ν_{max}): 18.5, 20.3, 22.7 cm^{-1}.

[TiI$_4${*o*-C$_6$H$_4$(PMe$_2$)$_2$}]

TiI$_4$ (0.20 g, 0.36 mmol) was dissolved in mildly refluxing dry CH$_2$Cl$_2$ (80 cm^3), with subsequent removal of undissolved solids *via* filtration affording a deep purple solution. Addition of *o*-C$_6$H$_4$(PMe$_2$)$_2$ (0.07 g, 0.36 mmol) in dry, degassed CH$_2$Cl$_2$ (10 cm^3) gave an immediate colour change and the resulting dark red solution was stirred for 30 min., then concentrated *in vacuo* to 5 cm^3. Dry, degassed *n*-hexane (20 cm^3) was added and CH$_2$Cl$_2$ was removed *in vacuo* to afford a dark purple precipitate that was filtered to give the required [TiI$_4${*o*-C$_6$H$_4$(PMe$_2$)$_2$}], (yield 0.08 g, 31 %). Required for [C$_{10}$H$_{16}$I$_4$P$_2$Ti]: C = 15.9, H = 2.1 %; found: C = 15.8, H = 2.2 %. ^{1}H NMR (300 K): δ 7.60-7.75 (*m*, *o*-C$_6$H$_4$), 2.28 (*m*, Me). ^{31}P{^{1}H} NMR (300 K): δ 18.0.

[TiI$_4${*o*-C$_6$H$_4$(AsMe$_2$)$_2$}]

As above, but using *o*-C$_6$H$_4$(AsMe$_2$)$_2$ (0.10 g, 0.36 mmol). A dark red/brown solid was isolated as the required [$TiI_4\{o\text{-}C_6H_4(AsMe_2)_2\}$] (yield 0.08 g, 26 %). Required for [$C_{10}H_{16}As_2Cl_4Ti$]: C = 14.3, H = 1.9 %; found: C = 14.5, H = 2.1 %. ^1H NMR: mixture of adducts. $^{13}C\{^1H\}$ NMR (193 K): no spectrum.

[$TiI_4\{o\text{-}C_6H_4(PMe_2)_2\}_2$]

As above, but using TiI_4 (0.10 g, 0.18 mmol) and 3 molar equivalents of $o\text{-}C_6H_4(PMe_2)_2$ (0.11 g, 0.54 mmol). A pale yellow solid was isolated as the required [$TiI_4\{o\text{-}C_6H_4(PMe_2)_2\}_2$] (yield 0.06 g, 34 %). Required for [$C_{20}H_{32}I_4P_4Ti$]: C = 24.2, H = 3.4 %; found: C = 25.0, H = 3.3 %. ^1H NMR(300 K): δ 7.5-7.8 (*m*, $o\text{-}C_6H_4$), 2.35 (*m*, Me), 1.33 (*s*, Me, free ligand). $^{31}P\{^1H\}$ NMR (300 K): δ -4.6, -52.5.

[$TiI_4\{o\text{-}C_6H_4(AsMe_2)_2\}_2$]

As above, but using TiI_4 (0.10 g, 0.18 mmol) and 3 molar equivalents of $o\text{-}C_6H_4(AsMe_2)_2$ (0.15 g, 0.54 mmol). An dark brown solid was isolated as the required [$TiBr_4\{o\text{-}C_6H_4(AsMe_2)_2\}_2$] (yield 0.05 g, 22 %). Required for [$C_{20}H_{32}As_4I_4Ti$]: C = 21.3, H = 2.9 %; found: C = 21.7, H = 3.0 %. ^1H NMR: mixture of adducts. $^{13}C\{^1H\}$ NMR (193 K): no spectrum.

Crystallographic Studies

Details of the crystallographic data collection and refinement parameters are given in Tables 4.9 and 4.10. Crystals of [$TiCl_4\{o\text{-}C_6H_4(PMe_2)_2\}$], [$TiCl_4\{o\text{-}C_6H_4(PMe_2)_2\}_2$], [$TiBr_4\{o\text{-}C_6H_4(PMe_2)_2\}_2$] and [$TiBr_4\{o\text{-}C_6H_4(AsMe_2)_2\}_2$] were grown by slow evaporation of CH_2Cl_2 solutions of the appropriate complex within a N_2 purged glove box . The crystals of [$TiCl_5(Ph_2PCH_2PHPh_2)$] were obtained as a hydrolysis product during similar slow evaporation of a CH_2Cl_2 solution of [$TiCl_4(Ph_2PCH_2PPh_2)$]. Whereas crystals of [$FeI_2\{o\text{-}C_6H_4(AsMe_2)_2\}_2$] and [$FeI_2\{o\text{-}C_6H_4(AsMe_2)_2\}_2$][$I_3$] were obtained as impurities by similar slow evaporation of solutions of [$TiI_4\{o\text{-}C_6H_4(AsMe_2)_2\}_2$]. Data collection used an Enraf Nonius Kappa CCD diffractometer equipped with an Oxford Systems open-flow cryostat operating at 150 K, with graphite monochromated Mo-K_α radiation (λ = 0.71073 A). Structure solution[38] and refinement[39,40,41] were routine except for the iron complexes, for which analysis of initial structure solutions modelling for Ti indicated the wrong choice of metal centre (see Section 4.2.3).

Table 4.9 Crystallographic data collection and refinement parameters for [$TiCl_4(L_2)$], [$TiX_4(L_2)_2$] and [$TiCl_5(Ph_2PCH_2PHPh_2)$].

	[$TiCl_4\{o\text{-}C_6H_4(PMe_2)_2\}$]	[$TiCl_4\{o\text{-}C_6H_4(PMe_2)_2\}_2$]	[$TiBr_4\{o\text{-}C_6H_4(PMe_2)_2\}_2$]	[$TiBr_4\{o\text{-}C_6H_4(AsMe_2)_2\}_2$]	[$TiCl_5(Ph_2PCH_2PHPh_2)$]
Formula	$C_{10}H_{16}Cl_4P_2Ti$	$C_{20}H_{32}Cl_4P_4Ti$	$C_{20}H_{32}Br_4P_4Ti$	$C_{20}H_{32}As_4Br_4Ti$	$C_{25}H_{23}Cl_5P_2Ti$
Formula weight	387.90	586.08	763.88	939.68	610.57
Crystal system	Orthorhombic	Tetragonal	Tetragonal	Tetragonal	Orthorhombic
Space group	*Pbca* (# 61)	$I\bar{4}$ (# 82)	$I\bar{4}$ (# 82)	$I\bar{4}$ (# 82)	$P2_12_12_1$ (# 19)
a / Å	13.1752(2)	9.0716(7)	9.1729(4)	9.3125(5)	10.4063(6)
b / Å	15.3631(2)	9.0716(7)	9.1729(4)	9.3125(5)	15.3834(9)
c / Å	16.6348(3)	16.1037(12)	16.2896(8)	16.4876 (9)	16.5893(11)
α / °	90	90	90	90	90
β / °	90	90	90	90	90
γ / °	90	90	90	90	90
U / Å^3	3367.08(8)	1325.2(2)	1370.64(9)	1429.85(12)	2655.2(2)
Z	8	2	2	2	4
$\mu(\text{Mo-K}_\alpha)$ / cm^{-1}	13.10	9.75	64.02	105.08	9.59
No. of unique reflections	3860	790	722	753	5781
R_{int} (based on F^2)	0.051	0.055	0.064	0.061	0.219
No. of obs. reflections [a]	2461	630	586	633	8136
No. of parameters	154	66	66	66	298
R [b]	0.037	0.083	0.044	0.046	0.060
R_w [c]	0.047	0.111	0.053	0.053	0.082

[a] Observed if [$I_o > 3\sigma(I_o)$] [b] $R = \sum (|F_{obs}|_i - |F_{calc}|_i) / \sum |F_{obs}|_i$ [c] $R_w = \sqrt{[\sum w_i(|F_{obs}|_i - |F_{calc}|_i)^2 / \sum w_i|F_{obs}|_i^2}$

Table 4.10 Crystallographic data collection and refinement parameters for [FeI$_2${*o*-C$_6$H$_4$(AsMe$_2$)$_2$}$_2$] and [FeI$_2${*o*-C$_6$H$_4$(AsMe$_2$)$_2$}$_2$][I$_3$].

	[FeI$_2${*o*-C$_6$H$_4$(AsMe$_2$)$_2$}$_2$]	[FeI$_2${*o*-C$_6$H$_4$(AsMe$_2$)$_2$}$_2$][I$_3$]
Formula	$C_{20}H_{32}As_4FeI_2$	$C_{20}H_{32}As_4FeI_5.CH_2Cl_2$
Formula weight	881.82	1347.46
Crystal system	Orthorhombic	Triclinic
Space group	*Pbca* (# 61)	$P\bar{1}$ (# 2)
a / Å	9.2286(2)	9.39850(10)
b / Å	16.3280(3)	9.53460(10)
c / Å	17.3743(4)	11.76270(10)
α / °	90	78.1370(6)
β / °	90	86.5600(6)
γ / °	90	70.5680(5)
U / Å^3	2618.04(8)	972.75(2)
Z	4	1
μ(Mo-K$_\alpha$) / cm^{-1}	90.96	78.81
No. of unique reflections	3044	3958
R_{int} (based on F^2)	0.063	0.105
No. of obs. reflections [a]	2043	3545
No. of parameters	124	166
R [b]	0.048	0.068
R$_w$ [c]	0.060	0.088

[a] Observed if $[I_o > 3\sigma(I_o)]$

[b] $R = \sum (|F_{obs}|_i - |F_{calc}|_i) / \sum |F_{obs}|_i$

[c] $R_w = \sqrt{[\sum w_i(|F_{obs}|_i - |F_{calc}|_i)^2 / \sum w_i|F_{obs}|_i^2}$

4.5 References

[1] H. Rose, *Poggendorff's Ann. Phys.*, 1832, **24**, 141, 259.

[2] F. Challenger, F. Pritchard, *J. Chem. Soc.*, 1924, 864.

[3] G. W. A. Fowles, R. A. Walton, *J. Chem. Soc.*, 1964, 4330.

[4] I. R. Beattie, R. A. Collis, *J. Chem. Soc. (A)*, 1969, 2960.

[5] A. D. Westland, L. Westland, *Can. J. Chem.*, 1965, **43**, 426.

[6] F. Calderazzo, S. A. Losi, B. P. Susz, *Helv. Chim. Acta*, 1971, **54**, 1157; *Inorg. Chim. Acta*, 1969, **3**, 329.

[7] J. E. Drake, C. Riddle, *Inorg. Nucl. Chem. Letters*, 1969, **5**, 665.

[8] R. Höltje, *Z. Anorg. Allg. Chem.*, 1930, **190**, 241.

[9] J. Chatt, R. G. Hayter, *J. Chem. Soc.*, 1963, 1343.

[10] R. J. H. Clark, R. H. U. Negrotti, *Chem. Ind.*, 1968, 154.

[11] R. J. H. Clark, J. Lewis, R. S. Nyholm, P. Pauling, G. B. Robertson, *Nature*, 1961, **192**, 222.

[12] R. J. H. Clark, J. Lewis, R. S. Nyholm, *J. Chem. Soc.*, 1962, 2460.

[13] R. J. H. Clark, *J. Chem. Soc.*, 1965, 5699.

[14] F. A. Cotton, C. A. Murillo, M. A. Petrukhina, *J. Organomet. Chem.*, 2000, **593-594**, 1; 1999, **573**, 78.

[15] R. J. H. Clark, R. H. U. Negrotti, R. S. Nyholm, *J. Chem. Soc., Chem. Commun.*, 1966, 486.

[16] D. L. Kepert, K. R. Trigwell, *Aust. J. Chem.*, 1975, **28**, 1245.

[17] W. P. Crisp, R. L. Deutscher, D. L. Kepert, *J. Chem. Soc. (A)*, 1970, 2199.

[18] R. J. H. Clark, W. Errington, *J. Chem. Soc. (A)*, 1967, 258.

[19] F. A. Cotton, J. H. Matonic, C. A. Murillo, M. A. Petrukhina, *Inorg. Chim. Acta*, 1998, **267**, 173.

[20] R. Hart, W. Levason, B. Patel, G. Reid, *Eur. J. Inorg. Chem.*, 2001, **11**, 2927.

[21] C. M. F. Rae, K. R. Seddon, *Inorg. Chim. Acta*, 1976, **17**, L35.

[22] I. R. Beattie, M. Webster, *J. Chem. Soc.*, 1964, 3507.

[23] R. J. H. Clark, C. J. Willis, *J. Chem. Soc. (A)*, 1971, 838.

[24] R. J. H. Clark, *Spectrochim. Acta*, 1965, **21**, 955.

[25] R. A. Cipriano, W. Levason, R. A. S. Mould, D. Pletcher, M. Webster, *J. Chem. Soc., Dalton Trans.*, 1990, 339.

[26] B. J. Brisdon, T. E. Lester, R. A. Walton, *Spectrochim. Acta*, 1967, **23A**, 1969.

[27] A. B. P. Lever, *Inorganic Electronic Spectroscopy*, 2nd Edition, Elsevier, 1984.

[28] C. Mahadevan, P. T. Manoharan, B. L. Ramakrishna, M. Seshasayee, *Acta Crystallogr., Sect. C*, 1985, **C41**, 38.

[29] P. K. Bernstein, H. B. Gray, R. Marsh, G. A. Rodley, *Inorg. Chem.*, 1972, **11**, 3040.

[30] D. Nicholls, *Complexes and First-Row Transition Elements*, The MacMillan Press Ltd, London, 1974.

[31] F. H. Allen, L. Brammer, O. Kennard, A. G. Orpen, R. Taylor, D. G. Watson, *J. Chem. Soc, Dalton Trans.*, 1989, **12**, S1.

[32] H. Hidaka, M. Kudo, K. Nishizawa, H. Sudo, *Jpn. Kokai Tokkyo Koho*, 1987, 5.

[33] T. I. Kirillova, T. M. Malyutina, V. A. Orlova, B. Y. Spivalov, *Zh. Anal. Khim.*, 1979, **34**, 161.

[34] H. C. E. McFarlane, W. McFarlane, *Polyhedron*, 1983, **2**, 303.

[35] R. L. Harris, E. P. Kyba, S.-T. Lui, *Organometallics*, 1983, **2**, 1877.

[36] R. D. Feltham, A. Kasenally, R. S. Nyholm, *J. Organomet. Chem.*, 1967, **7**, 285.

[37] W. Lange, A. Tzschach, *Chem. Ber.*, 1962, **95**, 1360.

[38] PATTY, The DIRDIF Program System, G. Admiraal, G. Beurskens, P. T. Beurskens, W. P. Bosman, S. Garcia-Granda, R. O. Gould, J. M. M. Smits, C. Smykalla, Technical Report of the Crystallography Laboratory, University of Nijmegen, 1992.

[39] TeXsan, Crystal Structure Analysis Package, Molecular Structure Corporation, Houston, Texas, 1995.

[40] R. H. Blessing, *Acta Crystallogr., Sect. A*, 1995, **51**, 33.

[41] H. D. Flack, *Acta Crystallogr., Sect. A*, 1983, **39**, 876.

Chapter 5

Zr(IV) and Hf(IV) Chloride Complexes with Bidentate Thio- and Seleno-ether Ligands

5.1 Introduction

The work discussed in Chapters 3 and 4 has shown that bidentate donor ligands of groups 15 and 16 form a variety of coordination complexes with Ti(IV) halides, despite the considerable mismatch between extremely hard Ti(IV) and soft σ-donor ligands. While the dichalcogenoether adducts exhibited only 6-coordination at Ti(IV),[1] reaction of TiX_4 (X = Cl, Br, I) with certain bidentate phosphine and arsine ligands revealed dodecahedral 8-coordinate complexes.[2] These higher coordination number adducts are however uncommon, consistent with the difficulty in arranging eight donor atoms around the small Ti(IV) centre. Such steric considerations are less consequential for the group IV congeners, due to the relatively large size of Zr(IV) and Hf(IV). Indeed, the reaction of MCl_4 with o-$C_6H_4(AsMe_2)_2$ has been reported to afford 8-coordinate $[MCl_4\{o\text{-}C_6H_4(AsMe_2)_2\}_2]$ (M = Zr, Hf) as early as 1961.[3,4] Although the equivalent bromo-adducts were reported in 1963[5] and 1966,[6] spectroscopic characterisation of the Zr(IV) and Hf(IV) adducts has been limited to melting points and analytical data, with far IR spectroscopic data reported separately for the chloro adducts only.[7] Comparison of the X-ray powder diffraction data with the reported structure of $[TiCl_4\{o\text{-}C_6H_4(AsMe_2)_2\}_2]$ indicated that these group IV adducts are isostructural, though no single crystal X-ray diffraction studies have been reported for these Zr(IV) and Hf(IV) complexes. Of note, the preparations of $[MX_4\{o\text{-}C_6H_4(AsMe_2)_2\}_2]$ (M = Zr, Hf; X = Cl, Br) showed some disparity, with the Zr(IV) reactions proceeding at significantly faster rates than the Hf(IV) reactions. This has been utilised to separate zirconium and hafnium mixtures, with the Zr(IV) adduct isolated pure in *ca.* 35 % yield from a 3:2 $ZrCl_4$:$HfCl_4$ mixture.[6]

In contrast to the analogous Ti(IV) chemistry, 6-coordinate 1:1 metal : ligand adducts were not observed for the reaction of Zr(IV) and Hf(IV) with o-$C_6H_4(AsMe_2)_2$. However, 6-coordinate complexes have been reported for the reaction of MX_4 with PR_3 (M = Zr, X = Cl; R = Et, Pr, Bu)[8] and $Ph_2E(CH_2)_2EPh_2$ (M = Zr, X = Cl, Br; M = Hf, X = Cl; E = P, As),[9] although again characterisation was limited to analytical data and far IR spectroscopy. Again, none of these complexes have been structurally characterised, however the structures of $[ZrMe_4\{Me_2P(CH_2)_2PMe_2\}_2]$ and $[HfCl_4\{Ph_2P(CH_2)_2PPh_2\}]$ have been reported more recently to reveal 8-coordinate dodecahedral and 6-coordinated distorted octahedral geometry, respectively.[10,11] The $Me_2P(CH_2)_2PMe_2$

ligand is also reported to form 8-coordinate $[ZrCl_4\{Me_2P(CH_2)_2PMe_2\}_2]$ upon reaction with $ZrCl_4$.[12,13]

Complexes of Zr(IV) and Hf(IV) with soft donor ligands of group 16 are much less common, possibly due to the poorer σ-donor properties of group 16 ligands compared with those of group 15. Thus, $ZrCl_4$ has been reported to form only 6-coordinate complexes $[ZrCl_4(Me_2E)_2]$[14,15,16] and $[ZrCl_4(C_4H_8OS)]$[17] on reaction with Me_2E (E = S, Se) or 1,4-thioxan (C_4H_8OS). For the latter complex, 6-coordination at Zr(IV) is achieved *via* O- and S-donor atoms from two independent, bridging ligands, as observed for the analogous Ti(IV) adduct (see Section 3.1, Chapter 3). However, the reported spectroscopic characterisation of these chalcogenoether Zr(IV) complexes is at best limited to far IR spectroscopy and analytical data. Improved characterisation has been reported during a thermodynamic study of cyclic C_4H_8S (tetrahydrothiophene, THT) addition to Zr(IV) and Hf(IV) halides.[18] Thus, the 6-coordinate 1:2 adducts $[MX_4(THT)_2]$ (M = Zr, X = Cl, Br; M = Hf, X = Cl) showed greater stability of $[ZrCl_4(THT)_2]$ over $[ZrBr_4(THT)_2]$, consistent with the lower Lewis acidity of $ZrBr_4$. Comparison of the Zr(IV) and Hf(IV) chloro adducts showed greater stability for $[HfCl_4(THT)_2]$, consistent with empty 5*d* orbitals of Hf(IV) being more polarisable than 4*d* orbitals of Zr(IV), and hence increased interaction with the polarised orbitals of the soft thioether donor. Eight coordination of soft group 16 ligands has been observed during the reaction of $ZrCl_4$ with $MeS(CH_2)_2SMe$ to afford $[ZrCl_4\{MeS(CH_2)_2SMe\}_2]$[19], in contrast to only 6-coordinate $[TiCl_4\{MeS(CH_2)_2SMe\}]$ discussed in Chapter 3. However, again spectroscopic characterisation of this 8-coordinate complex was restricted to analytical data and far IR spectroscopy. This general trend of limited characterisation of the Zr(IV) and Hf(IV) complexes can at least in part be attributed to the extreme moisture sensitivity of these invariably white complexes that show minimal solubility in non-coordinating solvents. Also of note, none of the above Zr(IV) or Hf(IV) complexes have been structurally characterised, hence there is essentially no data of sufficient detail to permit comparison of the interactions of soft donor ligands with the group IV halides.

This chapter investigates the coordination chemistry of bidentate thio- and selenoether ligands with zirconium and hafnium tetrachloride, in order to present the first structural investigation of these metal-ligand interactions. Thus, reported within is the development of a synthetic route to 6- and/or 8-coordinate Zr(IV) and Hf(IV) complexes with various thio- and seleno-ether ligands [Me_2S, $MeE(CH_2)_nEMe$ for E = S or Se, n = 2 or 3].[20] Also reported is the reaction of $ZrCl_4$ with the arsine ligand *o*-$C_6H_4(AsMe_2)_2$ in order to unequivocally establish the geometry at Zr(IV) and to allow comparison with the congenic Ti(IV) complexes discussed in Chapter 4. The complexes are very poorly soluble in non-coordinating solvents and hence characterisation was restricted to solid state studies *via* elemental analysis and IR spectroscopy. X-ray single crystal structure determinations are reported for the 6-coordinate adducts [$ZrCl_4(Me_2S)_2$], [$ZrCl_4\{MeS(CH_2)_3SMe\}$] and [$HfCl_4\{MeSe(CH_2)_2SeMe\}$]; and for the 8-coordinate complexes [$MCl_4\{MeS(CH_2)_2SMe\}_2$] (M = Zr, Hf) and [$ZrCl_4\{o\text{-}C_6H_4(AsMe_2)_2\}_2$]. Comparison of these data with the structurally characterised Ti(IV) complexes reported in Chapters 3 and 4 permits discussion of the consequences of changing the donor atom, ligand backbone and even group IV metal centre on the metal-donor interaction. A brief discussion on the instability of certain selenoether Zr(IV) adducts is also reported, including the structural characterisation of [Zr_2Cl_{10}][$Me_2S(CH_2Cl)$], formed during an attempted synthesis of [$ZrCl_4\{MeSe(CH_2)_3SeMe\}$].

5.2 Results and Discussion

Even more so than the Ti(IV) adducts reported in Chapters 3 and 4, the formation of Zr(IV) and Hf(IV) complexes with soft donor ligands has proved very challenging. Unlike liquid $TiCl_4$, both $ZrCl_4$ and $HfCl_4$ are polymeric solids exhibiting stable 6-coordination at the metal centres *via* bridging chlorides. The stability of this polymeric form presents the initial challenge of poor solubility in non-coordinating solvents. Thus, addition of excess bidentate thio- or seleno-ether ligand [$RE(CH_2)_nER$ for E = S or Se, R = Me, Ph, n = 2 or 3] to suspensions of $ZrCl_4$ in rigorously anhydrous CH_2Cl_2 afforded only partially substituted adducts even after several days of reaction at room temperature or at reflux. Presumably the expected weak interaction between hard Zr(IV) and the soft chalcogenoether donor atoms is insufficient to cause complete disruption of the polymeric $ZrCl_4$ structure. Increased solubility of $ZrCl_4$ was achieved using rigorously anhydrous $CHCl_3$, though again addition of excess bidentate thio- or seleno-ether ligand presented incomplete reaction even after several days reflux. These results clearly illustrate the difficulty in achieving thio- or seleno-ether coordination with Zr(IV) due to the strong preference of the hard metal centre for hard donor ligands.

In order to overcome the limited reactivity of $ZrCl_4$, an alternative Zr(IV) precursor was sought. The reported octahedral adduct *cis*-$[ZrCl_4(THF)_2]$ (THF = tetrahydrofuran, C_4H_8O) provided solubility in anhydrous CH_2Cl_2, however reaction with excess thio- or seleno-ether ligands again led to only partially substituted adducts after several days reflux. This difficulty in substituting the THF donor ligands is consistent with the preference of hard Zr(IV) for the hard O-donor ligand, despite the stabilisation proffered by a chelating bidentate ligand. Thus, reactions were repeated in anhydrous $CHCl_3$ with regular removal of solvent *in vacuo* and subsequent replenishment of anhydrous $CHCl_3$ in attempt to remove THF from the reaction solution. However, again incomplete substitution was observed. One notable exception was the reaction of $[ZrCl_4(THF)_2]$ in anhydrous CH_2Cl_2 with the bidentate selenoether ligand $PhSe(CH_2)_2SePh$. In contrast to the reactions with other thio- and seleno-ether ligands, an immediate colour change from colourless to orange was observed on addition of the ligand. Precipitation with anhydrous *n*-hexane allowed removal of unreacted $[ZrCl_4(THF)_2]$ and the residual filtrate was reduced to dryness *in vacuo* to afford a yellow solid. This solid readily dissolved in non-coordinating solvents and thus permitted characterisation *via* multinuclear NMR spectroscopy. The resulting ^1H NMR spectrum showed resonances corresponding to the phenyl protons of the ligand (δ 7.1 – 7.6), but no resonances corresponding to the protons of the dimethylene backbone. Similarly, $^{13}C\{^1H\}$ NMR spectroscopy revealed resonances characteristic of the phenyl groups (δ 127 – 130), but no methylene carbons. These data are consistent with the dealkylation of the selenoether ligand and indeed, $^{77}Se\{^1H\}$ NMR spectroscopy of the isolated solid revealed a single resonance at δ 460, consistent with the formation of PhSeSePh[21] This suggests that reaction of Zr(IV) with $PhSe(CH_2)_2SePh$ leads to the decomposition of the ligand to afford uncoordinated PhSeSePh. These results parallel the observed solution behaviour of the equivalent Ti(IV) adduct $[TiCl_4\{PhSe(CH_2)_2SePh\}]$ (see Section 3.4, Chapter 3), illustrating the poor interaction between the hard group IV metal centres and the soft weak σ-donor selenoether ligand.[1]

The difficulties encountered in achieving dithio- or diseleno-ether coordination at

Zr(IV) led us to reconsider the reported synthesis of other Zr(IV) chalcogenoether complexes. [$ZrCl_4(L)_2$] is obtained from reaction of excess monodentate thioether ligand L (L = Me_2S or THT) with a suspension of $ZrCl_4$ in rigorously anhydrous CH_2Cl_2 and precipitation with dry *n*-hexane. Along with microanalytical data, far IR spectroscopy revealed strong Zr-Cl stretching vibrations comparable with those previously reported to confirm the formulation as *cis*-[$ZrCl_4(L)_2$].[14] Good solubility of both complexes in anhydrous chlorinated solvents permitted ^1H NMR spectroscopic analysis, which revealed the expected ligand resonances shifted slightly to high frequency upon coordination [L = Me_2S, $\delta = 2.32$ (Me); L = THT, $\delta = 3.25$ (CH_2S), 2.10 (CH_2)]. It is not obvious why these bis-monodentate thioether complexes form so readily while coordination of the bidentate dithioether is incomplete after several days.

The high yield isolation and solubility of molecular *cis*-[$ZrCl_4(Me_2S)_2$] in non-coordinating solvents presented another possible precursor to Zr(IV) complexes with bidentate thio- and seleno-ether ligands. The volatility of Me_2S permits its removal *in vacuo* to drive the reaction equilibrium towards coordination of the bidentate donor ligands. Thus, a slight excess of thio- or seleno-ether ligand L_2 [L_2 = $MeE(CH_2)_nEMe$, E = S or Se, n = 2 or 3] was added to a solution of [$ZrCl_4(Me_2S)_2$] in rigorously anhydrous CH_2Cl_2 at room temperature (Figure 5.1). Subsequent slow removal of solvent under gentle vacuum and replenishment of anhydrous CH_2Cl_2 resulted in the gradual precipitation of a white solid isolated as the required [$ZrCl_4(L_2)$]. Similar reaction of [$ZrCl_4(Me_2S)_2$] with three equivalents of thio- or seleno-ether ligand L_2' [L_2' = $MeE(CH_2)_2EMe$, E = S or Se] resulted in the precipitation of white powdered solids [$ZrCl_4(L_2')_2$]. The equivalent Hf(IV) adducts were isolated *via* similar methods. Thus, reaction of $HfCl_4$ with Me_2S in rigorously anhydrous CH_2Cl_2 resulted in the formation of [$HfCl_4(Me_2S)_2$] in high yield. Subsequent substitution reactions with the bidentate thio- or seleno-ether ligands afforded the white complexes [$HfCl_4(L_2)$] and [$HfCl_4(L_2')_2$] according to stoichiometry, although the reactions proceeded at significantly slower rates compared with the Zr(IV) adducts. All of the complexes were isolated in moderate yields and microanalytical data confirmed the formulation of the respective adducts. The complexes were routinely handled and stored within a dry N_2 purged glove box in respect of the extreme moisture sensitivity of the analogous Ti(IV) adducts.

While the isolation of the bis-thioether Zr(IV) adduct [$ZrCl_4\{MeS(CH_2)_2SMe\}_2$] is consistent with the reported reactivity of $ZrCl_4$ with $MeS(CH_2)_2SMe$,[19] reaction of $[ZrCl_4(Me_2S)_2]$ with only one equivalent of the ligand also allowed the isolation of the 1:1 metal : ligand adduct $[ZrCl_4\{MeS(CH_2)_2SMe\}]$.

The bidentate arsine ligand o-$C_6H_4(AsMe_2)_2$ has also been reported to form 8-coordinate $[ZrCl_4\{o\text{-}C_6H_4(AsMe_2)_2\}_2]$ on reaction with $ZrCl_4$,[3,4] hence it may also be possible to form the 6-coordinate 1:1 adduct, as observed for the analogous Ti(IV) adducts.[2] However, reaction of $[ZrCl_4(Me_2S)_2]$ with o-$C_6H_4(AsMe_2)_2$ afforded the 1:2 adduct regardless of ligand stoichiometry used, with formulation confirmed by microanalytical data.

The isolated Zr(IV) and Hf(IV) bidentate ligand complexes are extremely insoluble in non-coordinating solvents. Thus, in contrast to the informative solution spectroscopic studies undertaken for the analogous Ti(IV) adducts reported in Chapters 3 and 4, no solution phase characterisation has been achieved to date for the Zr(IV) and Hf(IV) complexes. Attempts to collect ^1H and $^{13}C\{^1H\}$ NMR spectroscopic data from very dilute solutions of the adducts revealed only resonances corresponding to uncoordinated ligand, suggesting solubility is a result of dissociation and/or decomposition in solution. Therefore, further characterisation of these Zr(IV) and Hf(IV) complexes has been restricted to far IR spectroscopy and single crystal X-ray studies only.

Figure 5.1 Reaction scheme for the synthesis of $[MCl_4(L_2)_n]$ (M = Zr, Hf; n = 1, 2).

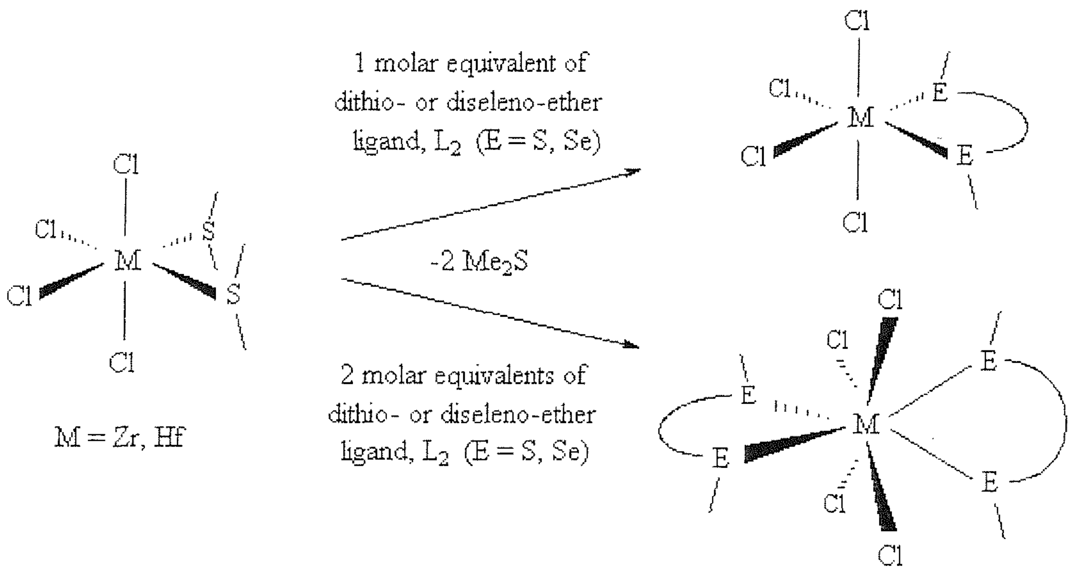

5.2.1 *IR spectroscopy*

Far IR spectroscopic data were recorded for MCl_4 (M = Zr, Hf) with the high moisture sensitivity of the complexes dictating the use of sodium dried-Nujol mulls pressed between CsI plates. The polymeric structure of MCl_4 comprises of $[MCl_6]^{2-}$ octahedra sharing two edges to maintain charge neutrality to present a zigzag chain structure. Far IR spectra revealed broad M-Cl stretching vibrations for the terminal [397 cm^{-1}, M = Zr; 379 cm^{-1}, M = Hf] and bridging [290 cm^{-1}, M = Zr; 280 cm^{-1}, M = Hf] chlorides, consistent with longer $M\text{-}Cl_{bridging}$ distances compared with $M\text{-}Cl_{terminal}$.[22,23]

The far IR spectra of the coordination complexes $[ZrCl_4(THT)_2]$, $[MCl_4(Me_2S)_2]$ and $[MCl_4(L_2)]$ (M = Zr, Hf; $L_2 = MeE(CH_2)_nEMe$, E = S or Se, n = 2 or 3) showed the loss of bridging chloride stretching vibrations, confirming the molecularity of the adducts. The spectra of complexes involving monodentate ligands revealed four M-Cl stretching vibrations in the range 357-308 (Zr-Cl), 346-301 cm^{-1} (Hf-Cl), consistent with C_{2v} *cis*-coordination ($2A_1 + B_1 + B_2$). However, only very broad vibrations were observed for the bidentate ligand adducts, with ν(Zr-Cl) observed at *ca.* 360 cm^{-1} and ν(Hf-Cl) at *ca.* 330 cm^{-1} for the 1:1 bidentate thio- and seleno-ether adducts. While the broadness of the bands prevented conclusive assignment of the geometry at Zr(IV) or Hf(IV), the small chain lengths of the bidentate ligands used here dictates only C_{2v} *cis*-coordination when chelating.

As observed for the structurally characterised 8-coordinate phosphine and arsine Ti(IV) adducts described in Chapter 4,[2] the 1:2 metal : ligand complexes formed here are expected to adopt D_{2d} dodecahedral geometry at the metal centre. Indeed, the far IR spectra of these 1:2 adducts revealed two M-Cl stretching vibrations ($B_2 + E$) at *ca.* 306, 300 cm^{-1} for ν(Zr-Cl) and *ca.* 282, 276 cm^{-1} for ν(Hf-Cl). These frequencies are significantly lower than for the 6-coordinate 1:1 complexes above, consistent with a lengthening of the M-Cl bonds as a result of increased steric crowding upon 8-coordination. The observed Zr-Cl stretching frequencies for $[ZrCl_4\{MeS(CH_2)_2SMe\}_2]$ (307, 301 cm^{-1}) and $[ZrCl_4\{o\text{-}C_6H_4(AsMe)_2\}_2]$ (296, 288 cm^{-1}) also show reasonable agreement with those previously reported (305 cm^{-1} and 303, 295 cm^{-1} respectively).[7,19] Interestingly, the spectra of $[ZrCl_4\{MeE(CH_2)_2EMe\}]$ reveal a mixture of the 1:1 and 1:2 adducts (Figure 5.2), suggesting the 1:2 adduct may be the favourable product as it forms at even relatively low ligand concentrations.

Figure 5.2 ν(Zr-Cl) region of [$ZrCl_4\{MeS(CH_2)_2SMe\}$] IR spectrum (Nujol Mull).

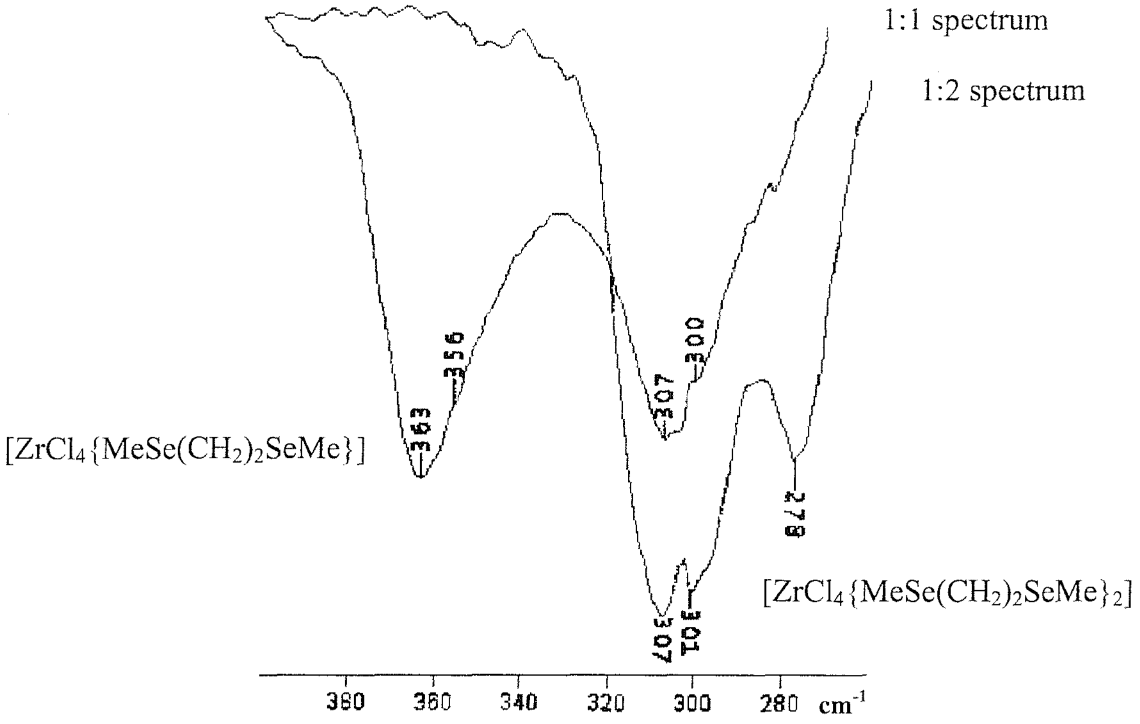

5.2.2 X-ray crystallographic studies

In view of the complete absence of structural reports on thio- and seleno-ether Zr(IV) and Hf(IV) complexes and due to the limited spectroscopic characterisation available, single crystal X-ray diffraction studies were undertaken on six of the complexes synthesised here. Thus, single crystals of [$ZrCl_4(Me_2S)_2$], [$ZrCl_4\{MeS(CH_2)_3SMe\}$], [$HfCl_4\{MeSe(CH_2)_2SeMe\}$], [$ZrCl_4\{MeS(CH_2)_2SMe\}_2$], [$HfCl_4\{MeS(CH_2)_2SMe\}_2$] and [$ZrCl_4\{o\text{-}C_6H_4(AsMe)_2\}_2$] were grown by slow evaporation of CH_2Cl_2 solutions of the complexes in a dry N_2 purged glove box. The solutions were obtained by filtration of reaction mixtures following synthesis of the respective complex in anhydrous CH_2Cl_2 (see section 5.4, Experimental). As these reaction filtrates may contain a mixture of adducts, the crystals obtained may result from a soluble impurity and not necessarily from the bulk sample. However, no disparity was observed between the microanalytical data and far IR spectra of the bulk solid and that obtained from the filtrates, suggesting the crystals are representative of the bulk complex. All attempts to grow crystals from dilute solutions of the isolated complexes were unsuccessful due to either insufficient complex in solution or dissociation of ligand on dissolution.

The structure of $[ZrCl_4(Me_2S)_2]$ (Figure 5.3, Tables 5.1, 5.2) reveals a distorted octahedral environment at Zr(IV) comprising four chloro ligands and two mutually *cis* thioether donor atoms. The bond angles reveal similar geometry at Zr(IV) to that observed for similar Ti(IV) six coordinate thio- and seleno-ether complexes discussed in Chapter 3. Thus, the chloride ligands appear to lean towards the thioether ligand to give distorted bond angles between the mutually *trans* chlorides, ∠Cl(1) – Zr(1) – Cl(2) = 157.14(8)° [cf. 162.91(3) – 165.7(2)° for Ti(IV)] and between the chlorides *trans* to thioethers, ∠Cl(3) – Zr(1) – Cl(4) = 104.72(10)° [cf. 102.8(1) – 109.28(7)° for Ti(IV)].

Table 5.1 Selected bond lengths for $[ZrCl_4(Me_2S)_2]$.

Bond	Distance / Å	Bond	Distance / Å
Zr(1) – S(1)	2.754(3)	Zr(1) – Cl(2)	2.425(2)
Zr(1) – S(2)	2.788(2)	Zr(1) – Cl(3)	2.361(2)
Zr(1) – Cl(1)	2.386(2)	Zr(1) – Cl(4)	2.386(3)

Table 5.2 Selected bond angles for $[ZrCl_4(Me_2S)_2]$.

Bond	Angle / °	Bond	Angle / °
S(1) – Zr(1) – S(2)	79.12(7)	S(2) – Zr(1) – Cl(4)	87.41(9)
S(1) – Zr(1) – Cl(1)	83.29(8)	Cl(1) – Zr(1) – Cl(2)	157.14(8)
S(1) – Zr(1) – Cl(2)	79.30(8)	Cl(1) – Zr(1) – Cl(3)	97.09(8)
S(1) – Zr(1) – Cl(3)	88.75(8)	Cl(1) – Zr(1) – Cl(4)	96.83(8)
S(1) – Zr(1) – Cl(4)	166.37(9)	Cl(2) – Zr(1) – Cl(3)	97.23(8)
S(2) – Zr(1) – Cl(1)	81.32(8)	Cl(2) – Zr(1) – Cl(4)	96.65(8)
S(2) – Zr(1) – Cl(2)	80.94(7)	Cl(3) – Zr(1) – Cl(4)	104.72(10)
S(2) – Zr(1) – Cl(3)	167.87(9)		

Figure 5.3 **View of the structure of [$ZrCl_4(Me_2S)_2$] with numbering scheme adopted. Ellipsoids drawn at 40%, H-atoms omitted for clarity.**

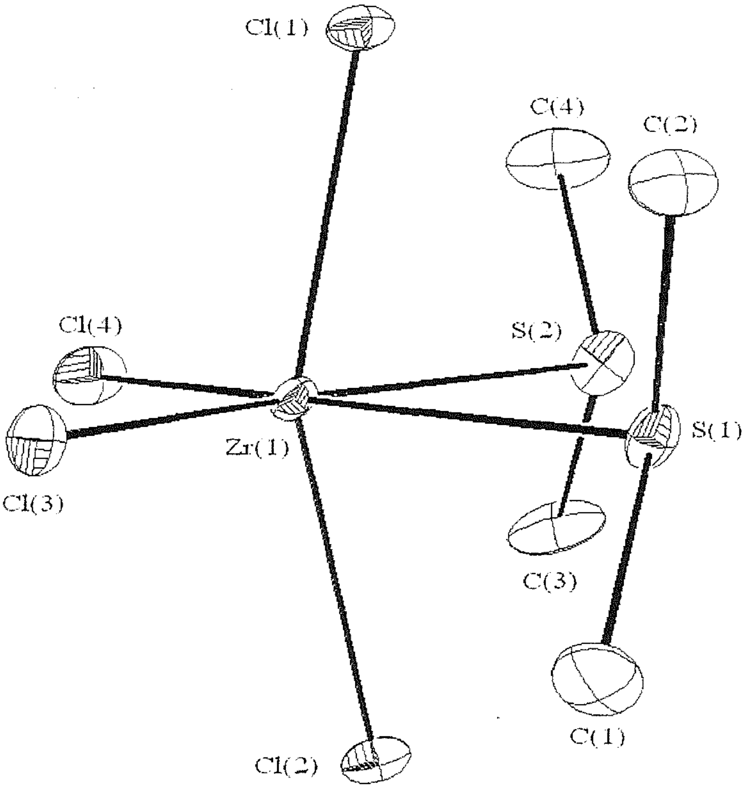

The structure of [$ZrCl_4\{MeS(CH_2)_3SMe\}$] (Figure 5.4, Tables 5.3, 5.4) reveals a binuclear adduct with two bidentate thioether ligands bridging two Zr(IV) centres. This 12-membered metallocyclic structure contrasts the mononuclear Ti(IV) species with the same ligand chelating described in Chapter 3, and appears to accommodate greater distortion of the geometry at the metal centre. Thus, the chloride ligands lean even further towards the thioether ligand than in [$ZrCl_4(Me_2S)_2$] (**1**) or the Ti(IV) equivalent complex [$TiCl_4\{MeS(CH_2)_3SMe\}$] (**2**), with $\angle Cl_{trans\ Cl} - Zr - Cl_{trans\ Cl}$ = 153.18(6), 156.05(7)° [cf. 157.14(8)° (**1**), 163.7(2)° (**2**)]. This unexpected geometry may suggest that the 6-membered ring formed on chelation of the $MeS(CH_2)_3SMe$ ligand proffers negligible stabilisation for Zr(IV) compared with that gained by reducing the steric constrictions of the chloride coordination sphere. The formation of this binuclear Zr(IV) adduct may also account for the failure to achieve 8-coordinate Zr(IV) upon addition of excess ligand, as this would require reorganisation of the bridging binding mode.

Figure 5.4 View of the structure of [$ZrCl_4\{MeS(CH_2)_3SMe\}$] with numbering scheme adopted. Ellipsoids drawn at 40%, H-atoms omitted for clarity.

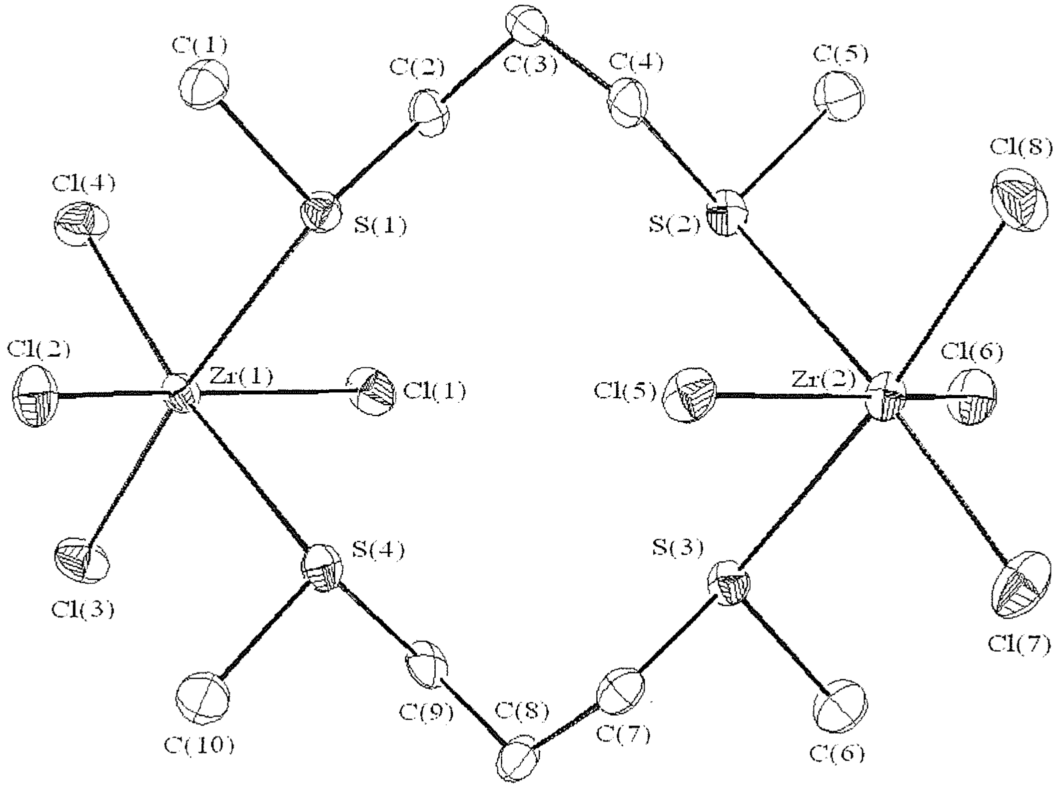

Table 5.3 Selected bond lengths for [$ZrCl_4\{MeS(CH_2)_3SMe\}$].

Bond	Distance / Å	Bond	Distance / Å
Zr(1) – S(1)	2.783(2)	Zr(2) – S(2)	2.792(2)
Zr(1) – S(4)	2.777(2)	Zr(2) – S(3)	2.761(2)
Zr(1) – Cl(1)	2.385(2)	Zr(2) – Cl(5)	2.395(2)
Zr(1) – Cl(2)	2.404(2)	Zr(2) – Cl(6)	2.408(2)
Zr(1) – Cl(3)	2.370(2)	Zr(2) – Cl(7)	2.370(2)
Zr(1) – Cl(4)	2.370(2)	Zr(2) – Cl(8)	2.372(2)

Table 5.4 Selected bond angles for [$ZrCl_4\{MeS(CH_2)_3SMe\}$].

Bond	Angle / °	Bond	Angle / °
S(1) – Zr(1) – S(4)	79.52(5)	S(2) – Zr(2) – S(3)	85.29(5)
S(1) – Zr(1) – Cl(1)	82.18(5)	S(2) – Zr(2) – Cl(5)	83.05(5)
S(1) – Zr(1) – Cl(2)	79.84(5)	S(2) – Zr(2) – Cl(6)	76.93(5)
S(1) – Zr(1) – Cl(3)	170.21(6)	S(2) – Zr(2) – Cl(7)	173.33(6)
S(1) – Zr(1) – Cl(4)	90.17(5)	S(2) – Zr(2) – Cl(8)	87.28(6)
S(4) – Zr(1) – Cl(1)	81.89(6)	S(3) – Zr(2) – Cl(5)	83.44(5)
S(4) – Zr(1) – Cl(2)	79.40(5)	S(3) – Zr(2) – Cl(6)	77.36(5)
S(4) – Zr(1) – Cl(3)	90.78(6)	S(3) – Zr(2) – Cl(7)	88.42(6)
S(4) – Zr(1) – Cl(4)	169.57(6)	S(3) – Zr(2) – Cl(8)	171.99(6)
Cl(1) – Zr(1) – Cl(2)	156.05(7)	Cl(5) – Zr(2) – Cl(6)	153.18(6)
Cl(1) – Zr(1) – Cl(3)	97.85(6)	Cl(5) – Zr(2) – Cl(7)	98.47(6)
Cl(1) – Zr(1) – Cl(4)	98.37(6)	Cl(5) – Zr(2) – Cl(8)	98.65(6)
Cl(2) – Zr(1) – Cl(3)	97.21(6)	Cl(6) – Zr(2) – Cl(7)	99.53(6)
Cl(2) – Zr(1) – Cl(4)	97.37(6)	Cl(6) – Zr(2) – Cl(8)	98.03(6)
Cl(3) – Zr(1) – Cl(4)	99.49(6)	Cl(7) – Zr(2) – Cl(8)	98.87(7)

The crystals obtained for [$HfCl_4\{MeSe(CH_2)_2SeMe\}$] were of slightly lower quality and hence the final structure solution reveals slightly higher than normal residuals and estimated standard deviations (e.s.d.'s). Nevertheless, the structure (Figure 5.5, Tables 5.5, 5.6) reveals a mononuclear adduct with similar geometry at the metal centre as [$ZrCl_4(Me_2S)_2$] (**1**) and the similar Ti(IV) complex [$TiCl_4\{MeS(CH_2)_2SMe\}$] (**3**, see Chapter 3), eg. $\angle Cl_{trans\ Se} - Hf - Cl_{trans\ Se}$ = 104.3(2)° [cf. 104.72(10)° (**1**), 105.66(3)° (**3**)], $\angle Cl_{trans\ Cl} - Hf - Cl_{trans\ Cl}$ = 161.6(2)° [cf. 157.14(8)° (**1**), 162.91(3)° (**1**)]. Notably the structure does not adopt the binuclear arrangement observed for

[$ZrCl_4$\{$MeS(CH_2)_3SMe$\}] and this is attributed to the strong stabilisation proffered by the 5-membered ring formed on *DL* chelation of the $MeSe(CH_2)_2SeMe$ ligand. Interestingly, the ligand bite angle, [∠Se – Hf – Se = 79.86(7)°], is comparable with the equivalent angle in (**1**) [79.12(7)°] despite the absence of chelate constraints for the dimethyl-sulfide ligands.

Figure 5.5 View of the structure of [$HfCl_4$\{$MeSe(CH_2)_2SeMe$\}] with numbering scheme adopted. Ellipsoids drawn at 40%, H-atoms omitted for clarity.

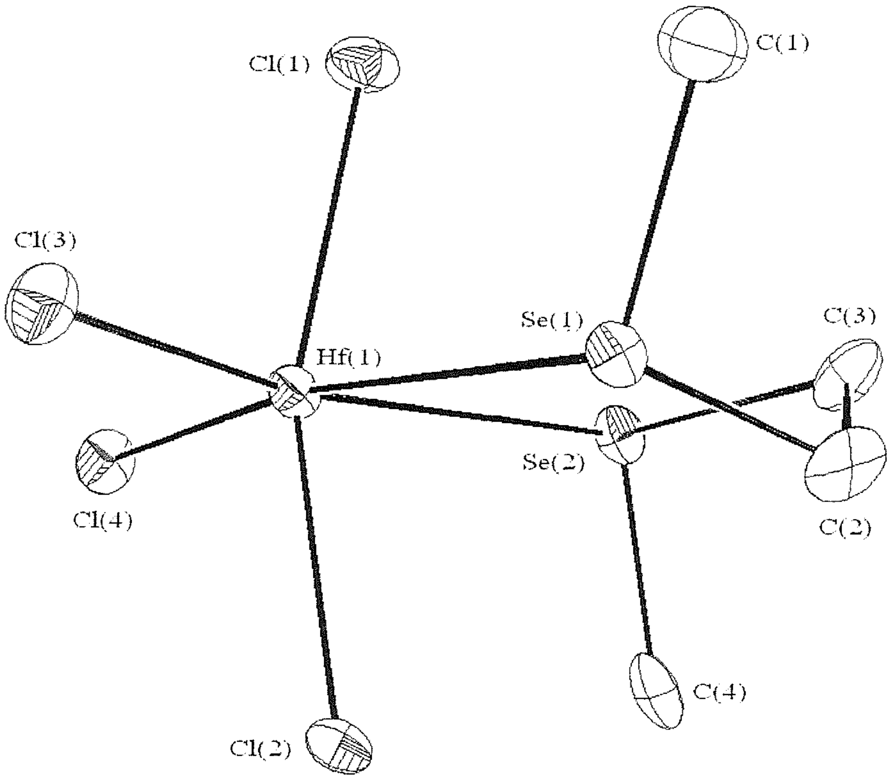

Table 5.5 Selected bond lengths for [$HfCl_4$\{$MeSe(CH_2)_2SeMe$\}].

Bond	Distance / Å	Bond	Distance / Å
Hf(1) – Se(1)	2.844(2)	Hf(1) – Cl(2)	2.397(5)
Hf(1) – Se(2)	2.848(2)	Hf(1) – Cl(3)	2.348(6)
Hf(1) – Cl(1)	2.396(6)	Hf(1) – Cl(4)	2.364(6)

Table 5.6 Selected bond angles for [$HfCl_4\{MeSe(CH_2)_2SeMe\}$].

Bond	Angle / °	Bond	Angle / °
Se(1) – Hf(1) – Se(2)	79.86(7)	Se(2) – Hf(1) – Cl(4)	91.6(2)
Se(1) – Hf(1) – Cl(1)	88.8(2)	Cl(1) – Hf(1) – Cl(2)	161.6(2)
Se(1) – Hf(1) – Cl(2)	78.4(2)	Cl(1) – Hf(1) – Cl(3)	95.3(2)
Se(1) – Hf(1) – Cl(3)	84.8(2)	Cl(1) – Hf(1) – Cl(4)	96.2(2)
Se(1) – Hf(1) – Cl(4)	169.2(2)	Cl(2) – Hf(1) – Cl(3)	96.7(2)
Se(2) – Hf(1) – Cl(1)	78.7(2)	Cl(2) – Hf(1) – Cl(4)	94.6(2)
Se(2) – Hf(1) – Cl(2)	86.0(2)	Cl(3) – Hf(1) – Cl(4)	104.3(2)
Se(2) – Hf(1) – Cl(3)	163.6(2)		

Although the above 6-coordinate Zr(IV) and Hf(IV) complexes show the same gross geometry at the metal centres, comparison of the bond distances does reveal some differences. Analysis of the M-E bond lengths reveals comparable Zr-S bond lengths for [$ZrCl_4(Me_2S)_2$] and [$ZrCl_4\{MeS(CH_2)_3SMe\}$] {2.754(3), 2.788(2) Å and 2.761(2) – 2.792(2) Å respectively}, while the Hf-Se bond distances in [$HfCl_4\{MeSe(CH_2)_2$-$SeMe\}$] are longer [2.844(2), 2.848(2) Å], consistent with the larger radius and softer character of Se over S donor atoms. The M-Cl bond distances show a similar trend to that observed for the Ti(IV) thio- and seleno-ether complexes, with the bond distances for the chlorides *trans* to the donor ligand [2.286(3) – 2.348(6) Å] significantly shorter than those of the mutually *trans* chlorides [2.385(2), 2.425(2) Å]. This indicates a *trans* influence of Cl > S, Se, illustrating the preference of the hard Zr(IV) and Hf(IV) centres for the hard chloride ligands over the softer chalcogenoether donor atoms. While this *trans* influence order is consistent with that observed for the analogous Ti(IV) adducts, the order is the reverse of that observed for late transition metals, where the soft metal centres show coordination preference for soft donor ligands. All of the observed bond lengths also show an increase of *ca.* 0.11 – 0.14 Å in comparison with those observed in similar Ti(IV) adducts, consistent with the larger radii of the Zr(IV) and Hf(IV) centres.

The structure of the 8-coordinate complex [$ZrCl_4\{MeS(CH_2)_2SMe\}_2$] (Figure 5.6, Tables 5.7, 5.8) reveals a 2-fold pseudo-dodecahedral geometry at the metal centre, with four S donor atoms occupying the A-type vertices and four chloro ligands occupying B vertices. A similar coordination geometry was observed for the 8-coordinate Ti(IV) complexes discussed in Chapter 4 involving the phosphine and arsine ligands *o*-$C_6H_4(EMe_2)_2$ for E = P, As. The thioether ligands once again adopt the *DL* configuration, though one of the ligands exhibits disorder in the dimethylene backbone. This was modelled to reveal alternative positions for the backbone carbon atoms while still retaining the *DL* arrangement of the ligand. Similar disorder associated with coordinated $MeS(CH_2)_2SMe$ has been previously reported in the mixed valence adduct $[Cu\{MeS(CH_2)_2SMe\}_2][ClO_4]_{4/3}$.[24] The Zr-S bond lengths [2.828(2), 2.853(2) Å] are longer (*ca.* 0.06 Å) than those in the 6-coordinate adduct $[ZrCl_4\{MeS(CH_2)_3SMe\}]$ involving a similar thioether ligand, consistent with increased steric crowding upon increasing coordination number at Zr(IV). The Zr-Cl bond lengths [2.485(2), 2.486(2) Å] show approximately twice this increase in bond length (*ca.* 0.10 – 0.12 Å) compared to the similar 1:1 adduct. This may be attributed to the differing *trans* influences in the respective adducts and is consistent with that observed for similar phosphine and arsine Ti(IV) complexes discussed in Chapter 4. The longer M-Cl bond distances in the 1:2 adduct compared with the 1:1 adduct also correlates well with the lower frequency M-Cl (M = Zr, Hf) stretching vibrations observed for the 1:2 adducts during far IR spectroscopy of these complexes (see Section 5.2.1). The increase in Zr-S bond lengths in the 1:2 adduct also leads to a more acute bite-angle for the chelating ligand [71.28(9), 71.89(9)°] compared with the the 6-coordinate structure [79.52(5), 85.29(5)°].

The crystals obtained of the equivalent Hf(IV) complex $[HfCl_4\{MeS(CH_2)_2SMe\}_2]$ were of lower quality and hence the structure solution reveals residuals slightly higher than normal. Nevertheless, the crystals were isostructural with those of the above Zr(IV) 1:2 adduct, with no significant geometry differences (Figure 5.7, Tables 5.7, 5.8).

Figure 5.6 **View of the structure of [ZrCl$_4${MeS(CH$_2$)$_2$SMe}$_2$] with numbering scheme adopted. Ellipsoids drawn at 40%, H-atoms omitted for clarity.**

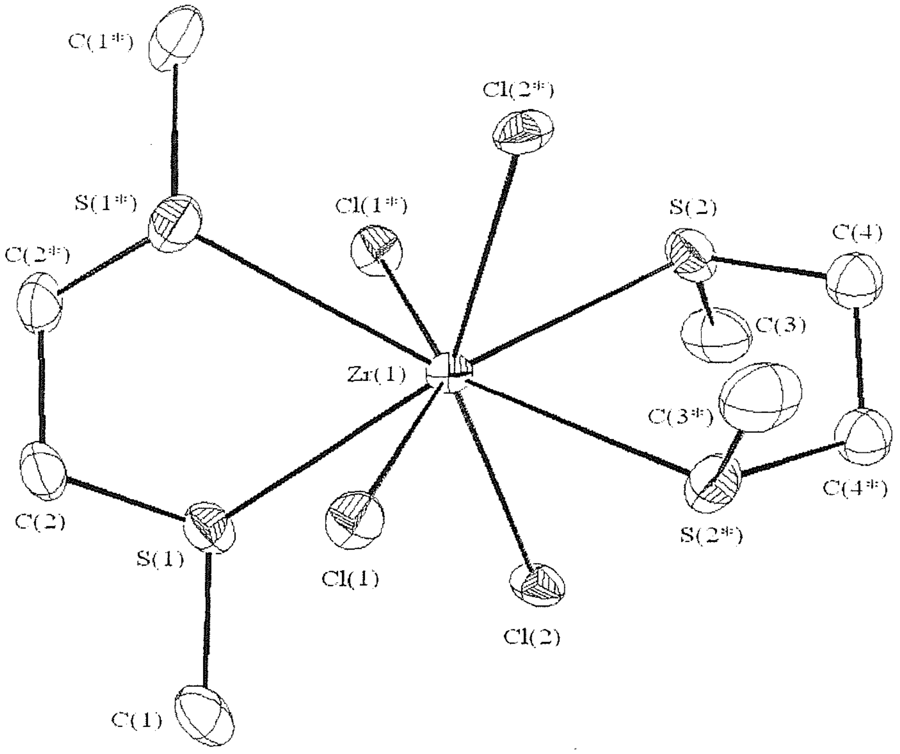

Figure 5.7 **View of the structure of [HfCl$_4${MeS(CH$_2$)$_2$SMe}$_2$] with numbering scheme adopted. Ellipsoids drawn at 40%, H-atoms omitted for clarity.**

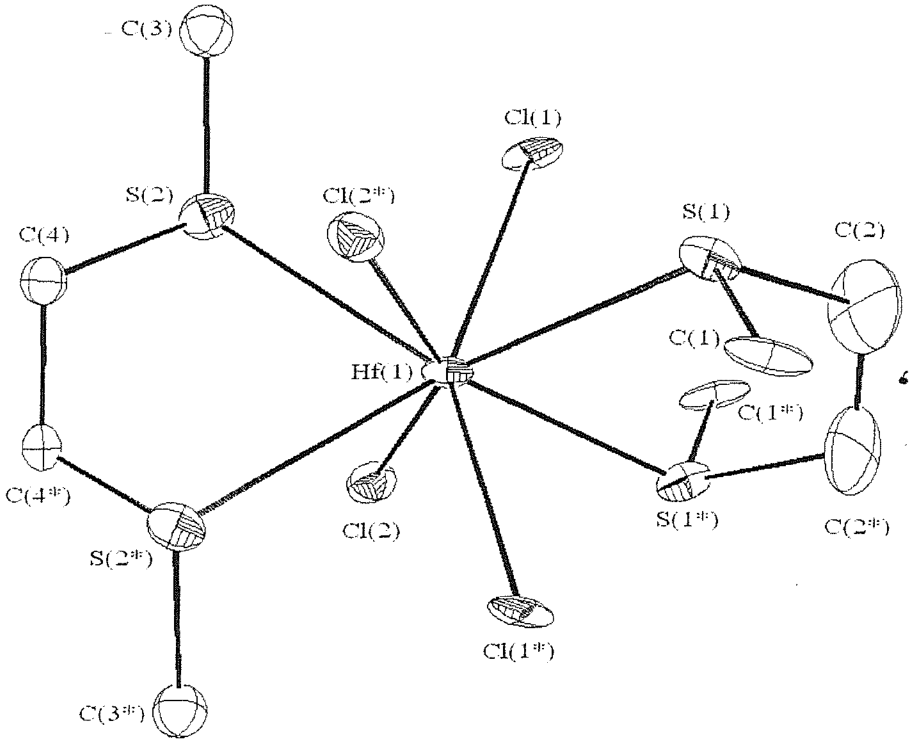

Table 5.7 Selected bond lengths for $[MCl_4\{MeS(CH_2)_2SMe\}_2]$ for M = Zr, Hf.

	Distance / Å	
Bond (M = Zr, Hf)	$[ZrCl_4\{MeS(CH_2)_2SMe\}_2]$	$[HfCl_4\{MeS(CH_2)_2SMe\}_2]$
M(1) – S(1)	2.853(2)	2.819(7)
M(1) – S(2)	2.828(2)	2.846(7)
M(1) – Cl(1)	2.486(2)	2.470(6)
M(1) – Cl(2)	2.485(2)	2.473(6)

Table 5.8 Selected bond angles for $[MCl_4\{MeS(CH_2)_2SMe\}_2]$ for M = Zr, Hf.

	Angle / °	
Bond (M = Zr, Hf)	$[ZrCl_4\{MeS(CH_2)_2SMe\}_2]$	$[HfCl_4\{MeS(CH_2)_2SMe\}_2]$
S(1) – M(1) – S(2)	133.03(7)	128.6(2)
S(1) – M(1) – S(1)*	71.28(9)	72.7(3)
S(1) – M(1) – S(2)*	129.31(6)	133.4(2)
S(1) – M(1) – Cl(1)	77.94(7)	80.8(2)
S(1) – M(1) – Cl(2)	71.75(6)	71.8(2)
S(1) – M(1) – Cl(1)*	73.83(7)	71.7(2)
S(1) – M(1) – Cl(2)*	142.91(7)	143.3(2)
S(2) – M(1) – S(2)*	71.89(9)	71.2(3)
S(2) – M(1) – Cl(1)	142.92(7)	142.7(2)
S(2) – M(1) – Cl(2)	80.08(7)	77.9(2)
S(2) – M(1) – Cl(1)*	71.81(6)	71.5(2)
S(2) – M(1) – Cl(2)*	71.92(7)	73.5(2)
Cl(1) – M(1) – Cl(2)	95.68(7)	94.0(2)
Cl(1) – M(1) – Cl(1)*	145.09(10)	145.8(3)
Cl(1) – M(1) – Cl(2)*	94.58(7)	96.2(2)
Cl(2) – M(1) – Cl(2)*	145.31(10)	144.6(3)

The work described in Chapter 4 has shown the structural characterisation of a series of 6- and 8-coordinate Ti(IV) adducts involving the phosphine and arsine ligands o-$C_6H_4(EMe)_2$ for E = P, As, with comparison of the structures revealing the effects of changing coordination number, halide and group 15 donor atom. In view of extending this series to show the effects of changing the group IV metal centre on the coordination geometry, single crystal X-ray diffraction studies were conducted on the Zr(IV) arsine complex isolated here. Thus, $[ZrCl_4\{o\text{-}C_6H_4(AsMe)_2\}_2]$ (Figure 5.8, Tables 5.9, 5.10) is isostructural with $[TiCl_4\{o\text{-}C_6H_4(AsMe)_2\}_2]$ (see Chapter 4) and is similar to the above 8-coordinate Zr(IV) and Hf(IV) thioether complexes. The Zr-Cl [2.507(3) Å] and Zr-As [2.845(2) Å] bond lengths are longer than those reported for the equivalent Ti(IV) complex $[TiCl_4\{o\text{-}C_6H_4(AsMe_2)_2\}_2]$ [2.46(2) Å and 2.71(2) Å respectively],[3,4] consistent with the larger radius of the Zr(IV) centre compared with Ti(IV). Furthermore, the increase in the M-As bond length (*ca.* 0.14 Å) is almost three times the increase in the M-Cl distance. Such dramatic disparity between the effect of changing the metal centre for the respective donor ligands indicates a significant change in the hardness of the metal. Thus, while the distances to the hard chloro ligands apparently show only increases due to the larger radius of the metal centre, the bond lengths to the soft arsine ligands reflect a significantly reduced interaction with hard Zr(IV). As a consequence, the observed bite angles for the chelating arsine ligand are significantly reduced [70.49(6)° Zr(IV), c.f. 72.6(2)° Ti(IV)] due to the constraints of the ligand backbone, while the bond angles between the unrestrained chloro ligands are relatively unchanged [e.g. 146.5(2)° Zr(IV), c.f. 145.6(3)° Ti(IV)]. Although these observations are consistent with the reported anomalous 'soft' behaviour of Ti(IV) with respect to the preferential thioether coordination in mixed S- and O- donor ligands (see Chapter 3),[17,25,26] the observed differences may be partly attributed to the large e.s.d.'s associated with the early reported Ti(IV) structure.

Table 5.9 Selected bond lengths for $[ZrCl_4\{o\text{-}C_6H_4(AsMe)_2\}_2]$.

Bond	Distance / Å	Bond	Distance / Å
Zr(1) – As(1)	2.845(2)	Zr(2) – Cl(1)	2.507(3)

Table 5.10 Selected bond angles for [$ZrCl_4\{o\text{-}C_6H_4(AsMe)_2\}_2$].

Bond	Angle / °	Bond	Angle / °
As(1) – Zr(1) – As(1a)	70.49(6)	As(1) – Zr(1) – As(1b/c)	131.84(4)
As(1) – Zr(1) – Cl(1)	76.35(9)	As(1) – Zr(1) – Cl(1a)	76.42(9)
As(1) – Zr(1) – Cl(1b)	71.51(9)	As(1) – Zr(1) – Cl(1c)	142.00(9)
Cl(1) – Zr(1) – Cl(1a)	146.5(2)	Cl(1) – Zr(1) – Cl(1b/c)	94.77(5)

Figure 5.8 View of the structure of [$ZrCl_4\{o\text{-}C_6H_4(AsMe)_2\}_2$] with numbering scheme adopted. Ellipsoids drawn at 40%, H-atoms omitted for clarity.

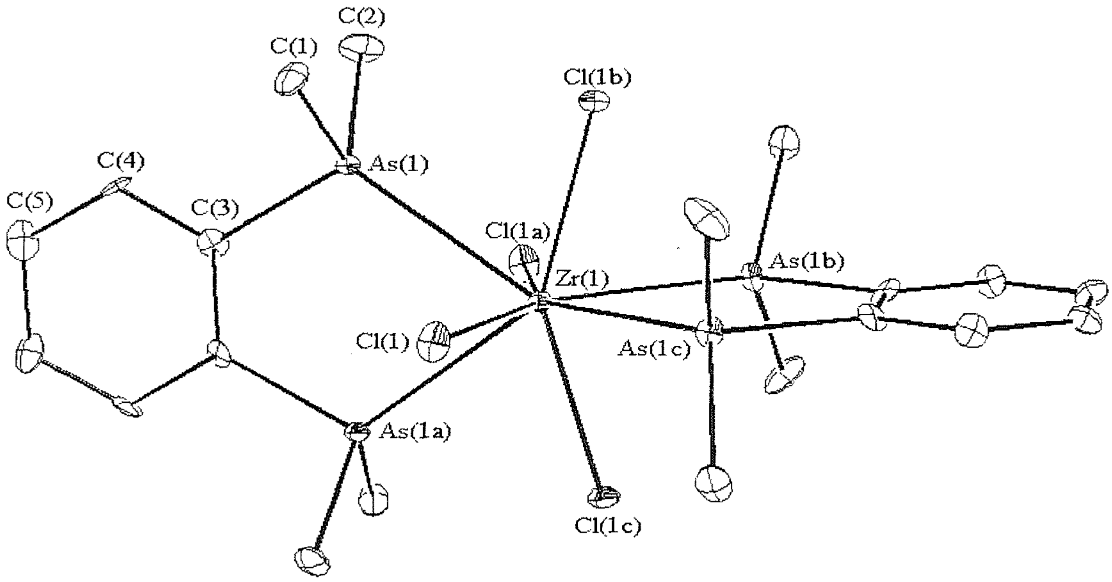

Following unsuccessful attempts to grow single crystals of the Zr(IV) selenoether adducts *via* slow evaporation as utilised for the above structures, crystallisation was attempted *via* slow formation of the required adduct. Thus, separate dilute CH_2Cl_2 solutions of [$ZrCl_4(Me_2S)_2$] and $MeSe(CH_2)_nSeMe$ ($n = 2, 3$) were allowed to slowly diffuse together in a sealed sample vial within a dry N_2 purged glove box. The crystals resulting from the respective ligand solutions surprisingly gave the same unit cell dimensions, indicating the crystals represent the same species despite the differing ligand architecture. Thus, single crystal X-ray diffraction studies were conducted and the resulting structure (Figure 5.9, Tables 5.10, 5.12) reveals the decomposition of the Zr(IV) precursor to [Zr_2Cl_{10}][Me_2SCH_2Cl]$_2$. This indicates that under these sealed reaction conditions, the stabilisation proffered by the chelation of the bidentate selenoether ligand is insufficient to displace the monodentate thioether ligands. Whereas under the gentle vacuum conditions of the bulk synthesis, volatile Me_2S is removed from the reaction mixture to drive the equilibrium towards selenoether coordination.

Analysis of the geometry at the Zr(IV) centres reveals similar distortions as in the 6-coordinate Zr(IV) and Hf(IV) complexes described earlier. Thus, the terminal chloride ligands lean towards the bridging unit, resulting in an acute angle between the *cis*-bridging chlorides [78.47(9)°]. This again suggests the extent of the observed distortions may be due to the spatial requirements of the electron rich terminal chlorides. The bond distances also show a similar trend to the thio- and seleno-ether adducts, with Zr-Cl distances significantly shorter for chlorides *trans* to the bridging chlorides [2.358(3), 2.389(3) Å] compared with the mutually *trans* terminal chlorides [2.416(2), 2.435(3) Å]. This indicates the terminal chlorides prefer to reside *trans* to the less strongly coordinating bridging chlorides, consistent with the observed long $Zr\text{-}Cl_{bridging}$ distances [2.577(3), 2.650(3) Å]. Other structurally characterised complexes involving the $[Zr_2Cl_{10}]^{2-}$ dianion have been reported previously,[27,28,29,30] each showing similar coordination geometry at the Zr(IV) centres to that observed here. Notably, crystals of $[Zr_2Cl_{10}][C_6H_3(OMe)_3H]^+$ were isolated due to the low solubility of the required compound in CH_2Cl_2, as observed for the equivalent crystals formed in this work.

Figure 5.9 View of the structure of $[Zr_2Cl_{10}][Me_2SCH_2Cl]_2$ with numbering scheme adopted. Ellipsoids drawn at 40%.

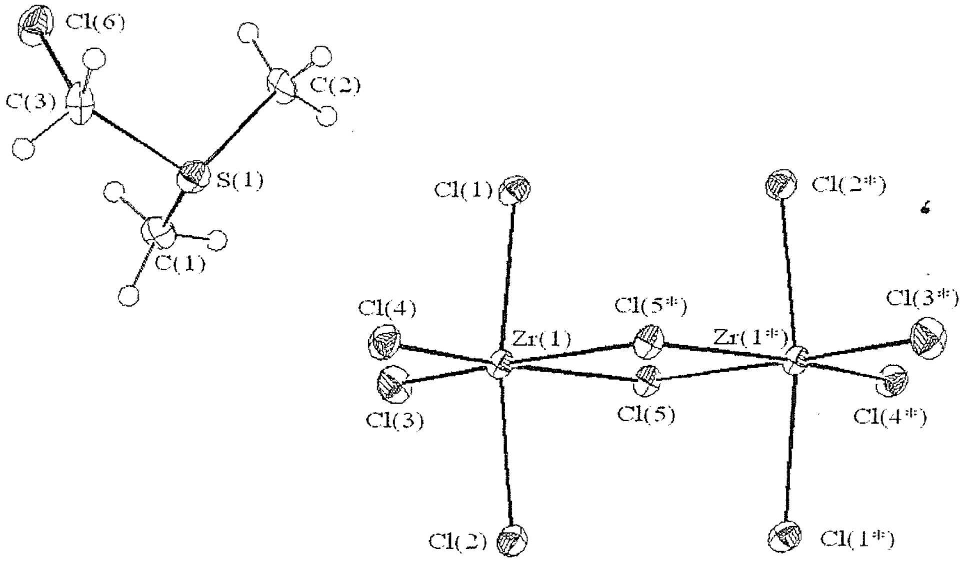

Table 5.11 Selected bond lengths for $[Zr_2Cl_{10}][Me_2SCH_2Cl]_2$.

Bond	Distance / Å	Bond	Distance / Å
Zr(1) – Cl(1)	2.416(2)	Zr(1) – Cl(2)	2.435(3)
Zr(1) – Cl(3)	2.358(3)	Zr(1) – Cl(4)	2.389(3)
Zr(1) – Cl(5)	2.577(3)	Zr(1) – Cl(5)*	2.650(3)

Table 5.12 Selected bond angles for $[Zr_2Cl_{10}][Me_2SCH_2Cl]_2$.

Bond	Angle / °	Bond	Angle / °
Cl(1) – Zr(1) – Cl(2)	171.62(9)	Cl(1) – Zr(1) – Cl(3)	93.22(9)
Cl(1) – Zr(1) – Cl(4)	92.06(9)	Cl(1) – Zr(1) – Cl(5)	87.03(9)
Cl(1) – Zr(1) – Cl(5*)	86.30(8)	Cl(2) – Zr(1) – Cl(3)	92.89(9)
Cl(2) – Zr(1) – Cl(4)	92.49(9)	Cl(2) – Zr(1) – Cl(5)	86.80(8)
Cl(2) – Zr(1) – Cl(5*)	86.92(8)	Cl(3) – Zr(1) – Cl(4)	100.31(10)
Cl(3) – Zr(1) – Cl(5)	94.30(10)	Cl(3) – Zr(1) – Cl(5*)	172.77(10)
Cl(4) – Zr(1) – Cl(5)	165.39(9)	Cl(4) – Zr(1) – Cl(5*)	165.39(9)
Cl(5) – Zr(1) – Cl(5*)	78.47(9)	Zr(1) – Cl(5) – Zr(2)	101.53(9)

5.3 Conclusions

While reaction of bidentate thio- and seleno-ether ligands with $ZrCl_4$ or $[ZrCl_4(THF)_2]$ leads to incomplete substitution adducts, addition of excess Me_2S to MCl_4 (M = Zr, Hf) affords $[MCl_4(Me_2S)_2]$ in high yield. Reaction of $[MCl_4(Me_2S)_2]$ with one equivalent of dichalcogenoether ligand L_2 [L_2 = $MeE(CH_2)_nEMe$, E = S, Se; n = 2, 3] or three equivalents of L_2' [L_2' = $MeE(CH_2)_2EMe$] affords 6-coordinate $[MCl_4(L_2)]$ or 8-coordinate $[MCl_4(L_2')_2]$ upon gentle pumping to remove Me_2S. IR spectroscopic data indicated the 6- and 8-coordinate complexes adopt C_{2v} and D_{2d} local symmetry respectively at Zr(IV) and Hf(IV). The M-Cl stretching frequencies decrease significantly upon increasing coordination number at the metal centre, indicating a lengthening of the M-Cl bonds in the sterically crowded 8-coordinate complexes.

Single crystal X-ray diffraction studies of $[ZrCl_4(Me_2S)_2]$, $[ZrCl_4\{MeS(CH_2)_3SMe\}]$, $[HfCl_4\{MeSe(CH_2)_2SeMe\}]$, $[ZrCl_4\{MeS(CH_2)_2SMe\}_2]$, $[HfCl_4\{MeS(CH_2)_2SMe\}_2]$ and $[ZrCl_4\{o\text{-}C_6H_4(AsMe)_2\}_2]$ have been described and these represent the first such studies of thio- or seleno-ether Zr(IV) or Hf(IV) adducts. The structures of the 6-coordinate adducts confirm *cis* coordination of the chalcogenoether ligands, although the structure of $[ZrCl_4\{MeS(CH_2)_3SMe\}]$ revealed a binuclear adduct with bridging thioether ligands. This may in part be due to the lower stabilisation proffered by 6-membered rings when the ligand is chelating. The structures revealed significant distortion from regular octahedral geometry, with chloride ligands leaning towards the chalcogenoether ligands. Notably, bond angles between S- or Se- donor atoms were relatively unaffected by ligand denticity, coordination mode, donor atom or even metal centre; suggesting the observed distortions are most influenced by the spatial requirements of the chloro ligands. As observed for the analogous Ti(IV) adducts, longer M-Cl bond lengths between chlorides *trans* to Cl compared to those *trans* to S or Se indicated a *trans* influence of Cl > S, Se; consistent with the preference of hard Zr(IV) and Hf(IV) for hard Cl. Comparison of the structures with those of similar Ti(IV) adducts revealed the expected increase in bond lengths involving the metal centre, consistent with the larger size of Zr(IV) and Hf(IV).

The crystals of the 8-coordinate thioether complexes are isostructural and show dodecahedral geometry at the metal centre. Comparison with the 6-coordinate structures above revealed the expected increase in bond lengths with increased coordination number, with greatest disparity in the M-Cl bond lengths consistent with the reduced *trans* influence in the 8-coordinate adducts. The 8-coordinate $[ZrCl_4\{o\text{-}C_6H_4(AsMe)_2\}_2]$ is isostructural with the equivalent Ti(IV) adducts, with bond lengths again reflecting the increased size of Zr(IV). Greatest disparity was observed in the M-As bond lengths, suggesting increased hard Lewis acid behaviour of Zr(IV) over Ti(IV).

Attempted crystallisation *via* reaction of $[ZrCl_4(Me_2S)_2]$ and selenoether ligand solutions afforded crystals of the decomposition product $[Zr_2Cl_{10}][Me_2SCH_2Cl]_2$. The Zr(IV) dianion showed similar distortions as the above 6-coordinate adducts, again suggesting the geometry at Zr(IV) is most influenced by chloro ligands.

5.4 Experimental

The bidentate thio- and seleno-ether ligands were prepared *via* the literature procedures,[31,32,33] while Me_2S, THT, $ZrCl_4$, $ZrCl_4(THF)_2$ and $HfCl_4$ were used as received from Aldrich Chemical Company. Rigorously anhydrous *n*-hexane and CH_2Cl_2 were freshly distilled over sodium/benzophenone and CaH_2 respectively, and degassed with dry N_2. All reactions were performed under an N_2 atmosphere using standard Schlenk techniques. The products were transferred and stored in a dry, continuously N_2-purged glove box, as were all sample preparations.

[$ZrCl_4(THT)_2$]

THT (3.52 g, 40 mmol) in dry, degassed CH_2Cl_2 (10 cm^3) was added to a suspension of $ZrCl_4$ (2.33 g, 10 mmol) in CH_2Cl_2 (50 cm^3) and the solution stirred at room temperature under N_2 for 2 hours to complete $ZrCl_4$ dissolution. The solution was concentrated *in vacuo* to 10 cm^3, with subsequent addition of dry, degassed *n*-hexane (30 cm^3) affording a white solid that was filtered, washed with *n*-hexane (10 cm^3) and dried *in vacuo* to give the required [$ZrCl_4(THT)_2$] (yield 3.15 g, 77 %). Required for [$C_8H_{16}Cl_4S_2Zr$]: C = 23.5, H = 3.9 %; found: C = 23.5, H = 4.0 %. ^1H NMR: δ 3.25 (*s*, CH_2S), 2.10 (*s*, CH_2). IR ν(ZrCl): 353, 343, 331, 315 cm^{-1}.

[$ZrCl_4(Me_2S)_2$]

As [$ZrCl_4(THT)_2$], but using Me_2S (2.48 g, 40 mmol). A white solid was isolated as the required [$ZrCl_4(Me_2S)_2$] (yield 3.03 g, 85 %). Required for [$C_4H_{12}Cl_4S_2Zr$]: C = 13.4, H = 3.4 %; found: C = 13.9, H = 3.6 %. ^1H NMR: δ 2.32 (*s*, Me). IR ν(ZrCl): 357, 341, 319, 308 cm^{-1}.

[$HfCl_4(Me_2S)_2$]

As [$ZrCl_4(Me_2S)_2$], but using $HfCl_4$ (3.20 g, 10 mmol). A white solid was isolated as the required [$HfCl_4(Me_2S)_2$] (yield 3.65 g, 82 %). Required for [$C_4H_{12}Cl_4HfS_2$]: C = 10.8, H = 2.7 %; found: C = 11.2, H = 2.9 %. IR ν(HfCl): 346, 332, 311, 301 cm^{-1}.

[$ZrCl_4${$MeS(CH_2)_2SMe$}]

$MeS(CH_2)_2SMe$ (0.076 g, 0.62 mmol) in dry, degassed CH_2Cl_2 (10 cm^3) was added to a solution of [$ZrCl_4(Me_2S)_2$] (0.20 g, 0.56 mmol) in CH_2Cl_2 (50 cm^3). The solution was slowly concentrated *in vacuo* to 20 cm^3 and stirred under N_2 for 24 hours. Further concentration and addition of *n*-hexane (10 cm^3) afforded a white solid that was filtered, washed with *n*-hexane (10 cm^3) and dried *in vacuo* to give the required [$ZrCl_4${$MeS(CH_2)_2SMe$}] (yield 0.12 g, 61 %). Required for [$C_4H_{10}Cl_4S_2Zr$]: C = 13.5, H = 2.8 %; found: C = 13.5, H = 2.9 %. IR ν(ZrCl): 363 br cm^{-1}.

[$ZrCl_4${$MeS(CH_2)_3SMe$}]

As above, but using $MeS(CH_2)_3SMe$ (0.084 g, 0.62 mmol). A white solid was isolated as the required [$ZrCl_4${$MeS(CH_2)_3SMe$}] (yield 0.11 g, 54 %). Required for [$C_5H_{12}Cl_4S_2Zr$]: C = 16.3, H = 3.3 %; found: C = 15.9, H = 3.3 %. IR ν(ZrCl): 364 br cm^{-1}.

[$ZrCl_4${$MeSe(CH_2)_2SeMe$}]

As above, but using $MeSe(CH_2)_2SeMe$ (0.134 g, 0.62 mmol). A white solid was isolated as the required [$ZrCl_4${$MeSe(CH_2)_2SeMe$}] (yield 0.15 g, 58 %). Required for [$C_4H_{10}Cl_4Se_2Zr$]: C = 10.7, H = 2.2 %; found: C = 11.0, H = 2.5 %. IR ν(ZrCl): 364 br cm^{-1}.

[$ZrCl_4${$MeSe(CH_2)_3SeMe$}]

As above, but using $MeS(CH_2)_3SMe$ (0.143 g, 0.62 mmol). A white solid was isolated as the required [$ZrCl_4${$MeSe(CH_2)_3SeMe$}] (yield 0.12 g, 46 %). Required for [$C_5H_{12}Cl_4Se_2Zr$]: C = 13.0, H = 2.6 %; found: C = 12.7, H = 2.8 %. IR ν(ZrCl): 366 br cm^{-1}.

[$ZrCl_4${$MeS(CH_2)_2SMe$}$_2$]

As [$ZrCl_4${$MeS(CH_2)_2SMe$}], but using [$ZrCl_4(Me_2S)_2$] (0.10 g, 0.28 mmol) and three equivalents of $MeS(CH_2)_2SMe$ (0.103 g, 0.84 mmol). A white solid was isolated as the required [$ZrCl_4${$MeS(CH_2)_2SMe$}$_2$] (yield 0.10 g, 72 %). Required for [$C_8H_{20}Cl_4S_4Zr$]: C = 20.1, H = 4.2 %; found: C = 20.4, H = 4.0 %. IR ν(ZrCl): 307, 301 cm^{-1}.

$[ZrCl_4\{MeSe(CH_2)_2SeMe\}_2]$

As above, but using $MeSe(CH_2)_2SeMe$ (0.181 g, 0.84 mmol). A white solid was isolated as the required $[ZrCl_4\{MeSe(CH_2)_2SeMe\}_2]$ (yield 0.13 g, 68 %). Required for $[C_8H_{20}Cl_4Se_4Zr]$: C = 14.5, H = 3.0 %; found: C = 14.8, H = 2.8 %. IR ν(ZrCl): 305, 299 cm^{-1}.

$[ZrCl_4\{$*o*-$C_6H_4(AsMe)_2\}_2]$

As above, but using *o*-$C_6H_4(AsMe)_2$ (0.240 g, 0.84 mmol). A white solid was isolated as the required $[ZrCl_4\{$*o*-$C_6H_4(AsMe)_2\}_2]$ (yield 0.17 g, 77 %). Required for $[C_{20}H_{32}As_4Cl_4Zr]$: C = 29.8, H = 4.0 %; found: C = 30.1, H = 4.0 %. IR ν(ZrCl): 296, 288 cm^{-1}.

$[HfCl_4\{MeS(CH_2)_2SMe\}]$

As $[ZrCl_4\{MeS(CH_2)_2SMe\}]$, but using $[HfCl_4(Me_2S)_2]$ (0.25 g, 0.56 mmol), $MeS(CH_2)_2SMe$ (0.076 g, 0.62 mmol) and reaction stirred for 48 hours. A white solid was isolated as the required $[HfCl_4\{MeS(CH_2)_2SMe\}]$ (yield 0.14 g, 55 %). Required for $[C_4H_{10}Cl_4HfS_2]$: C = 10.9, H = 2.3 %; found: C = 11.1, H = 2.5 %. IR ν(HfCl): 329 br cm^{-1}.

$[HfCl_4\{MeSe(CH_2)_2SeMe\}]$

As above, but using $MeSe(CH_2)_2SeMe$ (0.134 g, 0.62 mmol). A white solid was isolated as the required $[HfCl_4\{MeSe(CH_2)_2SeMe\}]$ (yield 0.14 g, 47 %). Required for $[C_4H_{10}Cl_4HfSe_2]$: C = 9.0, H = 1.9 %; found: C = 9.2, H = 2.0 %. IR ν(HfCl): 329 br cm^{-1}.

$[HfCl_4\{MeS(CH_2)_2SMe\}_2]$

As $[HfCl_4\{MeS(CH_2)_2SMe\}]$, but using $[HfCl_4(Me_2S)_2]$ (0.125 g, 0.28 mmol) and three equivalents of $MeS(CH_2)_2SMe$ (0.103 g, 0.84 mmol). A white solid was isolated as the required $[HfCl_4\{MeS(CH_2)_2SMe\}_2]$ (yield 0.09 g, 58 %). Required for $[C_8H_{20}Cl_4HfS_4]$: C = 17.0, H = 3.6 %; found: C = 16.7, H = 3.4 %. IR ν(HfCl): 283, 279 cm^{-1}.

[$HfCl_4${MeSe(CH_2)$_2$SeMe}$_2$]

As above, but using MeSe(CH_2)$_2$SeMe (0.181 g, 0.84 mmol). A white solid was isolated as the required [$HfCl_4${MeSe(CH_2)$_2$SeMe}$_2$] (yield 0.11 g, 52 %). Required for [C_8H_{20}-Cl_4HfSe_4]: C = 12.8, H = 2.7 %; found: C = 12.6, H = 2.5 %. IR ν(HfCl): 280, 273 cm^{-1}.

Crystallographic Studies

Details of the crystallographic data collection and refinement parameters are given in Tables 5.13 and 5.14. Crystals of [$ZrCl_4(Me_2S)_2$], [$ZrCl_4${MeS(CH_2)$_3$SMe}], [$HfCl_4${MeSe(CH_2)$_2$SeMe}], [$ZrCl_4${MeS(CH_2)$_2$SMe}$_2$], [$HfCl_4${MeS(CH_2)$_2$SMe}$_2$] and [$ZrCl_4${*o*-C_6H_4(AsMe)$_2$}$_2$] were grown in a dry N_2 purged glove box *via* slow evaporation of CH_2Cl_2 filtrates obtained from the respective complex syntheses. The crystals of [Zr_2Cl_{10}][Me_2SCH_2Cl]$_2$ were also obtained as a decomposition product during attempted crystallisation of [$ZrCl_4${MeS(CH_2)$_n$SMe}] (n = 2, 3) *via* slow reaction of CH_2Cl_2 solutions of [$ZrCl_4(Me_2S)_2$] and selenoether ligand. Data collection used an Enraf Nonius Kappa CCD diffractometer equipped with an Oxford Systems open-flow cryostat operating at 150 K, with graphite monochromated Mo-K_α radiation (λ = 0.71073 A). Structure solution[34] and refinement[35,36,37] were routine except for [$ZrCl_4${MeS(CH_2)$_2$SMe}$_2$], which revealed disorder in the carbon backbone of one of the thioether ligands. This was adequately modelled by assigning alternative positions for the carbon atoms in a 67 : 33 ratio, with these carbon atoms refined isotropically. Although this necessitates disorder in the methyl substituents on the S-donor atoms, no alternative positions were located and hence the disorder was modelled by slightly larger than normal anisotropic thermal parameters for these methyl carbons.

Table 5.13 Crystallographic data collection and refinement parameters for $[ZrCl_4(Me_2S)_2]$, $[MCl_4(L_2)]$ and $[MCl_4(L_2)_2]$, M = Zr, Hf

	$[ZrCl_4(Me_2S)_2]$	$[(ZrCl_4)_2\{MeS(CH_2)_3SMe\}_2]$	$[HfCl_4\{MeSe(CH_2)_2SeMe\}]$	$[ZrCl_4\{MeS(CH_2)_2SMe\}_2]$	$[HfCl_4\{MeS(CH_2)_2SMe\}_2]$
Formula	$C_4H_{12}Cl_4S_2Zr$	$C_{10}H_{24}Cl_8S_4Zr_2$	$C_4H_{10}Cl_4HfSe_2$	$C_8H_{20}Cl_4S_4Zr$	$C_8H_{20}Cl_4HfS_4$
Formula weight	357.29	738.60	536.34	477.52	564.79
Crystal system	Monoclinic	Orthorhombic	Monoclinic	Tetragonal	Tetragonal
Space group	*Cc* (# 9)	P*bca* (# 61)	P2$_1$ (# 4)	P4_12_12 (# 92)	P4_32_12 (# 96)
a / Å	6.4219(2)	15.8646(2)	7.4864(2)	9.9696(3)	9.9760(2)
b / Å	25.7274(8)	15.4382(2)	11.5652(4)	9.9696(3)	9.9760(2)
c / Å	8.3971(3)	21.6118(4)	8.1257(2)	17.5265(4)	17.4881(4)
α / °	90	90	90	90	90
β / °	106.9050(11)	90	116.501(2)	90	90
γ / °	90	90	90	90	90
U / Å^3	1327.09(7)	5293.18(12)	629.61(3)	1742.01(7)	1740.43(6)
Z	4	8	2	4	4
μ(Mo-K$_\alpha$) / cm^{-1}	18.97	19.06	148.47	17.01	70.54
No. of unique reflections	1376	5961	1359	1111	1112
R_{int} (based on F^2)	0.048	0.062	0.104	0.067	0.120
No. of obs. reflections [a]	1308	3205	1281	867	898
No. of parameters	98	217	99	77	78
R [b]	0.043	0.042	0.056	0.041	0.080
R_w [c]	0.063	0.049	0.068	0.053	0.108

[a] Observed if $[I_o > 3\sigma(I_o)]$ [b] $R = \sum (|F_{obs}|_i - |F_{calc}|_i) / \sum |F_{obs}|_i$ [c] $R_w = \sqrt{}[\sum w_i(|F_{obs}|_i - |F_{calc}|_i)^2 / \sum w_i|F_{obs}|_i^2$

Table 5.14 Crystallographic data collection and refinement parameters for $[ZrCl_4\{o\text{-}C_6H_4(AsMe_2)_2\}_2]$ and $[Zr_2Cl_{10}][Me_2SCH_2Cl]_2$.

	$[ZrCl_4\{o\text{-}C_6H_4(AsMe_2)_2\}_2]$	$[Zr_2Cl_{10}][Me_2SCH_2Cl]_2$
Formula	$C_{20}H_{32}Cl_4As_4Zr$	$C_6H_{16}Cl_{12}S_2Zr_2$
Formula weight	805.19	760.20
Crystal system	Tetragonal	Monoclinic
Space group	$I\bar{4}$ (# 82)	$P2_1/n$ (# 14)
a / Å	9.2424(2)	9.2646(3)
b / Å	9.2424(2)	14.5290(5)
c / Å	16.6704(7)	9.3074(4)
α / °	90	90
β / °	90	91.9700(11)
γ / °	90	90
U / Å^3	1424.00(6)	1252.09(7)
Z	2	4
μ(Mo-K$_\alpha$) / cm^{-1}	53.82	49.21
No. of unique reflections	753	2659
R_{int} (based on F^2)	0.066	0.100
No. of obs. reflections [a]	701	1349
No. of parameters	66	100
R [b]	0.057	0.053
R_w [c]	0.082	0.061

[a] Observed if $[I_o > 3\sigma(I_o)]$

[b] $R = \sum (|F_{obs}|_i - |F_{calc}|_i) / \sum |F_{obs}|_i$

[c] $R_w = \sqrt{[\sum w_i(|F_{obs}|_i - |F_{calc}|_i)^2 / \sum w_i|F_{obs}|_i^2}$

5.5 References

[1] W. Levason, B. Patel, G. Reid, V.-A. Tolhurst, M. Webster, *J. Chem. Soc., Dalton Trans.*, 2000, 3001.

[2] R. Hart, W. Levason, B. Patel, G. Reid, *Eur. J. Inorg. Chem.*, 2001, **11**, 2927.

[3] R. J. H. Clark, J. Lewis, R. S. Nyholm, P. Pauling, G. B. Robertson, *Nature*, 1961, **192**, 122.

[4] R. J. H. Clark, J. Lewis, R. S. Nyholm, *J. Chem. Soc.*, 1962, 2460.

[5] R. J. H. Clark, D. L. Kepert, R. S. Nyholm, *Nature*, 1963, **199**, 559.

[6] R. J. H. Clark, W. Errington, J. Lewis, R. S. Nyholm, *J. Chem. Soc. (A)*, 1966, 989.

[7] R. J. H. Clark, *Spectrochim. Acta*, 1965, **21**, 955.

[8] J. H. Wengrovius, R. R. Schrock, C. S. Day, *Inorg. Chem.*, 1981, **20**, 1844.

[9] T. C. Ray, A. D. Westland, *Inorg. Chem.*, 1965, **4**, 1501.

[10] G. S. Girolami, M. B. Hursthouse, M. Thornton-Pett, G. Wilkinson, *J. Chem. Soc., Dalton Trans.*, 1984, 2789.

[11] F. A. Cotton, P. A. Kibala, W. A. Wojtczak, *Acta Crytstallogr., Sect. C*, 1991, C47, 82.

[12] R. P. Beatty, T. J. McNeese, *J. Am. Chem. Soc.*, 1979, **101**, 1053.

[13] R. P. Beatty, S. Datta, S. S. Wreford, *Inorg. Chem.*, 1965, **4**, 1501.

[14] D. Hugi-Cleary, M. Turin-Rossier, A. E. Merbach, *Inorg. Chim. Acta*, 1990, **167**, 245.

[15] M. Valloton, A. E. Merbach, *Helv. Chim. Acta*, 1975, **58**, 2272.

[16] I. R. Beattie, M. Webster, *J. Chem. Soc.*, 1964, 3507.

[17] E. C. Alyea, E. G. Torrible, *Can. J. Chem.*, 1965, **43**, 3468.

[18] F. M. Chung, A. D. Westland, *Can. J. Chem.*, 1969, **47**, 195.

[19] J. B. Hamilton, R. E. McCarley, *Inorg. Chem.*, 1970, **9**, 1339.

[20] W. Levason, B. Patel, G. Reid, submitted for publication.

[21] Z-C. Chen, Z-D. Liu, *Synth. Commun.*, 1993, **23**, 2673.

[22] B. Krebs, *Angew. Chem., Int. Ed. Engl.*, 1969, **8**, 146.

[23] H. Jacobs, R. Niewa, *Z. Krystallogr.*, 1995, **210**, 687.

[24] R. M. Kessler, W. K. Musker, M. M. Olmstead, *Inorg. Chem.*, 1981, **20**, 151.

[25] G. W. A. Fowles, R. A. Walton, *J. Chem. Soc.*, 1964, 4330.

[26] A. J. McAlees, R. McCrindle, A. R. Woon-Fat, *Inorg. Chem.*, 1976, **15**, 1065.

[27] S. J. Coles, M. B. Hursthouse, D. G. Kelly, N. M. Walker, *Acta Crystallogr., Sect. C*, 1999, **55**, 1789.

[28] M. V. Borzov, A. V. Churakov, J. A. Howard, D. P. Krut'ko, E. N. Veksler, *Polyhedron*, 1998, **17**, 3889.

[29] A. I. Brusilovets, A. N. Chernega, E. B. Rusanov, *Zh. Obshch. Khim.*, 1995, **65**, 1819.

[30] K. Dehnicke, J. Eicher, U. Müller, *Z. Anorg. Allg. Chem.*, 1985, **521**, 37.

[31] F. R. Hartley, W. Levason, C. A. McAuliffe, S. G. Murray, H. E. Soutter, *Inorg. Chim. Acta*, 1979, **35**, 265.

[32] D. J. Gulliver, E. G. Hope, W. Levason, G. L. Marshall, S. G. Murray, D. M. Potter, *J. Chem. Soc., Perkin Trans. II*, 1984, 429.

[33] R. D. Feltham, A. Kasenally, R. S. Nyholm, *J. Organomet. Chem.*, 1967, **7**, 285.

[34] PATTY, The DIRDIF Program System, G. Admiraal, G. Beurskens, P. T. Beurskens, W. P. Bosman, S. Garcia-Granda, R. O. Gould, J. M. M. Smits, C. Smykalla, Technical Report of the Crystallography Laboratory, University of Nijmegen, 1992.

[35] TeXsan, Crystal Structure Analysis Package, Molecular Structure Corporation, Houston, Texas, 1995.

[36] R. H. Blessing, *Acta Crystallogr., Sect. A*, 1995, **51**, 33.

[37] H. D. Flack, *Acta Crystallogr., Sect. A*, 1983, **39**, 876.

Chapter 6

Ti(IV) and Zr(IV) Halide Complexes with Tridentate Soft Donor Ligands

6.1 Introduction

While the work discussed in Chapter 3 has established that bidentate thio- and seleno-ether ligands form only 6-coordinate complexes with Ti(IV) halides,[1] certain bidentate phosphine and arsine ligands have been shown to stabilise 8-coordination at Ti(IV) in Chapter 4.[2] Furthermore, the larger ionic radii of congenic Zr(IV) and Hf(IV) have been shown to accommodate both 6- and 8-coordination depending on chain length and stoichiometry of bidentate thio- or seleno-ether ligand in Chapter 5.[3] These results suggest that coordination numbers greater than 6 are attainable for these group IV metal centres *via* careful design of ligand donor properties and reaction conditions. One may therefore expect reaction of group IV halides with tridentate donor ligands may lead to 7-coordination at the metal centres.

There are few reported examples of 7-coordinate Ti(IV), Zr(IV) or Hf(IV) complexes involving neutral donor ligands, and all of these involve strong σ-donor arsine ligands. Reaction of TiX_4 (X = F, Cl, Br or I) and $ZrBr_4$ with the tridentate ligand L_3, $MeAs\{(CH_2)_3AsMe_2\}_2$ affords $[(TiF_4)_3(L_3)]$, $[(TiCl_4)_2(L_3)]$, $[MBr_4(L_3)]$ (M = Ti, Zr) and $[TiI_3(L_3)][I]$.[4] The formulation of these adducts was based primarily on elemental analyses, together with supporting conductivity measurements, molecular weight determinations and electronic and IR spectroscopy. However, uncertainty still remains as to the actual coordination number at the metal centre due to the absence of structural characterisation. Furthermore, the inference that 7-coordination is more readily accessible for $TiBr_4$ compared with $TiCl_4$ adducts contrasts the greater steric crowding caused by the bulkier bromo ligands. Indeed, the only other reported examples of 7-coordinate Ti(IV) with neutral donor ligands involve reaction of $TiCl_4$ with the tridentate arsine ligands L_3', $MeAs\{o\text{-}C_6H_4(AsMe_2)\}_2$ or $MeC(CH_2AsMe_2)_3$, to afford $[TiCl_4(L_3')]$.[5] While the formulation of these adducts was confirmed as above, ^1H NMR spectra were also measured to ascertain the coordination geometry at Ti(IV). Thus, the spectrum for the $MeAs\{o\text{-}C_6H_4(AsMe_2)\}_2$ adduct showed resonances corresponding to both CH_3 environments shifted to high frequency by *ca.* 0.6 – 0.9 ppm compared with the free ligand. Moreover, the shifts of the CH_3 resonances associated with the terminal As-donor arms are similar, and this, together with molecular models indicating bidentate coordination is unfavoured compared with tridentate, suggested the complex was indeed 7-coordinate. Similar high frequency shifts (*ca.* 0.3 – 0.8 ppm) were also observed for the CH_3-As and CH_2 resonances of the $MeC(CH_2AsMe_2)_3$ adduct, and hence the original report postulated that this complex was also 7-coordinate.

Reaction of similar tripodal ligands MeC(X)(Y)(Z) [X = Y = Z = CH_2OMe; X = Y = CH_2OMe, Z = CH_2SMe or CH_2NMe_2; X = CH_2OMe, Y = CH_2SMe, Z = CH_2NMe_2] with $TiCl_4$ has been reported to afford [$TiCl_4${MeC(W)(Y)(Z)}].[6] Room temperature ^1H NMR spectroscopy of these adducts again showed high frequency shifts for the CH_3-E (E = N, O, S) and CH_2 resonances upon ligand coordination. However, these resonances resolved on cooling the sample to reveal uncoordinated donor arm resonances less shifted to high frequency, and in some cases, additional resonances due to free ligand. This suggested the ligands act as bidentates only to give 6-coordinate [$TiCl_4${η^2-MeC(W)(Y)(Z)}], with the room temperature spectra showing fast exchange between coordinated and uncoordinated donor arms. Surprisingly, even the ligands involving small, hard O- or N-donor atoms were unable to form 7-coordinate complexes with the hard Ti(IV) centre.

These results prompted a re-examination of the earlier proposition of 7-coordinate [$TiCl_4${$MeC(CH_2AsMe_2)_3$}].[5] Comparison of the ^1H NMR spectra for this complex with that of 6-coordinate [$TiCl_4${$MeC(CH_2OMe)_3$}] revealed similarities indicating both complexes are indeed 6-coordinate. For example, while each spectrum revealed CH_3-E resonances shifted to high frequency compared to free ligand due to coordinated donor arms (0.80 ppm, E = As; 0.88 ppm, E = O), resonances less shifted to high frequency were also observed indicating the presence of uncoordinated donor arms (0.30 ppm, E = As; 0.17 ppm, E = O). These data suggest that 7-coordination at Ti(IV) may be restricted to the specific donating properties of the tridentate *o*-phenylene ligand MeAs{*o*-$C_6H_4(AsMe_2)$}$_2$, similar to the observation that the majority of 8-coordinate Ti(IV) complexes involve the *o*-phenylene ligands *o*-$C_6H_4(EMe_2)_2$ (E = P, As).[7,8,9] However, it is possible that similar oversights in the interpretation of the ^1H NMR spectra were made for [$TiCl_4${MeAs{*o*-$C_6H_4(AsMe_2)$}$_2$}], as the two tridentate arsine adducts were characterised within the same study.

While the above complexes indicating 7-coordination at Ti(IV) have not been structurally characterised, one example of 7-coordinate Ti(IV) involving anionic thiocarbamate ligands has been structurally authenticated. Thus, reaction of $TiCl_4$ with sodium *N,N*-dialkyldithiocarbamates affords 6-, 7- and 8-coordinate complexes

$[TiCl_2(S_2CNR_2)_2]$, $[TiCl(S_2CNR_2)_3]$ and $[Ti(S_2CNR_2)_4]$ (R = Me, ^{i}Pr, ^{i}Bu) depending on stoichiometry of the reaction mixture.[10] The structure of $[TiCl(S_2CNMe_2)_3]$ confirms the 7-coordinate formulation, showing distorted pentagonal bipyramidal geometry at Ti(IV), with the chloride ligand occupying an axial position. Similar structures have been reported for other 7-coordinate complexes involving anionic ligands, including congenic $[ZrCl(acac)_3]$[11] (acac = $C_5H_7O_2^-$). Other spectroscopically characterised 7-coordinate Ti(IV) complexes include $[TiCl(tropolone)_3]$[12] (tropolone = $C_7H_5O_2^-$) and $[TiCl(oxine)_3]$ (oxine = 8-quinolinol, $C_9H_6NO^-$).[13]

This chapter investigates the coordination chemistry of tridentate group 15 and 16 neutral donor ligands with group IV halides, with a view to establishing both solution and solid state properties of a range of potentially 7-coordinate complexes. Thus, reported within is the synthesis and spectroscopic characterisation of a series of TiX_4 (X = Cl, Br, I) and $ZrCl_4$ complexes with the tripodal ligands $Me(CH_2EMe)_3$ (E = S, Se) and $Me(CH_2AsMe_2)_3$ and the macrocyclic ligands $[9]aneS_3$ (1,4,7-trithiacyclononane) and $[10]aneS_3$ (1,4,7-trithiacyclodecane).[2,3] The only previously reported macrocyclic thioether adduct with Ti(IV) is the structurally characterised distorted octahedral complex $[TiCl_2(NBu^t)([9]aneS_3)]$.[14] The Ti(IV) complexes formed here have been characterised by elemental analysis and IR, UV-visible and multinuclear (^1H, $^{13}C\{^1H\}$, $^{77}Se\{^1H\}$) NMR spectroscopy, with the poor solubility of the Zr(IV) adducts in non-coordinating solvents limiting characterisation to elemental analysis and IR spectroscopy. Single crystal X-ray structure determinations are reported for the complexes $[TiBr_4\{Me(CH_2AsMe_2)_3\}]$ and $[ZrCl_4([9]aneS_3)]$ in order to unequivocally establish the coordination geometry at the metal centres. The structure of $[ZrCl_4\{Me(CH_2AsMe_2)_3\}_2]$ has also been determined during the attempted structural characterisation of $[ZrCl_4\{Me(CH_2AsMe_2)_3\}]$. Comparison of these structures with related 6- and 8-coordinate Ti(IV) and Zr(IV) structures discussed in the previous chapters may establish the consequences of changing the coordination number or ligand type, where relevant.

6.2 Results and Discussion

Reaction of $TiCl_4$ with one molar equivalent of tripodal ligand, L_3 [L_3 = $MeC(CH_2EMe)_3$ (E = S, Se) and $MeC(CH_2AsMe_2)_3$] in rigorously anhydrous *n*-hexane at room temperature resulted in the immediate precipitation of bright yellow and orange solids, [$TiCl_4(L_3)$], in high yield (Figure 6.1). Similarly, dissolution of $TiBr_4$ in rigorously anhydrous CH_2Cl_2 followed by addition of one molar equivalent of L_3 afforded orange and red coloured solutions of [$TiBr_4(L_3)$]. Intensely coloured solids were isolated in high yield *via* precipitation with *n*-hexane. As with the iodo-adducts discussed in Chapters 3 and 4, reactions with TiI_4 required comparatively large volumes of CH_2Cl_2 due to the poor solubility of TiI_4 in non-coordinating solvents. Subsequent addition of one molar equivalent of L_3 resulted in a colour change to give dark red/purple solutions of [$TiI_4(L_3)$]. While the arsine tripod adduct was isolated in low yield as a deep purple solid *via* precipitation with *n*-hexane, the thio- and seleno-ether adducts proved particularly difficult to isolate as powdered solids, affording only oily residues that were unsuitable for characterisation purposes and hence not pursued further. Equivalent reactions of TiX_4 (X = Cl, Br, I) with the macrocyclic tridentate ligands [9]aneS_3 and [10]aneS_3 resulted in the high yield precipitation of bright yellow, orange and purple solids, very poorly soluble in non-coordinating solvents. Similarly, reaction of [$ZrCl_4(Me_2S)_2$] with one molar equivalent of tridentate ligand L_3' [L_3' = $MeC(CH_2EMe)_3$ (E = S, Se), $MeC(CH_2AsMe_2)_3$ and [Z]aneS_3 (Z = 9, 10)] in rigorously anhydrous CH_2Cl_2 resulted in the precipitation of white [$ZrCl_4(L_3')$] upon slow removal of Me_2S *in vacuo*.

All of the isolated complexes are extremely moisture sensitive, with the Ti(IV) adducts visibly decolourising and liberating the free ligand within one minute of exposure to moist air. Notably, the macrocyclic Ti(IV) adducts are markedly more stable than the tripodal complexes, consistent with the increased stabilisation proffered by macrocyclic coordination (see Chapter 1). The formulation of the complexes as [$TiX_4(L_3)$] (X = Cl, Br, I) and [$ZrCl_4(L_3')$] was confirmed *via* microanalytical data. However, as with the Ti(IV) complexes reported in Chapters 3 and 4, mass spectrometry gave no useful information.

Figure 6.1 Reaction scheme for the synthesis of [$TiX_4(L_3)$] and [$ZrCl_4(L_3')$].

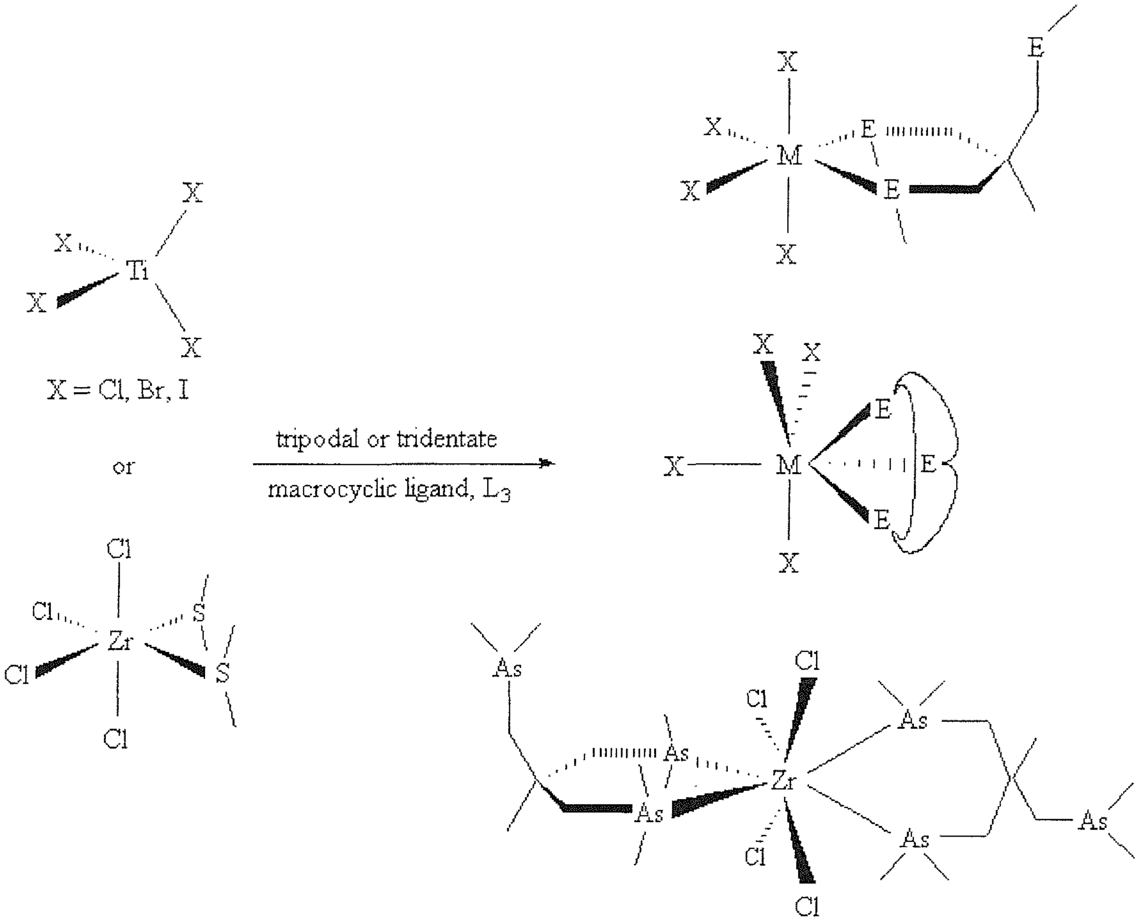

6.2.1 *IR spectroscopy*

Seven coordinate complexes can adopt a number of geometries including pentagonal bipyramidal, capped trigonal prismatic or capped octahedral.[15] For the donor atom sets involved in the [$TiX_4(L_3)$] (X = Cl, Br, I) and [$ZrCl_4(L_3')$] complexes formed here, a number of isomers can exist for each of the coordination geometries. Analysis of the more commonly observed possible isomers reveals point group symmetries of C_{3v}, C_{2v} or the elemental point group C_1. Therefore, the number of metal-halide stretching vibrations expected is either three for C_{3v} symmetry or four for all other geometries. Unfortunately, four such vibrations were also observed for the six-coordinate complexes involving bidentate soft donor ligands discussed in Chapters 3-5. Hence, the number of vibrations observed for the complexes formed here is unlikely to establish either the coordination number or geometry at the metal centres.

Far IR data were recorded for [$TiX_4(L_3)$] (X = Cl, Br, I) and [$ZrCl_4(L_3')$], with the sensitivity of the complexes dictating the glove-box preparation of sodium dried-Nujol mulls pressed between CsI plates. The spectra of the Ti(IV) tripodal ligand adducts showed up to four Ti-X stretching vibrations in the range ν(Ti-Cl) 411-368 cm^{-1} and ν(Ti-Br) 333-284 cm^{-1}. These stretching frequencies compare remarkably well with those observed for the 6-coordinate Ti(IV) complexes involving bidentate arsine or thio- or seleno-ether discussed in Chapters 3 and 4, with ν(Ti-Cl) 422-373 cm^{-1} and ν(Ti-Br) 332-285 cm^{-1}. This may be surprising considering the greater steric crowding in the proposed seven-coordinate complexes is expected to increase Ti-X bond distances compared with those of the six-coordinate adducts. The IR spectra of the macrocyclic Ti(IV) adducts revealed Ti-X stretching vibrations at significantly different frequencies [ν(Ti-Cl) 443-384 cm^{-1} and ν(Ti-Br) 359-338 cm^{-1}] compared with the six-coordinate adducts, possibly indicating a change in coordination geometry at the metal centre.

The spectra of the thio- and seleno-ether Zr(IV) adducts revealed broad unresolved stretching vibrations, similar to those observed for the equivalent six- and eight-coordinate Zr(IV) complexes reported in Chapter 5. Notably, the stretching frequencies observed for the proposed seven-coordinate complexes formed here (*ca.* 330 cm^{-1}) reside approximately midway between those observed for the similar six- (*ca.* 360 cm^{-1}) and eight-coordinate (*ca.* 300 cm^{-1}) Zr(IV) adducts (Figure 6.2). Although other factors may influence the frequency of stretching vibrations, the observed trend is consistent with increasing Zr-Cl bond distances and thus decreasing stretching frequencies upon increasing the coordination number and hence steric crowding at Zr(IV). However, the spectrum of the tripodal arsine Zr(IV) adduct revealed a pair of Zr-Cl stretching vibrations at 300 and 304 cm^{-1}, remarkably similar to those observed for structurally characterised eight coordinate [$ZrCl_4\{o\text{-}C_6H_4(AsMe_2)_2\}_2$] described in Chapter 5. This suggests the tripodal arsine complex formed here is also eight-coordinate and may adopt the equivalent 1:2 metal ligand composition [$ZrCl_4\{MeC(CH_2AsMe_2)_3\}_2$], with two uncoordinated As donor atoms. This contrasts the 1:1 formulation postulated from microanalytical data, however it is possible that the moisture sensitive complex may partially decompose upon exposure to air during the acquisition of analytical data.

Figure 6.2 **Comparison of the ν(Zr-Cl) region of the IR spectra of [$ZrCl_4${MeS-$(CH_2)_2$SMe}$_n$] (n = 1, 2) and [$ZrCl_4$([9]aneS$_3$)] (Nujol Mull).**

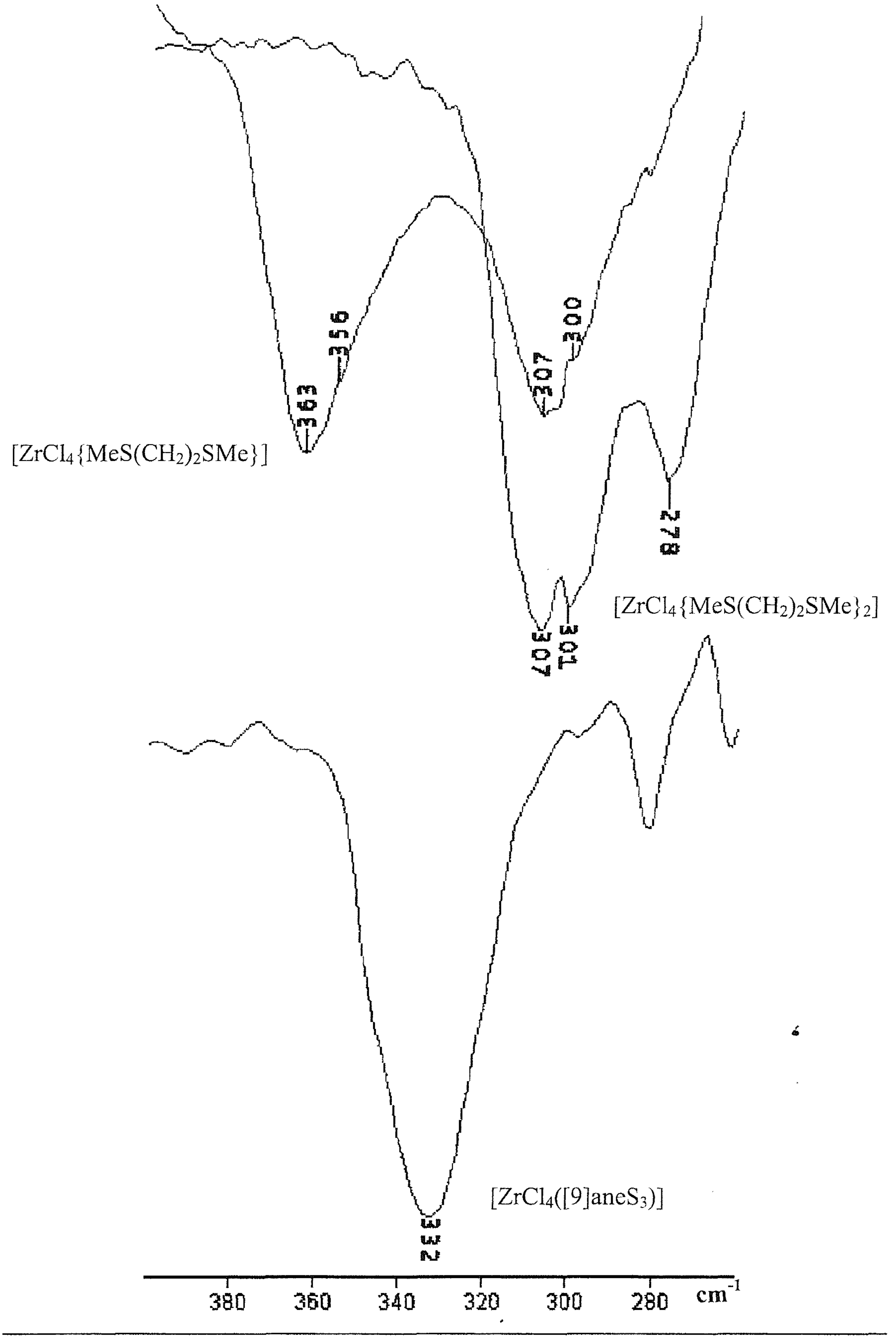

6.2.2 NMR spectroscopy

While the poor solubility of the Zr(IV) adducts in non-coordinating solvents prevented solution phase characterisation, the work described in Chapters 3 and 4 has shown that NMR spectroscopy can establish the solution stability of the more soluble Ti(IV) complexes. Thus, ^1H and $^{13}C\{^1H\}$ NMR spectroscopic studies were undertaken for the Ti(IV) complexes formed here. The room temperature ^1H NMR spectrum of $[TiCl_4\{MeC(CH_2SMe)_3\}]$ showed the expected shift to high frequency upon coordination for the three ^1H resonances [δ 2.87 (CH_2), 2.36 (MeS), 1.24 (MeC)], consistent with reduced electron density at the thioether following σ-donation to the Ti(IV) centre. On cooling, the resonances broadened and split, indicating the slowing of dynamic processes in solution. At 180 K, the resonances began to sharpen once again, suggesting the processes were now slow on the NMR time-scale. Analysis of these resonances revealed the presence of at least two of the possible *meso-1*, *-2* or *DL* invertomers *via* pyramidal inversion at S (see Chapter 1), giving multiple methyl and methylene proton resonances associated with coordinated S-donor arms [δ 3.2 (br, *m*, CH_2); 2.53, 2.51 (MeS)]. Resonances were also observed at frequencies indicative of free thioether ligand [δ 2.55 (CH_2), 2.01 (MeS)], suggesting ligand dissociation is fast at room temperature, but slow at 180 K on the NMR time-scale. However, additional resonances were also observed to slightly higher frequency than the free ligand resonances [δ 2.68 (CH_2), 2.07 (MeS)] and these are consistent with the presence of uncoordinated donor arms. Unfortunately, the presence of overlapping resonances prevented accurate integration of the ^1H environments, however comparison of the coordinated and uncoordinated arm resonances revealed an approximate 2:1 ratio. This suggests that the tripodal ligand actually behaves as a bidentate ligand, with one uncoordinated free donor arm to afford six-coordinate $[TiCl_4\{\eta^2\text{-}MeC(CH_2SMe)_2\}]$.

While the above postulation that the tripodal thioether ligand gives only six-coordinate Ti(IV) adducts may be surprising considering eight-coordination at Ti(IV) has been reported in Chapter 4, the result is consistent with the reported[6] bidentate coordination of mixed O-, N-, and S-donor tripodal ligands with $TiCl_4$. Furthermore, the observations from bidentate thio- and seleno-ether complexes with Ti(IV) in Chapter 3 have shown that the stabilisation offered by 6-membered chelate rings is significantly lower than that by 5-membered rings, leading to increased ligand dissociation in solution. Similar fast ligand exchange on the NMR time-scale between coordinated and uncoordinated donor arms of the η^2-coordinated tripodal ligand may account for the earlier observation of only coordinated donor arm resonances at room temperature. The $^{13}C\{^1H\}$ NMR spectrum confirms this fast donor exchange, with the room temperature spectrum showing singlets for each of the four carbon environments [δ 47.9 (**a**, CH_2), 39.8 (**b**, C), 25.1 (**c**, Me), 22.9 (**d**, MeS)]. On cooling, the resonances associated with the donor arms split to reveal coordinated [δ 49.2, 47.4 (**a'**, CH_2); 25.9, 25.7 (**c'**, MeS)] and uncoordinated [δ 44.8 (**e**, CH_2), 18.0 (**f**, MeS)] donor arm resonances (Figure 6.3). The absence of free ligand resonances may be due to the lower sensitivity of $^{13}C\{^1H\}$ compared with ^1H NMR spectroscopy, and suggests ligand dissociation is not extensive for this chloro-adduct.

Figure 6.3 VT $^{13}C\{^1H\}$ NMR spectra of $[TiCl_4\{MeC(CH_2SMe)_3\}]$ (CH_2Cl_2/CD_2Cl_2)

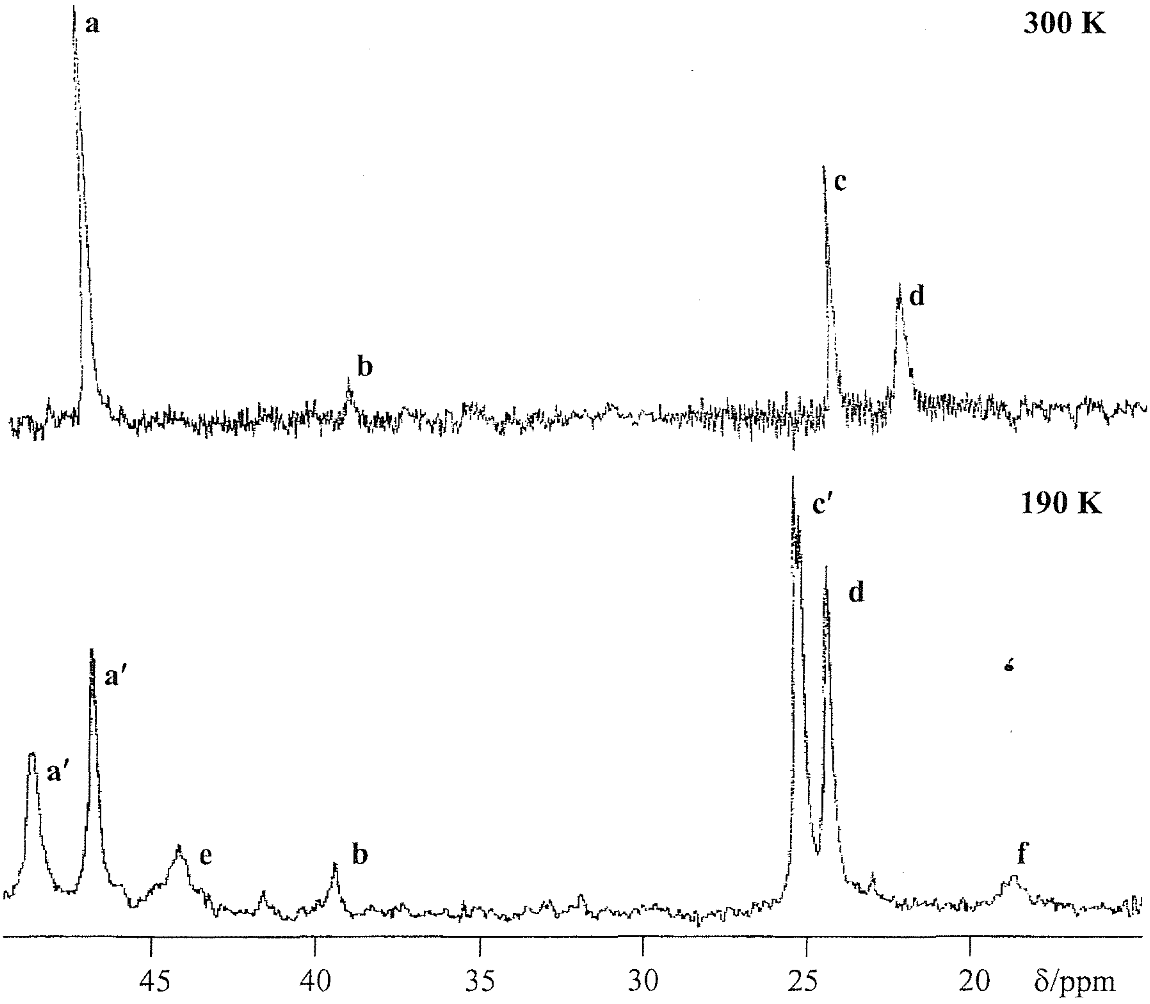

The VT-NMR spectra obtained for the analogous bromo-adduct [$TiBr_4${MeC-($CH_2SMe)_3$}] showed similar resonances consistent with bidentate coordination of the potentially tridentate ligand (Figure 6.4). However, here the low temperature $^{13}C\{^1H\}$ NMR spectrum did reveal the presence of free ligand resonances suggesting a greater degree of ligand dissociation for this bromo-adduct. This is consistent with weaker interactions between the soft donor ligand and the poorer Lewis acid $TiBr_4$ compared with $TiCl_4$, as observed for the analogous adducts involving bidentate thio- and seleno-ether ligands (see Chapter 3). The spectra of the selenoether tripod complexes continue this trend, with the softer Se donor compared with S, forming weaker interactions with the Ti(IV) centres. Thus, no room temperature $^{13}C\{^1H\}$ NMR spectrum was observed for [$TiCl_4${MeC($CH_2SeMe)_3$}], while extensive ligand dissociation in the bromo-adduct presented an ill-defined room temperature ^1H NMR spectrum and no $^{13}C\{^1H\}$ NMR spectrum even at 180 K. The presence of these fast dissociation and exchange processes also prevented the detection of $^{77}Se\{^1H\}$ NMR resonances for either complex even at low temperatures. Nevertheless, the low temperature ^1H NMR spectra do confirm the complexes involve only η^2-coordinated tripodal ligands, as observed for the above thioether ligands.

Figure 6.4 LT ^1H NMR spectrum of [$TiBr_4${MeC($CH_2SMe)_3$}] (180 K, CD_2Cl_2)

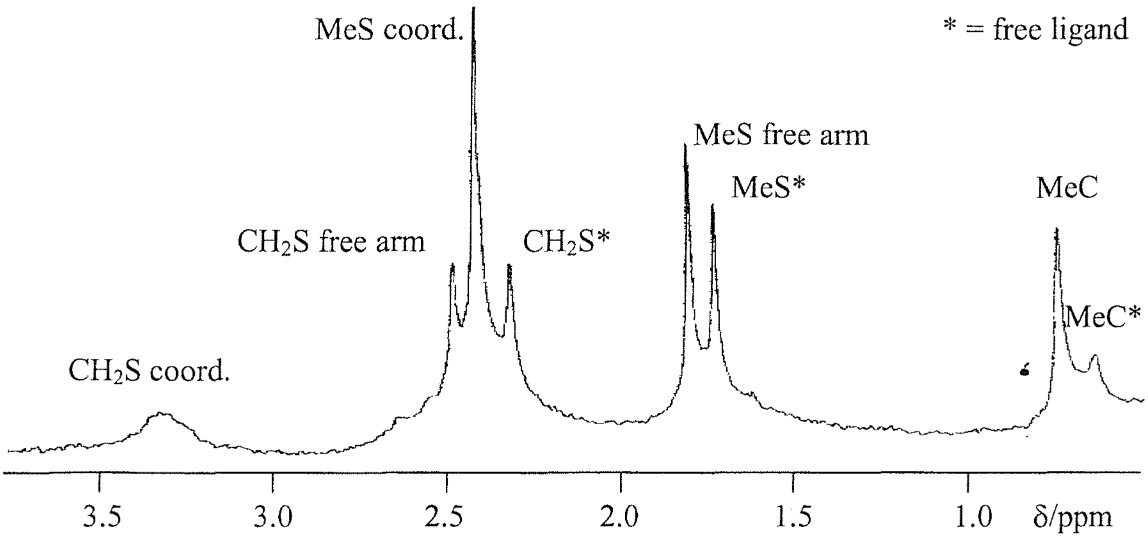

The VT ^1H NMR spectra of the arsine tripod Ti(IV) complexes also confirmed the formulation [$TiX_4\{\eta^2$-MeC($CH_2AsMe_2)_3$}] (X = Cl, Br), with resonances observed corresponding to both coordinated and free As-donor arms. Unlike the Group 16 ligand adducts above, no resonances were observed for free ligand even for the $TiBr_4$ adduct, consistent with the stronger σ-donor ability of Group 15 ligands over those of Group 16.

Unfortunately, the macrocyclic ligand Ti(IV) adducts showed poor solubility in non-coordinating solvents, preventing detailed solution phase characterisation. Nevertheless, $[TiCl_4([9]aneS_3)]$ did provide sufficient solubility in anhydrous $MeNO_2$/ d^3-$MeNO_2$ to allow analysis *via* ^1H and $^{13}C\{^1H\}$ NMR spectroscopy. However the bright yellow solutions of the complex were very sensitive to decomposition, resulting in decolourisation of the solution even upon transferral in a dry N_2 purged glove box. Consequently, the ^1H and $^{13}C\{^1H\}$ NMR spectra of even freshly prepared solutions revealed weak resonances due to a decomposition product in addition to strong resonances due to the required complex. The ^1H NMR spectrum showed a complex second order pattern at δ 4.2(*m*) and 3.8(*m*) corresponding to $[TiCl_4([9]aneS_3)]$ and a similar, but weaker pattern at δ 3.8(*m*) and 3.6(*m*) (Figure 6.5). Both patterns are consistent with the tridentate binding of the $[9]aneS_3$ ligand, as bidentate coordination would remove the second order coupling. Also, the complex appears to show no ligand exchange or macrocycle 'ring-whizzing' on the NMR time-scale, as both of these processes would present only a singlet ^1H resonance. The $^{13}C\{^1H\}$ NMR spectrum confirmed the symmetrical binding of the macrocycle, revealing a singlet at δ 43.1. Weaker resonances were also observed at δ 40.8, 39.8, 38.6, suggesting reduced symmetry in the decomposition product.

Figure 6.5 ^1H NMR spectrum of $[TiCl_4([9]aneS_3)]$ (d^3-$MeNO_2$)

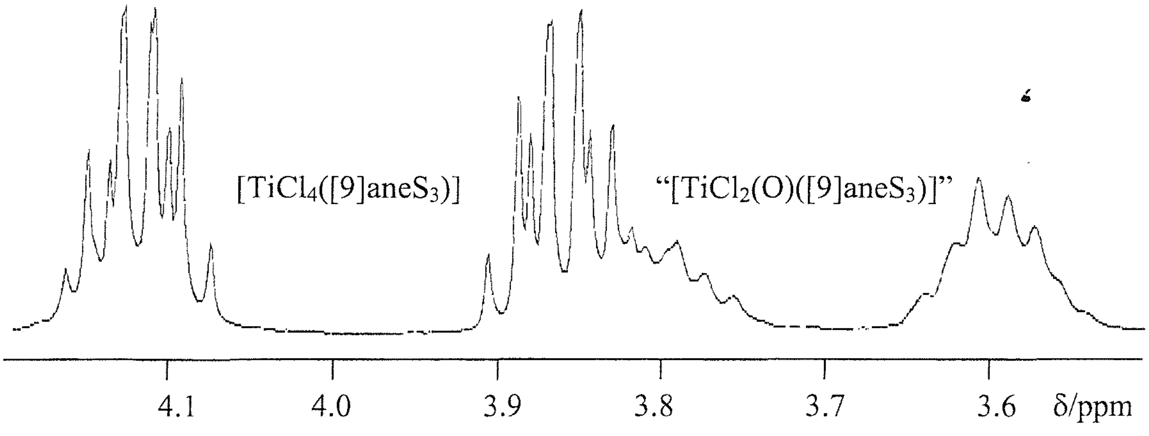

While these data for the decomposition product are insufficient to conclusively establish its identity, it is likely that the coordination of [9]aneS_3 with Ti(IV) would show similar behaviour to that of similar Me_3[9]aneN_3. Indeed, both the thia- and aza-macrocyclic ligands are known to form Ti(IV) adducts [$TiCl_2$(NBu^t)([9]aneS_3)] and [$TiCl_2$(NBu^t)(Me_3[9]aneN_3)], with structural characterisation revealing similar six-coordinate distorted octahedral structures.[14] The aza-macrocyclic ligand is also known to form the isoelectronic complex [$TiCl_2$(O)(Me_3[9]aneN_3)],[16] thus it is possible that [9]aneS_3 may also stabilise such a structure. It is therefore suggested that the [$TiCl_4$([9]aneS_3)] adduct formed here partially hydrolyses in solution to afford a decomposition product of formulation [$TiCl_2$(O)([9]aneS_3)], which is entirely consistent with the above NMR data. Conductivity experiments with $MeNO_2$ solutions of [$TiCl_4$([9]aneS_3)] confirmed the complex is a non-electrolyte, and suggests the complex is indeed a rare example of seven-coordinate Ti(IV). While similar NMR studies were not possible for the other poorly soluble macrocyclic Ti(IV) complexes, analytical data and similar IR spectra suggest these [TiX_4([Z]aneS_3)] (X = Cl, Br, I, Z = 9, 10) complexes all adopt similar seven-coordinate structures.

6.2.3 X-ray crystallographic studies

In order to confirm that the observations from NMR spectroscopy also extend to solid state behaviour, single crystal X-ray diffraction studies were undertaken on one of the tripodal complexes formed here. Thus, single crystals of [$TiBr_4${MeC-($CH_2AsMe_2)_3$}] were grown by slow evaporation of a CH_2Cl_2 solution of the complex in a dry N_2 purged glove box. The resulting structure (Figure 6.6, Tables 6.1, 6.2) confirmed that the tripod ligands indeed behave only as bidentates, revealing distorted octahedral geometry at Ti(IV) comprising four bromo ligands and two mutually *cis* arsine donor atoms from the potentially tridentate ligand. The free donor arm extends away from the Ti(IV) centre to present a mononuclear species with an uncoordinated arsine donor atom. The complex adopts a remarkably similar geometry at the metal centre compared with other Ti(IV) structures involving bidentate soft donor ligands (see Chapters 3 and 4). Thus, the bromo ligands lean towards the arsine ligand, with angles between mutually *cis* bromides greater than that expected for octahedral geometry and the angle between the mutually *trans* bromides contracted [162.3(1)°]. Also the Ti-Br bond distances for these mutually *trans* bromides [2.445(3), 2.471(3) Å] are significantly longer than those *trans* to As [2.403(3), 2.407(3) Å], indicating a *trans* influence of Br > As. The structure of [$TiBr_4\{o\text{-}C_6H_4(AsMe_2)_2\}_2$] discussed in Chapter 4 provides another rare opportunity to compare the bonding characteristics of similar donor ligands in 6- and 8-coordinate complexes. Thus, the Ti-As bond distances in the 6-coordinate complex [2.680(3), 2.688(3) Å] are *ca.* 0.05 Å shorter than those in the 8-coordinate complex, consistent with an increased steric crowding leading to longer metal-ligand distances in the latter. The Ti-Br distances also increase upon increasing coordination number, though the magnitude of the difference is more than three times that observed for the Ti-As distances. This is consistent with the high *trans* influence in the 6-coordinate adduct leading to short Ti-Br distances *trans* to As, while the absence of formally *trans* ligands in the 8-coordinate complex leads to increased bond distances beyond that expected for increasing the coordination number alone. These data parallel the observations from directly comparable 6- and 8-coordinate $TiCl_4$ adducts involving the bidentate phosphine ligand $o\text{-}C_6H_4(PMe_2)_2$ discussed in Chapter 4.

Figure 6.6 View of the structure of [$TiBr_4\{MeC(CH_2AsMe_2)_3\}$] with numbering scheme adopted. Ellipsoids drawn at 40%, H-atoms omitted for clarity.

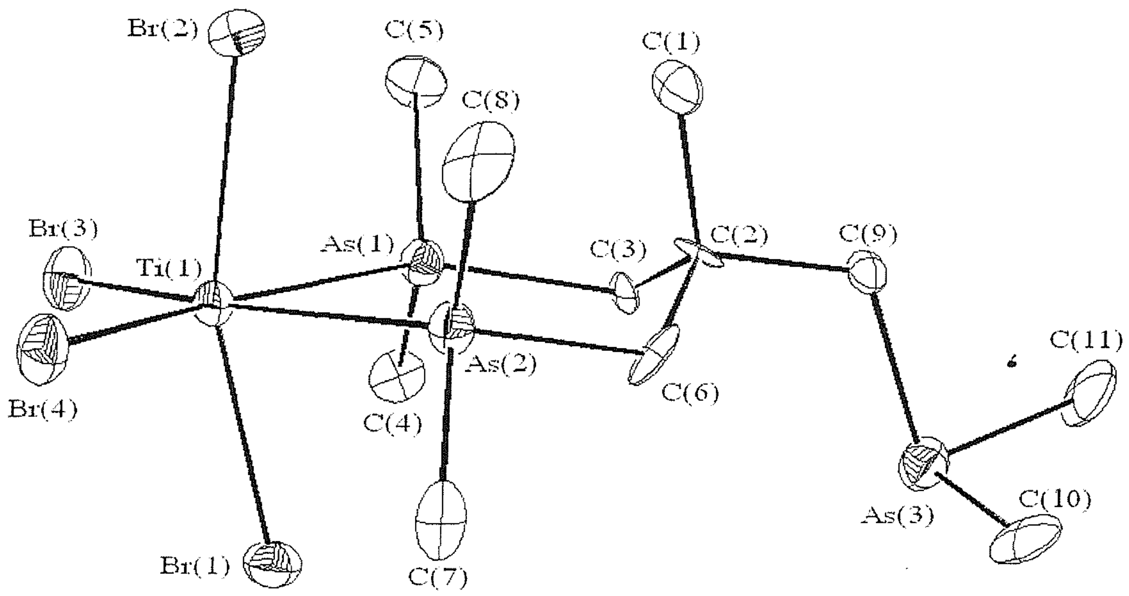

Table 6.1 Selected bond lengths for [$TiBr_4\{MeC(CH_2AsMe_2)_3\}$].

Bond	Distance / Å	Bond	Distance / Å
Ti(1) – As(1)	2.680(3)	Ti(1) – As(2)	2.688(3)
Ti(1) – Br(1)	2.471(3)	Ti(1) – Br(2)	2.445(3)
Ti(1) – Br(3)	2.407(3)	Ti(1) – Br(4)	2.403(3)

Table 6.2 Selected bond angles for [$TiBr_4\{MeC(CH_2AsMe_2)_3\}$].

Bond	Angle / °	Bond	Angle / °
As(1) – Ti(1) – As(2)	82.97(9)	As(1) – Ti(1) – Br(1)	82.57(10)
As(1) – Ti(1) – Br(2)	84.78(10)	As(1) – Ti(1) – Br(3)	83.36(10)
As(1) – Ti(1) – Br(4)	168.4(1)	As(2) – Ti(1) – Br(1)	81.53(10)
As(2) – Ti(1) – Br(2)	84.70(10)	As(2) – Ti(1) – Br(3)	166.30(13)
As(2) – Ti(1) – Br(4)	85.39(10)	Br(1) – Ti(1) – Br(2)	162.3(1)
Br(1) – Ti(1) – Br(3)	95.93(11)	Br(1) – Ti(1) – Br(4)	95.97(11)
Br(2) – Ti(1) – Br(3)	94.84(12)	Br(2) – Ti(1) – Br(4)	93.93(11)
Br(3) – Ti(1) – Br(4)	108.29(13)		

Also, in view of the paucity of structurally characterised seven-coordinate Ti(IV) and Zr(IV) complexes, crystal growing attempts were undertaken for the macrocyclic adducts formed here. However, the extremely poor solubility of the complexes in non-coordinating solvents prevented crystallisation by slow evaporation, while the high sensitivity of weak $MeNO_2$ solutions of [$TiCl_4$([9]aneS_3)] afforded only slow decomposition in solution. Thus, crystal growth was attempted by reaction of slowly diffusing solutions of the metal halide precursor and the macrocyclic ligand. No crystals were observed for the Ti(IV) adducts, with diffusion affording only the precipitation of the complex as a fine powder. However, single crystals of [$ZrCl_4$([9]aneS_3)] were obtained *via* slow diffusion of weak CH_2Cl_2 solutions of [$ZrCl_4(Me_2S)_2$] and [9]aneS_3 in a dry N_2 purged glove box. Unfortunately, the crystals obtained were extremely small and weakly diffracting, and repeated attempts to grow larger crystals by other methods were unsuccessful. Nevertheless, the resulting structure (Figure 6.7, Table 6.3, 6.4) clearly shows facial coordination of all three S-donor atoms of the macrocyclic ligand, with retention of the four chloro ligands presenting a rare 7-coordinate structure. Close inspection of the coordination environment at Zr(IV) reveals the chloro ligands lie almost coplanar to form the trigonal equatorial plane, with bond angles between these chlorides close to 120° [$\angle Cl_{eq}$ – Ti – Cl_{eq}' = 115.0(4), 119.2(4), 120.9(4)°]. These planar chlorides lean slightly towards the fourth chloride positioned in the remaining axial site [$\angle Cl_{ax}$ – Ti – Cl_{eq} = 81.7(4), 81.9(4), 84.1(4)°], presumably in order to reduce repulsion from the sterically crowded macrocycle site. Unfortunately, the weak diffraction data obtained from the small crystals resulted in higher than normal residuals, thus precluding more detailed discussion of the geometric parameters. Nevertheless, the observed Zr-Cl bond lengths [av. 2.423(11) Å] are longer than those in the 6-coordinate Zr(IV) complex [$ZrCl_4\{MeS(CH_2)_3SMe\}$] [av. 2.384(2) Å] and shorter than those in 8-coordinate [$ZrCl_4\{MeS(CH_2)_2SMe\}_2$ [av. 2.486(2) Å]. This is consistent with the expected increase in Zr-Cl bond lengths on increasing coordination number and hence steric crowding at the metal centre. These data also support the conclusions from IR spectroscopy of these adducts, which shows a significant decrease in Zr-Cl stretching frequency upon increasing coordination number.

Figure 6.7 View of the structure of [$ZrCl_4([9]aneS_3)$] with numbering scheme adopted. Ellipsoids drawn at 40%, H-atoms omitted for clarity.

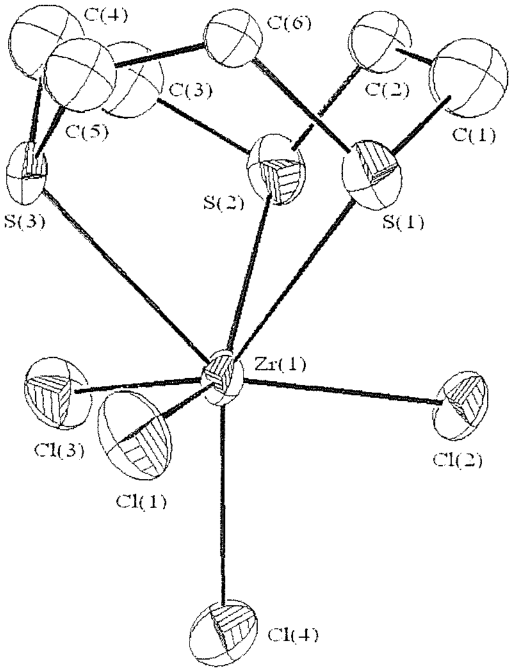

Table 6.3 Selected bond lengths for [$ZrCl_4$([9]aneS_3)].

Bond	Distance / Å	Bond	Distance / Å
Zr(1) – S(1)	2.778(10)	Zr(1) – S(2)	2.711(13)
Zr(1) – S(3)	2.752(11)	Zr(1) – Cl(1)	2.432(11)
Zr(1) – Cl(2)	2.401(10)	Zr(1) – Cl(3)	2.423(10)
Zr(1) – Cl(4)	2.455(12)		

Table 6.4 Selected bond angles for [$ZrCl_4$([9]aneS_3)].

Bond	Angle / °	Bond	Angle / °
S(1) – Zr(1) – S(2)	73.7(4)	S(1) – Zr(1) – S(3)	74.5(3)
S(2) – Zr(1) – S(3)	73.4(4)	S(1) – Zr(1) – Cl(1)	75.7(4)
S(1) – Zr(1) – Cl(2)	75.1(3)	S(1) – Zr(1) – Cl(3)	142.1(4)
S(1) – Zr(1) – Cl(4)	133.7(4)	S(2) – Zr(1) – Cl(1)	139.9(4)
S(2) – Zr(1) – Cl(2)	76.6(4)	S(2) – Zr(1) – Cl(3)	77.3(4)
S(2) – Zr(1) – Cl(4)	138.4(4)	S(3) – Zr(1) – Cl(1)	74.0(4)
S(3) – Zr(1) – Cl(2)	142.0(4)	S(3) – Zr(1) – Cl(3)	74.2(3)
S(3) – Zr(1) – Cl(4)	136.1(4)	Cl(1) – Zr(1) – Cl(2)	119.2(4)
Cl(1) – Zr(1) – Cl(3)	115.0(4)	Cl(1) – Zr(1) – Cl(4)	81.7(4)
Cl(2) – Zr(1) – Cl(3)	120.9(4)	Cl(2) – Zr(1) – Cl(4)	81.9(4)
Cl(3) – Zr(1) – Cl(4)	84.1(4)		

Following the unexpected observation by IR spectroscopy of an 8-coordinate Zr(IV) complex with $MeC(CH_2AsMe_2)_3$, single X-ray diffraction studies were undertaken to establish the identity of the complex. Thus, single crystals were grown by slow evaporation of the weak CH_2Cl_2 filtrate obtained from the attempted synthesis of [$ZrCl_4\{MeC(CH_2AsMe_2)_3\}$]. The resulting structure (Figure 6.8, Tables 6.5, 6.6) confirms the presence of dodecahedral 8-coordinate Zr(IV), showing four As-donor atoms occupying A-type vertices and four chloro ligands occupying the B vertices. The arsine donor set comprises two mutually *cis* coordinated donor atoms from two independent tripodal ligands behaving as bidentates. As with the 6-coordinate Ti(IV) adduct with this ligand, the third donor arms extend away from the metal centre and remain uncoordinated. This is consistent with the observation that reaction of Zr(IV) with the bidentate arsine ligand *o*-$C_6H_4(AsMe_2)_2$ affords 8-coordinate [$ZrCl_4${*o*-$C_6H_4(AsMe_2)_2$}$_2$] even at low ligand concentrations (Chapter 5). Indeed, the structure of the tripodal complex reported here shows comparable local geometry at Zr(IV) to that observed for [$ZrCl_4${*o*-$C_6H_4(AsMe_2)_2$}$_2$]. One notable difference is the increased ligand bite angle [74.71(4)°] compared with the *o*-$C_6H_4(AsMe_2)_2$ structure [70.49(6)°], consistent with the greater flexibility of the tripodal ligand. While the reaction filtrate crystallisation method utilised here presents the possibility that the observed species is simply an impurity, the structure is consistent with the conclusions of 8-coordinate Zr(IV) from IR spectroscopy of the bulk complex. Thus, it appears that the tripodal ligand preferentially stabilises 8-coordination at Zr(IV), with the inconsistent analytical data attributed to decomposition of the solid during data acquisition. This could be confirmed by comparing powder X-ray diffraction data from the bulk sample with that of the crystal structure and by obtaining microanalytical data for the crystalline form.

Figure 6.8 View of the structure of [$ZrCl_4${$MeC(CH_2AsMe_2)_3$}$_2$] with numbering scheme adopted. Ellipsoids drawn at 40%, H-atoms omitted for clarity.

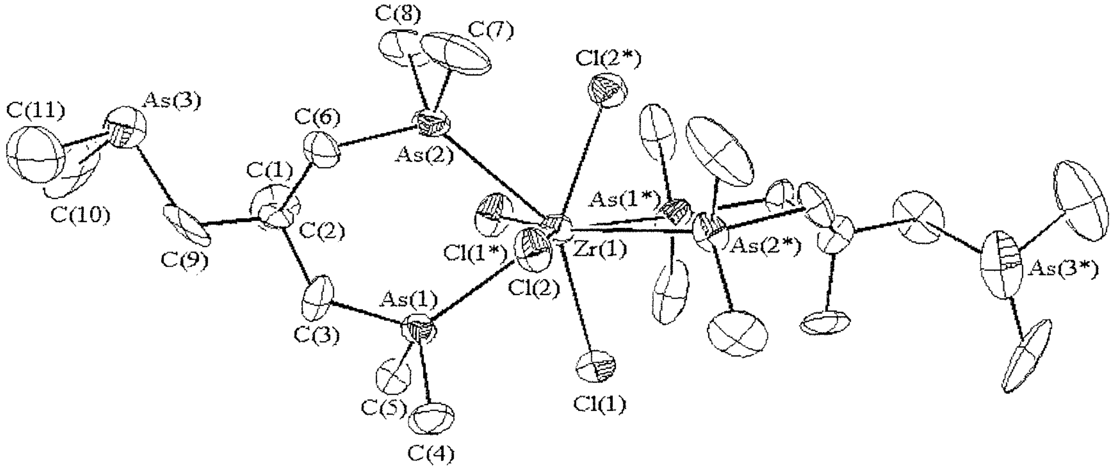

Table 6.5 Selected bond lengths for $[ZrCl_4\{MeC(CH_2AsMe_2)_3\}_2]$.

Bond	Distance / Å	Bond	Distance / Å
Zr(1) – As(1)	2.895(2)	Zr(1) – As(2)	2.909(2)
Zr(1) – Cl(1)	2.530(4)	Zr(1) – Cl(2)	2.492(4)

Table 6.6 Selected bond angles for $[ZrCl_4\{MeC(CH_2AsMe_2)_3\}_2]$.

Bond	Angle / °	Bond	Angle / °
As(1) – Zr(1) – As(2)	74.71(4)	As(1) – Zr(1) – As(1)*	122.57(9)
As(1) – Zr(1) – As(2)*	130.56(4)	As(2) – Zr(1) – As(2)*	132.55(9)
As(1) – Zr(1) – Cl(1)	70.27(9)	As(1) – Zr(1) – Cl(2)	78.94(9)
As(1) – Zr(1) – Cl(1)*	73.49(10)	As(1) – Zr(1) – Cl(2)*	146.68(9)
As(2) – Zr(1) – Cl(1)	144.88(9)	As(2) – Zr(1) – Cl(2)	76.62(10)
As(2) – Zr(1) – Cl(1)*	72.71(9)	As(2) – Zr(1) – Cl(2)*	72.09(9)
Cl(1) – Zr(1) – Cl(2)	93.91(13)	Cl(1) – Zr(1) – Cl(1)*	99.4(2)
Cl(1) – Zr(1) – Cl(2)*	143.01(12)	Cl(2) – Zr(1) – Cl(2)*	95.9(2)

6.3 Conclusions

The complexes $[TiX_4(L_3)]$ {X = Cl, Br, L_3 = $MeC(CH_2EMe)_3$ (E = S, Se); X = Cl, Br, I, L_3 = $MeC(CH_2AsMe_2)_3$ and [Z]aneS_3 (Z = 9, 10)} have been prepared *via* the reaction of TiX_4 with the respective tridentate ligand, L_3 in anhydrous *n*-hexane (X = Cl) or CH_2Cl_2 (X = Br, I). Similarly, reaction of $[ZrCl_4(Me_2S)_2]$ with L_3' {L_3' = MeC-$(CH_2EMe)_3$ (E = S, Se) and [Z]aneS_3 (Z = 9, 10)} in anhydrous CH_2Cl_2 afforded the complexes $[ZrCl_4(L_3')]$ upon gentle pumping to remove Me_2S. Whereas reaction of $[ZrCl_4(Me_2S)_2]$ with $MeC(CH_2AsMe_2)_3$ yields 8-coordinate $[ZrCl_4\{MeC(CH_2$-$AsMe_2)_3\}_2]$ even at low ligand concentrations.

While the geometry at Ti(IV) and Zr(IV) could not be ascertained with confidence from far IR spectroscopy, the observed metal-halide stretching frequencies have been informative. Thus, the tripodal ligand Ti(IV) adducts exhibit frequencies comparable with those observed for similar 6-coordinate Ti(IV) complexes, while the macrocyclic adduct frequencies are shifted significantly to low frequency, possibly indicating a change in geometry at Ti(IV). Furthermore, the stretching frequencies of the Zr(IV) adducts lie midway between those observed for similar 6- and 8-coordinate Zr(IV) adducts, suggesting 7-coordination. One exception was the Zr(IV) adduct with $MeC(CH_2AsMe_2)_3$, which exhibited Zr-Cl stretching frequencies almost identical to those observed for structurally authenticated 8-coordinate $[ZrCl_4\{o\text{-}C_6H_4(AsMe_2)_2\}_2]$.

Variable temperature ^1H and $^{13}C\{^1H\}$ NMR spectroscopy of the tripodal ligand Ti(IV) adducts confirmed the complexes are indeed 6-coordinate, with the tripodal ligand behaving as a bidentate. The spectra also revealed the solution stability of the complexes, with increased ligand dissociation observed on decreasing the Lewis acidity of the metal centre ($TiBr_4$ cf. $TiCl_4$) or increasing the softness of the donor atom (Se cf. S). The macrocyclic adduct $[TiCl_4([9]aneS_3)]$ exhibited slight solubility in anhydrous $MeNO_2$, with the resulting NMR spectra confirming symmetric coordination of the ligand to present a rare example of 7-coordinate Ti(IV). The NMR spectra also revealed the presence of a partially hydrolysed decomposition product, tentatively assigned as $[TiCl_2(O)([9]aneS_3)]$.

X-ray crystallography of $[TiBr_4\{MeC(CH_2AsMe_2)_3\}]$ confirmed the tripodal ligand behaves as a bidentate, with geometry at Ti(IV) comparable with similar 6-coordinate complexes involving bidentate ligands. The structure of $[ZrCl_4([9]aneS_3)]$ confirmed symmetrical coordination of the ligand to reveal a rare example of 7-coordinate Zr(IV). The observed Zr-Cl bond distances are midway between those observed for similar 6- and 8-coordinate thioether Zr(IV) complexes, consistent with the observations from IR spectroscopy. The structure of $[ZrCl_4\{MeC(CH_2AsMe_2)_3\}_2]$ confirms bis-coordination of tripodal ligands acting as bidentates to afford 8-coordinate Zr(IV). The observed structure is comparable with similar $[ZrCl_4\{o\text{-}C_6H_4(AsMe_2)_2\}_2]$, though with increased ligand bite angle for the more flexible tripodal ligand.

6.4 Experimental

Tripodal arsine,[17] thio-[18] and seleno-ether[19] ligands and [9]aneS$_3$[20] were prepared *via* literature procedures, while [10]aneS$_3$ and TiX$_4$ were used as received from Aldrich Chemical Company and [ZrCl$_4$(Me$_2$S)$_2$] prepared as described in Chapter 5. Rigorously anhydrous *n*-hexane and CH$_2$Cl$_2$ were freshly distilled over sodium/ benzophenone and CaH$_2$ respectively, and degassed with dry N$_2$. All reactions were performed under an N$_2$ atmosphere using standard Schlenk techniques. The products were transferred and stored in a dry, continuously N$_2$-purged glove box, as were all sample preparations.

[TiCl$_4${MeC(CH$_2$SMe)$_3$}]

TiCl$_4$ (0.10 cm^3, 0.91 mmol) was added *via* degassed syringe to a solution of MeC(CH$_2$SMe)$_3$ (0.19 g, 0.91 mmol) in dry, degassed *n*-hexane (20 cm^3), affording the immediate precipitation of a bright yellow solid. This was filtered, washed with *n*-hexane (5 cm^3) and dried *in vacuo* to give the required [TiCl$_4${MeC(CH$_2$SMe)$_3$}] (yield 0.35 g, 87 %). Required for [C$_8$H$_{18}$Cl$_4$S$_3$Ti]: C = 24.0, H = 4.5 %; found: C = 23.8, H = 4.4 %. ^{1}H NMR (300 K): δ 2.87 (br, *s*, CH$_2$, 6H), 2.36 (br, *s*, CH$_3$S, 9H), 1.24 (br, *s*, CH$_3$C, 3H); (180 K): 3.2 (br, *s*, CH$_2$, 6H), 2.68 (*s*, CH$_2$ free arm, 3H), 2.55 (*s*, CH$_2$ free ligand), 2.53, 2.51 (*s*, CH$_3$S, 6H), 2.07 (*s*, CH$_3$S free arm, 3H), 2.01 (*s*, CH$_3$S free ligand), 1.17 (*s*, CH$_3$C, 3H), 1.07 (*s*, CH$_3$C free ligand). ^{13}C{^{1}H} NMR (300 K): δ 47.9 (CH$_2$), 39.8 (C), 25.1 (Me), 22.9 (MeS); (180 K): 49.2, 47.4 (CH$_2$), 44.8 (CH$_2$ free arm), 40.1 (C), 25.9, 25.7 (MeS) 24.9 (Me), 18.0 (MeS free arm). IR ν(TiCl): 411, 399, 389, 379 cm^{-1}.

[TiCl$_4${MeC(CH$_2$SeMe)$_3$}]

As above, but using MeC(CH$_2$SeMe)$_3$ (0.32 g, 0.91 mmol). An orange solid was isolated as the required [TiCl$_4${MeC(CH$_2$SeMe)$_3$}] (yield 0.44 g, 82 %). Required for [C$_8$H$_{18}$Cl$_4$Se$_3$Ti]: C = 17.8, H = 3.5 %; found: C = 17.9, H = 3.4 %. ^{1}H NMR (300 K): δ 2.74 (br, *s*, CH$_2$, 6H), 2.49 (br, *s*, CH$_3$S, 9H), 1.30 (br, *s*, CH$_3$C, 3H); (180 K): 3.1 (br, *s*, CH$_2$, 6H), 2.70 (*s*, CH$_2$ free arm, 3H), 2.63 (*s*, CH$_2$ free ligand), 2.45, 2.43 (*s*, CH$_3$S, 6H), 1.98 (*s*, CH$_3$S free arm, 3H), 1.93 (*s*, CH$_3$S free ligand), 1.20 (*s*, CH$_3$C, 3H), 1.11

(*s*, CH_3C free ligand). $^{13}C\{^1H\}$ NMR (300 K): no spectrum; (180 K): δ 46.1, 45.1 (CH_2), 39.9 (C), 37.1 (CH_2 free arm), 26.7 (Me), 18.5, 18.1 (MeS), 8.5 (MeS free arm). IR ν(TiCl): 402, 396, 389, 384 cm^{-1}.

$[TiCl_4\{MeC(CH_2AsMe_2)_3\}]$

As above, but using $MeC(CH_2AsMe_2)_3$ (0.35 g, 0.91 mmol). An orange solid was isolated as the required $[TiCl_4\{MeC(CH_2AsMe_2)_3\}]$ (yield 0.49 g, 86 %). Required for $[C_{11}H_{27}As_3Cl_4Ti]$: C = 23.0, H = 4.7 %; found: C = 23.0, H = 4.9 %. ^1H NMR (300 K): δ 2.15 (*m*, CH_2, 4H), 1.74 (*s*, CH_2 free arm, 2H), 1.58 (*s*, CH_3As, 12H), 1.23 (*s*, CH_3C, 3H), 0.95 (*s*, CH_3As free arm, 6H). IR ν(TiCl): 400, 375, 368, 354 cm^{-1}.

$[TiCl_4([9]aneS_3)]$

As above, but using $[9]aneS_3$ (0.16 g, 0.91 mmol). A yellow solid was isolated as the required $[TiCl_4([9]aneS_3)]$ (yield 0.34 g, 92 %). Required for $[C_6H_{12}Cl_4S_3Ti]$: C = 19.5, H = 3.3 %; found: C = 19.3, H = 3.3 %. ^1H NMR (CD_3NO_2, 300 K): δ 4.17-4.07, 3.91-3.81 (*m*, CH_2, 6H). $^{13}C\{^1H\}$ NMR (CD_3NO_2, 300 K): 43.1(*s*, CH_2). IR ν(TiCl): 443, 416(br), 384 cm^{-1}.

$[TiCl_4([10]aneS_3)]$

As above, but using $[10]aneS_3$ (0.18 g, 0.91 mmol). A dull yellow solid was isolated as the required $[TiCl_4([10]aneS_3)]$ (yield 0.30 g, 78 %). Required for $[C_7H_{14}Cl_4S_3Ti]$: C = 21.9, H = 3.8 %; found: C = 21.7, H = 4.0 %. IR ν(TiCl): 427, 409, 401 cm^{-1}.

$[TiBr_4\{MeC(CH_2SMe)_3\}]$

$MeC(CH_2SMe)_3$ (0.17 g, 0.82 mmol) in dry, degassed CH_2Cl_2 (10 cm^3) was added to a solution of $TiBr_4$ (0.30 cm^3, 0.82 mmol) in CH_2Cl_2 (30 cm^3). The resulting red solution was stirred for 30 min. then concentrated *in vacuo* to 5cm^3. Addition of dry, degassed *n*-hexane (20cm^3) afford an orange solid that was filtered, washed with *n*-

hexane (5 cm^3) and dried *in vacuo* to give the required [$TiBr_4\{MeC(CH_2SMe)_3\}$] (yield 0.44 g, 76 %). Required for [$C_8H_{18}Br_4S_3Ti$]: C = 16.6, H = 3.1 %; found: C = 16.5, H = 3.1 %. ^{1}H NMR (300 K): δ 2.90 (br, *s*, CH_2, 6H), 2.40 (br, *s*, CH_3S, 9H), 1.20 (br, *s*, CH_3C, 3H); (180 K): 3.4 (br, *s*, CH_2, 6H), 2.63 (*s*, CH_2 free arm, 3H), 2.59, 2.57 (*s*, CH_3S, 6H), 2.50 (*s*, CH_2 free ligand), 2.06 (*s*, CH_3S free arm, 3H), 2.01 (*s*, CH_3S free ligand), 1.18 (*s*, CH_3C, 3H), 1.07 (*s*, CH_3C free ligand). $^{13}C\{^1H\}$ NMR (300 K): no spectrum; (180 K): δ 49.4, 47.2 (CH_2), 43.4 (CH_2 free arm), 42.7 (CH_2 free ligand), 38.9 (C), 27.4, 27.3 (MeS) 23.7 (Me), 18.0 (MeS free arm), 17.1 (MeS free ligand). IR ν(TiBr): 333, 325, 315, 307 cm^{-1}.

[$TiBr_4\{MeC(CH_2SeMe)_3\}$]

As above, but using $MeC(CH_2SeMe)_3$ (0.29 g, 0.82 mmol). A red solid was isolated as the required [$TiBr_4\{MeC(CH_2SeMe)_3\}$] (yield 0.51 g, 72 %). Required for [$C_8H_{18}Br_4Se_3Ti$]: C = 13.4, H = 2.5 %; found: C = 13.7, H = 3.0 %. ^{1}H NMR (300 K): no spectrum; (180 K): δ 3.3 (br, *s*, CH_2, 6H), 2.73 (*s*, CH_2 free arm, 3H), 2.70 (*s*, CH_2 free ligand), 2.55, 2.52 (*s*, CH_3S, 6H), 2.03 (*s*, CH_3S free arm, 3H), 2.00 (*s*, CH_3S free ligand), 1.23 (*s*, CH_3C, 3H), 1.12 (*s*, CH_3C free ligand). $^{13}C\{^1H\}$ NMR: no spectrum. IR ν(TiBr): 322, 307, 301, 295 cm^{-1}.

[$TiBr_4\{MeC(CH_2AsMe_2)_3\}$]

As above, but using $MeC(CH_2AsMe_2)_3$ (0.32 g, 0.82 mmol). A red solid was isolated as the required [$TiBr_4\{MeC(CH_2AsMe_2)_3\}$] (yield 0.54 g, 72 %). Required for [$C_{11}H_{27}As_3Br_4Ti$]: C = 17.6, H = 3.6 %; found: C = 18.1, H = 3.7 %. ^{1}H NMR (300 K): δ 2.2 (*m*, CH_2, 4H), 1.75 (*s*, CH_2 free arm, 2H), 1.71, (*s*, CH_3As, 12H), 1.26 (*s*, CH_3C, 3H), 0.96 (*s*, CH_3As free arm, 6H). IR ν(TiBr): 326, 313, 284, 279 cm^{-1}.

[$TiBr_4([9]aneS_3)$]

As above, but using $[9]aneS_3$ (0.15 g, 0.82 mmol). An orange solid was isolated as the required [$TiBr_4([9]aneS_3)$] (yield 0.47 g, 87 %). Required for [$C_6H_{12}Br_4S_3Ti$]: C = 13.2, H = 2.2 %; found: C = 13.0, H = 2.4 %. IR ν(TiBr): 358, 345, 339 cm^{-1}.

[TiBr$_4$([10]aneS$_3$)]

As above, but using [10]aneS$_3$ (0.16 g, 0.82 mmol). An orange solid was isolated as the required [TiBr$_4$([10]aneS$_3$)] (yield 0.41 g, 73 %). Required for [$C_7H_{14}Br_4S_3Ti$]: C = 15.0, H = 2.5 %; found: C = 14.6, H = 2.4 %. IR ν(TiBr): 359, 345, 338 cm^{-1}.

[TiI$_4${MeC(CH$_2$AsMe$_2$)$_3$}]

TiI$_4$ (0.20 g, 0.36 mmol) was dissolved in mildly refluxing dry CH_2Cl_2 (80 cm^3), with subsequent removal of undissolved solids *via* filtration affording a deep purple solution. Addition of MeC(CH$_2$AsMe$_2$)$_3$ (0.14 g, 0.36 mmol) in dry, degassed CH_2Cl_2 (10 cm^3) gave an immediate colour change and the resulting red solution was stirred for 30 min., then concentrated *in vacuo* to 5 cm^3. Dry, degassed *n*-hexane (20 cm^3) was added and CH_2Cl_2 was removed *in vacuo* to afford a dark purple *n*-hexane solution with some dark precipitate. This was filtered to give the required [TiI$_4${MeC(CH$_2$AsMe$_2$)$_3$}], though the partial solubility of the complex in *n*-hexane gave a reduced yield (0.30 g, 32 %). Required for [$C_{11}H_{27}As_3I_4Ti$]: C = 14.1, H = 2.9 %; found: C = 14.0, H = 3.2 %.

[TiI$_4$([9]aneS$_3$)]

As above, but using [9]aneS$_3$ (0.07 g, 0.36 mmol). A purple solid was isolated as the required [TiI$_4$([9]aneS$_3$)] (yield 0.32 g, 43 %). Required for [$C_6H_{12}I_4S_3Ti$]: C = 9.8, H = 1.6 %; found: C = 9.6, H = 1.7 %.

[TiI$_4$([10]aneS$_3$)]

As above, but using [10]aneS$_3$ (0.07 g, 0.36 mmol). A purple solid was isolated as the required [TiI$_4$([10]aneS$_3$)] (yield 0.23 g, 31 %). Required for [$C_7H_{14}I_4S_3Ti$]: C = 11.2, H = 1.9 %; found: C = 11.5, H = 2.0 %.

[ZrCl$_4${MeC(CH$_2$SMe)$_3$}]

MeC(CH$_2$SMe)$_3$ (0.13 g, 0.62 mmol) in dry, degassed CH_2Cl_2 (10 cm^3) was added to a solution of [ZrCl$_4$(Me$_2$S)$_2$] (0.20 g, 0.56 mmol) in CH_2Cl_2 (50 cm^3). The solution was slowly concentrated *in vacuo* to 20 cm^3 and stirred under N_2 for 24 hours. Further concentration and addition of *n*-hexane (10 cm^3) afforded a white solid that was filtered, washed with *n*-hexane (10 cm^3) and dried *in vacuo* to give the required [$ZrCl_4$-{$MeC(CH_2SMe)_3$}] (yield 0.27 g, 61 %). Required for [$C_8H_{18}Cl_4S_3Zr$]: C = 21.7, H = 4.1 %; found: C = 21.5, H = 4.3 %. IR ν(ZrCl): 328 br cm^{-1}.

[$ZrCl_4${$MeC(CH_2SeMe)_3$}]

As above, using $MeC(CH_2SeMe)_3$ (0.22 g, 0.62 mmol). A white solid was isolated as the required [$ZrCl_4${$MeC(CH_2SeMe)_3$}] (yield 0.31 g, 54 %). Required for [C_8H_{18}-Cl_4Se_3Zr]: C = 16.5, H = 3.1 %; found: C = 16.1, H = 3.3 %. IR ν(ZrCl): 324 br cm^{-1}.

[$ZrCl_4$([9]aneS_3)]

As above, but using [9]aneS_3 (0.11 g, 0.62 mmol). A white solid was isolated as the required [$ZrCl_4$([9]aneS_3)] (yield 0.34 g, 82 %). Required for [$C_6H_{12}Cl_4S_3Zr$]: C = 17.4, H = 2.9 %; found: C = 17.1, H = 3.3 %. IR ν(ZrCl): 332 br cm^{-1}.

[$ZrCl_4$([10]aneS_3)]

As above, but using [10]aneS_3 (0.12 g, 0.62 mmol). A white solid was isolated as the required [$ZrCl_4$([10]aneS_3)] (yield 0.28 g, 65 %). Required for [$C_6H_{12}Cl_4S_3Zr$]: C = 19.7, H = 3.3 %; found: C = 19.2, H = 3.0 %. IR ν(ZrCl): 320 br cm^{-1}.

[$ZrCl_4${$MeC(CH_2AsMe_2)_3$}$_2$]

From attempted synthesis of [$ZrCl_4${$MeC(CH_2AsMe_2)_3$}], using $MeC(CH_2AsMe_2)_3$ (0.24 g, 0.62 mmol). A white solid was isolated as [$ZrCl_4${$MeC(CH_2AsMe_2)_3$}$_2$] (yield 0.31 g, 74 % with respect to ligand concentration). Required for [$C_{22}H_{54}Cl_4As_6Zr$]: C = 26.4, H = 5.4 %; found: C = 21.0, H = 4.2 %. Required for [$ZrCl_4${$MeC(CH_2AsMe_2)_3$}], [$C_8H_{18}Cl_4Se_3Zr$]: C = 21.4, H = 4.4 %. IR ν(ZrCl): 300, 304 cm^{-1}.

Crystallographic Studies

Details of the crystallographic data collection and refinement parameters are given in Table 6.7. Crystals of [$TiBr_4$\{$MeC(CH_2AsMe_2)_3$\}] were grown in a dry N_2 purged glove box *via* slow evaporation of a CH_2Cl_2 solution of the complex, while crystals of [$ZrCl_4$\{$MeC(CH_2AsMe_2)_3$\}$_2$] were grown similarly from the CH_2Cl_2 filtrate obtained from the complex synthesis. Crystals of [$ZrCl_4$([9]aneS_3)] were grown *via* slow diffusion of weak CH_2Cl_2 solutions of [$ZrCl_4(Me_2S)_2$] and [9]aneS_3 in a dry N_2 purged glove box. Data collection used an Enraf Nonius Kappa CCD diffractometer equipped with an Oxford Systems open-flow cryostat operating at 150 K, with graphite monochromated Mo-K_α radiation (λ = 0.71073 A). Structure solution[21] and refinement[22,23,24] were routine.

Table 6.7 Crystallographic data collection and refinement parameters for $[TiBr_4\{MeC(CH_2AsMe_2)_3\}]$, $[ZrCl_4\{MeC(CH_2AsMe_2)_3\}_2]$ & $[ZrCl_4([9]aneS_3)]$.

	$[TiBr_4\{MeC(CH_2AsMe_2)_3\}]$	$[ZrCl_4\{MeC(CH_2AsMe_2)_3\}_2]$	$[ZrCl_4([9]aneS_3)]$
Formula	$C_{11}H_{27}As_3Br_4Ti$	$C_{22}H_{54}As_6Cl_4Zr$	$C_6H_{12}Cl_4S_3Zr$
Formula weight	751.62	1001.23	413.37
Crystal system	Orthorhombic	Tetragonal	Monoclinic
Space group	$Pna2_1$ (# 33)	$P4_12_12$ (# 92)	$P2_1/c$ (# 14)
a / Å	23.4808(5)	10.6325(2)	11.5442(10)
b / Å	9.4899(2)	10.6325(2)	8.4604(7)
c / Å	9.9052(2)	33.0844(8)	13.9222(13)
α / °	90	90	90
β / °	90	90	98.270(4)
γ / °	90	90	90
U / Å^3	2207.18(7)	3740.19(12)	1345.6(2)
Z	4	4	4
μ(Mo-K$_\alpha$) / cm^{-1}	121.05	58.61	20.36
No. of unique reflections	3509	2568	3973
R_{int} (based on F^2)	0.074	0.082	0.218
No. of obs. reflections [a]	1769	1811	725
No. of parameters	171	150	127
R [b]	0.047	0.063	0.097
R_w [c]	0.051	0.076	0.111

[a] Observed if $[I_o > 3\sigma(I_o)]$

[b] $R = \sum (|F_{obs}|_i - |F_{calc}|_i) / \sum |F_{obs}|_i$

[c] $R_w = \sqrt{[\sum w_i(|F_{obs}|_i - |F_{calc}|_i)^2 / \sum w_i|F_{obs}|_i^2}$

6.5 References

[1] W. Levason, B. Patel, G. Reid, V.-A. Tolhurst, M. Webster, *J. Chem. Soc., Dalton Trans.*, 2000, 3001.

[2] R. Hart, W. Levason, B. Patel, G. Reid, *Eur. J. Inorg. Chem.*, 2001, **11**, 2927.

[3] W. Levason, B. Patel, G. Reid, submitted for publication.

[4] G. A. Barclay, I. K. Gregor, M. J. Lambert, S. B. Wild, *Aus. J. Chem.*, 1967, **20**, 1571.

[5] R. J. H. Clark, M. L. Greenfield, R. S. Nyholm, *J. Chem. Soc. (A)*, 1966, 1254.

[6] A. J. McAlees, R. McCrindle, A. R. Woon-Fat, *Inorg. Chem.*, 1976, **15**, 1065.

[7] R. J. H. Clark, J. Lewis, R. S. Nyholm, *J. Chem. Soc.*, 1962, 2460.

[8] R. J. H. Clark, R. H. U. Negrotti, R. S. Nyholm, *J. Chem. Soc., Chem. Commun.*, 1966, 486.

[9] W. P. Crisp, R. L. Deutscher, D. L. Kepert, *J. Chem. Soc. (A)*, 1970, 2199.

[10] A. N. Bhat, R. C. Fay, D. F. Lewis, A. F. Lindmark, S. H. Strauss, *Inorg. Chem.*, 1974, **13**, 886.

[11] R. C. Fay, J. J. Stezowski, R. B. VonDreele, *J. Am. Chem. Soc.*, 1971, **93**, 2887.

[12] E. L. Muetterties, C. M .Wright, *J. Am. Chem. Soc.*, 1965, **87**, 4706.

[13] M. J. Frazer, Z. Goffer, *J. Chem. Soc. (A)*, 1966, 544.

[14] A. J. Blake, P. Mountford, M. Schröder, P. J. Wilson, *J. Chem. Soc., Chem. Commun.*, 1998, 1007.

[15] M. G. Drew, *Prog. Inorg. Chem.*, 1977, **23**, 67.

[16] G. Haselhorst, P. Jeske, B. Nuber, T. Weyhermüller, K. Wieghardt, *Inorg. Chem.*, 1994, **33**, 2462.

[17] R. D. Feltham, A. Kasenally, R. S. Nyholm, *J. Organomet. Chem.*, 1967, **7**, 285.

[18] R. Ali, S. J. Higgins, W. Levason, *Inorg. Chim. Acta.*, 1984, **84**, 65.

[19] D. J. Gulliver, E. G. Hope, W. Levason, S. G. Murray, D. M. Potter, G. L. Marshall, *J. Chem. Soc., Perkin Trans., II*, 1984, 429.

[20] D. Sellmann, L. Zapf, *Angew. Chem. Int. Ed., Engl.*, 1984, **23**, 807.

[21] PATTY, The DIRDIF Program System, G. Admiraal, G. Beurskens, P. T. Beurskens, W. P. Bosman, S. Garcia-Granda, R. O. Gould, J. M. M. Smits, C. Smykalla, Technical Report of the Crystallography Laboratory, University of Nijmegen, 1992.

[22] TeXsan, Crystal Structure Analysis Package, Molecular Structure Corporation, Houston, Texas, 1995.

[23] R. H. Blessing, *Acta Crystallogr., Sect. A*, 1995, **51**, 33.

[24] H. D. Flack, *Acta Crystallogr., Sect. A*, 1983, **39**, 876.

APPENDIX

Microanalytical data for air stable complexes were collected by the University of Strathclyde analytical laboratory, while the moisture sensitive complexes were analysed by Prof. W. Levason at the University of Southampton using an F&M Model 185 Analyser. Electrospray mass spectrometry, where utilised, was performed using MeCN as the carrier solvent to a VG Biotech Platform. Infrared spectra were recorded using a Perkin Elmer FT-IR 1710 spectrophotometer and electronic spectra were recorded by diffuse reflectance on a Perkin Elmer Lambda 19 UV/visible spectrometer.

Room temperature ^{1}H NMR spectra were recorded using a Bruker AM300 spectrometer operating at 300 MHz and referenced to TMS, while for all other NMR spectra, a Bruker AM360 spectrometer was used. ^{1}H and ^{13}C{^{1}H} NMR spectra were recorded at 360 and 90.6 MHz operational frequency respectively and referenced to $SiMe_4$. ^{31}P{^{1}H} and ^{77}Se{^{1}H} NMR spectra were recorded at 145.5 and 68.7 MHz and referenced to an external 85% aqueous H_3PO_4 solution and to neat Me_2Se, respectively. ^{55}Mn NMR spectra were recorded at 24.84 MHz operating frequency using an aqueous $KMnO_4$ solution as an external reference.

Single crystal X-ray diffraction data were collected on either a Rigaku AFC7S four-circle diffractometer or an Enraf Nonius Kappa CCD diffractometer. Both utilised Mo-Kα X-radiation of wavelength 0.71073 Å. The X-ray source for the former is a sealed X-ray tube, while a Nonius FR591 rotating anode X-ray generator was used for the latter. In all cases, carefully selected crystals were mounted onto a glass fibre with grease and subsequently frozen during low temperature (150 K) collection using an Oxford Systems open-flow cryostat.